NASA

National Aeronautics and
Space Administration

NASA CR-134594

# FEASIBILITY STUDY OF INLET SHOCK STABILITY SYSTEM OF YF-12



BY
G. E. Blausey
D. M. Coleman
and
D. S. Harp

LOCKHEED AIRCRAFT CORPORATION
ADVANCED DEVELOPMENT PROJECTS



Prepared for:
National Aeronautics and Space Administration
Lewis Research Center

| 1. Report No. | 2. Government Accession No. | 3. Recipient's Catalog No. |
|---|---|---|
| CR 134594 | | |

| 4. Title and Subtitle | 5. Report Date |
|---|---|
| Feasibility Study of Inlet Shock Stability System of YF-12 | November 1972 |
| | 6. Performing Organization Code |

| 7. Author(s) | 8. Performing Organization Report No. |
|---|---|
| G. C. Blausey, D. M. Coleman and D. S. Harp | SP-1964 |
| | 10. Work Unit No. |
| | Y0E5538 |

| 9. Performing Organization Name and Address | 11. Contract or Grant No. |
|---|---|
| Lockheed Aircraft Corporation<br>P.O. Box 551<br>Burbank, California 91520 | |
| | 13. Type of Report and Period Covered |
| | Contractor's Report |

| 12. Sponsoring Agency Name and Address | 14. Sponsoring Agency Code |
|---|---|
| National Aeronautics & Space Administration<br>Lewis Research Center<br>Washington, D.C. 20546 | |

15. Supplementary Notes

16. Abstract

The feasibility of self-actuating bleed valves as a shock stabilization system in the inlet of the YF-12 is considered for vortex valves, slide valves, and poppet valves. Analytical estimation of valve performance indicates that only the slide and poppet valves located in the inlet cowl can meet the desired steady state stabilizing flows, and of the two the poppet valve is substantially faster in response to dynamic disturbances. The poppet valve is, therefore, selected as the best shock stability system for the YF-12 inlet.

| 17. Key Words (Suggested by Author(s)) | 18. Distribution Statement |
|---|---|
| Inlets<br>Inlet Flow Stability<br>Bleed Systems<br>Supersonic Inlets | Unclassified - Unlimited |

| 19. Security Classif. (of this report) | 20. Security Classif. (of this page) | 21. No. of Pages | 22. Price* |
|---|---|---|---|
| Unclassified | Unclassified | 144 | |

* For sale by the National Technical Information Service, Springfield Virginia 22151

TABLE OF CONTENTS

## SUMMARY

A study of the feasibility of using self-actuating bleed valves as a shock stabilization system in the inlet of the YF-12 airplane has been made. The candidate stability valve types included vortex valves, slide valves, and poppet valves. Performance of the valves installed in the inlet cowl and in the inlet shock trap bleed plenum was predicted using analytical methods. In addition, the high temperature friction characteristics of linear bearings similar to those considered for use in the slide valve were measured in the laboratory. Results of the analytical investigation showed adequate steady state flow capacity for only the slide and poppet type valves located in the inlet cowl. Dynamic analyses showed that response of the poppet valve was substantially faster than that of the slide valve. The test data indicated that further development work would be necessary before a satisfactory linear bearing for the slide valve could be obtained. For these reasons poppet type valves installed in the inlet cowl have been selected as the best shock stability system for the YF-12 inlet.


## INTRODUCTION

An inlet shock stability system has been proposed for flight demonstration on the YF-12 airplane. The project will be a part of the continuing NASA research program on the inlet of this aircraft. An initial feasibility evaluation is to be followed by wind tunnel proof testing on a full scale inlet. Upon successful demonstration of the system in the wind tunnel, one inlet of the YF-12 aircraft will be modified to demonstrate the stability system in flight.

The stability system will consist of self-actuating bleed valves located in the inlet nacelle. The valves will open in response to the increase in duct pressure produced by a transient excursion of the inlet terminal shock forward from its steady state position. As the valves open, inlet bleed air will be diverted overboard, thereby increasing the stability range of the inlet. The valves will close when the transient disturbance subsides and the shock retreats to its steady state position.

To determine the feasibility of such a system, an analytical evaluation of several inlet shock stability valves has been made. The candidate valve types included vortex valves, mechanical slide valves, and mechanical poppet valves. Installation locations in the inlet cowl and in the inlet shock trap bleed plenum were considered. An enlarged shock trap bleed entrance was considered in addition to the present configuration.

Installation studies determined the number and size of each type of valve which can be installed at each of the locations. Maximum steady state flow rates through each combination were estimated. Analytical dynamic models of the most promising configurations were then constructed and the dynamic response determined.

Friction data were obtained from an overboard bypass door assembly having linear bearings similar to those which would be used on the slide valve. Data were obtained with transverse loads ranging from 0 to 2240 newtons and at temperatures from 294 to 664 degrees kelvin.

## STABILITY VALVE CONFIGURATIONS

### Principle of Operation

The YF-12 airplane has a translating centerbody, axisymmetric, mixed compression inlet as shown schematically in Figure 1. Cowl bleed removed from a shock trap bleed at the inlet throat is exhausted overboard through the secondary passage of the engine nozzle. Bleed from the porous centerbody is exhausted overboard through the centerbody support struts. A variable overboard bypass is located aft of the inlet throat as indicated in Figure 1.

Two locations have been proposed for the installation of shock stability valves. One is in the cowl bleed plenum and the other is just forward of the inlet throat as shown in Figure 1. In either case, the self-actuating valves sense an inlet flow instability as a rapid increase in pressure. The increase in pressure causes the valves to divert inlet air overboard, thus preventing the instability from unstarting the inlet.

Vortex valves and self-acting mechanical valves have been investigated for this application. The operational features of vortex valves designed for use in supersonic inlets are discussed in Reference 1. Two types of self-acting mechanical valves have also been considered: a slide valve and a poppet type valve. The method of operation of these valves is discussed below.

1. Slide Valve with No Overboard Bleed - A schematic diagram of a piston actuated slide valve is shown in Figure 2(a). Two bleed plenum arrangements have been considered. One has three plenums, denoted B1, B2 and B3 in Figure 2(a), with the pressure in B3 acting as the driving force on the piston. The other has four plenums, B1, B2, B3 and B4 as shown in Figure 2(a), with the pressure in plenum B4 acting on the piston. The configuration studied initially had three compartments. Analysis showed that the decrease in pressure in B3 due to flow through the valve produced an undesirable reduction in valve travel. Consequently, the final configuration employs four plenums.

To operate the valve without overboard bleed, orifice No. 1 is not used. The valve is held in the closed position by a spring located behind the piston. If the pressure in the aft bleed plenum increases rapidly, the resulting pressure differential across the piston forces the piston to open. As the piston moves, it covers orifice No. 2 leaving plenums G and H sealed except for leakage around the piston. The valve will remain open until the pressure in the aft bleed plenum decreases or until the pressure in plenums G and H rises sufficiently due to piston leakage to allow the spring to force the valve shut. If the valve is open when the bleed plenum pressure returns to its original value, the piston will begin to close. When this happens, the pressure in plenum G will decrease closing the damper valve between plenums G and H. Now the valve closing rate is restricted by the damper valve and the valve closes slowly as air flows from plenum H into plenum G through orifice No. 3. The closing rate can be adjusted by changing the size of orifice No. 3. When the valve reaches its full closed position, orifice No. 2 is exposed allowing the plenum pressures to equalize again. The valve will not respond properly to another rapid pressure rise until these pressures are equalized.

2. Slide Valve With Overboard Bleed - When an overboard orifice (orifice No. 1) is added to the configuration described above and shown in Figure 2(a), the valve operation exhibits the following differences. Orifice No. 2 is sized so that when the valve is closed, the pressure in plenum G is approximately 0.1 $N/cm^2$ less than the bleed plenum pressure acting on the piston. The valve is held shut by a spring. When the bleed pressure rises rapidly, the piston moves and covers orifice No. 2. Piston leakage increases as a result of the bleed pressure increase. However, orifice No. 1 can be sized to provide an overboard flow rate equal to the flow rate into plenum G when the aft bleed plenum pressure rises just sufficiently to produce full valve opening. For bleed pressure changes equal to or greater than this amount, the valve will remain fully open until the bleed pressure decreases. Pressure changes less than this which produce only partial opening may be followed by valve drift toward the open position as the pressure in plenums G and H decays.

The original configuration used a damper (orifice No. 3) to reduce the magnitude of oscillations incurred during valve closure. Subsequently, the valve friction was found to be higher than originally assumed and the additional damping force made the damper unnecessary. The piston-operated valve with overboard bleed was selected as the final configuration for the slide valve.

3. Slide Valve With Bellows - A schematic diagram of a bellows-operated slide valve is shown in Figure 2(b). The forward face of the

actuating piston is exposed to the bleed plenum pressure in the aft compartment. The rear face is exposed to ambient pressure outside the nacelle on the outside of the bellows and engine face static pressure on the inside of the bellows. Because the supply lines to the rear of the piston are large relative to the leakage area around the piston, the operation of this valve is essentially independent of piston leakage. The ratio of the bellows and piston areas is set to match the pressure levels of the three pressures acting on the piston. The damper valve and orifice serve the same function as those in the valve shown in Figure 2(a) and, with adequate friction levels, may be omitted.

This valve will remain open as long as the pressure increase in the aft bleed plenum persists. Upon termination of the bleed pressure transient, the valve is ready to respond to the next one. One of the major disadvantages of this configuration is its reliance upon accurately known and consistently available reference pressures.

4. Poppet Valve With No Overboard Bleed - A piston actuated poppet valve is shown in schematic form in Figure 3(a). To operate the valve without overboard bleed, orifice No. 1 would not be used. Orifice No. 4 is required in order to allow some leakage from the plenum B into plenum G. Otherwise, during a prolonged pressure step in plenum B, the air in plenum G would leak out around the piston and the valve might get "stuck" open. The operation of this valve is the same as that of the slide valve with no overboard bleed. The same two limitations apply: the valve will drift closed during a long duration bleed pressure step, and it will not respond properly to a succeeding transient until the pressures in plenums B, G and H have equalized. The original configuration used the orifice damper No. 3 to provide damping during valve closure. Subsequently, an adjustable mechanical friction damper on the poppet stem replaced the orifice damper.

5. Poppet Valve With Overboard Bleed - The addition of orifice No. 1 (Figure 3(a)) produces a system which operates in the same manner as the slide valve with overboard bleed. This valve, with the stem-mounted mechanical friction damper, was selected as the final configuration for the unshielded poppet valve.

6. Poppet Valve With Bellows - A schematic diagram of a bellows-operated poppet valve is shown in Figure 3(b). The principle of operation, the advantages and disadvantages are the same as for the bellows-operated slide valve. Since a cowl installation requires valves at two axial positions, it is necessary to use different size bellows for the corresponding valves to accommodate the differences in bleed plenum pressure.

7. Poppet Valve With Overboard Bleed and Flow Shield - A modified version of the poppet valve for use in a cowl installation is shown in Figure 4. A poppet flow shield is used here to allow the poppet to be driven directly by duct pressure rather than the bleed plenum pressure. There are two advantages achieved by the shield: (1) aerodynamic forces due to airflow are minimized, and (2) the driving pressure does not decrease drastically due to opening of the valve. Furthermore, it becomes possible to actuate the forward row of valves with air ducted forward from a pickup location further aft in the duct. This permits faster actuation of the forward valves when the duct pressure starts to increase just forward of the throat as the shock moves forward.

Since this valve concept appeared to be the best of those investigated, more design refinements were made to the design than to the ones shown in Figures 2 and 3. For example, Figure 4 shows an additional orifice (No. 4) which was added to the poppet stem. This orifice prevents the pressure above the poppet from bleeding down too far when a small increase in duct pressure moves the piston across orifice No. 2. This ensures tha complete valve closure is always obtained when the inlet transient disturbance subsides.

## Assembly and Installation Layouts

As part of the shock stability system feasibility study, assembly and installation layout drawings have been prepared. These drawings show the alternate configurations and installation locations which have been investigated. Because of the large number of drawings in this report, they have been segregated from the figures, given drawing numbers rather than figure numbers, and placed at the end of the report following the figures. Dimensions are given in centimeters. Since existing detail and assembly drawings of the inlet are dimensioned in inches, some of the important centimeter dimensions in this report are followed, in parentheses, by inches. All design work was done using the inch as the unit of measurement.

1. System Schematics - Drawings 1, 2 and 3 are system schematics of the recommended installations for the slide valves, unshielded poppet valves, and shielded poppet valves, respectively. The valves are located in the cowl just forward of the inlet shock trap. Both the inlets to and the exits from the poppet and slide valves are compartmented axially and circumferentially. All valves exhaust overboard through louver exits. Each of the slide valves is connected to a large common plenum as indicated in Drawing 1. Each of the forward poppet valves

is connected to a common plenum and each of the aft poppet valves is connected to another common plenum as shown in Drawings 2 and 3. In each of these plenums, there is an adjustable overboard orifice. The slide or poppet valves can be closed manually by actuating a solenoid valve which admits high pressure air into the valve plenums. The high pressure air is obtained from ram scoops located in the inlet duct just downstream of the throat. Installation layouts for full-scale and three-quarter scale vortex valves are shown in Drawings 4 and 5, respectively.

2. Slide Valves

a. Drawing 6 shows a preliminary slide valve assembly and its installation in the cowl.

b. Drawing 7 shows the installation of twenty-four slide valves in the shock trap plenum. To facilitate flow around the valve end, the shock trap exit duct was shortened slightly, adjacent to the duct wall.

c. Drawing 8 shows the installation of the slide valve in the cowl. Changes or additions to Drawing 6 are:

- Number of valves increased from 24 to 25.
- A proposed typical louver box over each valve.
- Duct wall perforation details.

3. Poppet Valves - In the initial concept of the poppet valve, bleed flow pressure losses in valve entry ports brought about a substantial degradation in valve performance. The design was revised to allow bleed plenum flow directly into the poppet area. Two designs resulted. The first used restrictor check valves for damping and the second used light friction devices.

Drawing 9 is the original version and Drawing 10 is the final version of the unshielded poppet valve. The shielded version is shown in Drawing 11. Drawing 12 is the original version and Drawing 13 is the final version of a bellows-operated poppet valve.

Drawings 14, 15 and 16 show installations of the poppet valves in the cowl and shock trap bleed plenum. The original installation of the valves at these two locations is shown in Figure 14. Space requirements dictated a reduction in size of the forward valves. Since a reduction in flow capacity was undesirable, subsequent work was directed to increasing the size of the forward valves. The final cowl installation for the poppet valves, Drawings 15 and 16, uses valves of the same height at both the forward and aft positions.

Drawing 15 shows the placement of the twenty-five valves around the nacelle. The outboard chine shown here would be present on the airplane installation, but not on the wind tunnel model. Drawing 15 also shows the duct wall perforation details and the plumbing which connects each valve with its reference pressure plenum. Details of the exit louver box are shown in Drawing 16.

4. Wind Tunnel Valve Actuator - Drawing 17 shows the proposed arrangement of an electrically operated bleed valve system for use in a wind tunnel test. This system could be used to remotely vary the overboard bleed flow rate in order to determine how much steady state bleed flow is required to prevent adverse recirculation effects through the porous cowl wall.

5. Variable Overboard Orifice - Drawing 18 shows the proposed design for the variable overboard orifice required at each valve plenum, and its installation in the skin of the nacelle.

6. Bleed Shut-Off System - Drawing 19 shows the pneumatic system required to hold the bleed valves closed on command from the cockpit or from outside the wind tunnel.

7. Centerbody Perforations - Drawing 20 shows the perforated centerbody skins. They are replaceable by a set of solid skins to return to the original bleed configuration.

## PERFORMANCE ANALYSIS

### Design Pressures

1. Internal Pressures - The valve designs are based on internal cowl pressure distributions obtained from NASA/Lewis full-scale wind tunnel tests of the YF-12 inlet. The data used are shown in Figures 5 through 8.

Flight test data were used to define conditions in the shock trap bleed since these properties depend upon the engine ejector characteristics and nacelle leakage. For flight at the design Mach number, it was determined that the total pressure recovery of the shock trap bleed is 0.27 and the bleed mass flow ratio is 0.08.

2. External Pressures - Since the bleed valve flow will be discharged overboard through louvers, it is necessary to know the external pressure on the nacelle to size the valve exit louvers properly. Data from a recent NASA/Ames wind tunnel test of a 1/12-scale airplane model define these pressures. The results are shown in Figures 9 through 20. Figure 9 identifies the circumferential orientation of the symbols appearing in Figures 10 through 20. From these curves, it is seen that the lower inboard side of the nacelle is the only region experiencing unusually large positive pressures during high angle of attack conditions.

Inlet Bleed Characteristics

1. Porous Bleed Recirculation - According to the data of Figure 6, there is a significant variation in the cowl static pressure ahead of the inlet throat. If this region is perforated, with a plenum beneath the perforations, a recirculation flow will ensue with flow entering the plenum where the duct pressure is high and reentering the duct in the forward region where the pressure is low. An analysis of the recirculation was made assuming, as a first approximation, that the recirculation did not affect the duct pressure distribution. The data of Reference 2 were used to define the characteristics of flow from the duct into the plenum. The results are summarized in Figures 21 and 22. The data of References 3 and 4 were used to estimate the flow from the plenum back into the duct. The results were approximated by the correlation shown in Figure 23. Figures 21, 22 and 23 were used to determine the match point at which the flows entering and leaving the plenum were equal. The match point is shown in Figure 24.

The analysis indicates a recirculation mass flow ratio of about 2 percent. A one-dimensional analysis of the blockage effect of the flow emerging from the front of the porous bleed region indicates that this quantity of flow will restrict the duct flow to the extent that the minimum aerodynamic area will occur several inches upstream of the minimum geometric area.

Although recirculation of this magnitude would undoubtedly alter the duct wall static pressure distribution, it is apparent that a nonflowing bleed region of this length will have potentially adverse recirculation problems. Similarly, circumferential pressure variation, an example of which is shown in Figure 25, can induce recirculation problems. Consequently, it is recommended that cowl porous bleed regions forward of the shock trap be compartmented both axially and circumferentially.

A comparison of Figures 6 and 24 shows that the computed match point bleed plenum pressure is close to the mean value of the external static pressure on the porous region. Consequently, for determination of plenum pressures for the cases in which the bleed was compartmented axially, it was assumed that the plenum pressure with bleed valves closed would be approximately equal to the mean duct pressure exerted on the porous wall supplying air to the plenum.

2. Shock Trap Flow Characteristics - Steady state shock trap match point flow rates and recoveries are available from both wind tunnel and flight test data. However, no inlet data is available for the case where the terminal shock is in an equilibrium position ahead of the shock trap. Consequently, the performance of the shock trap bleed under these conditions has been estimated using wind tunnel data obtained during a Lockheed test of various bleed configurations in a simulated inlet. Some of the results are shown in Figures 26 and 27. Figure 26 shows a shock trap bleed very similar to the present airplane bleed while Figure 27 is for the same configuration with the streamwise opening enlarged by 55 percent. The curves show the mass flow vs. recovery characteristics of the bleeds for various terminal shock positions. Shock position is measured by the wall static pressure level at a point upstream of the bleed as indicated on Figures 26 and 27. The reference mass flow, $w_{TOTAL}$, is the calculated tunnel flow rate ahead of the bleed.

To match flight test data, it is necessary that the total pressure recovery of the shock trap bleed be 0.27 and that the mass flow ratio be 0.08. The data of Figure 26 indicate that for supercritical inlet operation, these match points can be attained if we let $w_{TOTAL}/w_o = .708$. This method of matching the bleed test data with flight test results has been used to define the operating characteristics of the shock traps.

Steady State Valve Performance

1. Vortex Valves - Flow characteristics for a variety of vortex valve installation designs with a wide range of operating conditions were examined to determine optimum performance available with this type of valve. Data for the high capacity, compact valves described in Reference 1 were used for this analysis. This reference developed two sets of flow characteristics for vortex valves: one based on test data from a set of one-sixth scale valves, from which a "recommended design" was developed; the other defined from actual flow characteristics of a full-scale valve built to the recommended design--referred to as the "full-scale test" data. These two data sets were selected as limiting performance curves for the probable range of flow characteristics exhibited by vortex valves of this

design. The "recommended design" performance curve shows a much steeper radial flow gain near the cutoff condition than the "full-scale test" curve, indicating greater performance potential (larger bleed flow increase with rise in bleed pressure at optimum nozzle pressure). The more linear flow characteristics of the "full-scale test" curve, however, indicate greater stability when subjected to off-design operating conditions.

The number of vortex valves that can be used and their size is limited by the space available for installation in the cowl and shock trap areas of the nacelle. The maximum practical valve size is 3/4-scale, based on full-scale dimensions of the "recommended design". Since valve outlet flow varies as the orifice area, or as the square of the scale factor, flows for 3/4-scale valves are approximately 56 percent of full-scale valve flows under the same operating conditions. A total of 96 valves with a total flow area of 310 $cm^2$ can be installed in each area. The valves in the cowl area can be separated into two sets of 48, denoted the forward and aft cowl valves. Each set reacts independently to different local bleed pressures.

The vortex valve installation design assumes that valve outlet flow dumps into an exhaust plenum which exits to ambient through a set of louvers. A nominal louver exit area of 6.45 $cm^2$ per valve is assumed. The louvers back pressure the valves slightly as bleed flow increases, but changes in valve outlet pressure are accounted for in the flow characteristic curves.

Flow analyses for an installed vortex valve were performed to determine the effects of variations in valve design and in operating pressures. Performance of the valve is defined as the increment in bleed (radial) flow for a given increase in bleed pressure at a constant vortex nozzle supply pressure. Bleed leakage flow is defined as the bleed flow at normal operating bleed pressure. Leakage flow can be zero if the valve is operating at the cutoff condition. Optimized performance for a valve occurs at the nozzle supply pressure for which bleed flow increment vs. bleed pressure rise is maximized while leakage flow is acceptable.

A simple computer program was written to analyze valve performance while varying design and operating parameters over a wide range. The parameters varied include louver exit area, valve scale, valve design, and nozzle supply pressure. The valve configurations are indicated by three designators: the scale (relative to the full-scale valve described in Reference 1), louver exit area ($cm^2$), and valve design. The "RD" design refers to the "recommended design" and the "FST" design refers to the "full-scale test" valve. Valve performance and leakage flows were calculated for increases in bleed pressure up to 50 percent above normal.

The flight condition assumed was Mach 3+ at cruise altitude. Normal operating bleed pressures of 2.38, 2.93 and 3.77 $N/cm^2$ were assumed to cover the probable pressure range in the forward nacelle areas.

Results of varying louver exit area are shown in Figures 28 and 29. A 3/4-scale valve with "full-scale test" flow characteristics is assumed. Figure 28 presents the bleed flow increment for a 20 percent increase in bleed pressure for three exit areas. Figure 29 shows leakage flow at the three typical bleed pressures. All flows increase with greater exit area because of reduced back pressure at the valve outlets. Figure 28 shows that optimum valve performance occurs at a definite nozzle supply pressure for each design or operating condition, and performance is fairly sensitive to nozzle pressure variation near this peak. Leakage flows shown in Figure 29 decrease sharply as nozzle pressure increases until the cutoff point is reached. These are typical operating characteristics for vortex valves.

Figure 28 also shows that optimum nozzle supply pressure increases slightly for larger exit area. Therefore, if higher nozzle pressures are available, greater flow increments can be obtained by increasing exit area. Leakage flows would not increase significantly because the effect of higher nozzle pressure almost balances the effect of greater exit area. Because of space limitations and design considerations, a louver exit area of 6.45 $cm^2$ per valve was selected as a basic design for further parametric comparisons.

Figures 30 and 31 show differences in performance and leakage for the two flow characteristic curves. The "recommended design" valve almost doubles the peak bleed flow increments indicated for the "full-scale test" valve, although peaks for both valves occur at the same nozzle supply pressures. Leakage flows are significantly lower for the "recommended design" valve near optimum nozzle pressures. The steepness of the flow curves indicates much greater sensitivity to nozzle pressure variations for the "recommended design" valve.

Figure 32 presents a summary of optimized performance and leakage for the different valve configurations examined. The data are presented for the range of normal operating bleed pressure, and assume that nozzle supply pressure is adjusted to yield peak bleed flow increment. Figure 33 shows the same comparison on a percentage basis, using the 3/4-scale "full-scale test" valve design with 6.45 $cm^2$ louver area as a base. The "recommended design" flow characteristics indicate by far the highest performance and lowest leakage flows. Increasing valve scale from 3/4 to 7/8 (a 35 percent area increase) yields the expected scaled up increases in bleed increment and leakage flows. Increasing louver area yields a small increase in performance with little change in leakage flow, as explained above.

The effects of off-design operation are shown in Figures 34 and 35. For a 10 percent increase in nozzle supply pressure above the optimized value, bleed flow increment drops by approximately 30 percent for all valve configurations. For a 10 percent decrease in nozzle pressure, performance drops about 10 percent for "full-scale test" valves and nearly four times that amount for "recommended design" valves. The percent changes in leakage flow (Figure 35) show approximately double the sensitivity to nozzle pressure variation for valves with "recommended design" flow characteristics. These figures emphasize the importance of considering the effects of off-design operation when choosing between vortex valves and other type valves, or even between vortex valves with different flow characteristics. Under conditions where nozzle supply pressure may not be well defined and consistent, a large tolerance must be placed on the design performance of vortex valves of this type.

Figure 36 presents the installed performance and total flows for "recommended design" valves operating at optimum nozzle supply pressure. Flow increment with increase in bleed pressure up to 50 percent is shown as a percentage of inlet capture airflow for the three separate valve installations. Valves are 3/4-scale and louver area is 6.45 $cm^2$. The maximum total bleed flow increment for each set of 96 valves operating in the cowl and in the shock trap areas is less than 2 percent of total airflow for a local bleed pressure rise of 50 percent. The total leakage mass flow ratio is approximately .002 at either location. The drag penalty charged to the leakage flow was computed by assuming full ram drag, i.e., the drag coefficient based on inlet capture area is twice the bleed mass flow ratio based on inlet capture area. At both the cowl and shock trap plenum locations, the leakage drag coefficient, based on wing reference area, is less than .00005.

2. Slide Valves - The bleed flow rate through slide valves installed in the cowl is a function of duct Mach number (i.e., shock position) and valve position. The relation between shock position and duct Mach number is shown in Figure 37. The supersonic Mach numbers were computed from the data of Figure 6. Mach numbers behind the terminal shock were computed by normal shock theory. A linear variation in Mach number was taken between the value at the normal shock and an assumed value of 0.95 just ahead of the throat. The mean duct Mach number at each of the separate bleed compartments (tabulated in Figure 37) was used in flow rate computations.

The slide valve exit louver flow characteristics, based on test data, are defined in Figure 38. Steady state flow characteristics of the slide valve are shown in Figures 39, 40 and 41 as a function of bleed plenum pressure for the noted values of total pressure at the louver exit. The louver flow rates shown in Figure 38 were matched with those in

Figures 39 through 41 to give the performance of the valve/louver combination. At higher bleed plenum pressures, the flow was assumed choked at the louver exit when the valve was completely open or choked in the valve slots when the valve was partially open. The minimum area in each fully open valve slot and in each exit louver slot is 89.6 $cm^2$, Flow rates through the valve/louver combination are plotted in Figures 42 and 43. Also shown on Figures 42 and 43 are flow rates through the duct wall perforations. The data of Reference 2 were used to define the flow characteristics from the inlet duct into the bleed plenums.

Figures 42 and 43 may also be used to find the steady state flow through slide valves installed in the shock trap bleed plenums. In this case, the bleed plenum pressure shown in Figures 42 and 43 would be the shock trap plenum pressure and the perforation flow rates would not be pertinent.

It should be noted that the flow rates shown in Figures 38 through 43 are those through 24 valves, but through only one of the three rows of slots. To determine the total flow rate through 24 valves installed in the shock trap plenum, the mass flow ratio shown in Figures 42 and 43 would be tripled. To determine the flow rate through slide valves installed in the cowl, Figures 42 and 43 would be entered three times with the valve position (identical for all three) and the duct Mach number (different for all three--obtain from Figure 37). The summation of these three mass flow ratios is the flow through all three slots of 24 valves. Since the number of valves installed in the cowl is 25, the summation should be multiplied by 25/24 to obtain the total flow through 25 valves.

Leakage flow rates with the valves completely closed were estimated by assuming clearances of 0.008 cm and a leakage path 0.318 cm long by 58.4 cm wide for each valve. An iteration procedure was used to match the leakage flow with the available pressure differential across the closed valve. The drag penalty charged to the leakage flow was computed by assuming full ram drag. The total leakage mass flow ratio through all the valves was less than .0003 for installation in either the cowl, shock trap plenum, or the plenum of an enlarged shock trap bleed. The corresponding drag coefficients, based on wing reference area, were less than .000006.

3. Unshielded Poppet Valves - Steady state flow rates through the unshielded poppet valves were computed using the methods described above with appropriate values for the physical dimensions involved. The minimum area in each fully open valve is 53.7 $cm^2$. The relationship between shock position and duct Mach number at free stream Mach numbers of 3+ and

2.47 is shown in Figures 44 and 45. Flow characteristics of the valves and exit louvers are shown in Figures 46 and 47. Match point flows for a total louver area of 1858 $cm^2$ are superimposed in Figures 48, 49 and 50 on flow rates through the duct wall perforations. Flow matching determinations similar to these were also made for other exit louver areas. On the basis of these results, which are summarized in Figure 51, an exit area of 1858 $cm^2$ was chosen as a minimum design requirement and was used in subsequent flow rate computations.

Figures 48, 49 and 50 may also be used to find the flow rate through poppet valves installed in the shock trap plenum. The bleed plenum pressure shown in these figures would represent the shock trap plenum pressure and the perforation flow rate curves would not be applicable for this case.

Note that the flow rates shown in Figures 46 through 51 are those through 24 valves. The total flow through the 48 valves installed in the shock trap plenum is twice that obtained from Figure 48 or 49. Flow through the forward and aft poppet valves installed in the cowl is determined from Figures 48 through 50. Since there are 25 valves at each of two stations in the cowl, the values obtained from Figures 48 through 50 should be multiplied by 25/24 to obtain the flow through 25 valves.

Leakage flow through the poppet valves in the completely closed position was computed by assuming choked flow through an average leakage gap of 0.008 cm. Leakage drag was computed by assuming full ram drag. For installation locations in the cowl, the existing shock trap plenum, or an enlarged shock trap plenum, the leakage mass flow ratio for all the valves was less than .0008 and the drag coefficient based on wing reference area was less than .000018.

4. Shielded Poppet Valves - The relationships between valve position, bleed plenum pressure and bleed flow rate are the same as those for the unshielded poppet valves (shown in Figures 48 and 49). However, with the valve fully open, the minimum flow area in the valve, 47 $cm^2$, is less than that of the unshielded valve because of the blockage caused by the poppet shield entry pipe. Flow rates at maximum valve opening may be obtained from Figures 48 and 49 by using a valve opening $\Delta x$=1.987 cm, which corresponds to an area of 47 $cm^2$. Leakage flow rate and drag is the same as that for the unshielded poppet valve.

Valve Dynamic Performance

1. Computer Simulation - Mathematical models of the slide valve and poppet valve have been constructed in order to estimate the effects of various design parameters on the dynamic response characteristics of the

valves. The models incorporate provisions for considering various valve configurations. The digital computer simulation provides a time history of the valve motion resulting from a prescribed time history of flow properties in the inlet duct. The step integration is accomplished as follows.

The rate of change of pressure in the piston chamber due to piston travel, leakage around the piston, and flow through the various orifices is computed from the following relationship for adiabatic flow:

$$mV\frac{dP}{dt} + (kV\sum w_{out} + km\frac{dV}{dt})P - (kRm\sum T_{T_{in}} w_{in}) = 0$$

where:
- $m$ = mass of air in chambers above piston
- $w_{in}$ = mass flow rate into chambers above piston
- $w_{out}$ = mass flow rate out of chambers above piston
- $V$ = total volume of chambers above piston
- $P$ = piston chamber pressure
- $T_{T_{in}}$ = total temperature of air flowing into chambers above piston

Mass flow rates are based on the estimated piston leakage shown in Figure 52 and the orifice flow shown in Figure 53. The piston clearance parameter, $h^3/L$, as defined in Figure 52, was assumed to be $19.6 \times 10^{-8} cm^2$ for the slide valve and $1.022 \times 10^{-8} cm^2$ for the poppet valves.

Valve position is calculated as follows:

$$x = x_o + \dot{x}\Delta t + \ddot{x}\frac{\Delta t^2}{2}$$

where:
- $x$ = valve position at end of time interval, $\Delta t$
- $x_o$ = valve position at beginning of interval
- $\dot{x}$ = valve velocity at beginning of interval
- $\ddot{x}$ = valve acceleration at beginning of interval

The forces acting on the pistons of the poppet valves are somewhat different for the shielded and unshielded versions. Using the nomenclature defined in Figure 3(a) and letting $P_{pop}$ be the average pressure acting on the entire lower surface of the poppet, the pressure force acting on the unshielded poppet is

$$F_{pressure} = (P_{pop} - P_G) A_{pop}$$

where $A_{pop}$ is the area of the poppet normal to its axis. This can

be rewritten as

$$F_{pressure} = (P_B - P_G)A_{pop} - (P_B - P_{pop})A_{pop}$$

where $(P_B - P_G)A_{pop}$ is termed the "piston" force and $(P_B - P_{pop})A_{pop}$ is termed the "aerodynamic" force.

Using the nomenclature defined in Figure 4 and letting $P_{edge}$ be the pressure on the bottom edge of the poppet, the pressure force acting on the shielded poppet is

$$F_{pressure} = (P_D - P_G)A_{pop} - (P_D - P_{edge})A_{edge}$$

where $(P_D - P_G)A_{pop}$ is termed the "piston" force and $(P_D - P_{edge})A_{edge}$ is termed the "aerodynamic" force.

Similarly, the pressure force acting on the slide valve is

$$F_{pressure} = (P_{B4} - P_G)A_{piston} - F_{aerodynamic}$$

where the nomenclature is defined in Figure 2(a). The aerodynamic force here is the axial force on the sliding gate.

The aerodynamic forces, as defined above, have been estimated analytically for the various valve configurations. The results for the slide valve and the unshielded poppet valve are shown in Figures 54 and 55. For the shielded poppet valve the edge pressure is estimated to be 0.60 times the bleed plenum pressure $P_B$. The aerodynamic force on the shielded poppet valve, therefore, becomes

$$F_{aerodynamic} = (P_D - .60\,P_B)A_{edge}$$

where the edge area is 4.19 $cm^2$.

For any stability valve configuration, the acceleration of the piston may be computed as follows:

$$\ddot{x} = \frac{F_{piston} - F_{aerodynamic} - F_{friction} - F_{spring}}{m_{piston}}$$

where $F_{friction}$ = friction force
$F_{spring}$ = spring force
$m_{piston}$ = piston mass

Two types of transient disturbances were simulated on the computer to investigate the dynamic response of the slide and poppet valves. One was an input perturbation in bleed plenum pressure and the other was an input perturbation in inlet terminal shock position. Figures 42, 43, 48, 49 and 50 show the steady-state relationship between duct Mach number, valve position, and bleed plenum pressure. It was assumed that the valve response is slow compared to the flow response through the valves, so these relationships can also be used as an approximation for transient disturbances. Duct Mach number is related to shock position as shown in Figures 37, 44 and 45.

Bleed plenum pressure transients consisted of step and sinusoidal variations. Shock position transients were composed of a relatively slow shock movement from the normal operating point up to the inlet throat followed by a rapid movement from the throat to the leading edge of the porous bleed region on the cowl. With no flow through the bleed valves, it is estimated that the shock velocity relative to the duct will be about 97.5 m/s by the time the shock reaches the leading edge of the bleed. The shock moves from the throat to the bleed leading edge in about 6 milliseconds. An arbitrary value of 50 milliseconds was chosen for the movement from the steady state position up to the throat. These two components made up the shock position transient used in the computer analysis. For the case of the poppet valves, the 6 millisecond portion was further broken down into 4 milliseconds for the aft poppets and 2 milliseconds for the forward poppets.

2. Slide Valves - The physical characteristics used in computing the dynamic performance of the slide valve are tabulated on Drawing 1. Response of the slide valve to a 27 percent step in bleed plenum pressure is shown in Figure 56. Complete opening requires .068 seconds. Shock position transients are shown in Figures 57 and 58. Complete opening of the valve takes longer for these cases because the driving pressure on the piston builds up more slowly than for the case shown in Figure 56. By the time the terminal shock has reached the leading edge of the bleed, the valve is open about 1/4 or 1/2 cm, depending on the altitude. When the shock reaches this position, it is arbitrarily held in order to observe complete valve opening. Then the shock movement is reversed in order to observe valve closure.

Valve response to large amplitude 10 and 40 Hz oscillations in bleed plenum pressure is shown in Figures 59 and 60. The 10 Hz case shows a large amplitude valve oscillation out of phase with the driving pressure while the 40 Hz case shows nearly complete damping of the oscillation. The effect of adding the fourth compartment to the valve is shown in Figure 61. A small shock displacement opens the four compartment valve completely, but the decrease in bleed plenum pressure as the valve opens prevents complete opening of the three compartment valve.

Preliminary configurations of the slide valve included one with no overboard bleed and one with an orifice damper valve as shown in Figure 2(a). Due to piston leakage, the valve with no overboard bleed will eventually drift closed during a long duration transient such as a large change in aircraft angle of attack. The configuration with the damper valve showed satisfactory dynamic performance. The primary effect of the damper was to increase the time required for valve closure. Both configurations were dropped from further consideration—the former because of poor angle of attack behavior and the latter because the damper did not improve performance enough to warrant the added complexity and cost.

3. Unshielded Poppet Valves — The original poppet valve configuration had the orifice damper valve No. 3 shown in Figure 3(a). This arrangement exhibited two deficiencies, examples of which are shown in Figures 62 and 63. Figure 62 shows that during valve closure a high frequency oscillation will occur as a result of the spring effect of the small volume of air trapped above the poppet piston. Figure 63 illustrates a condition in which the valve will not close completely when the transient disturbance is removed, again because of the small volume of air trapped above the piston.

As a result of these deficiencies, the orifice damper was removed and a friction device was added to the poppet stem as shown in Drawing 10. Drawing 2 shows the installation of the valve in the nacelle and lists the physical characteristics of the valve. The performance of this configuration is shown in Figures 64 through 76. Figures 64 and 65 show that at freestream Mach numbers of 3+ and 2.47, the aft poppet valve will open fully in about .028 seconds following a 27 percent step change in bleed pressure. Response of the aft poppet to large amplitude 10 and 40 Hz oscillations in bleed plenum pressure is shown in Figures 66 and 67. As in the case of the slide valve, the 40 Hz response is considerably more damped than that at 10 Hz. However, in the 10 Hz case, the response of the poppet lags the driving pressure by only about 90 degrees whereas in the case of the slide valve the motion lags by about 180 degrees.

Shock position transients are shown in Figures 68 through 73. The performance of the aft and forward poppets at Mach 3+ is shown in Figures 68 through 71. Although the forward and aft poppets are identical in design, the forward poppets are less responsive to movements of the terminal shock because they do not benefit from a pressure rise preceding the terminal shock as in the case of the aft poppets (see Figure 44). Whereas the aft poppets have opened 29 to 51 percent (depending on altitude) by the time the terminal shock has reached the leading edge of the porous

bleed, the forward poppets have only opened about 1 percent. The usefulness of the forward poppet with this type of transient disturbance appears small unless the valve is exposed to a bleed pressure build-up considerably greater than the .002 seconds assumed in Figures 70 and 71. However, the forward valves should respond about as well as the aft valves in the case of aircraft angle of attack transients which build up over a substantially longer period of time.

Response of the aft poppet to a displacement of the terminal shock at freestream Mach number 2.47 is shown in Figures 72 and 73. The driving pressure disturbance in this case is substantially different than that at Mach 3+ as is evident by comparing the duct Mach numbers shown in Figures 44 and 45. At Mach 2.47, there is no increase in bleed plenum pressure as the shock approaches the throat and the change in duct Mach number as the shock passes over the bleed is smaller than at Mach 3+. The result is that the valve receives a small pressure impulse which is greatly diminished as the valve begins to open. The reduced bleed plenum pressure is not sufficient to hold the valve open as it did at Mach 3+ (see Figures 68 through 71). Large amplitude 17 and 25 Hz oscillations result. Increased friction forces were applied to the poppet in an attempt to damp the oscillation. The effect is shown in Figure 74. An 8.9N increase in friction produces acceptable valve motion after 3 cycles of ringing. However, a friction increase of this magnitude will produce undesirable effects at higher altitudes where the valve driving forces are much smaller. Consequently, the use of friction to damp the oscillations shown in Figures 72 and 73 does not appear feasible.

Although Figures 72 and 73 indicate an undesirable instability, they represent a very unlikely physical situation in that the terminal shock is forced to remain at the leading edge of the bleed while the valves oscillate. A more reasonable physical expectation is that the inlet will either unstart completely or else restart. The latter possibility has been investigated, with the results shown in Figure 75. No instability is evident. To further investigate valve damping, a weak bleed pressure step insufficient to produce complete opening was applied to the valve. The results, shown in Figure 76, indicate no instability in this case either.

It therefore appears likely that the poppet valve will be adequately damped when step changes in bleed plenum pressure are applied, but will be inadequately damped in some cases when step changes in terminal shock position are applied. The shielded version of the poppet valve was designed to eliminate this potential problem.

4. Shielded Poppet Valves - The shielded poppet valve, shown in Drawing 11, has the following characteristics. Nomenclature is defined in Figure 4.

| | | |
|---|---|---|
| Mass of moving poppet | .226 | kg |
| Spring preload | 13.35 | N |
| Spring rate | 7.01 | N/cm |
| Plenum "H" volume (per valve) | 2700. | $cm^3$ |
| Poppet friction, dynamic | 4.9 | N |
| Poppet friction, static | 9.8 | N |
| Area of orifice No. 1 (per valve) | .01032 | $cm^2$ |
| Area of orifice No. 2 | .0710 | $cm^2$ |
| Area of orifice No. 3 | .0129 | $cm^2$ |
| Area of orifice No. 4 | .0129 | $cm^2$ |
| Location of orifice No. 4, $\Delta x$ | 1.118 | cm |
| Min. area in exit louvers (per valve) | 74.2 | $cm^2$ |

The response of this valve to several types of transient disturbances is shown in Figures 77 through 85.

Figures 77 and 78 show response to step changes in $P_B$ and $P_D$ (see Figure 4 for nomenclature). Due to flows into and out of the reference pressure plenum, the reference pressure $P_G$ may gradually change after an inlet transient disturbance opens the valve and closes orifice No. 2. The result is that over a period of time, the poppet may gradually drift to one of three stable positions: fully open, half open, or fully closed. An example is shown in Figure 79. A 20 percent step in $P_B$ and $P_D$ produces nearly complete opening after 0.042 seconds. At this position, air is flowing into the piston chamber through orifice No. 4. At t = 0.54 seconds, the reference pressure has built up sufficiently to overcome the static friction and the poppet begins to close. At t = 0.59, the motion stops because the driving forces are less than the static friction. At the new poppet position, there is no flow through orifice No. 4 so the reference pressure will begin to decrease. When this pressure drops sufficiently, the static friction will be overcome and the poppet will begin to open. Since the lower tap on orifice No. 4 is located at $\Delta x$ = 1.118cm, the poppet will jump back and forth across this location over a longer period of time. In the presence of vibration, the motion would be less jerky than that shown in Figure 79. The final equilibrium position where motion would cease is a poppet opening of about 1.118cm where the flow rates into and out of the piston chamber are equal.

Figure 79 shows a transient disturbance which produces partial valve opening followed by a drift back to the half-open position. Two other types of long duration effects are possible. First, a weaker disturbance which produces an initial opening less than half-open will be followed by a drift up to the half-open position. Second, a stronger disturbance which produces complete opening will not be followed by poppet drift since orifice No. 4 will be closed.

Figures 80 through 82 show valve response to the terminal shock displacements indicated in the lower part of the figures. Where the response of the unshielded poppet differed significantly, it is shown as a dashed line. Use of the shield has eliminated the instability at $M_o$=2.47.

Figures 83 and 84 demonstrate the sensitivity of the valve to pressure oscillations when a prior increase in duct pressure has produced partial valve opening. The oscillations are produced by a $\pm$.03 variation in duct Mach number after a normal shock movement toward the throat has produced partial opening.

Response of the valve to single pressure pulses of varying duration is shown in Figure 85. The valve position shown here is the maximum displacement produced by the pulse. In all cases, the valve eventually closes since the pressure pulse is not recurrent. Below about 2 Hz the valve shows no response at all because the flow through the orifices into the piston chamber is sufficient to keep the pressure differential across the valve below the value required to unseat the poppet.

## Aircraft and Propulsion System Flight Performance

1. Propulsion System - The inlet bypass door control modulates the door position as required to maintain a scheduled value of the ratio of $P_{SD8}$ to $P_{PLM}$ where $P_{SD8}$ is a manifolded duct wall static pressure just downstream of the throat and $P_{PLM}$ is an external cowl pitot pressure. Available wind tunnel data show that substantial reductions in back pressure on the cowl shock trap bleed have relatively little effect on this signal pressure ratio.

The greatest potential effect on signal pressure occurs when bleed valves are used with a porous bleed ahead of the shock trap. Under these conditions when the terminal shock is just forward of the porous bleed, substantial quantities of bleed air will be removed by the valves in addition to the increased flow through the shock trap. If the signal pressure ratio drops below the scheduled value, the bypass door will be commanded to a closed position. Bypass closure could aggravate the condition which was causing the shock to be forward.

To examine this possibility, a simplified one-dimensional analysis of the duct flow was made assuming that a normal shock stood at the leading edge of the porous bleed region. $P_{SD8}$ was assumed to be equal to the theoretical static pressure at the cowl station location of the $P_{SD8}$ ports. $P_{PLM}$ was obtained from wind tunnel data, assuming that the overboard bleed flow did not affect this pressure. With 20 percent overboard bleed the computed signal pressure ratio $P_{SD8}/P_{PLM}$ was 1.96 and with 10 percent bleed, it was 1.81. The commanded signal pressure ratio is 1.56 at 6 degrees aircraft angle of attack and 1.45 at 4 degrees. The analysis, therefore, indicates that the bypass door will be commanded to open when the terminal shock is forward and the bleed valves are open, thereby aiding the shock reswallowing process.

2. Aircraft - Figure 86 shows the estimated effect of a complete and sustained opening of one nacelle's shock stability valves on aircraft motion at cruise altitude and Mach number. When the valves are fully open, a 30 percent loss of thrust occurs along with aerodynamic effects due to bleed air flowing over the wing. The aerodynamic effects were estimated from forward bypass door data. For the case shown, no pilot inputs or autopilot inputs were used to correct the right roll which builds up to 80 degrees in six seconds. However, the stability augmentation system (SAS) did command four degrees left roll control (maximum roll authority for SAS) and sufficient yaw control to limit sideslip angle to a maximum of 1.5 degrees. Due to uncertanties in estimating the effects of opening the shock stability valves, the aircraft response shown is probably more violent than an actual case would be. Also, in the case shown, the valves are ~~assumed to be open for the entire time of the~~ response. If the valves were open for a shorter period of time, the response would be less violent. The case shown here is considerably less violent than an inlet unstart at the same flight condition and would be controllable using pilot inputs which are well within the aircraft control capabilities.

## SLIDE VALVE BEARING TEST

### Apparatus and Procedure

In order to determine the friction characteristics and life span of linear bearings representative of those proposed for the slide valve, an existing bypass door assembly was tested in the laboratory. This door, supplied by NASA Lewis Research Center, ran on a pair of Schneeberger linear bearings. Each bearing consisted of a series of rollers, spaced by roller separators and operating in a linear race. Testing was conducted in the oven shown in Figure 87 at temperatures up to 664 degrees kelvin. Transverse loading on the door was accomplished by means of loading

blocks as shown in Figure 88. The rod extending through the left side of the oven wall in Figure 88 was attached to an external scale used to record the bearing friction force. The hydraulic servo installed on the opposite end of the door assembly was used to cycle the door. All testing was conducted without lubrication on the bearings. Measurements of static and dynamic friction were made at six positions along the path of door travel. Transverse loads ranged from 0 to 2240 newtons.

## Friction Measurements

Initial tests at room temperature yielded friction coefficients substantially higher than expected. Investigation showed that, under load, there was a slight binding or interference between the moving parts. Consequently, the bearing shim thickness was increased in steps from the original value of 0.023 cm up to a final value of 0.051 cm at which point no further interference was apparent. Friction measurements at room temperature yielded the results shown in Figure 89. The friction coefficient is the ratio of the friction force to the transverse load.

High temperature tests were then conducted with the oven filled with carbon dioxide. Prior to heating the door was cycled briefly at 1 Hz by the hydraulic servo to verify that the actuation system was functioning properly. After a 4-1/2 hour soak period in the heated oven, the door base had reached a temperature of 664K. Friction was measured with all the loading blocks installed. The data, shown in Figure 90, indicate a substantial increase in friction from the levels measured at room temperature. With the door temperature at 670K, an attempt to initiate life cycling of the door resulted in a hydraulic failure inside the oven and the test was terminated.

Friction was measured again when the door had cooled to room temperature. The data, shown in Figure 91, indicate friction levels even higher than those measured at 664K. The friction remained high when the door was unloaded and cleaned of hydraulic fluid condensate residue. It was noted that the bearing races had discolored to a dark blue. Moreover, a ratcheting sound and feel was noted when the door was actuated manually with a small transverse load. The bearings were therefore disassembled for closer inspection. Figure 92 shows the door assembly before disassembly. Warpage in the roller separator is evident. Figure 93 shows the disassembled bearing. Although the roller separator is severely distorted, no evidence of contact with the bearing race was observed. A slight warpage in the bearing race was noted near the center of the race and the bearing rollers were scored as though they had been sliding rather than rolling.

## DISCUSSION OF RESULTS

### Steady State Flow Comparison

The estimated flow rates through the shock stability valves have been added to the calculated engine ejector secondary flow and superimposed on the shock trap flow characteristics in Figures 94 and 95. These two figures define the steady state performance of the three types of stability valves in the bleed plenums of the present and the enlarged shock traps. The steepness of the curve of ejector plus slide valve or poppet valve flow in contrast to the much shallower slope of shock trap flow indicates that attempts to increase nacelle secondary flow area or valve exit area are not worthwhile because the potential increase in bleed flow is very small.

The steady state flow rates through fully open stability valves are summarized in Figure 96 for two conditions: bleed plenum pressures 27 percent higher than their normal steady state values, and the inlet terminal shock standing ahead of the bleed. Since inlet stability is affected by changes in ejector secondary flow as well as stability valve flow, two flow rates are tabulated in Figure 96. The first is the increase in stability valve flow due to the increase in pressure. This is a measure of valve flow capacity. The second is the change in the sum of valve flow plus ejector secondary flow, which represents the increase in flow removed from the inlet cowl at or ahead of the throat. This is a measure of the inlet stability.

Figure 96 shows that the installation of vortex valves in either the cowl or shock trap plenum provides the smallest flow capacity of the configurations studied. Moreover, it also shows that the installation of any type of stability valve in the plenums of either the present or enlarged shock trap will produce a net increase in shock trap mass flow ratio of less than 5 percent. Therefore, from steady state flow capacity considerations, the only feasible configurations appear to be slide valves or poppet valves installed in the cowl just ahead of the inlet throat.

### Dynamic Performance Comparison

The dynamic performance of those configurations acceptable in terms of steady state flow capacity is shown in Figure 97. The first column shows the time required for full valve opening following a 27 percent step increase in duct and bleed plenum pressures. The next two columns show the change in cowl bleed flow (valve flow plus shock trap bleed flow) .056 seconds after a transient displacement of the terminal shock is initiated. The shock displacement consists of a .050 second movement from the normal steady state position up to the throat followed by a

.006 second movement from the throat to the leading edge of the porous bleed. The last two columns show the natural frequency of the installed valve with the inlet terminal shock position fixed.

The two versions of the poppet valve are superior to the slide valve in two respects: faster response time and higher natural frequency. Because of the isolation of the poppets from the bleed plenum pressure, the shielded poppet valves have a lower natural frequency than the unshielded valves. However, the shielded poppets are superior in two important respects. First, the forward poppets now sense duct pressure at the same location as the aft poppets and hence respond faster to inlet shock movements. This is one reason that the shielded valves show higher flow rates after the .056 second shock position transient. Second, the valve ringing which occurred at Mach 2.47 was eliminated by addition of the shield.

Bearing Test

Experience obtained with the linear bearings indicates that considerable care must be taken to avoid interference when large lateral loads are applied. Testing at high temperature resulted in scoring of the bearing rollers, severe distortion of the roller separators, and a slight warpage of the bearing races. It is believed that the rollers skidded at high temperature, scoring the rollers and producing higher friction coefficients. It could not be determined whether the skidding occurred before or after the roller separators buckled.

## CONCLUSIONS

A feasibility study of proposed self-actuating inlet shock stability bleed valves for the YF-12 airplane has been made. The candidate valves included vortex valves, slide valves, and poppet valves. Installations in the inlet cowl and in the inlet shock trap bleed plenum were considered. Shielded and unshielded versions of the poppet valve were designed for installation in the cowl. In the shielded valve, inlet duct pressure acts as the driving force on the poppet while in the unshielded version the bleed plenum pressure is the driving force. The following conclusions have been reached:

1. The installation of any type of bleed valve in the plenum of the present shock trap, or in a lengthened shock trap, will produce a net gain in shock trap mass flow ratio of less than 5 percent. The steady

state shock trap mass flow ratio with the terminal shock standing ahead of the inlet throat is about 17 percent, or less, depending on the type of bleed valve and size of the shock trap, compared to about 12 percent without bleed valves.

2. The installation of vortex valves in the cowl yields steady state valve mass flow ratios of about 3 percent with the terminal shock ahead of the bleed.

3. For installations in the cowl, the steady state mass flow ratios with the terminal shock ahead of the bleed and the valves fully open are about 22 percent for twenty-five slide valves, 26 percent for fifty unshielded poppet valves, and 21 percent for fifty shielded poppet valves.

4. A 27 percent step increase in inlet duct and bleed plenum pressures at cruise Mach number and altitude will open the cowl slide valves in .068 seconds, the unshielded cowl poppet valves in .028 seconds, and the shielded cowl poppet valves in .025 seconds.

5. At cruise Mach number and the minimum altitude, a .050 second movement of the terminal shock from its steady state position up to the inlet throat followed by a .006 second movement from the throat to the leading edge of the porous bleed will produce partial opening of valves installed in the cowl. The increase in cowl bleed mass flow ratio (valves plus shock trap) during the .056 second transient is about .07 for the slide valves, .11 for the unshielded poppet valves, and .24 for the shielded poppet valves. At the maximum altitude, the corresponding increases in cowl bleed mass flow ratios are .04, .08, and .10 for the slide, unshielded poppet, and shielded poppet valves, respectively.

6. A step change in inlet shock position at Mach 2.5 causes ringing in the unshielded cowl poppet valve because of the dynamic interaction between the poppet and the driving pressure in the bleed plenum. Similar duct transients at the cruise Mach number do not produce this ringing. The shielded poppet valve does not exhibit this instability at either Mach number.

7. Laboratory tests of linear bearings showed that excessive distortion of the roller separators and sliding of the rollers can occur at high temperature. Production of satisfactory slide valve bearings will probably require additional bearing development work.

8. The bleed valves do not appear to adversely affect operation of the present inlet control system.

9. Aircraft response to a complete and sustained opening of all the bleed valves in one nacelle appears to be controllable and less violent than an inlet unstart.

In view of the potential development problems associated with linear bearings for a slide valve and the inherently faster response rate of the poppet valve, it is recommended that shielded poppet valves installed in the cowl be selected as the configuration for testing. The feasibility study indicates that this configuration will provide the performance required for the inlet shock stability system.

# APPENDIX

## Symbols

| | |
|---|---|
| A | area |
| $C_P$ | pressure coefficient, $\frac{P - P_o}{q_o}$ |
| F | force |
| k | ratio of specific heats |
| m | mass |
| M | Mach number |
| P | static pressure |
| $P_T$ | total pressure |
| q | dynamic pressure |
| R | gas constant |
| t | time |
| $T_T$ | total temperature |
| V | volume |
| w | mass flow rate |
| $w_o$ | mass flow rate through inlet reference area at free stream conditions |
| x | valve position |
| $\alpha$ | nacelle angle of attack |
| $\beta$ | nacelle angle of sideslip |
| $\delta$ | total pressure $(\frac{N}{cm^2}) \div 10.13$ |
| $\theta$ | total temperature (K) $\div$ 288 |

## Subscripts

| | |
|---|---|
| B | bleed plenum |
| D | inlet duct |
| EJ | ejector |
| G | valve piston chamber |
| L | exit louver plenum |
| V | valve |
| O | free stream conditions |
| 2 | engine face station |

## REFERENCES


1. Gebben, Vernon D.: "High Capacity, Compact Vortex Valve for Increasing Stability of Supersonic Mixed-Compression Inlets" NASA TN D-6662, Feb. 1972.

2. McLafferty, George: "A Study of Perforation Configurations for Supersonic Diffusers", United Aircraft Corporation Research Department Report R-53372-7, Dec. 1950.

3. Silsby, Norman S.: "External Interference Effects of Flow Through Static-Pressure Orifices of an NACA Airspeed Head at a Mach Number of 3", NACA TN 4122, Oct. 1957.

4. Dewey, Paul E.: "An Investigation of the Discharge and Drag Characteristics of Auxiliary Air Outlets Discharging into a Transonic Stream", NACA TN 3466, July 1955.

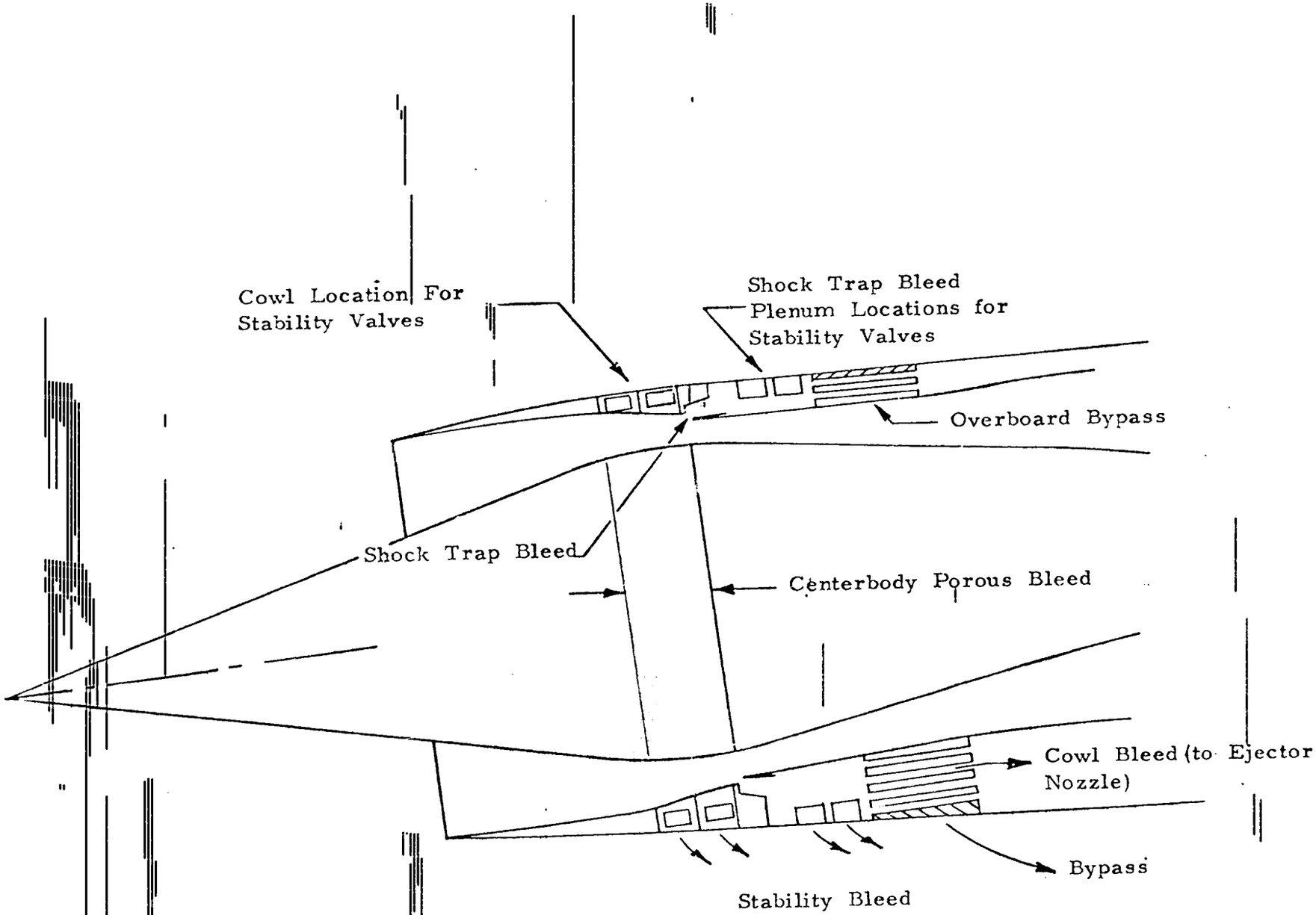


FIGURE 1. - YF-12 INLET SCHEMATIC

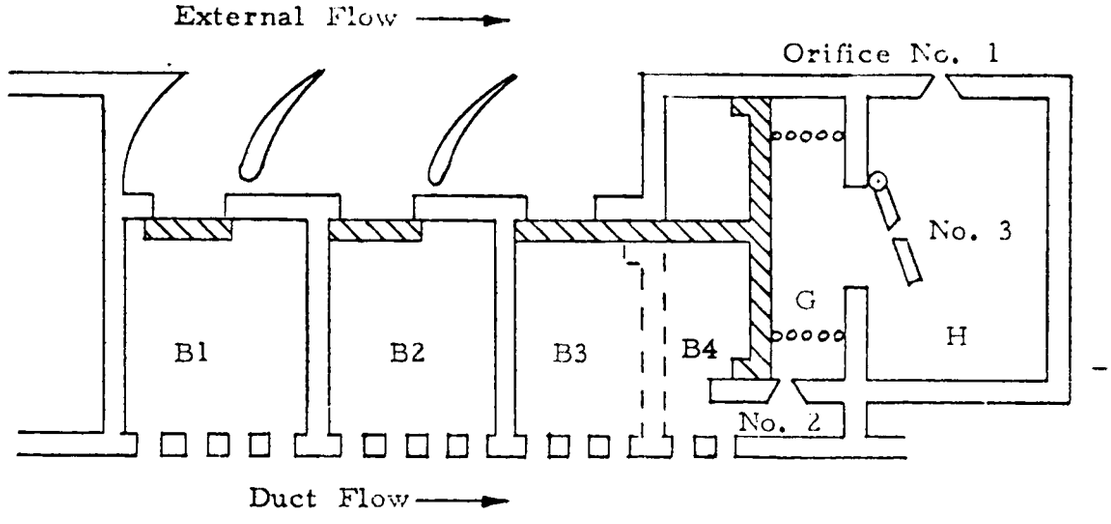


(a) Piston Actuated Valve

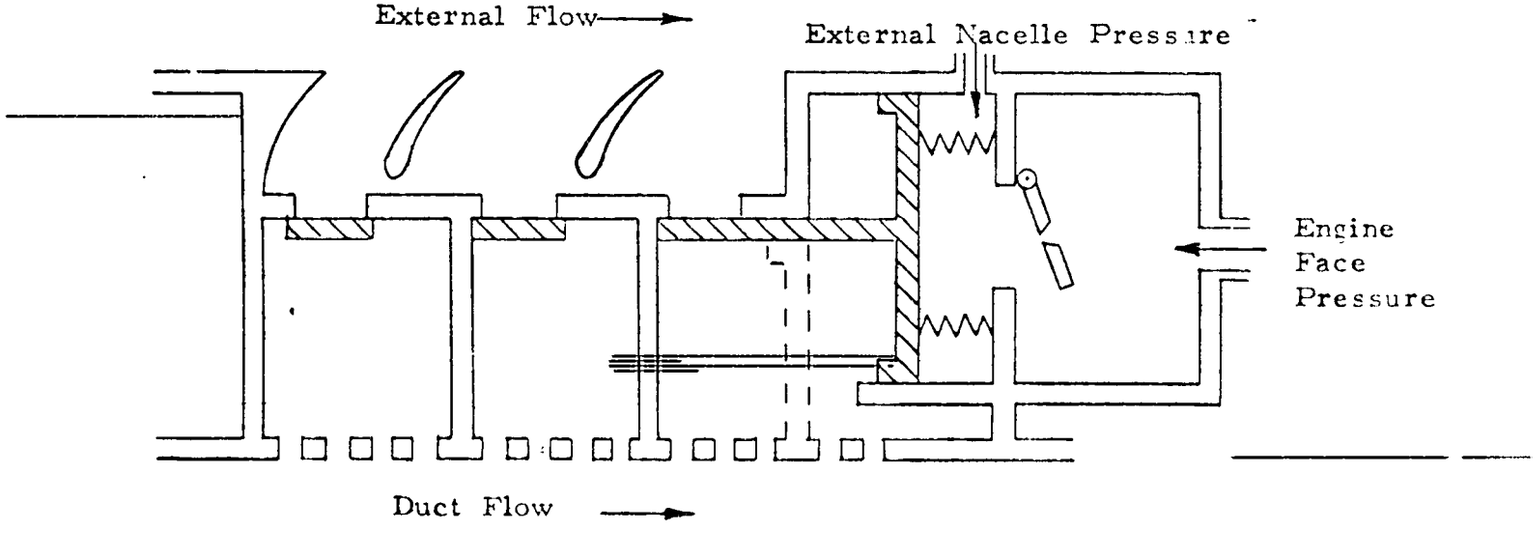


(b) Piston/Bellows Actuated Valve

FIGURE 2. - SLIDE VALVE SCHEMATICS

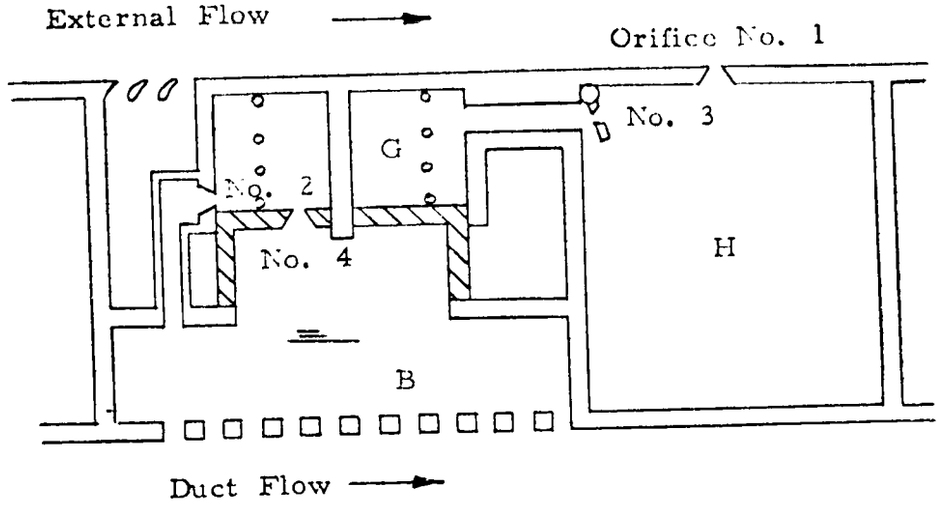


(a) Piston Actuated Valve

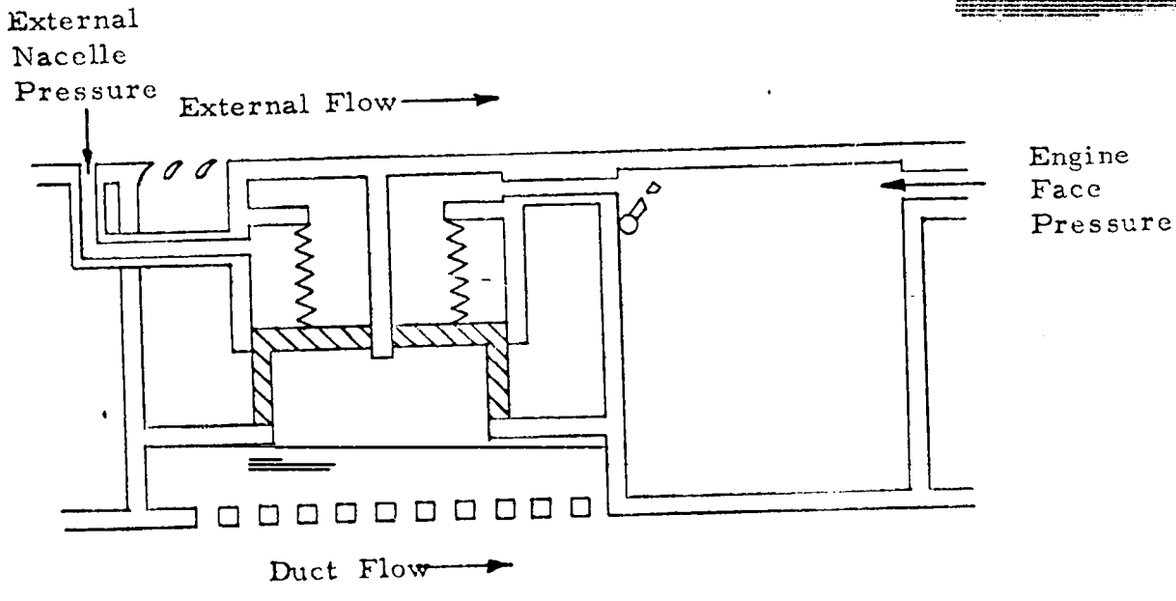


(b) Piston/Bellows Actuated Valve

FIGURE 3. - POPPET VALVE SCHEMATICS

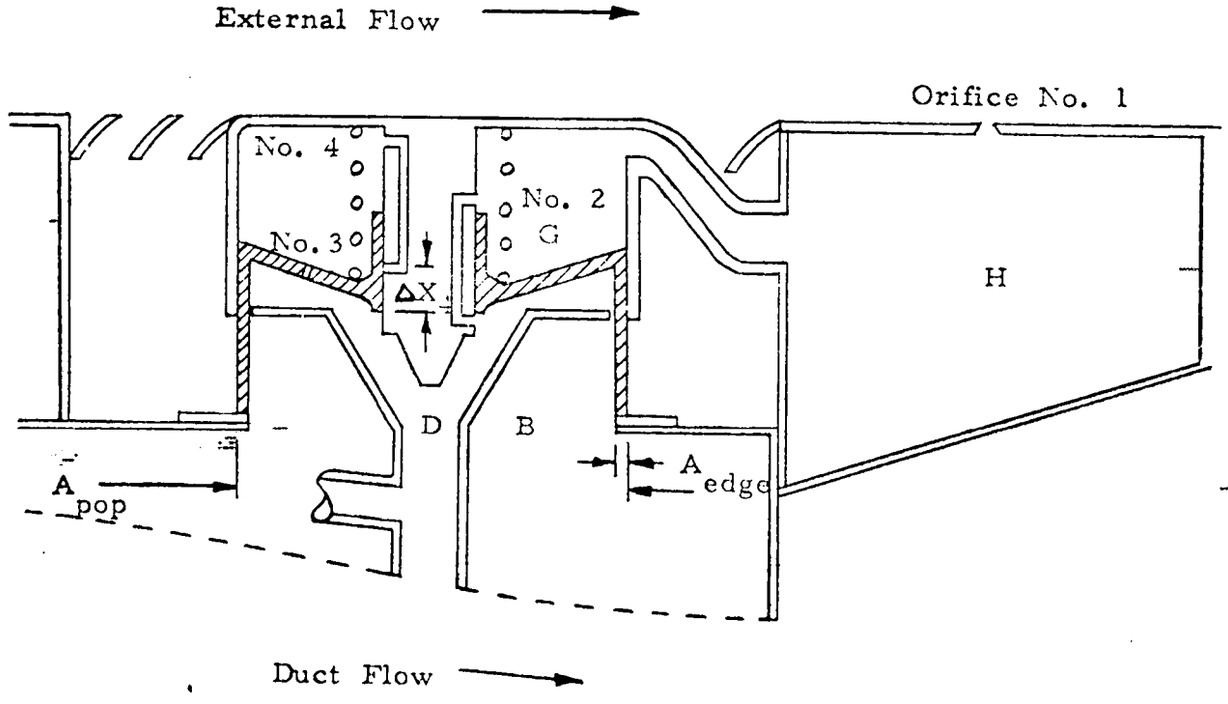


FIGURE 4. - SHIELDED POPPET VALVE SCHEMATIC

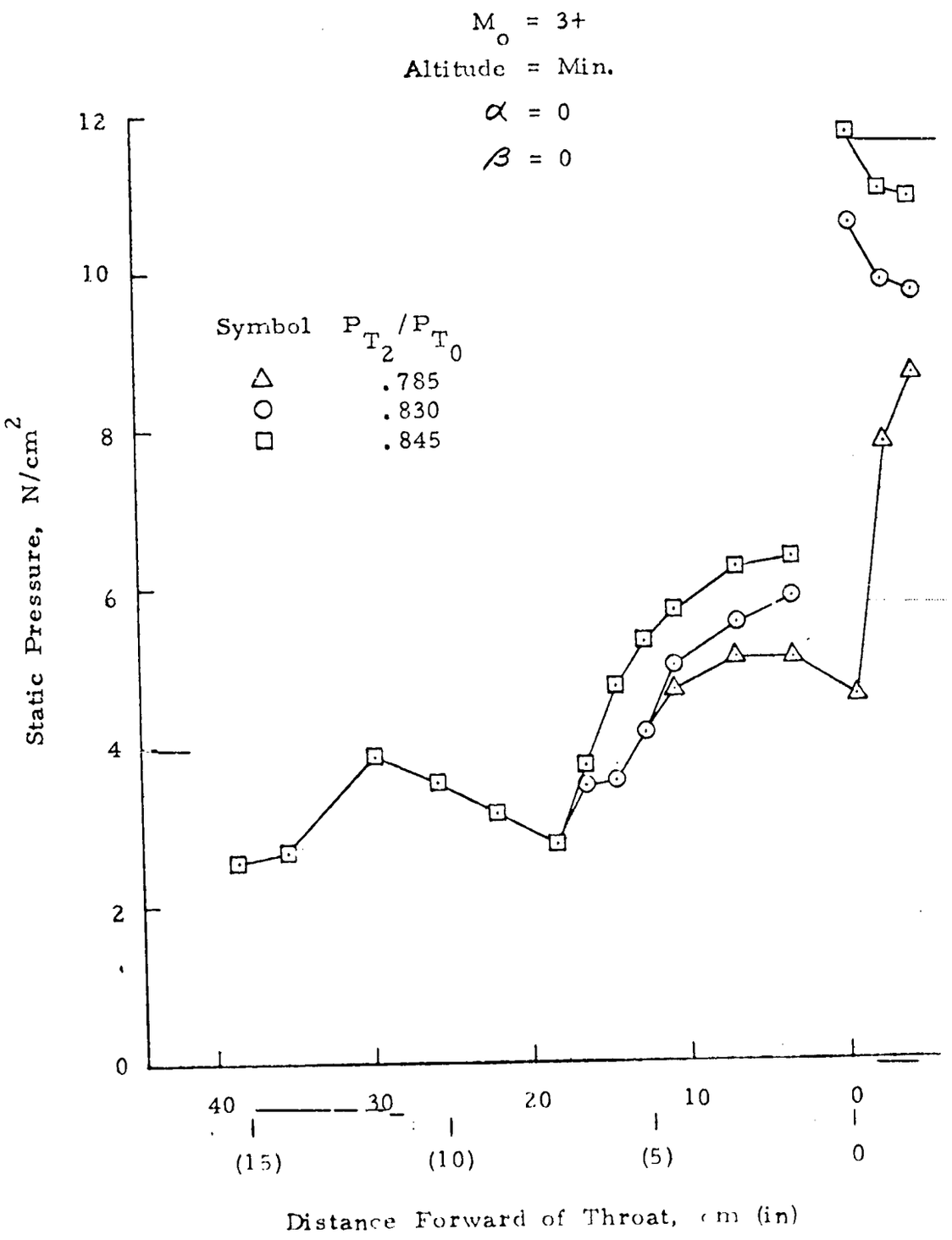


FIGURE 5. - COWL INTERNAL STATIC PRESSURE DISTRIBUTION

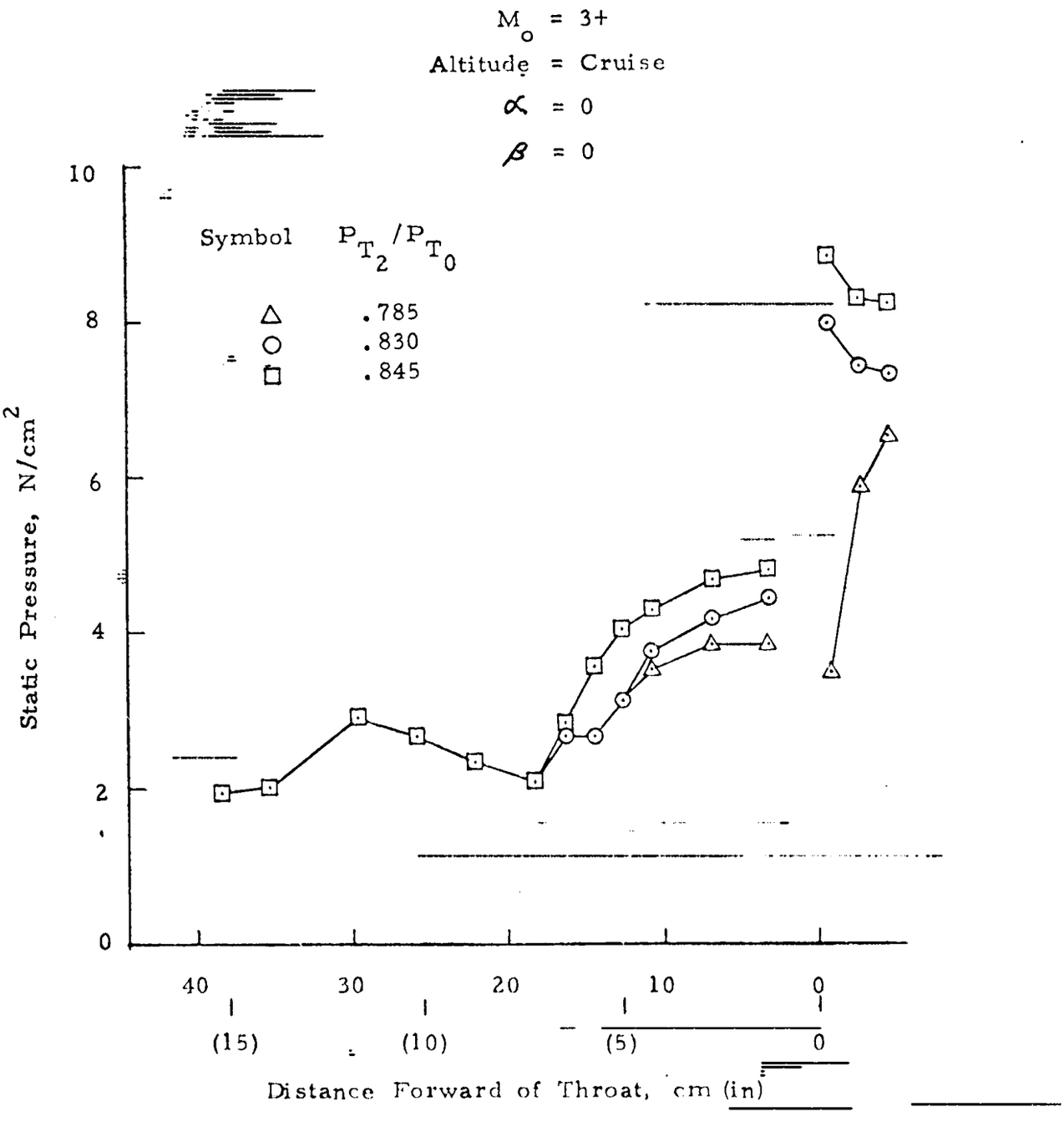


FIGURE 6. - COWL INTERNAL STATIC PRESSURE DISTRIBUTION

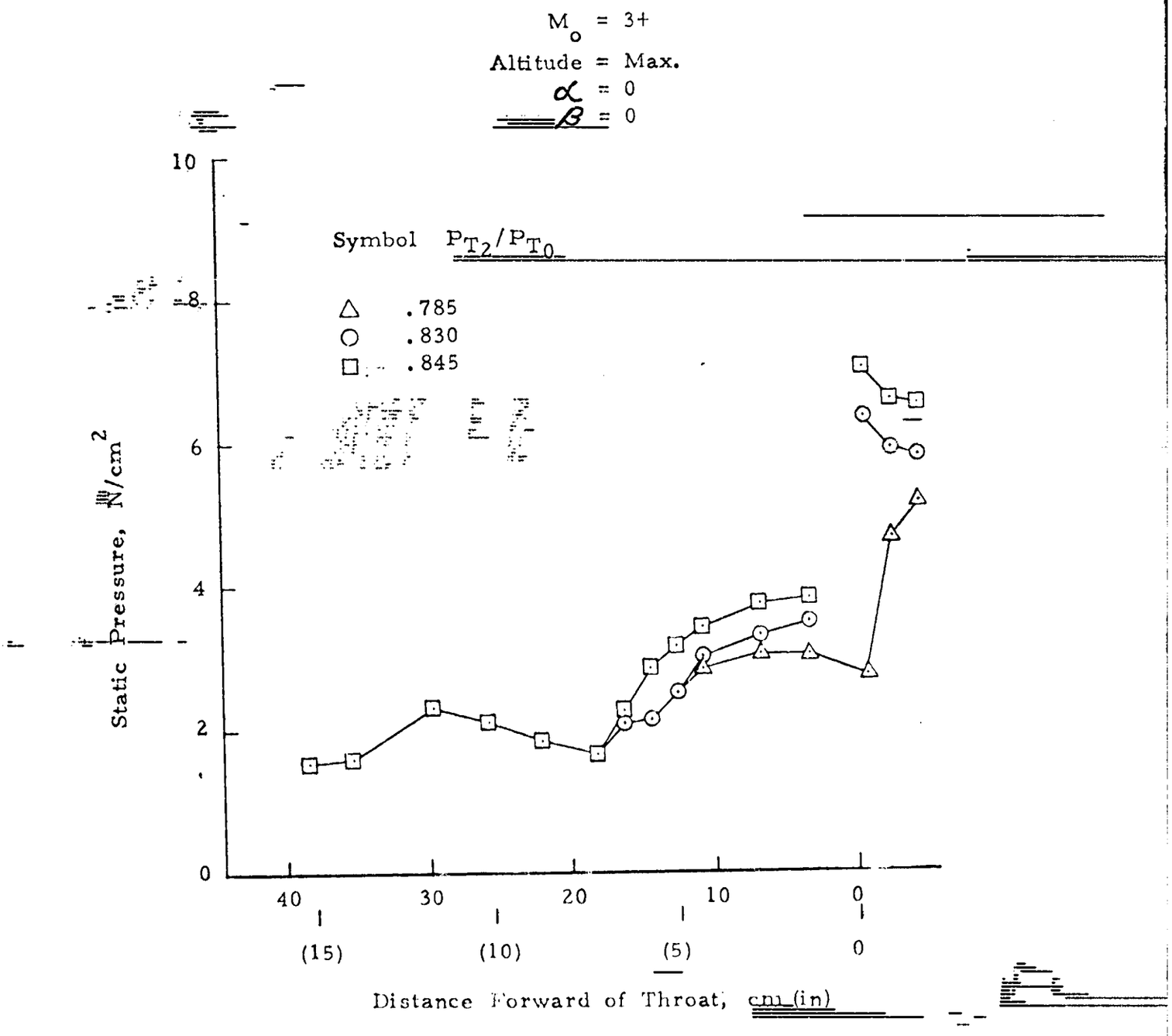


FIGURE 7. - COWL INTERNAL STATIC PRESSURE DISTRIBUTION

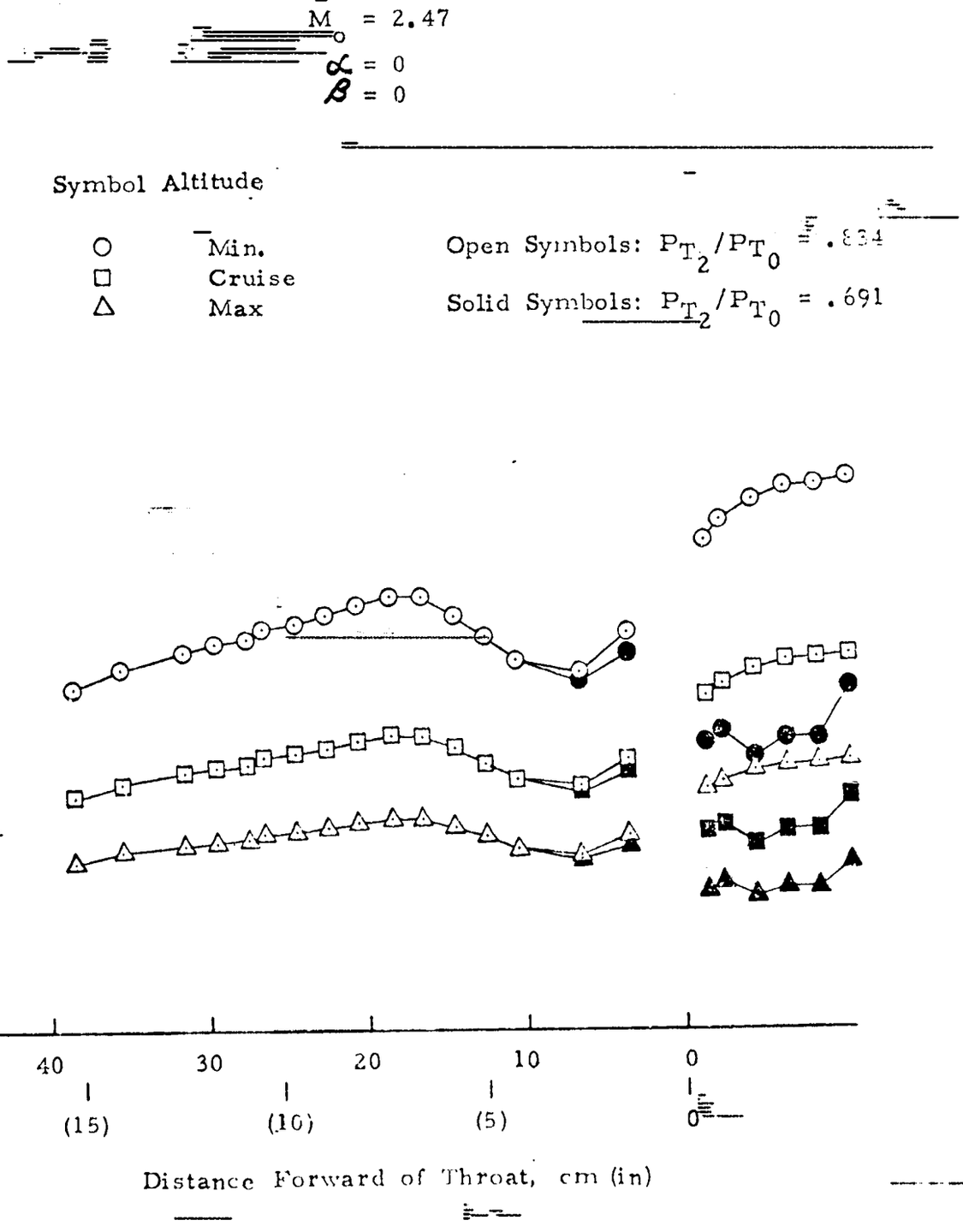


FIGURE 8. - COWL INTERNAL STATIC PRESSURE DISTRIBUTION

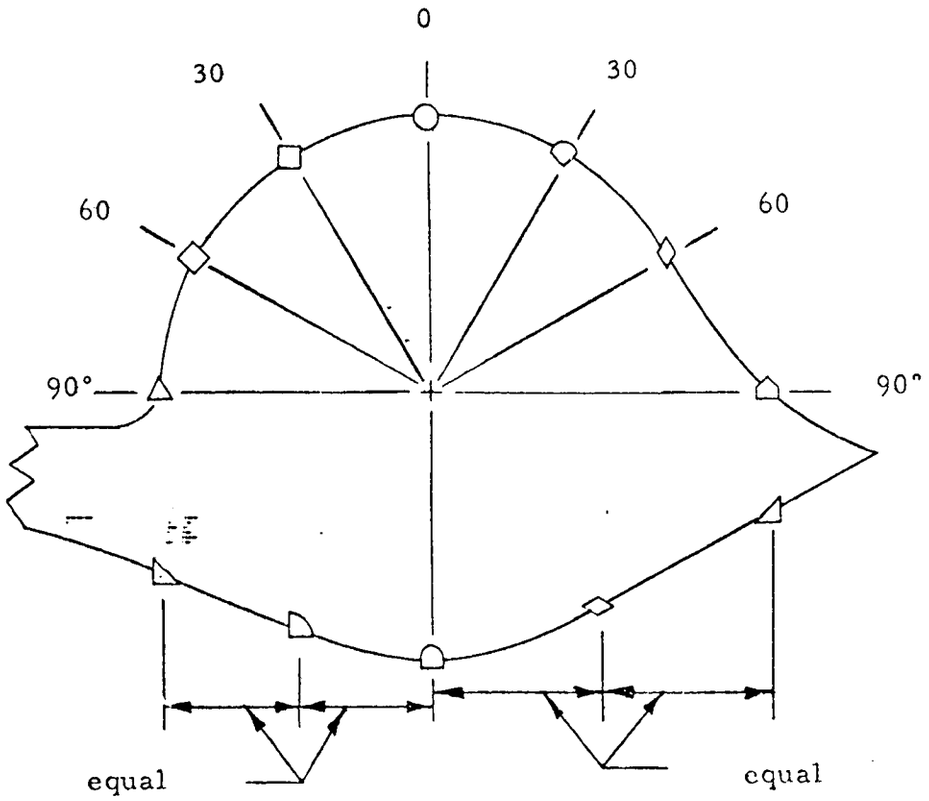


FIGURE 9. - LOCATION OF NACELLE PRESSURE PORTS

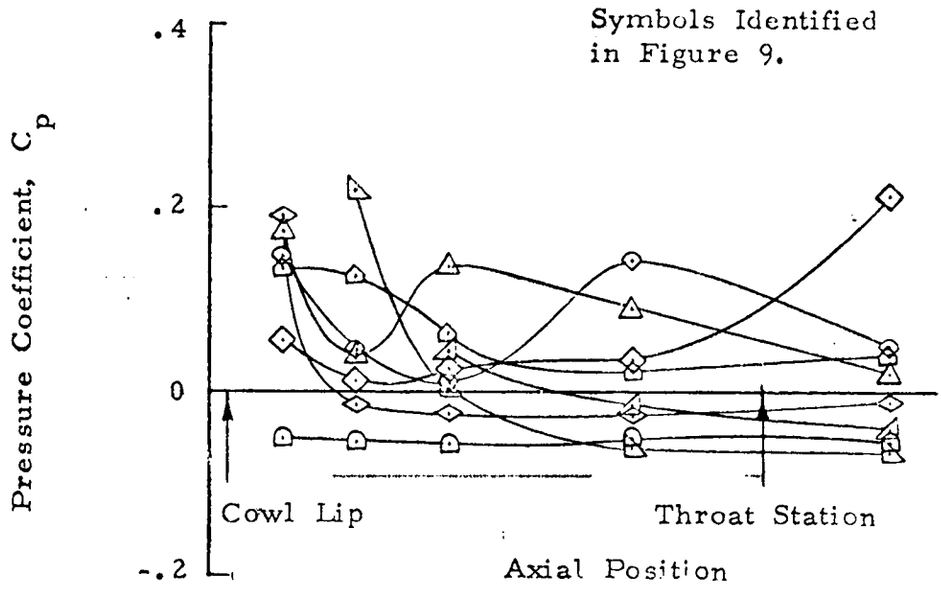


FIGURE 10. - NACELLE PRESSURE DISTRIBUTION, $\alpha = -1.56°$

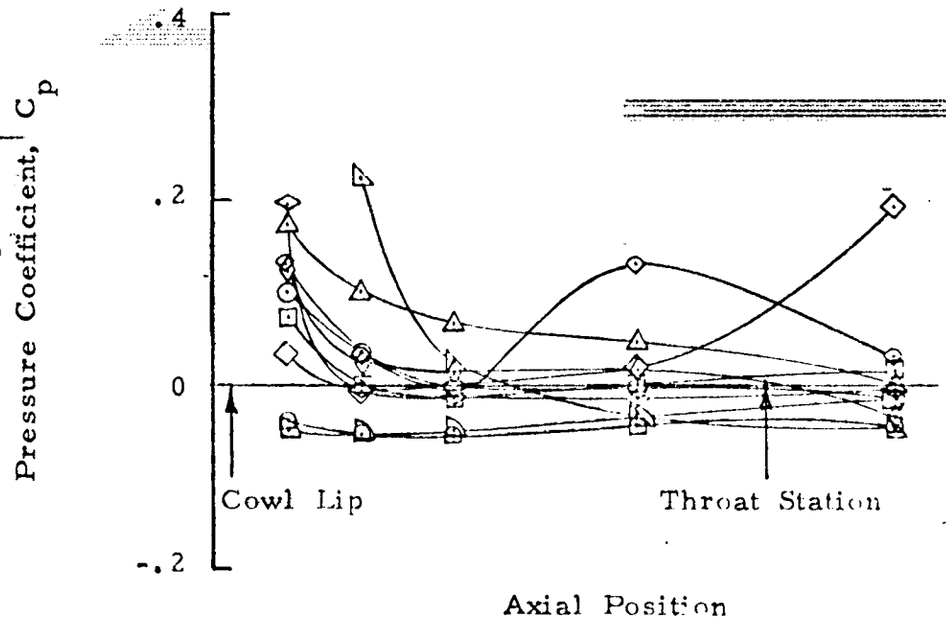


FIGURE 11. - NACELLE PRESSURE DISTRIBUTION, $\alpha = -.61°$

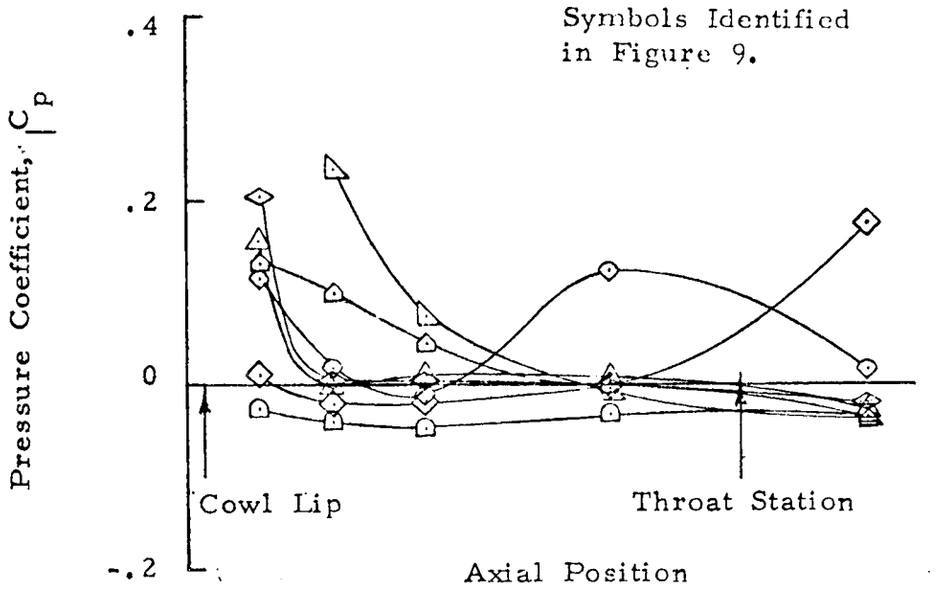


FIGURE 12. - NACELLE PRESSURE DISTRIBUTION, $\alpha$ = .35°

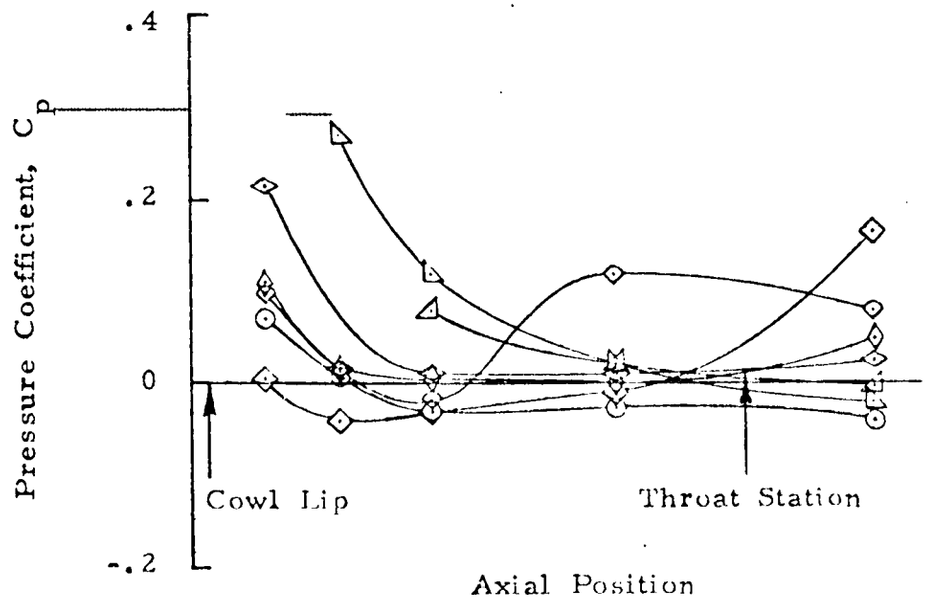


FIGURE 13. - NACELLE PRESSURE DISTRIBUTION, $\alpha$ = 1.29°

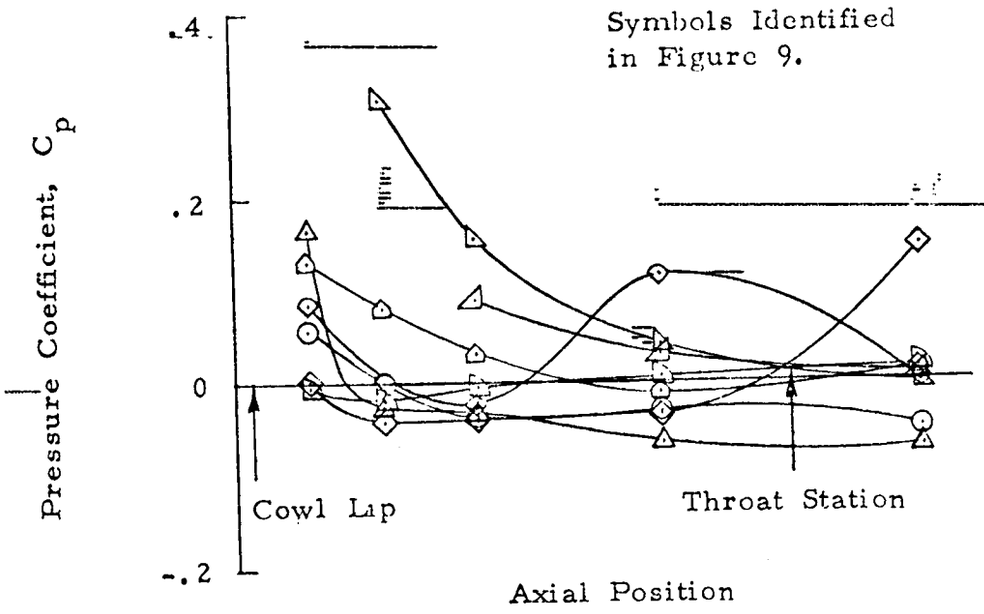


FIGURE 14. - NACELLE PRESSURE DISTRIBUTION, $\alpha = 2.25°$

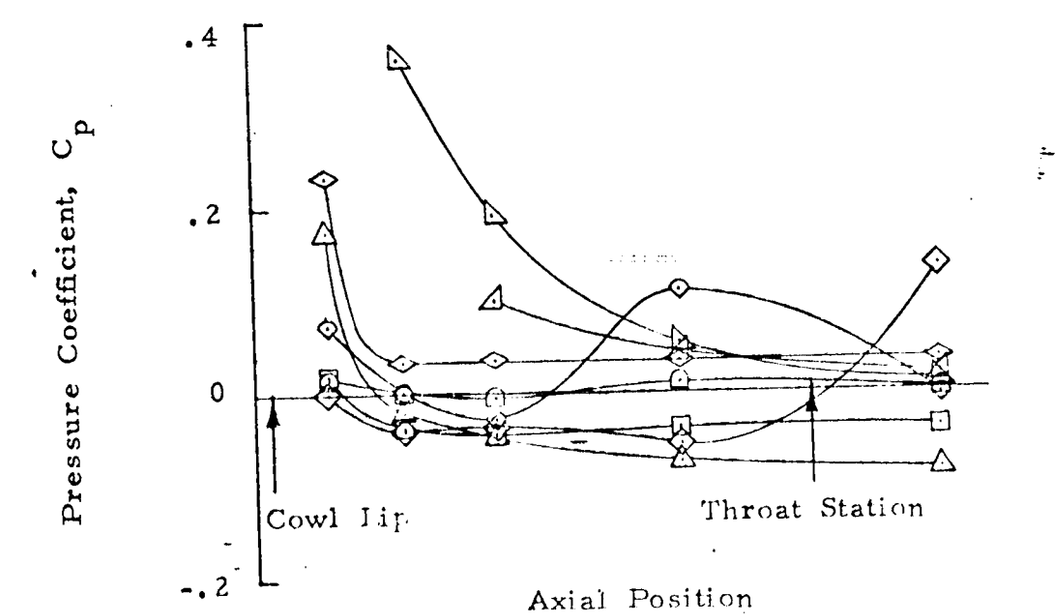


FIGURE 15. - NACELLE PRESSURE DISTRIBUTION, $\alpha = 3.19°$

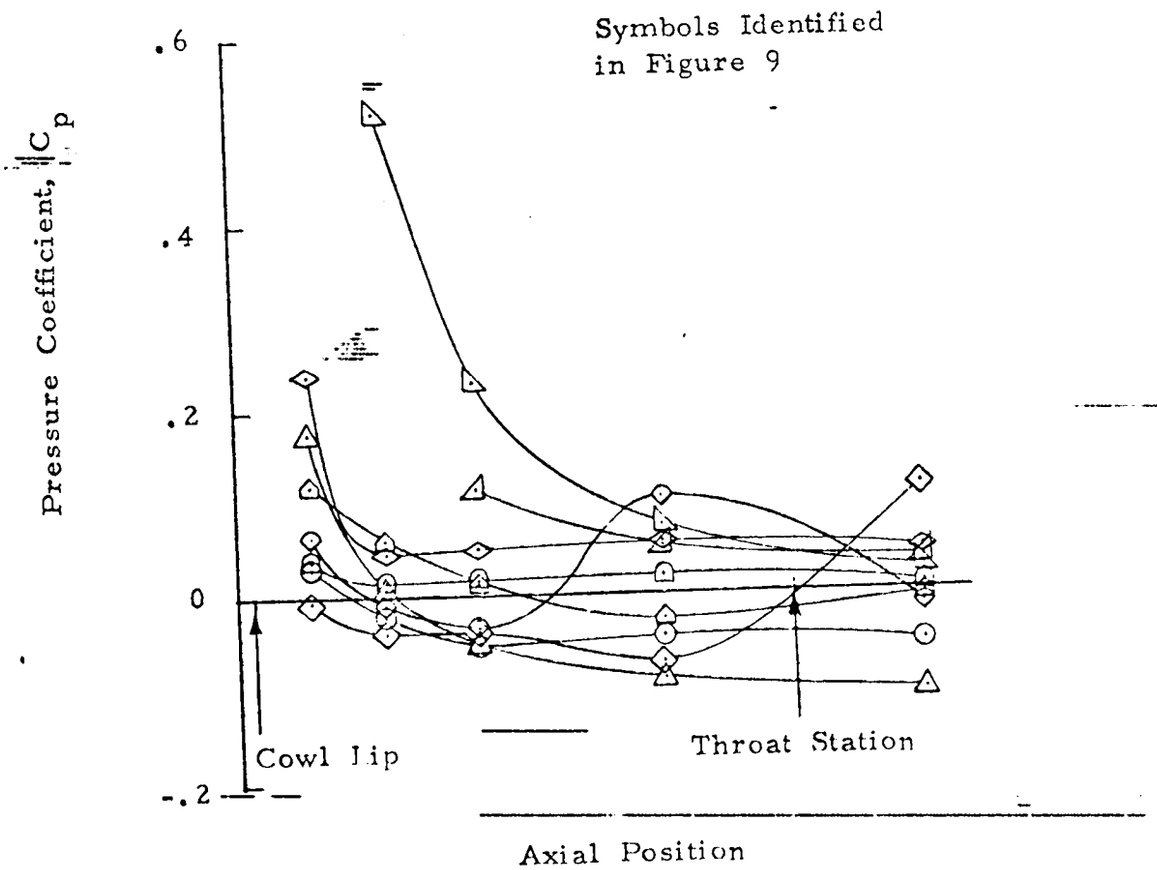


FIGURE 16. - NACELLE PRESSURE DISTRIBUTION, $\alpha$ = 4.14°

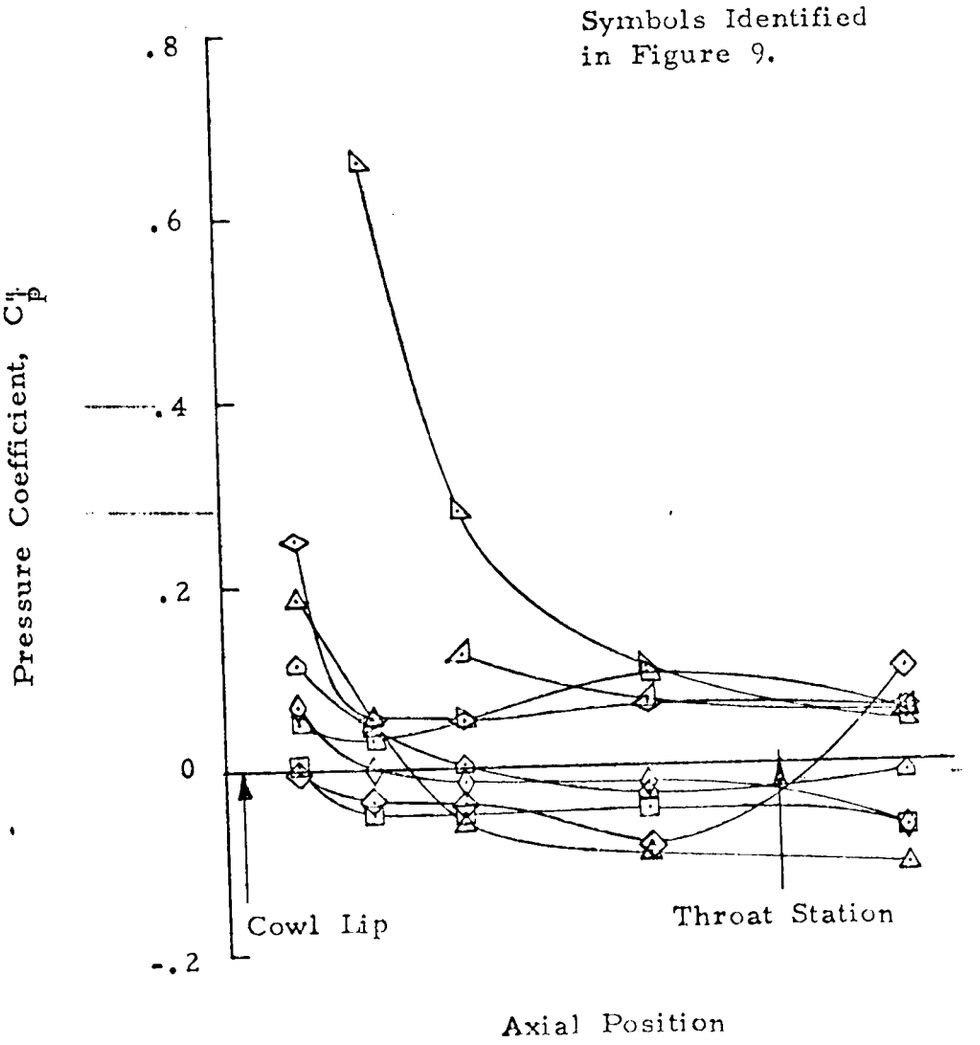


FIGURE 17. - NACELLE PRESSURE DISTRIBUTION, $\alpha$ = 5.09°

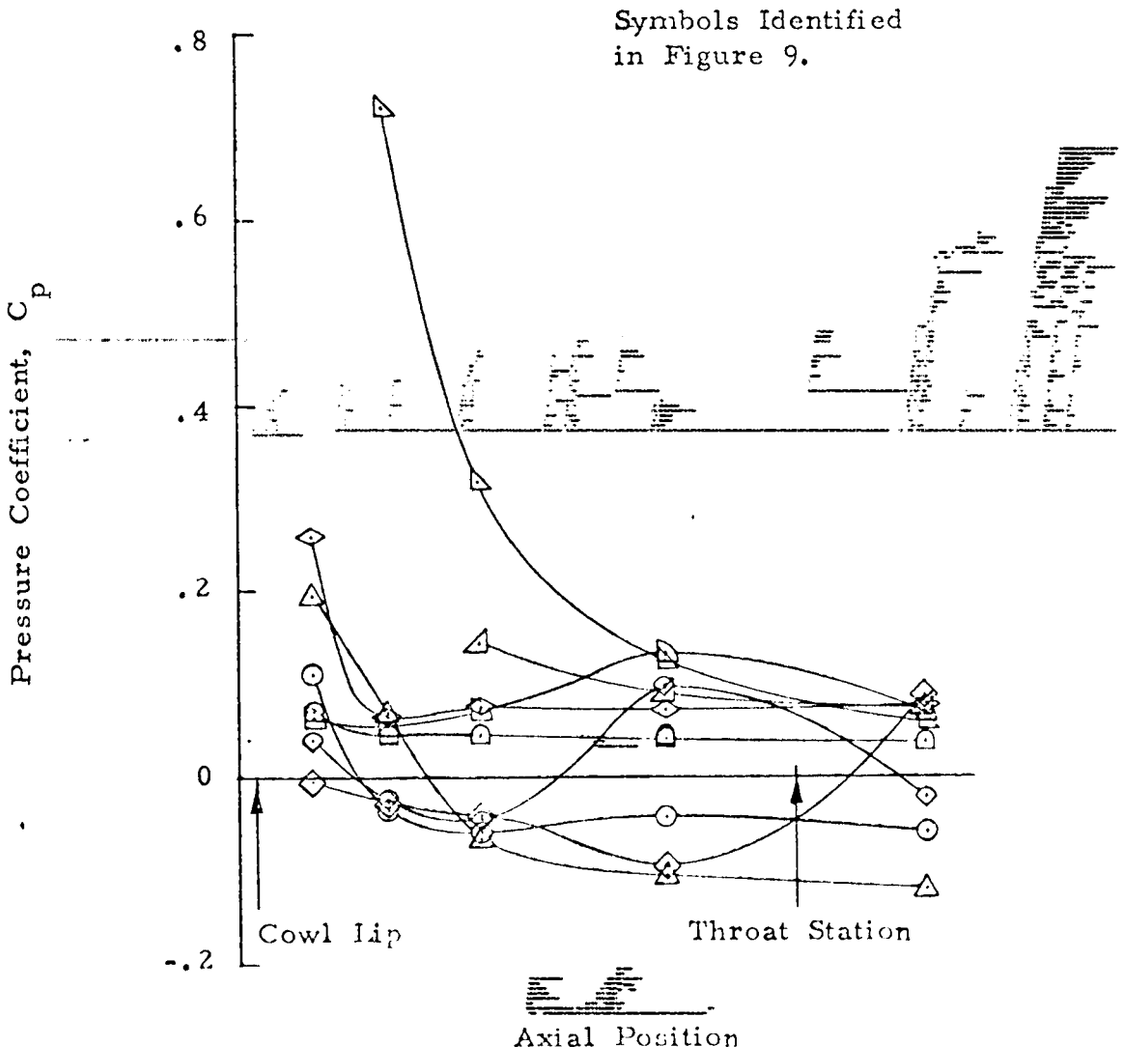


FIGURE 18. - NACELLE PRESSURE DISTRIBUTION, $\alpha = 4.03°$

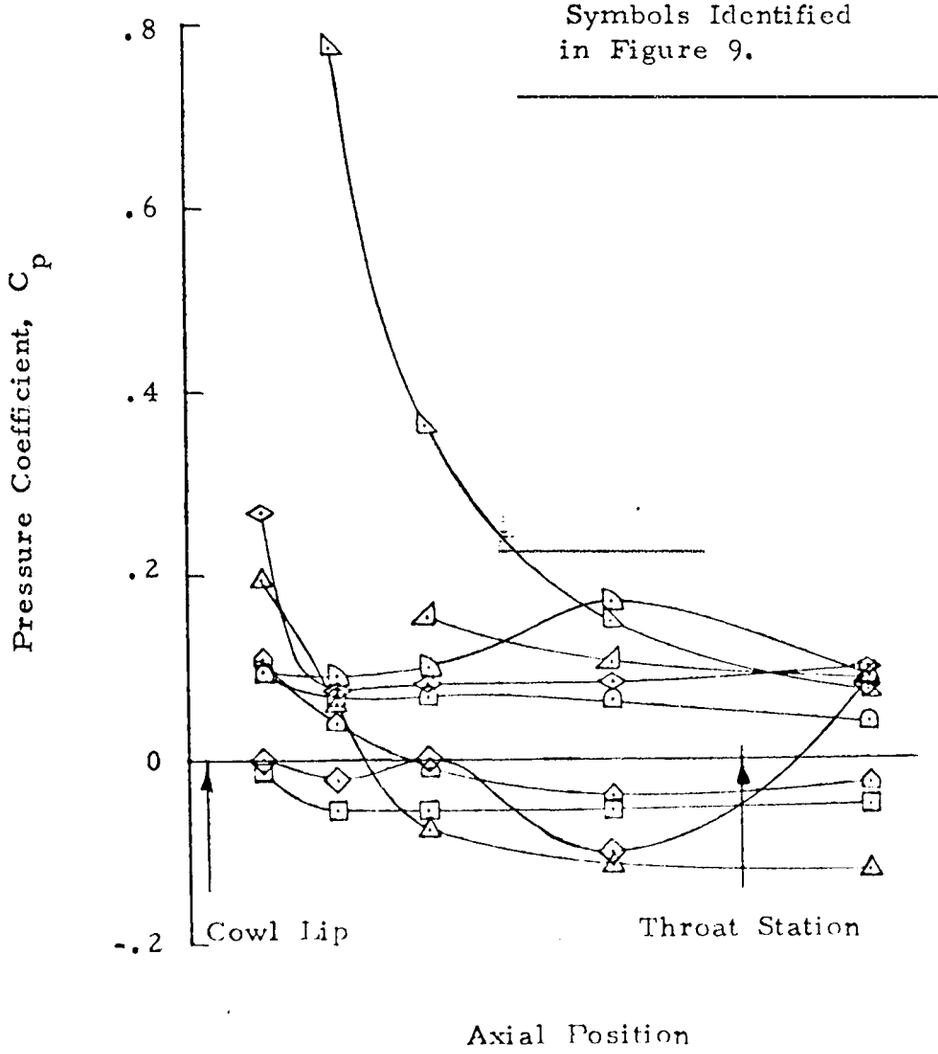


FIGURE 19. - NACELLE PRESSURE DISTRIBUTION, $\alpha$ = 6.98°

Symbols Identified
in Figure 9.

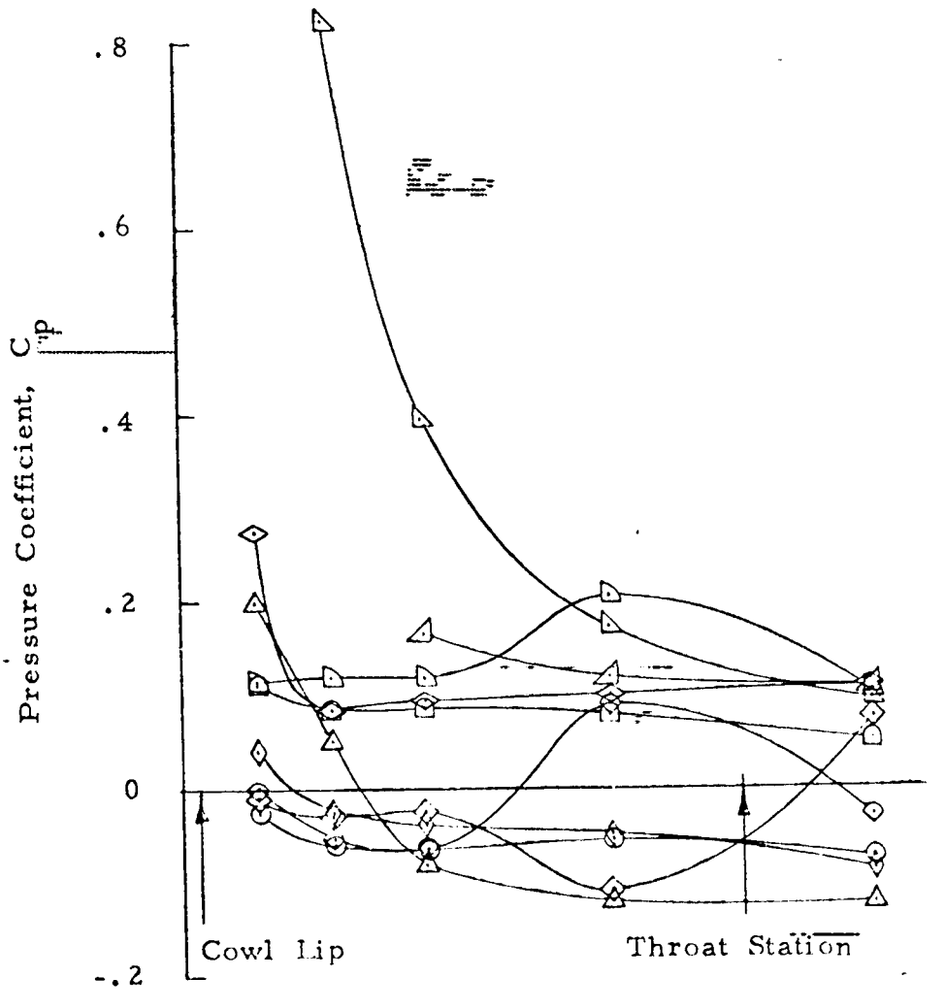


FIGURE 20. - NACELLE PRESSURE DISTRIBUTION, $\alpha$ = 7.92°

$w_{theo}$ = Theoretical inviscid two-dimensional flow rate.

$w_{sonic}$ = Sonic flow rate through perforation area at inlet duct total pressure

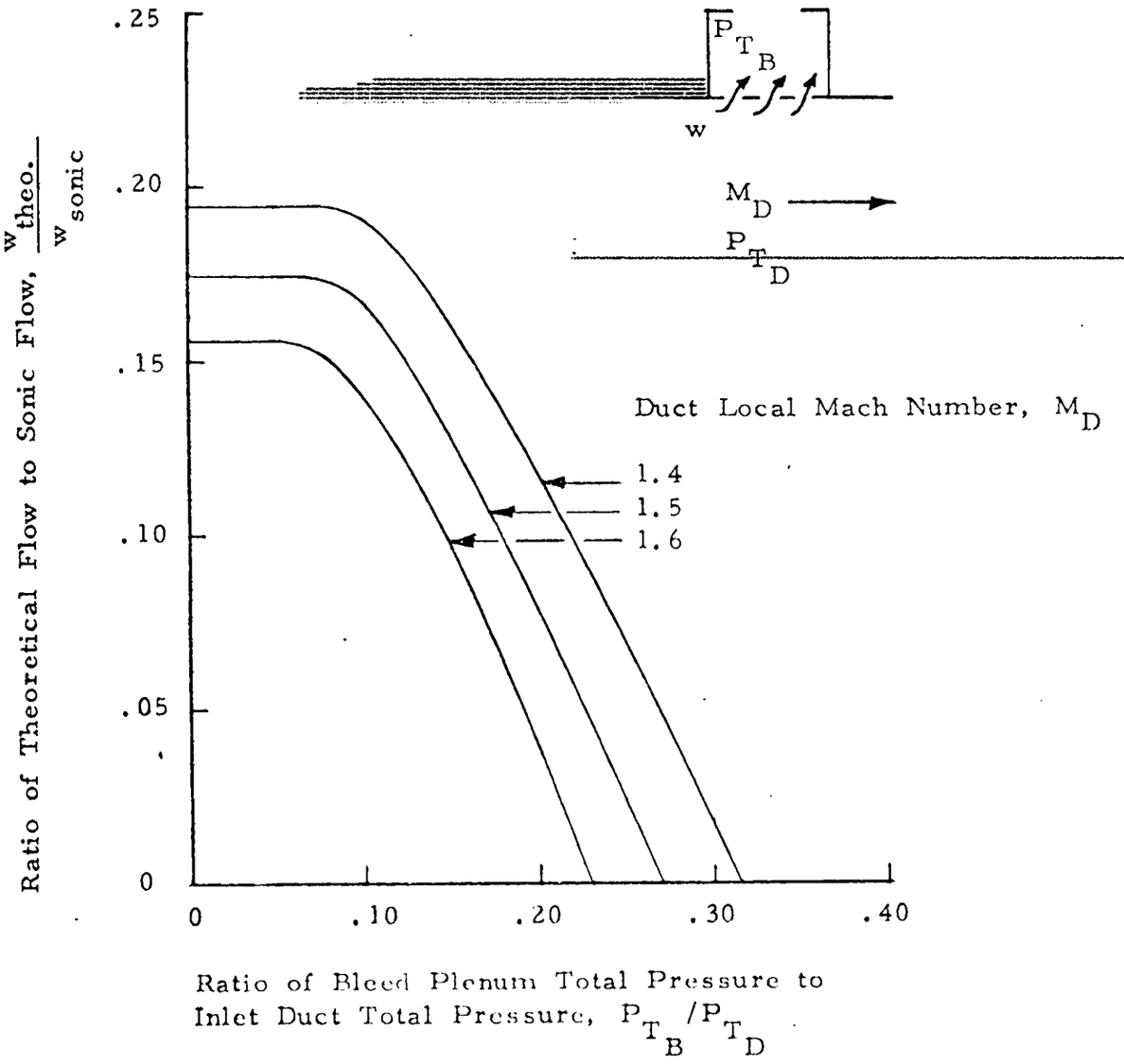


FIGURE 21. - THEORETICAL PERFORATION FLOW RATE

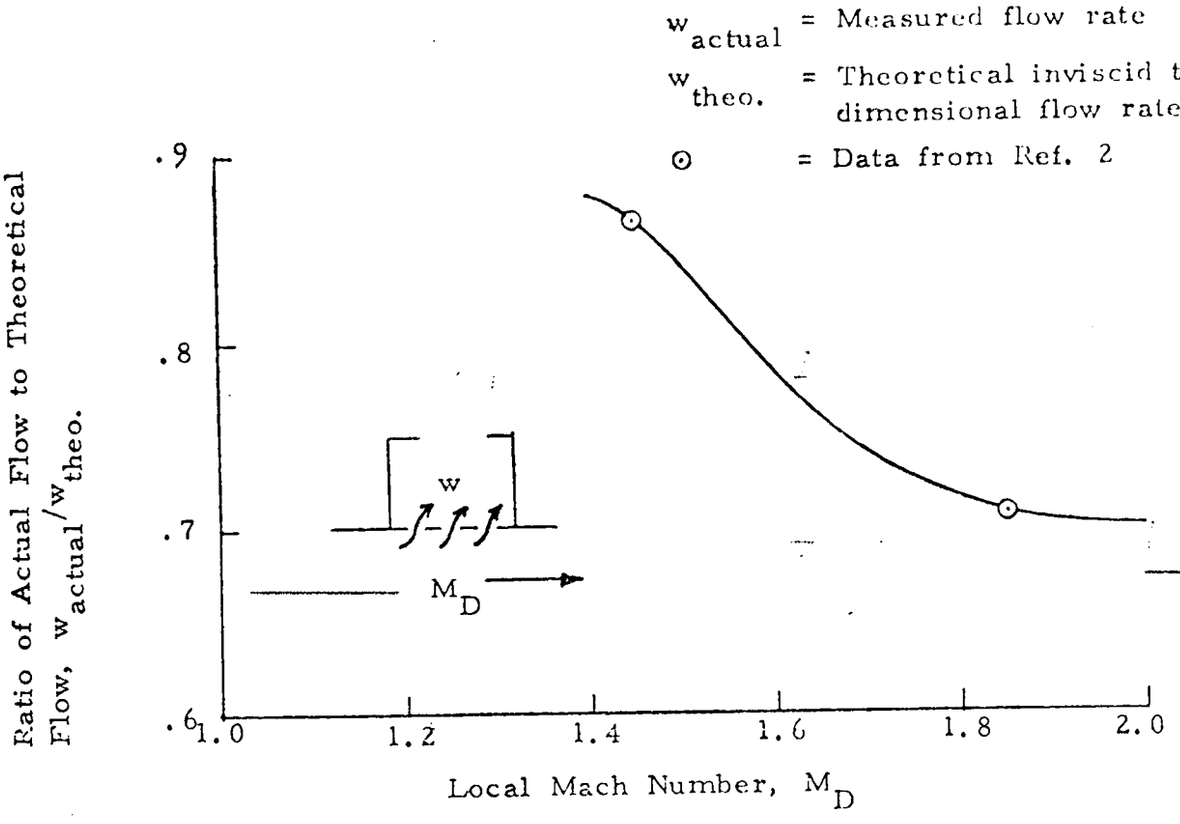


FIGURE 22. - EXPERIMENTAL PERFORATION FLOW RATE

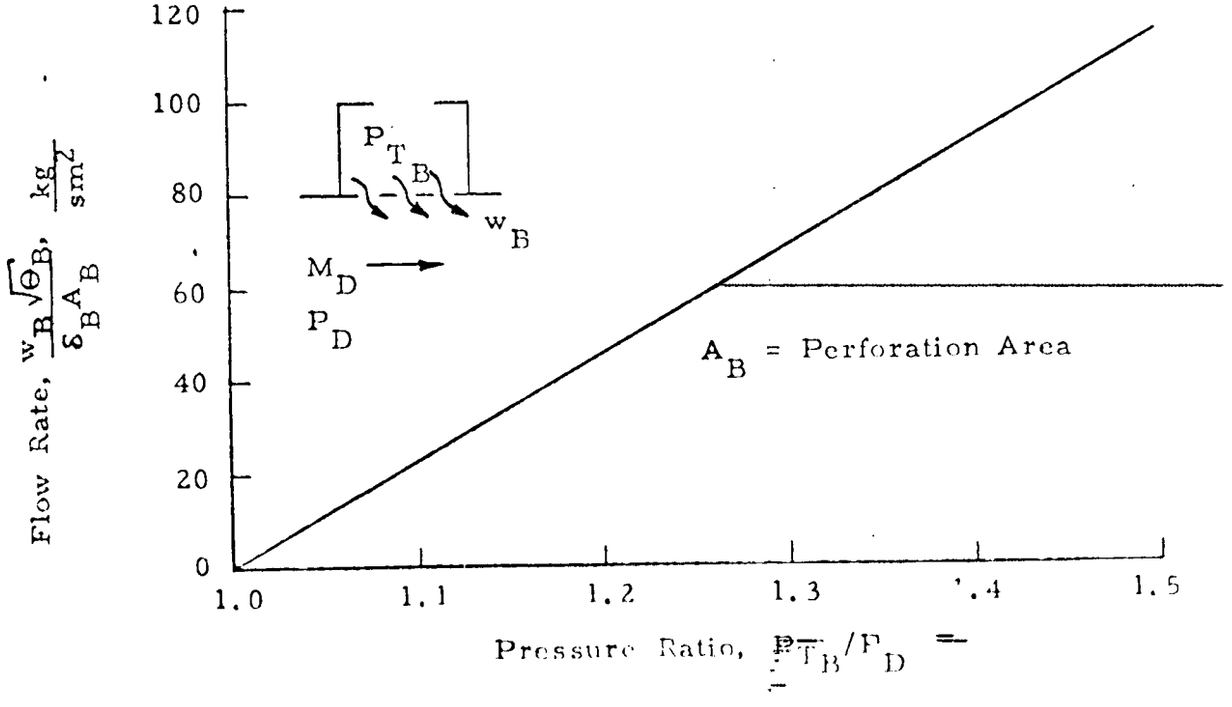


FIGURE 23. - ESTIMATED FLOW OUT OF POROUS COWL BLEED

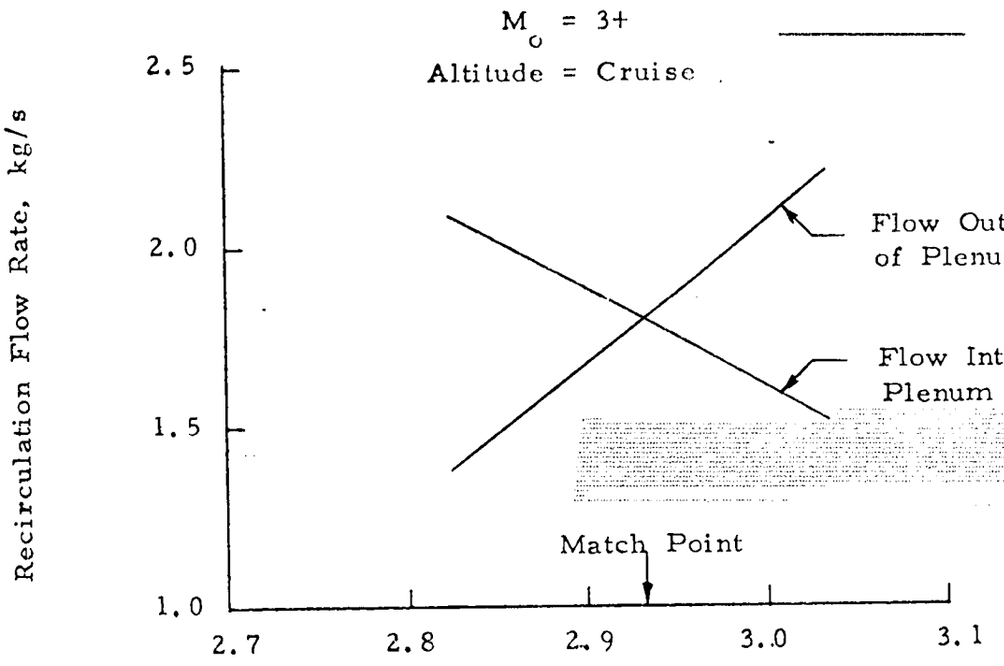


FIGURE 24. - COWL BLEED PLENUM PRESSURE MATCH POINT

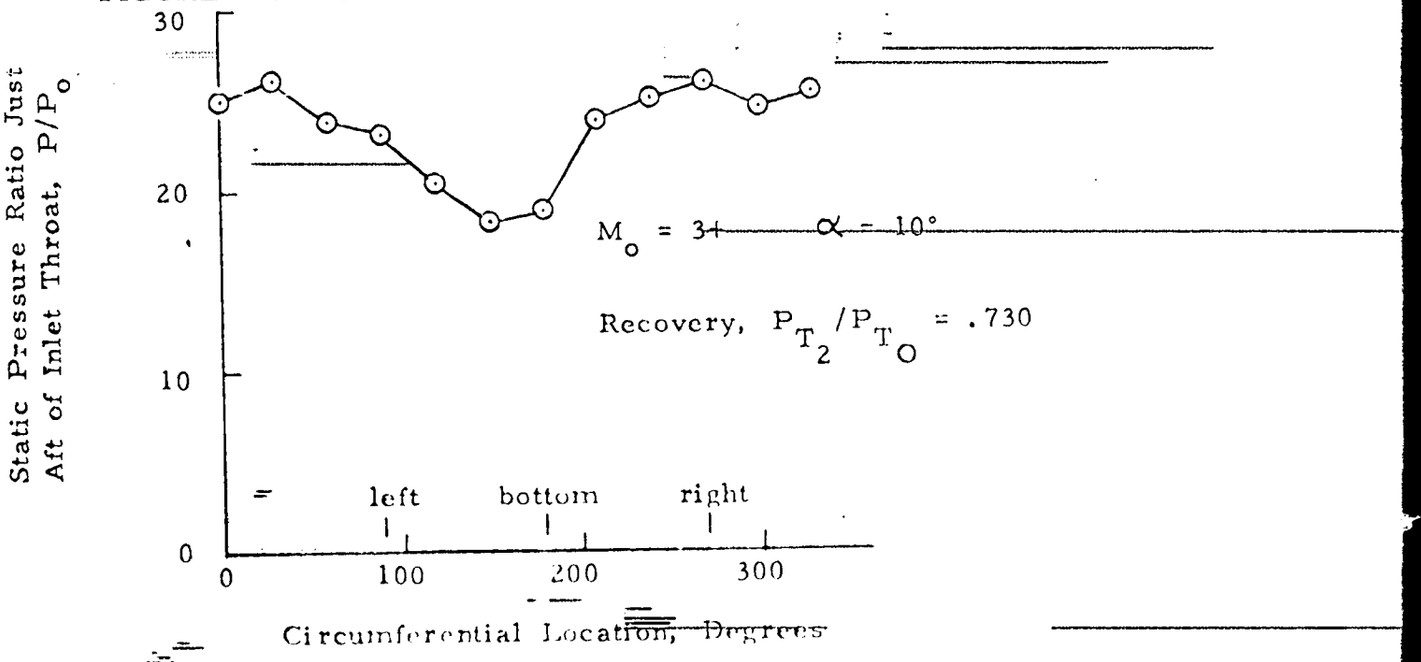


FIGURE 25. - COWL CIRCUMFERENTIAL PRESSURE DISTRIBUTION

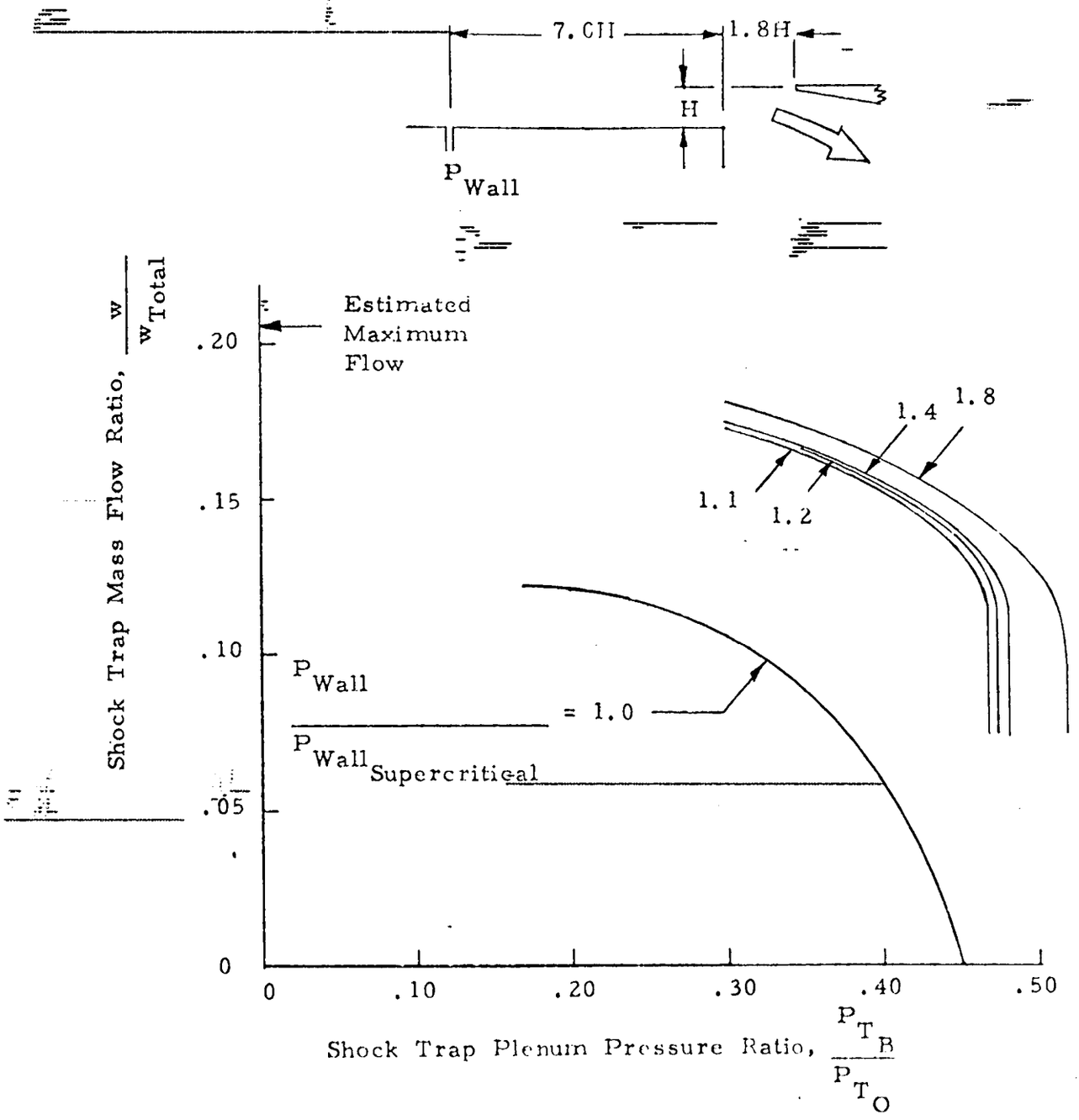


FIGURE 26. - EFFECT OF SHOCK POSITION ON FLOW CHARACTERISTICS OF SHOCK TRAP BLEED

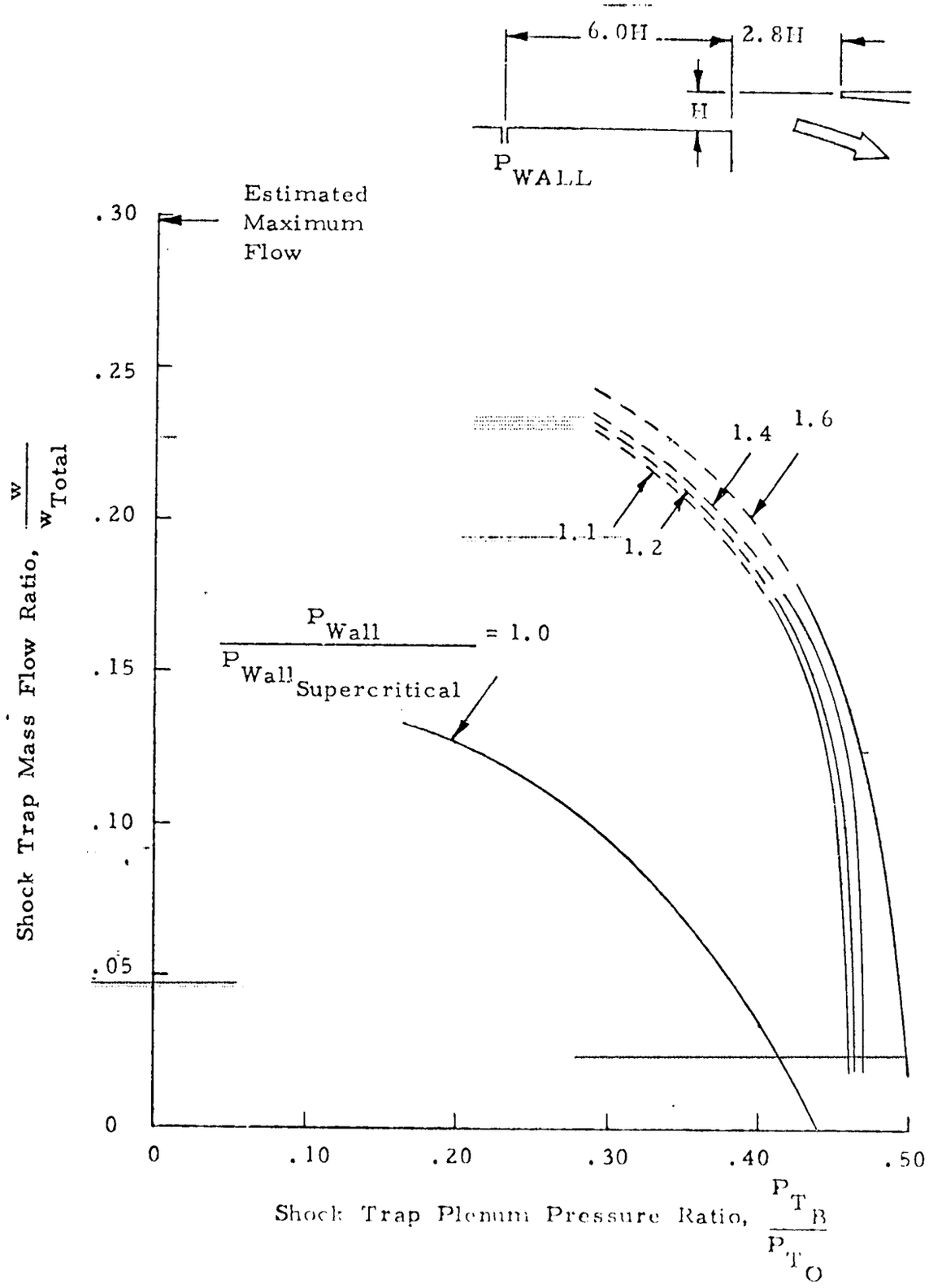


FIGURE 27. - EFFECT OF SHOCK POSITION ON FLOW CHARACTERISTICS OF MODIFIED SHOCK TRAP BLEED

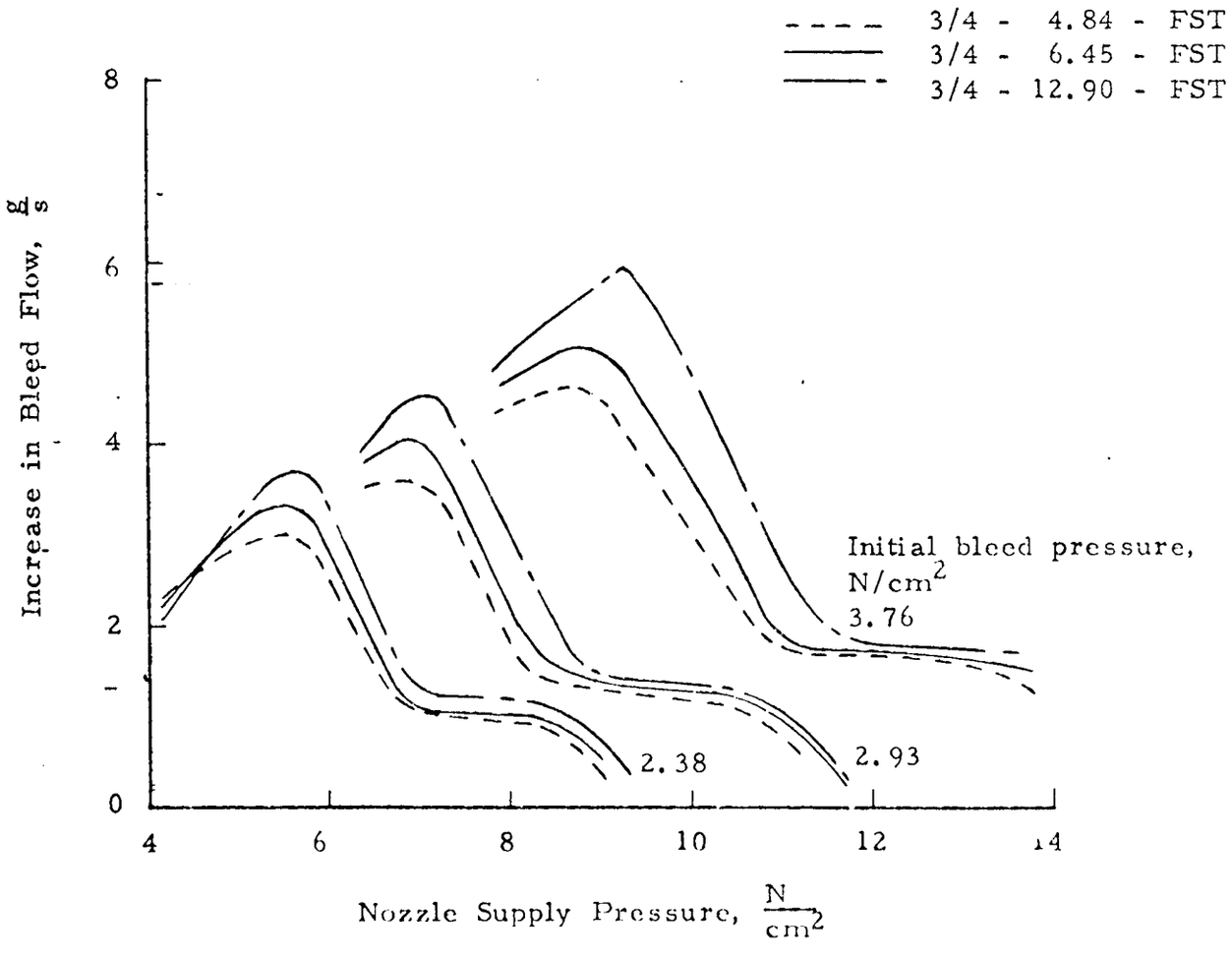


FIGURE 28. VORTEX VALVE BLEED FLOW INCREMENT DUE TO 20 PERCENT INCREASE IN BLEED PRESSURE

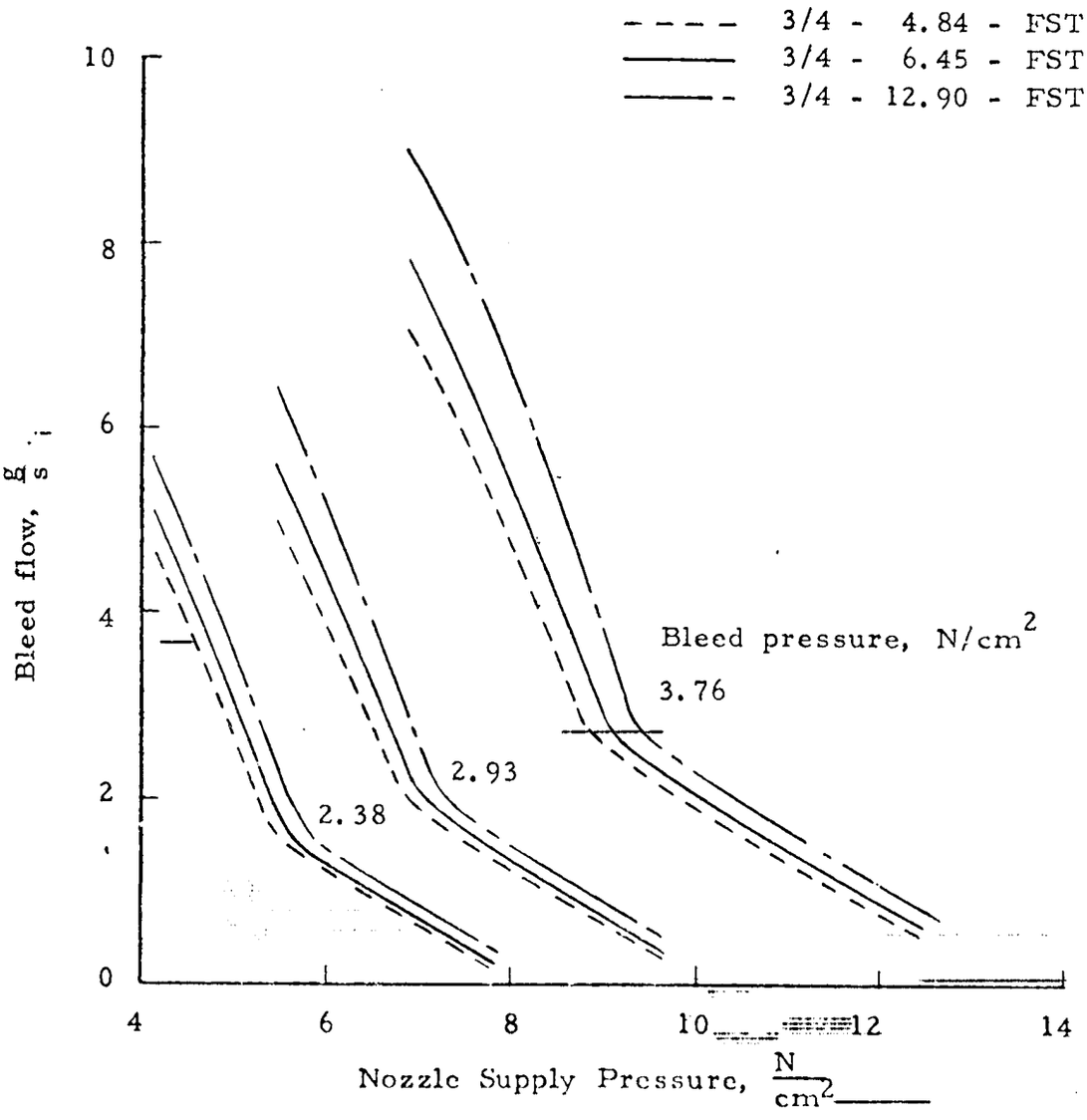


FIGURE 29. LEAKAGE BLEED FLOW IN VORTEX VALVE

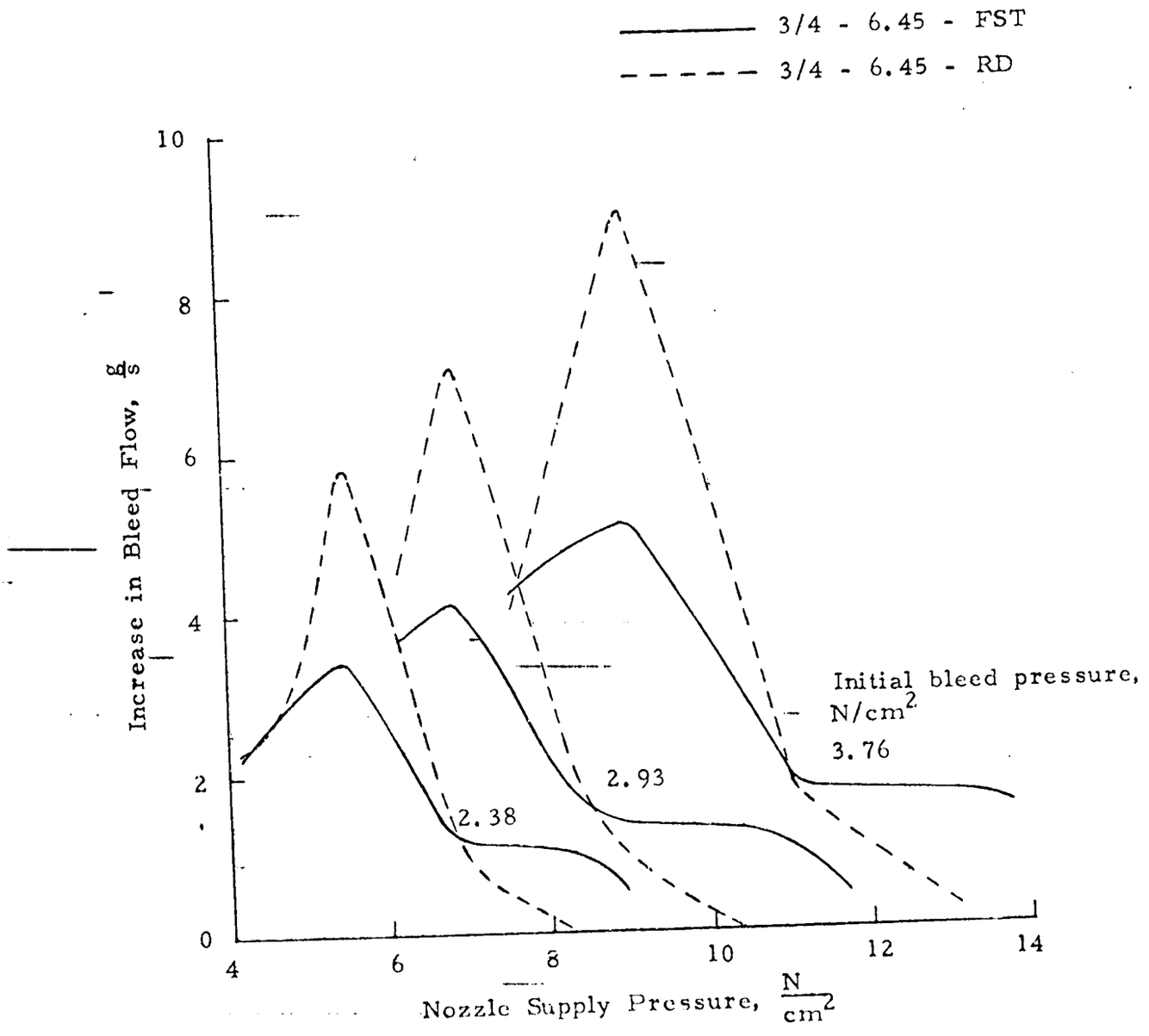


FIGURE 30. VORTEX VALVE BLEED FLOW INCREMENT DUE TO 20 PERCENT INCREASE IN BLEED PRESSURE

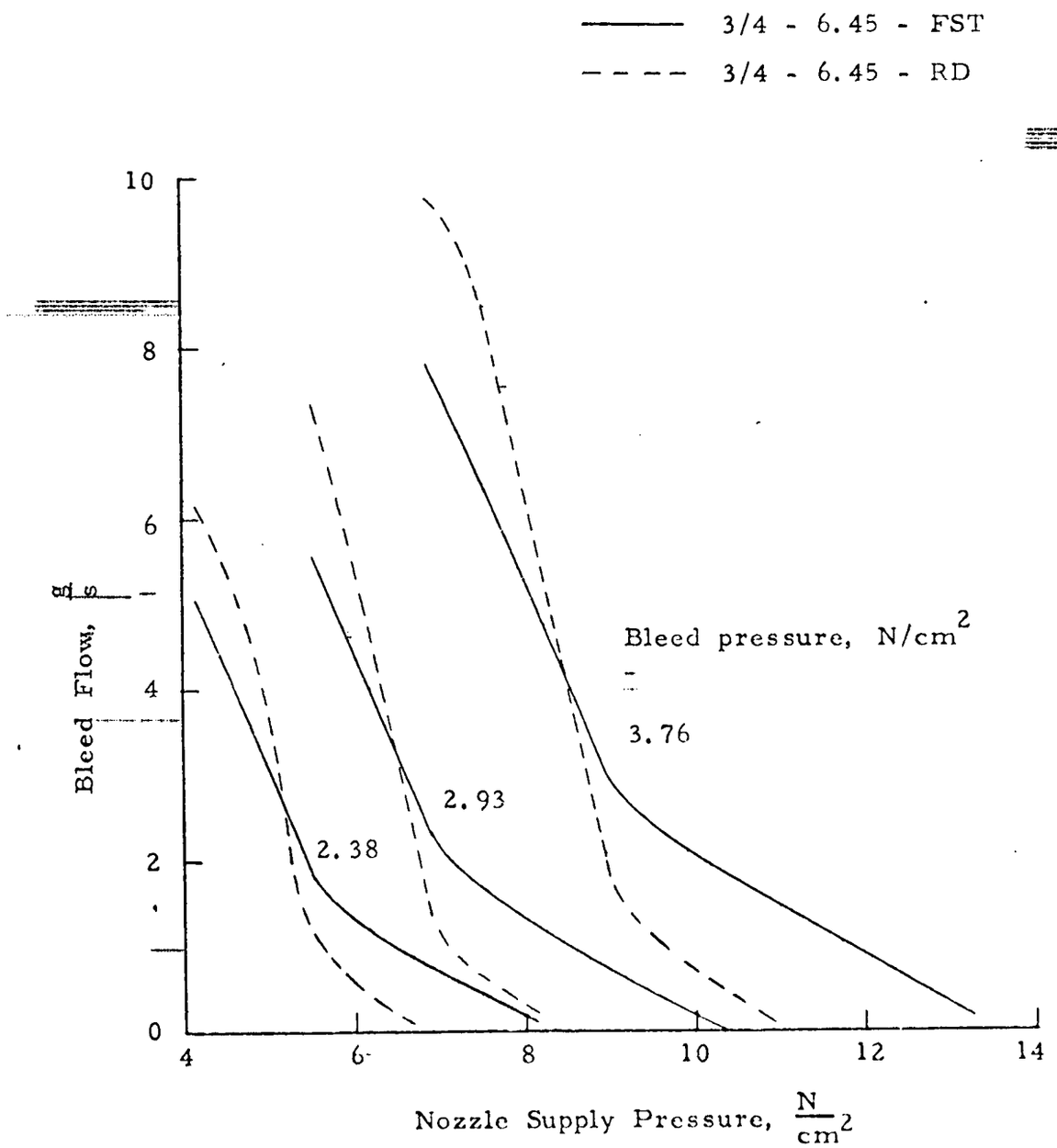


FIGURE 31. LEAKAGE BLEED FLOW IN VORTEX VALVE

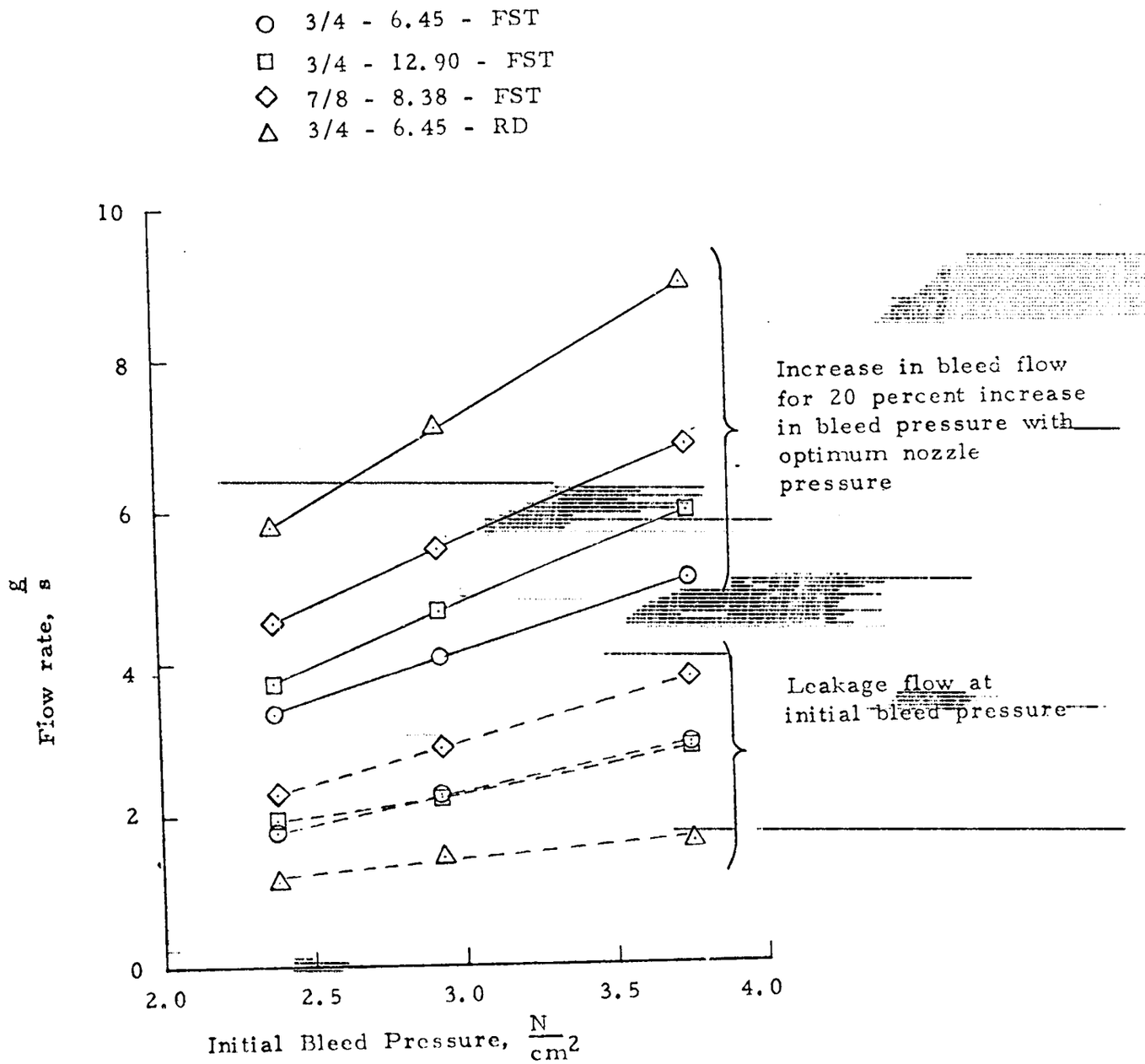


FIGURE 32. EFFECT OF BLEED PRESSURE ON VORTEX VALVE LEAKAGE AND INCREMENTAL BLEED FLOWS

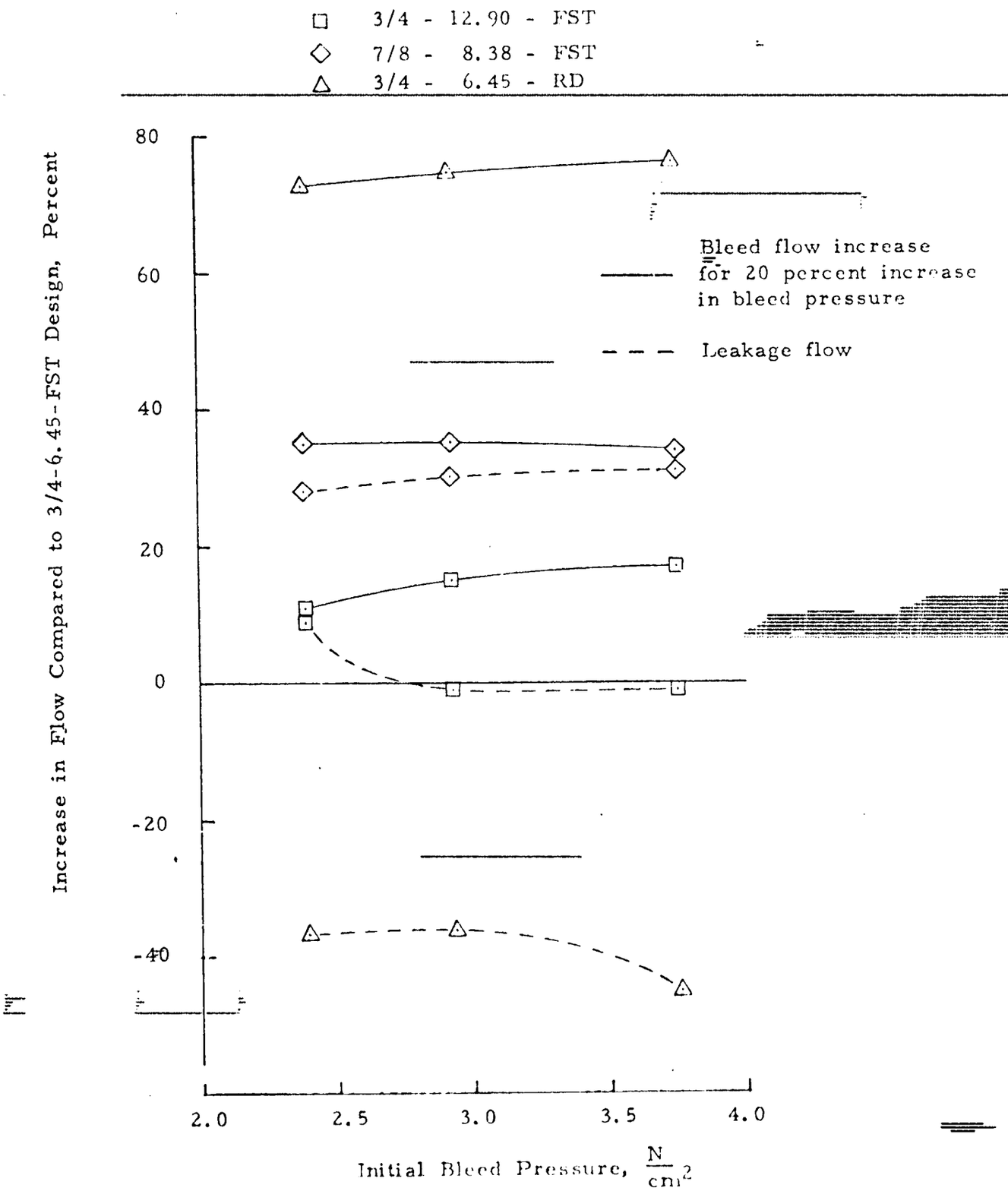


FIGURE 33. VORTEX VALVE BLEED AND LEAKAGE FLOWS COMPARED TO 3/4-6.45-FST DESIGN

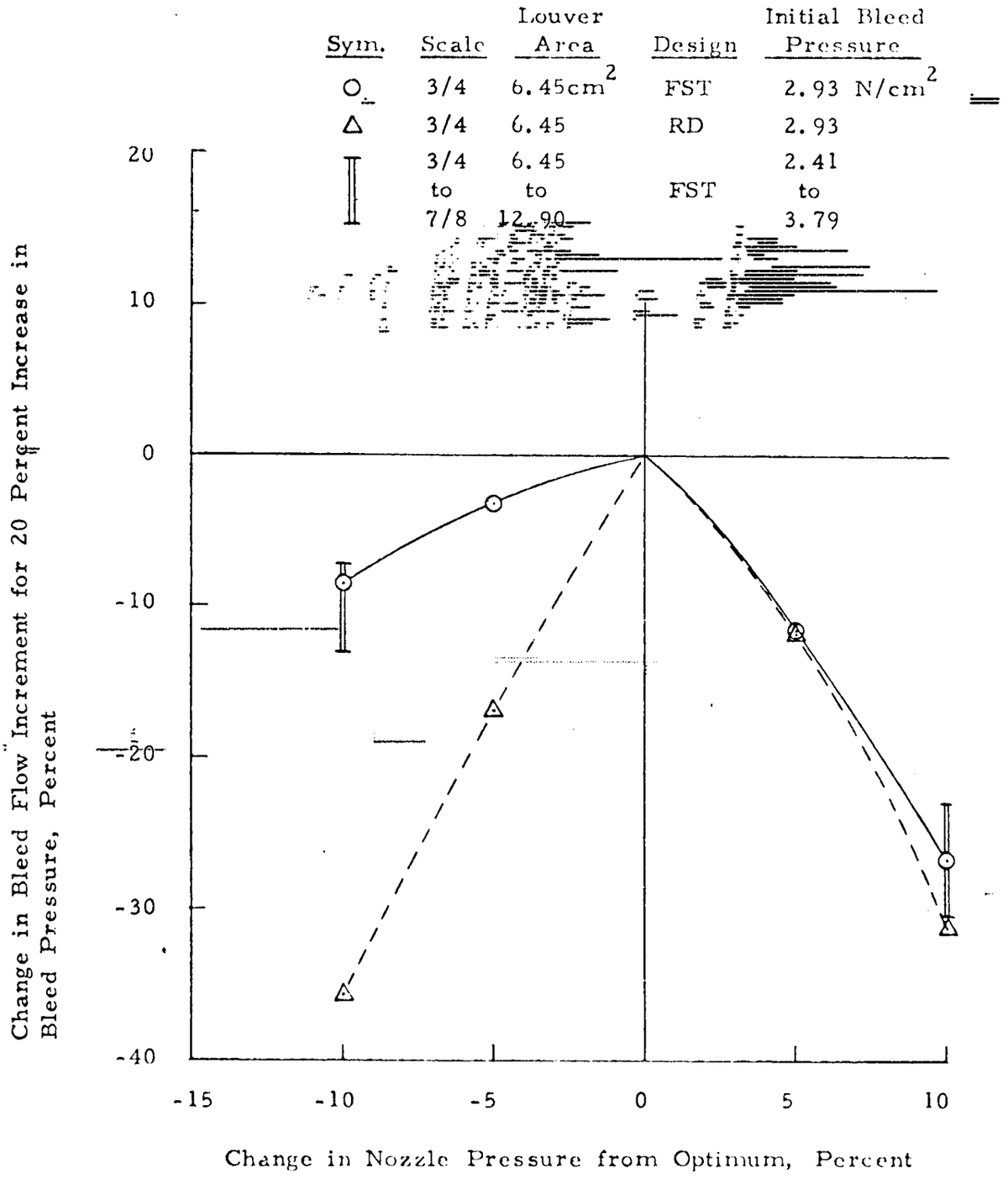


FIGURE 34. EFFECT OF NOZZLE PRESSURE ON BLEED FLOW INCREMENT

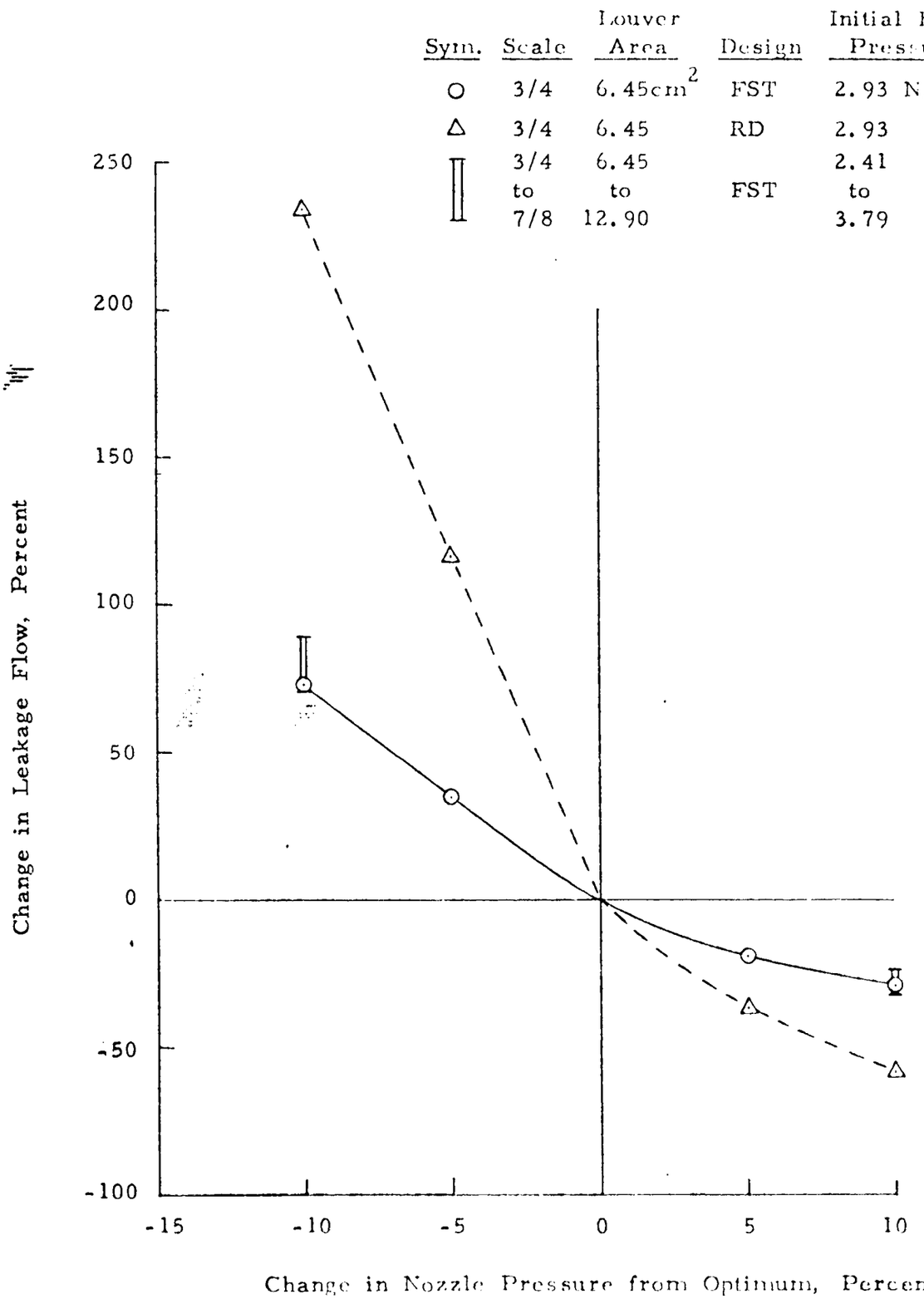


FIGURE 35. EFFECT OF NOZZLE PRESSURE ON LEAKAGE FLOW

| | Initial Bleed Pressure $N/cm^2$ | Nozzle Pressure $N/cm^2$ | Number of Valves | Leakage Flow Ratio $w_{Leakage}/w_o$ |
|---|---|---|---|---|
| Shock Trap | 3.76 | 9.03 | 96 | .00207 |
| Aft Cowl | 3.58 | 8.62 | 48 | .00103 |
| Fwd. Cowl | 2.41 | 5.52 | 48 | .00075 |

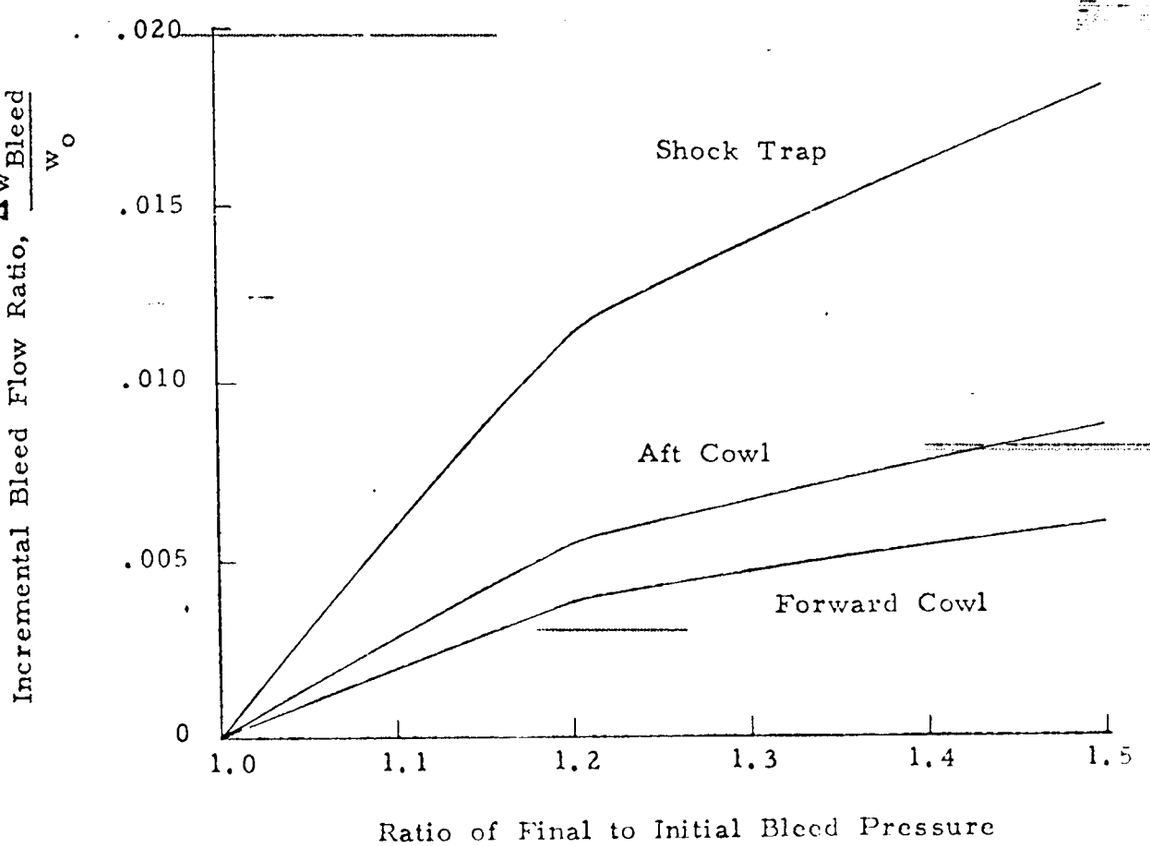


FIGURE 36. VORTEX VALVE BLEED FLOW INCREMENTS

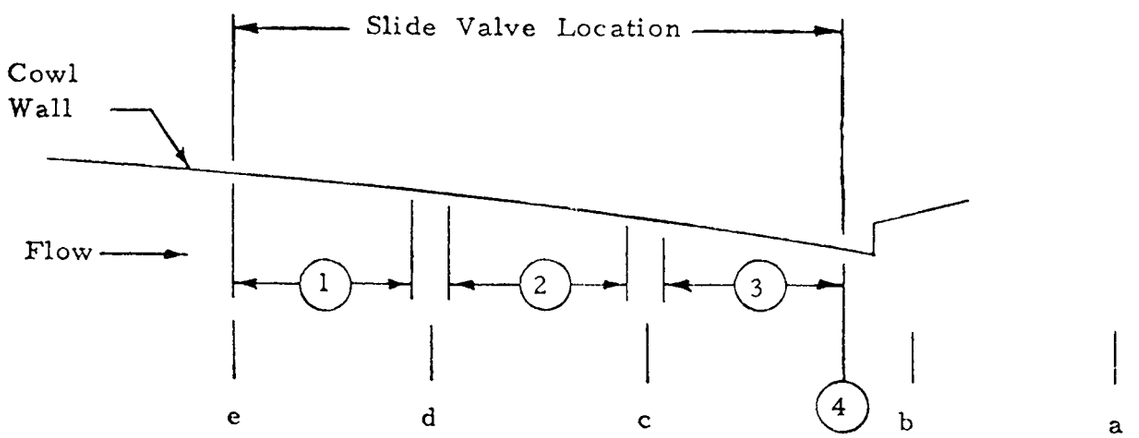


| Nominal Shock Location | $\bar{M}_1$ | $\bar{M}_2$ | $\bar{M}_3$ | $M_4$ |
|---|---|---|---|---|
| a* | 1.73 | 1.77 | 1.50 | 1.47 |
| b** | 1.73 | 1.67 | 1.35 | 1.32 |
| c | 1.73 | 1.53 | .87 | .95 |
| d | 1.73 | .70 | .86 | .95 |
| e | .70 | .80 | .90 | .95 |

* Normal operating condition

** Peak stable recovery

FIGURE 37. EFFECT OF TERMINAL SHOCK POSITION ON DUCT MACH NUMBERS AT SLIDE VALVE LOCATION, $M_O = 3+$

$M_O$ = 3+

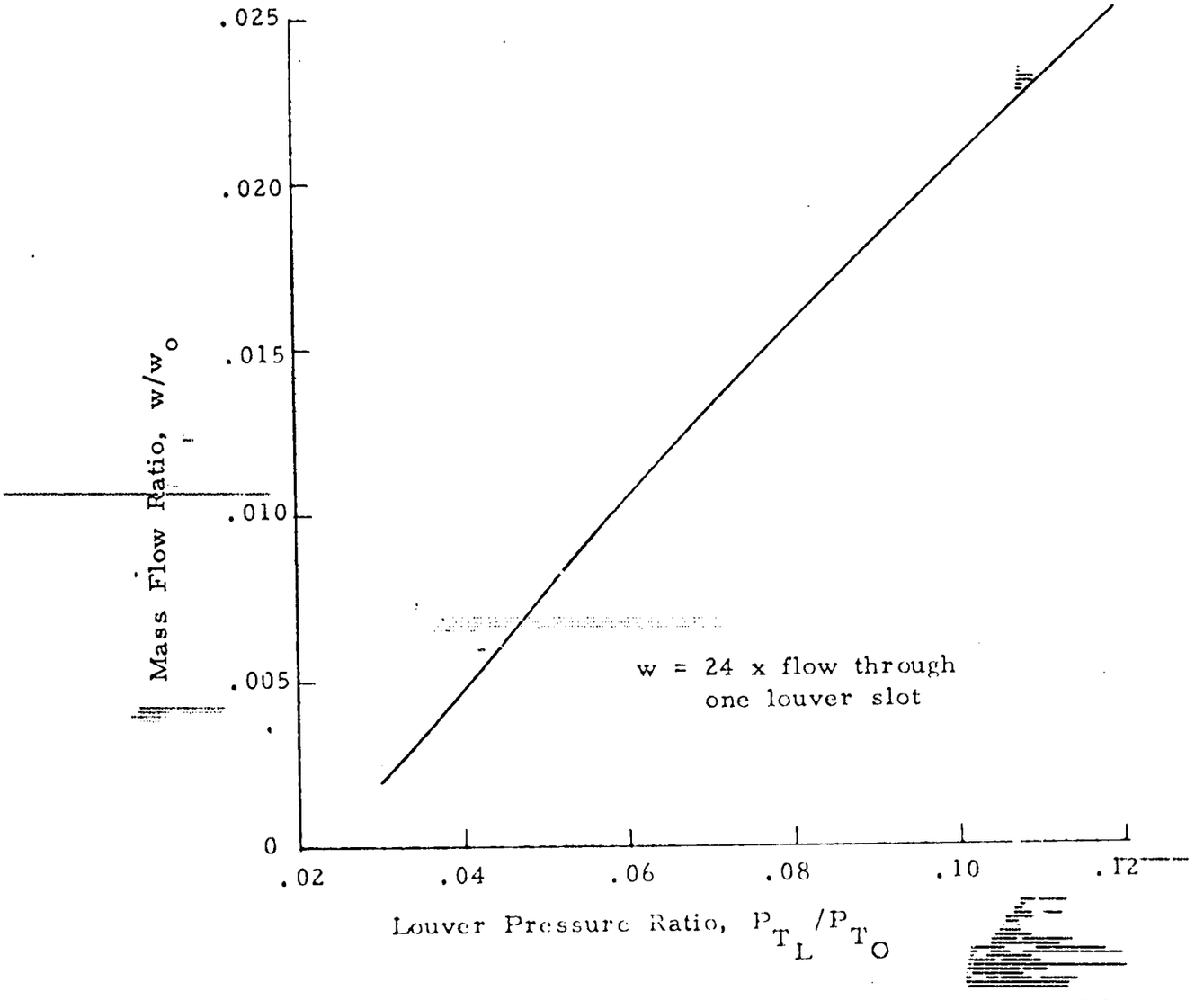


FIGURE 38. FLOW THROUGH SLIDE VALVE EXIT LOUVERS

$M_O = 3+$

$P_{T_L}/P_{T_O} = .06$

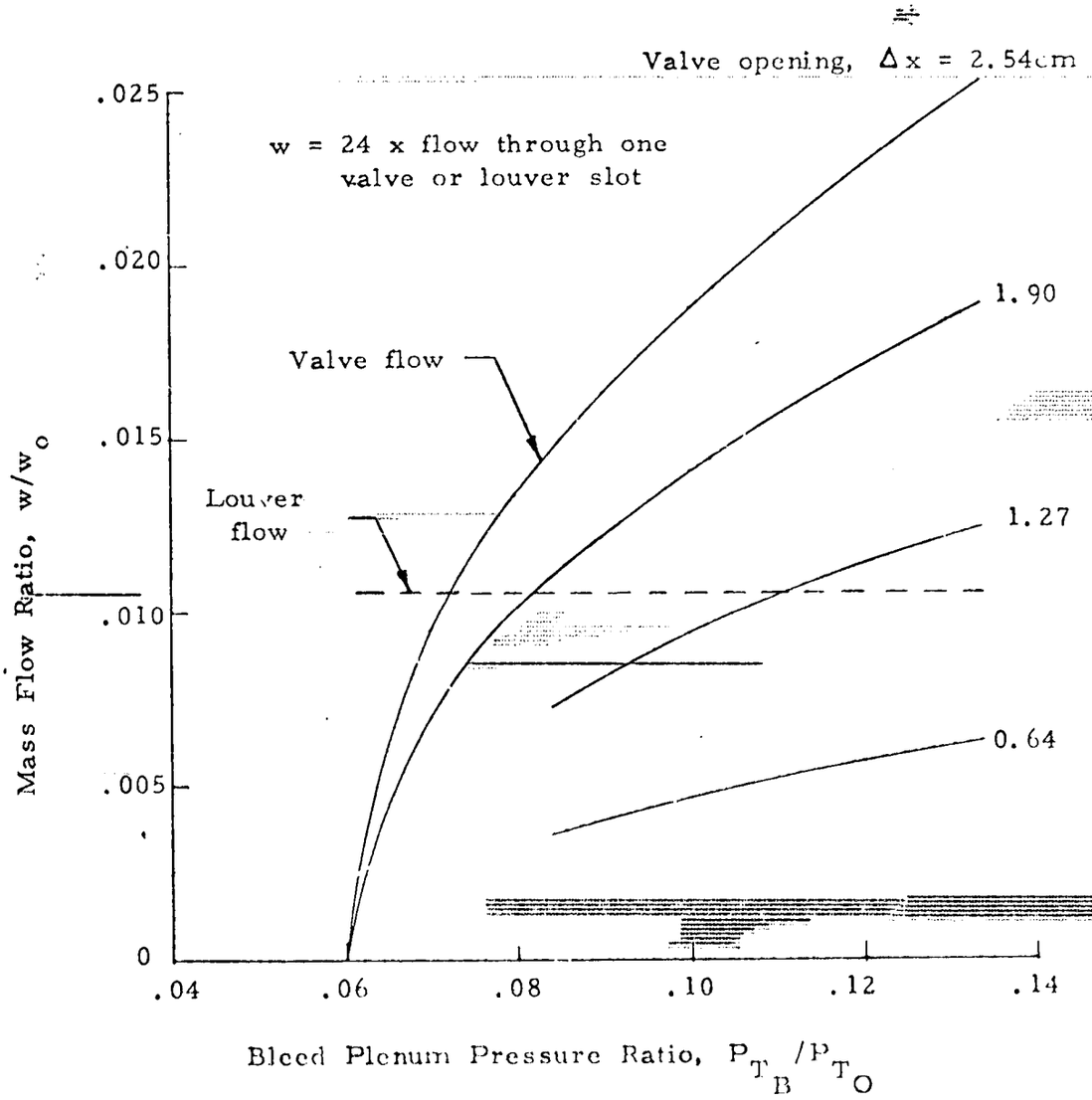


FIGURE 39. EFFECT OF VALVE ~~POSITION ON FLOW~~ THROUGH SLIDE VALVE

$M_O = 3.4$

$P_{T_L}/P_{T_O} = .085$

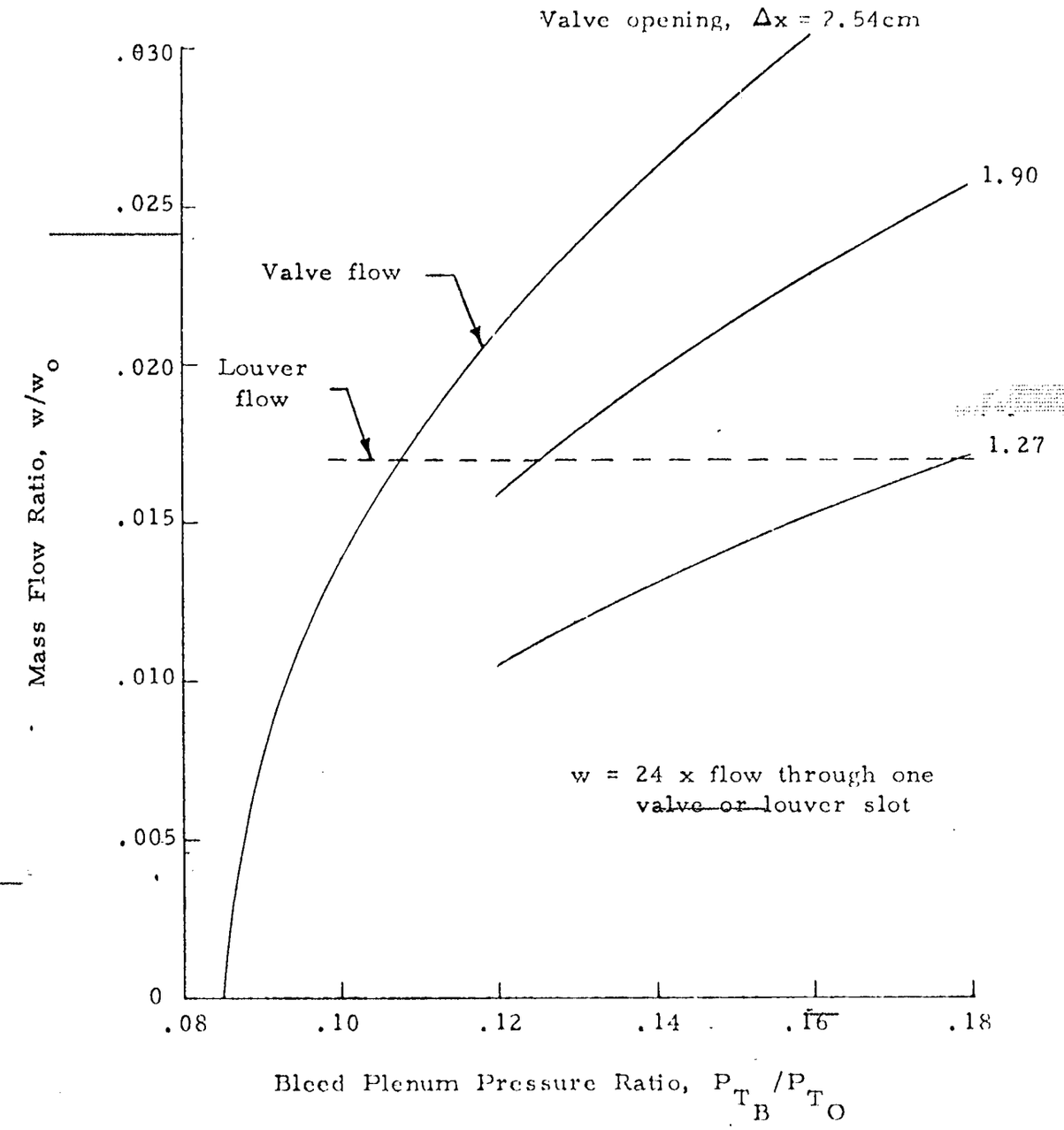


FIGURE 40. EFFECT OF VALVE POSITION ON FLOW THROUGH SLIDE VALVE

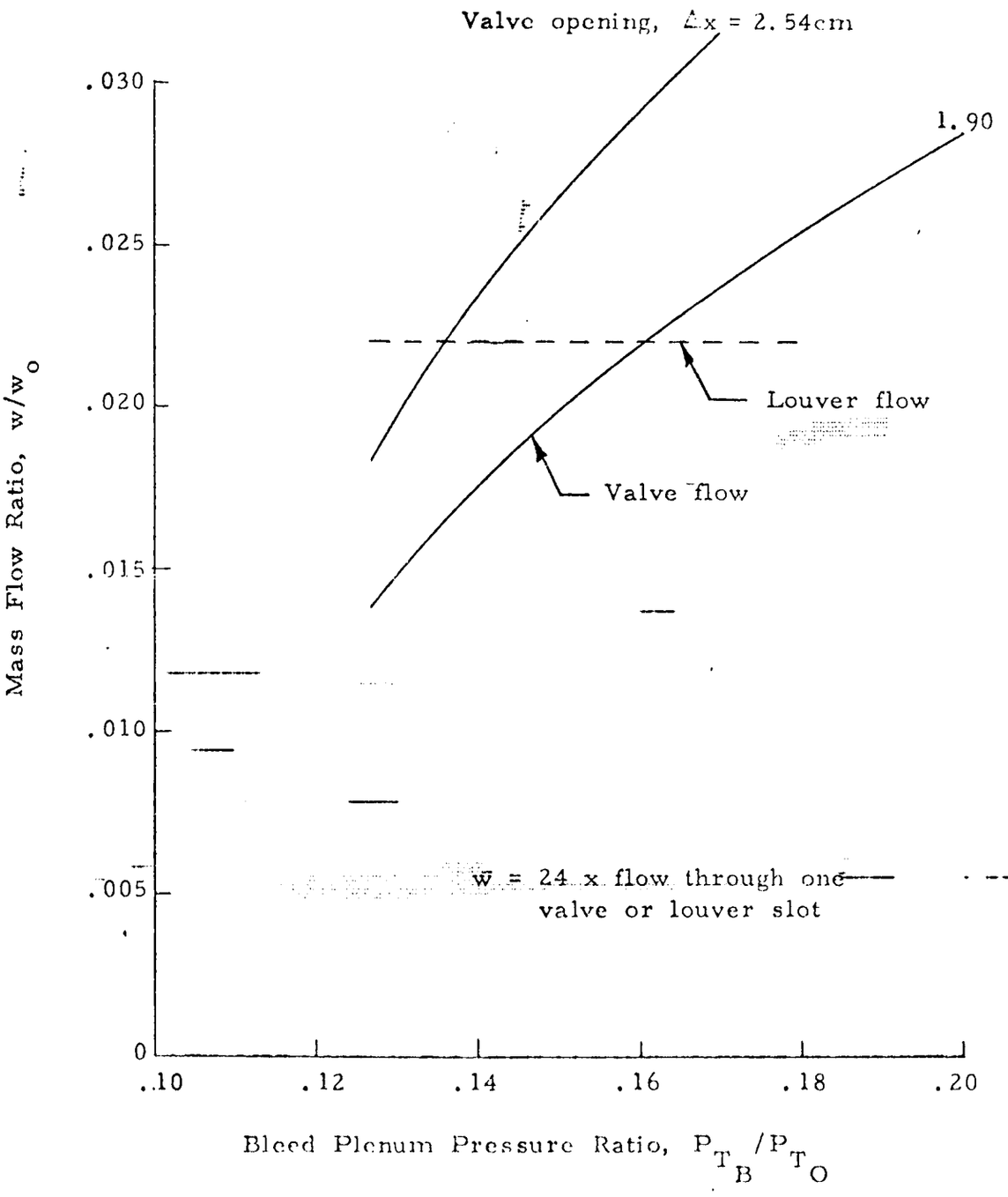


FIGURE 41. EFFECT OF VALVE POSITION ON FLOW THROUGH SLIDE VALVE

$M_O$ = 3+

w = 24 x flow through one of the three bleed compartments in a slide valve

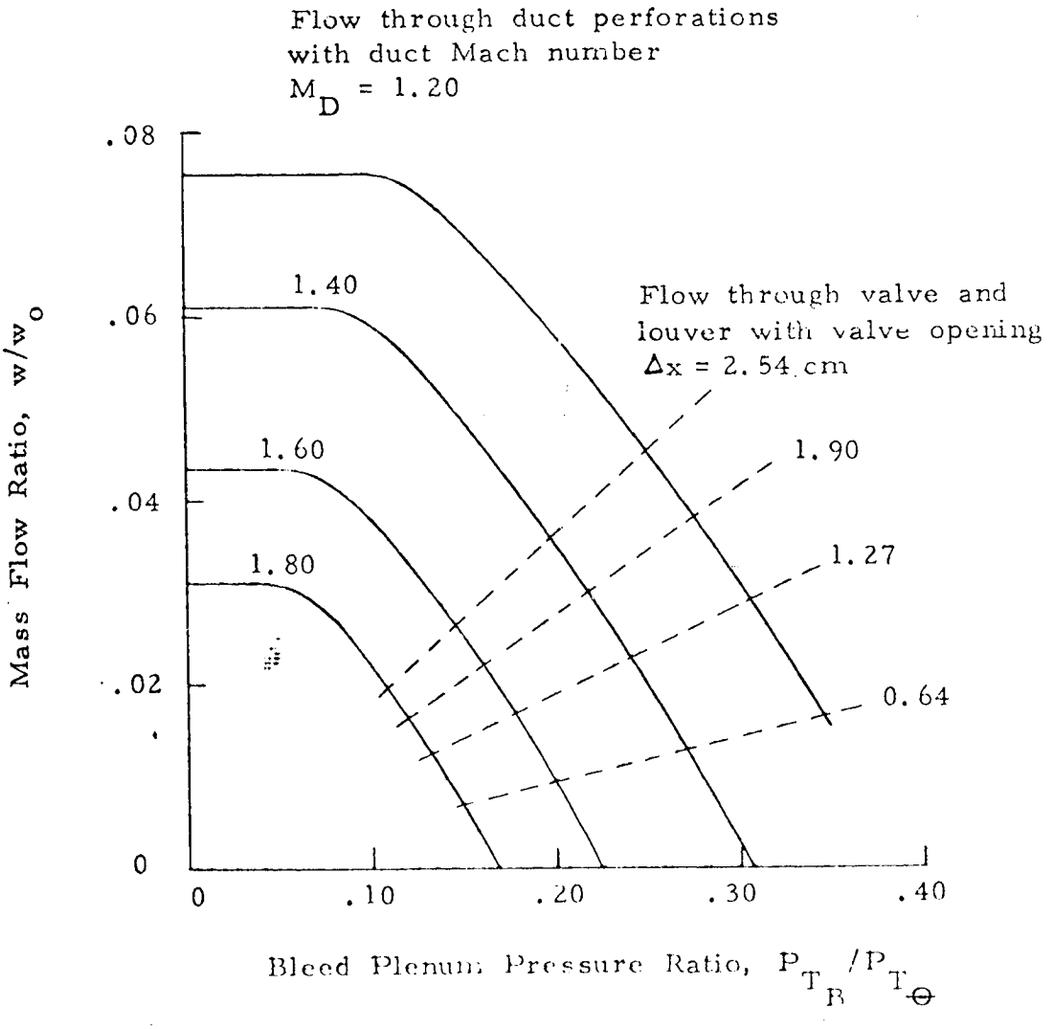


FIGURE 42. EFFECT OF DUCT MACH NUMBER AND VALVE POSITION ON FLOW THROUGH SLIDE VALVE

$M_O = 3+$

w = 24 x flow through one of the three bleed compartments in a slide valve

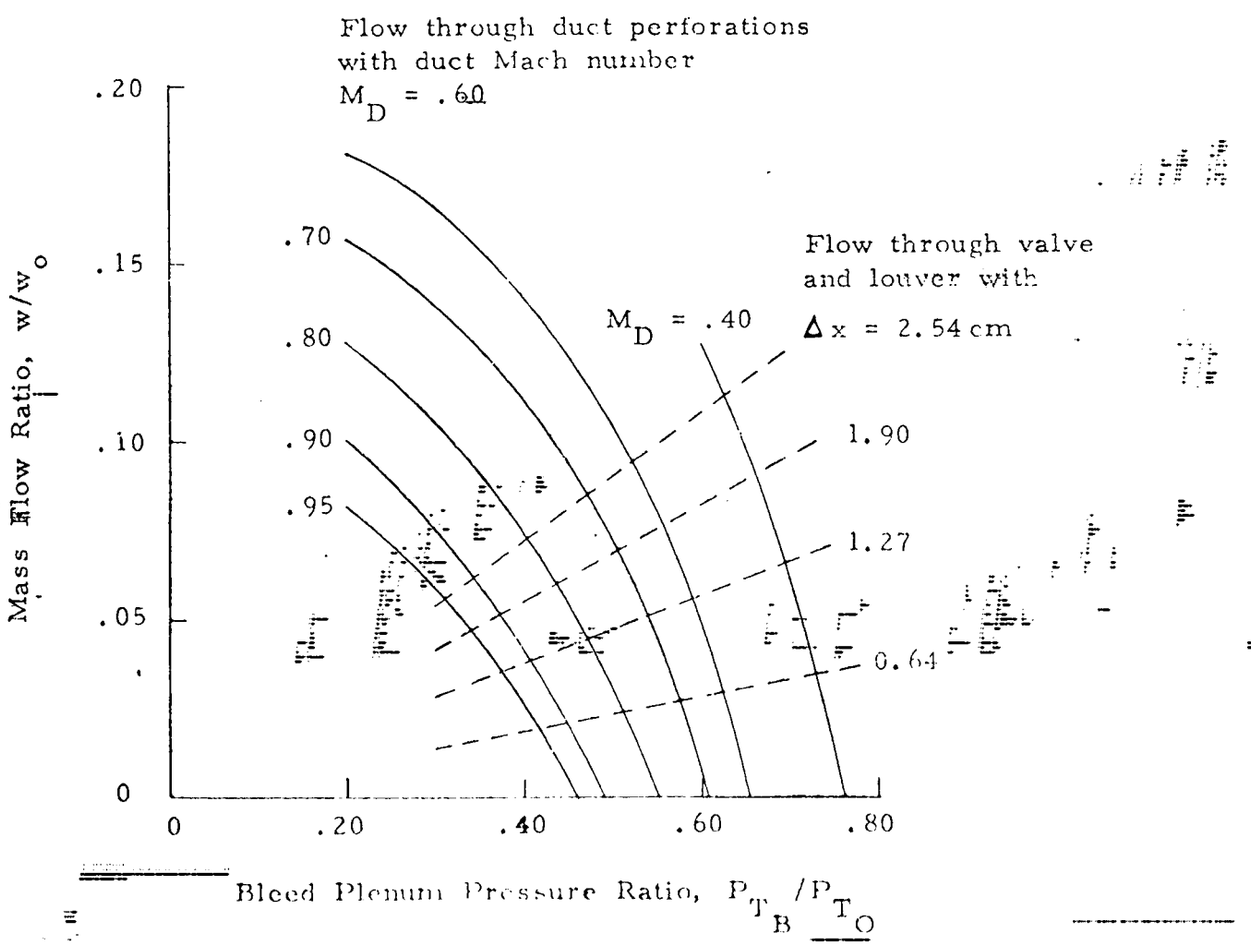


FIGURE 43. EFFECT OF DUCT MACH NUMBER AND VALVE POSITION ON FLOW THROUGH SLIDE VALVE

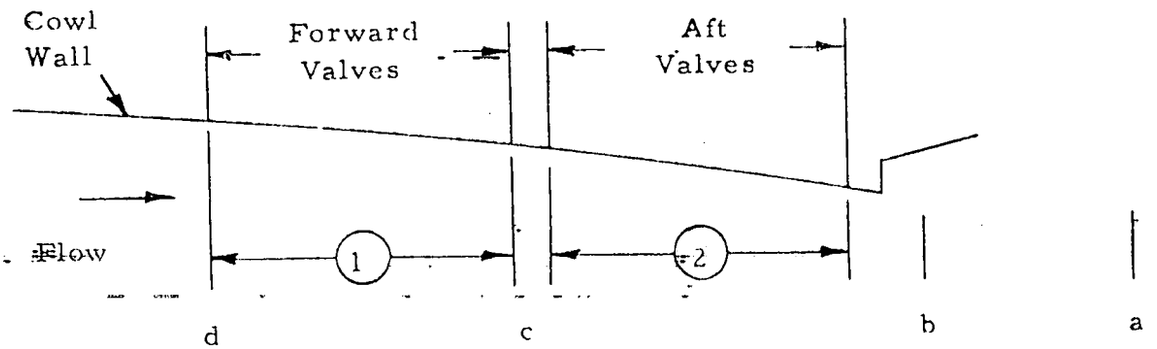


| Nominal Shock Location | $\bar{M}_1$ | $\bar{M}_2$ |
|---|---|---|
| a* | 1.749 | 1.590 |
| b** | 1.749 | 1.452 |
| c | 1.749 | .778 |
| d | .706 | .872 |

* Normal Operating Condition
** Peak Stable Recovery

FIGURE 44. EFFECT OF TERMINAL SHOCK POSITION ON DUCT MACH NUMBERS AT POPPET VALVE LOCATIONS, $M_0 = 3.4$

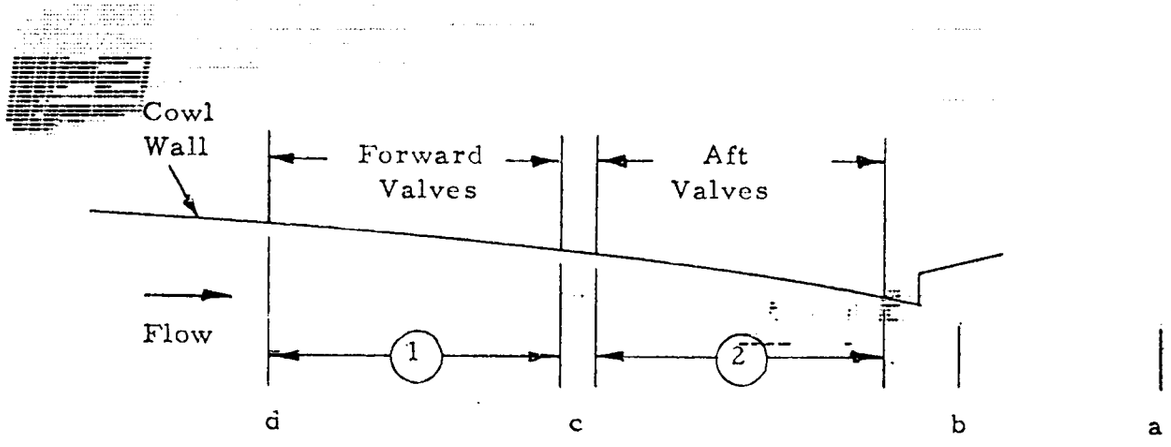


| Nominal Shock Location | $\overline{M}_2$ |
|---|---|
| a* | 1.227 |
| b** | 1.227 |
| c | .905 |
| d | .912 |

* Normal operating condition
** Peak stable recovery

FIGURE 45. EFFECT OF TERMINAL SHOCK POSITION ON DUCT MACH NUMBER AT POPPET VALVE LOCATION, $M_O = 2.47$

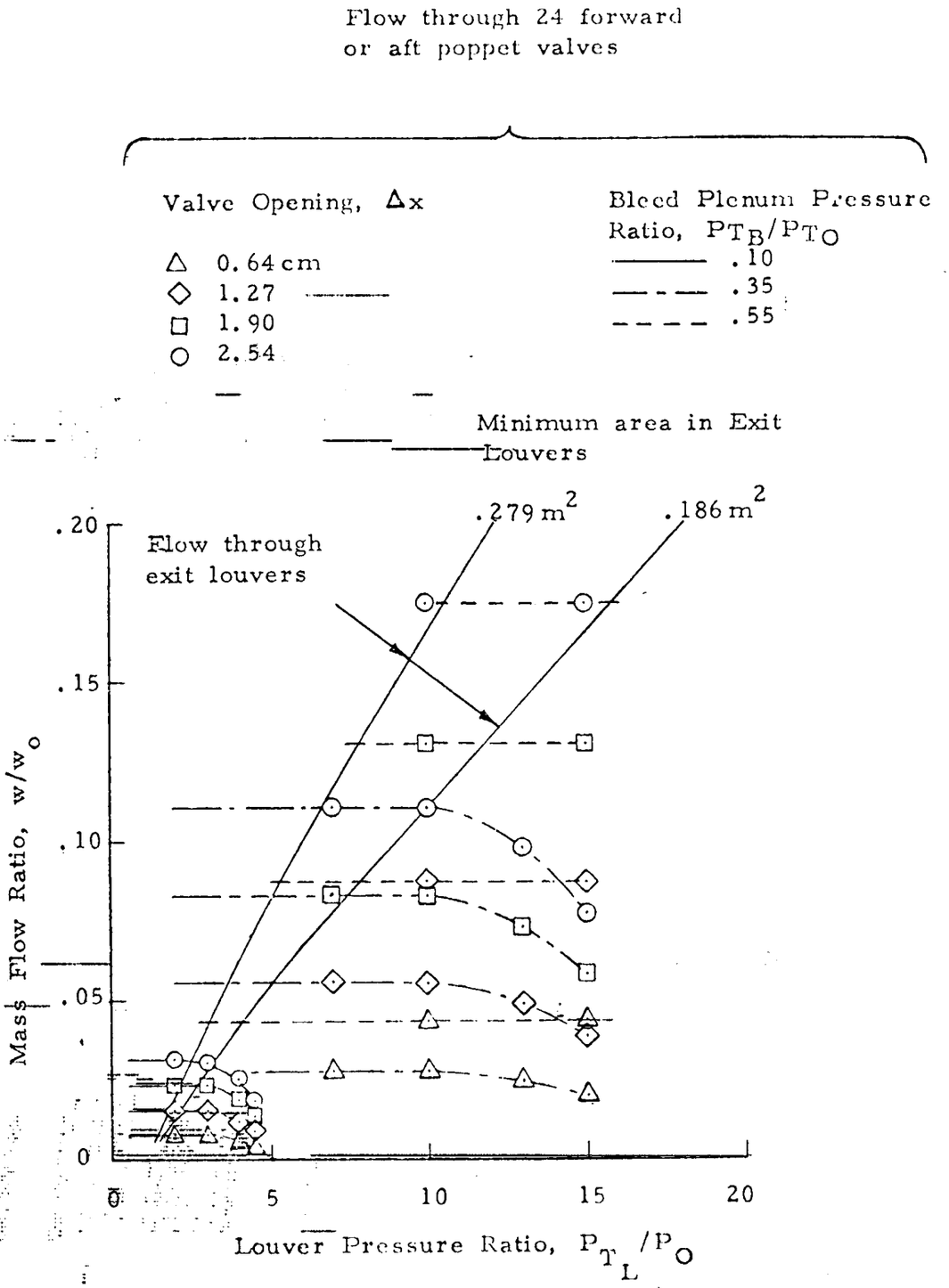


FIGURE 46. EFFECT OF PRESSURE AND VALVE POSITION ON FLOW THROUGH 24 FORWARD OR AFT POPPET VALVES, $M_O$ = 3+

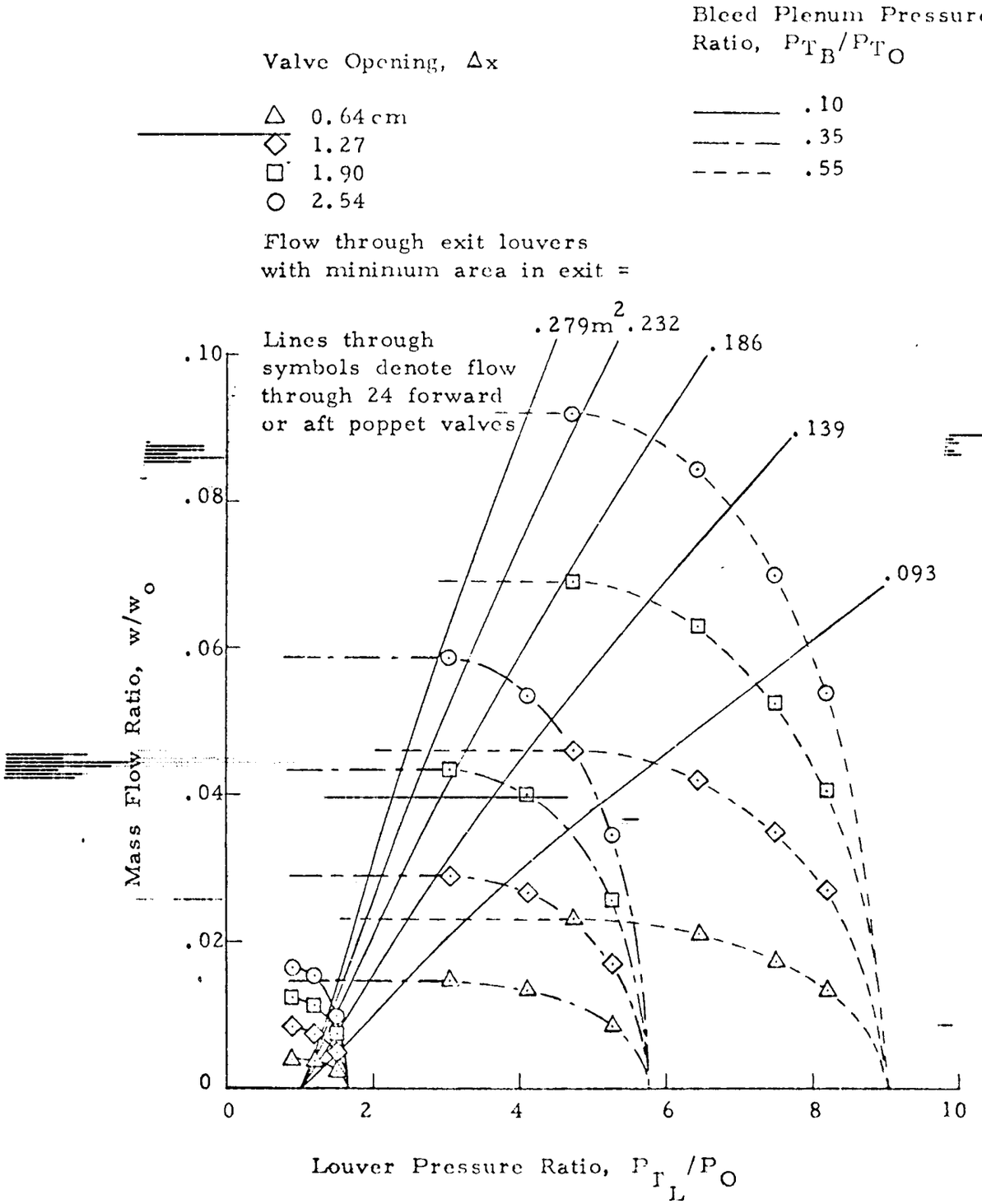


FIGURE 47. EFFECT OF PRESSURE AND VALVE POSITION ON FLOW THROUGH 24 FORWARD OR AFT POPPET VALVES, $M_O$ = 2.47

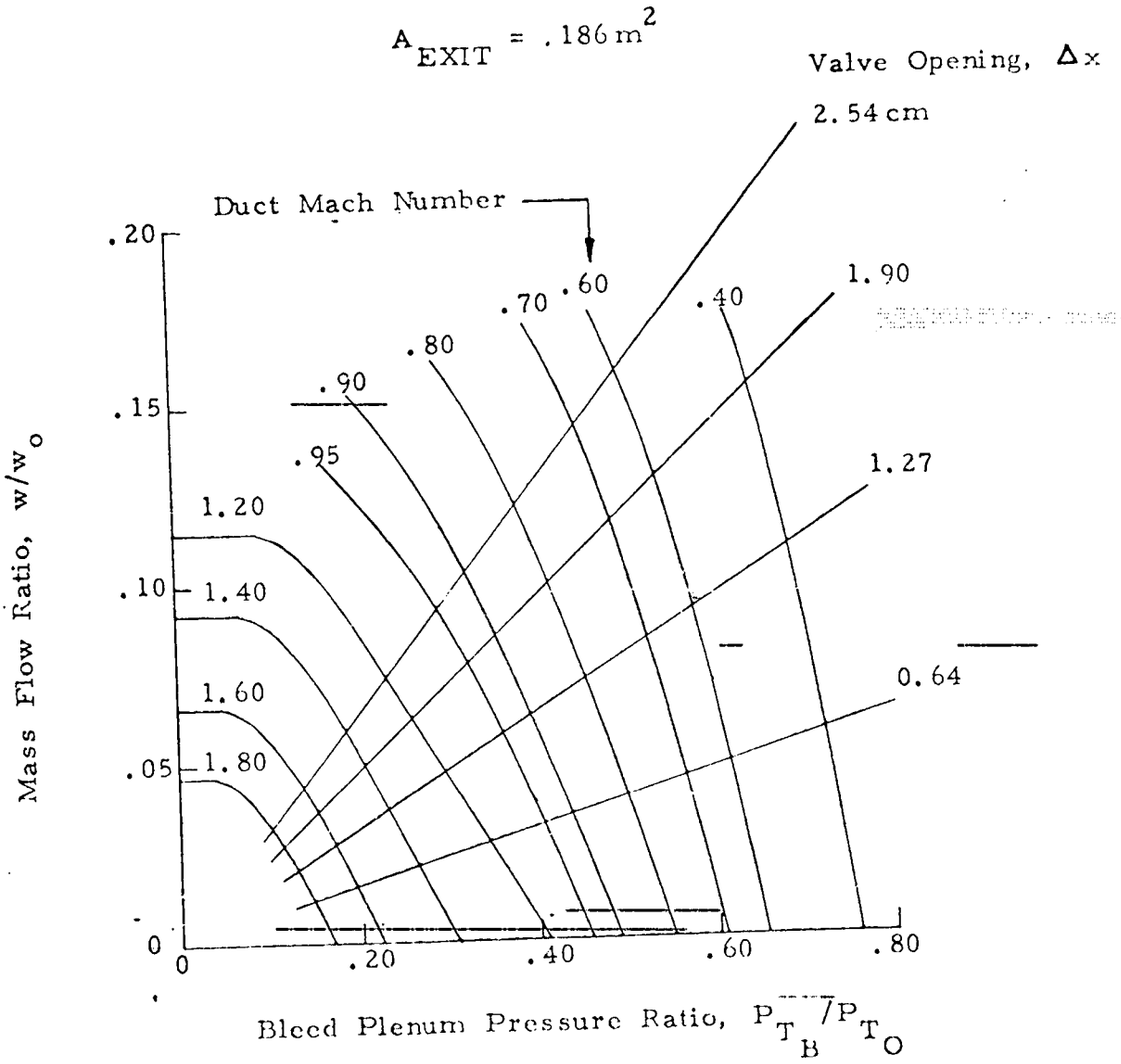


FIGURE 48. EFFECT OF DUCT MACH NUMBER AND VALVE POSITION ON FLOW THROUGH 24 AFT POPPET VALVES, $M_O = 34$

$$A_{EXIT} = .186\,m^2$$

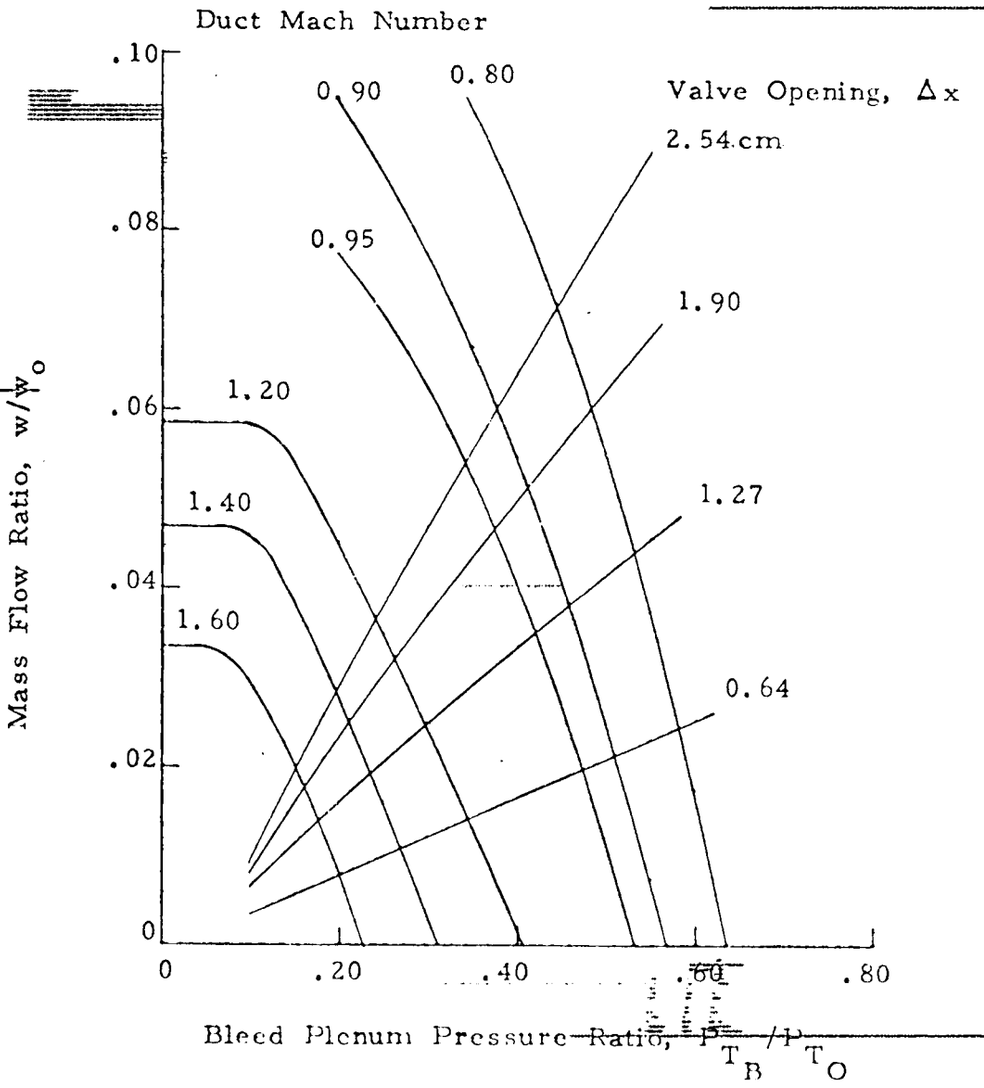


FIGURE 49. EFFECT OF DUCT MACH NUMBER AND VALVE POSITION ON FLOW THROUGH 24 AFT POPPET VALVES, $M_O = 2.47$

$A_{EXIT} = .186\,m^2$

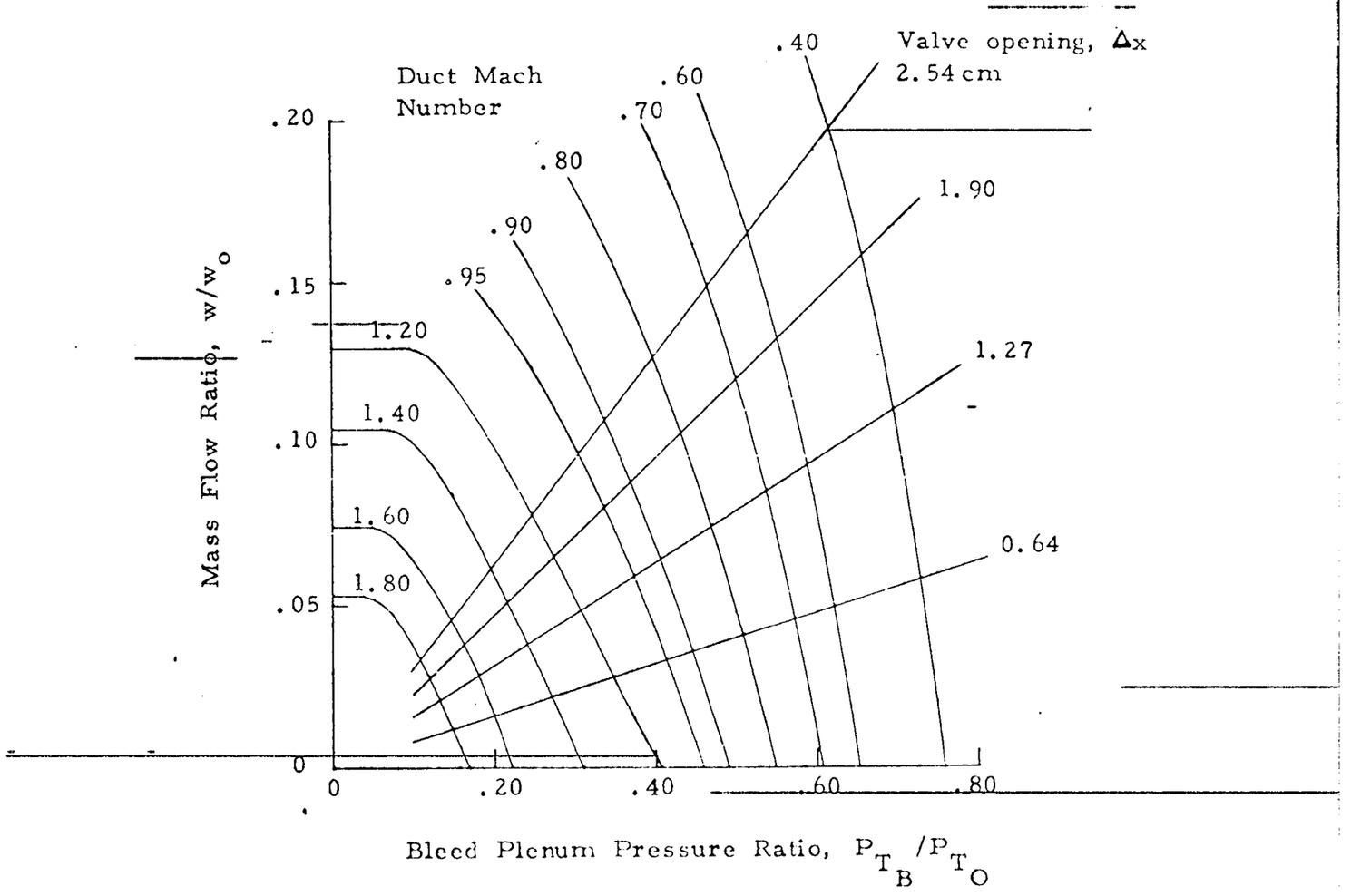


FIGURE 50. EFFECT OF DUCT MACH NUMBER AND VALVE POSITION ON FLOW THROUGH 24 FORWARD POPPET VALVES, $M_O$ = 3+

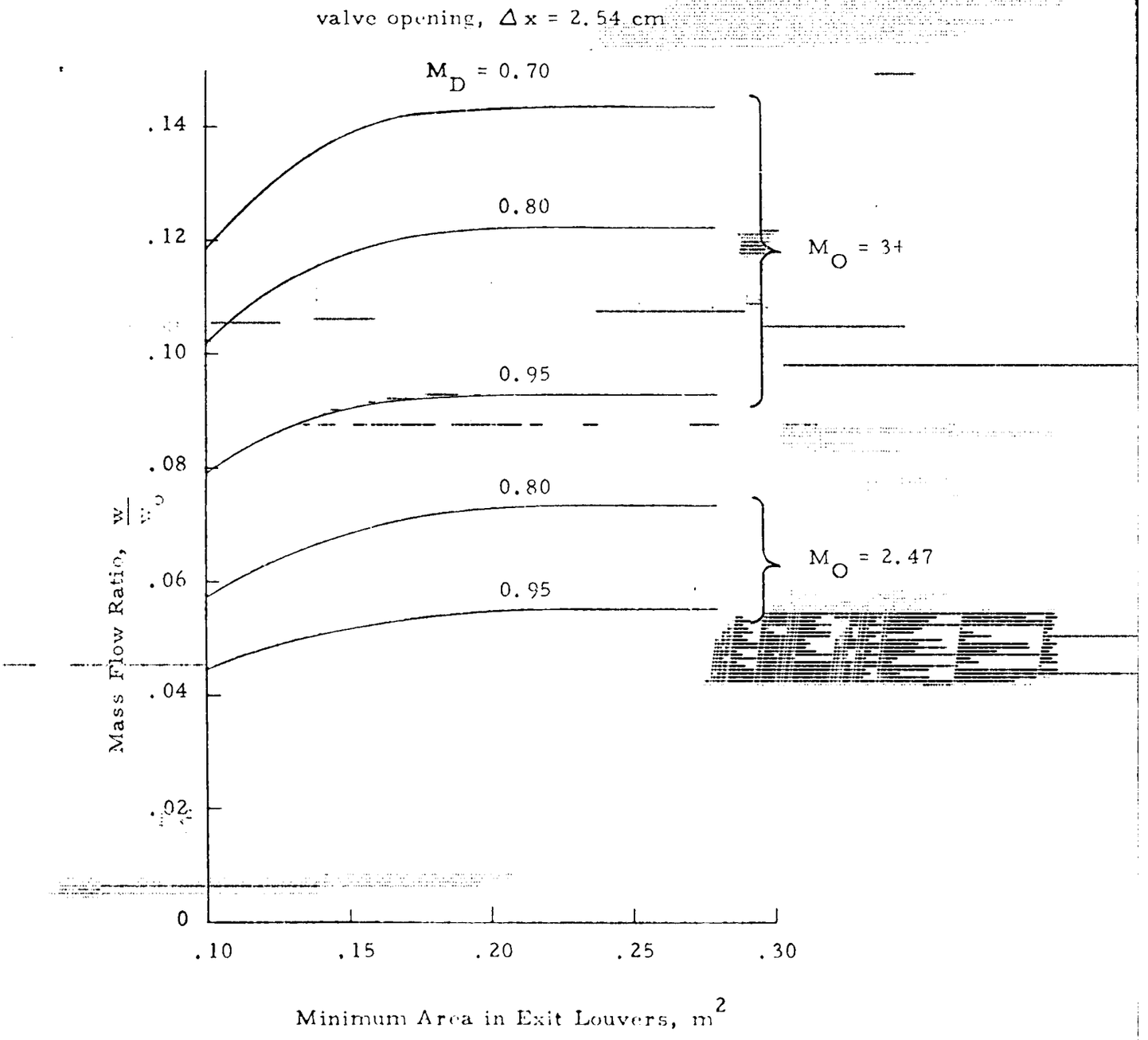


FIGURE 51. EFFECT OF EXIT LOUVER AREA ON FLOW THROUGH 24 AFT POPPET VALVES

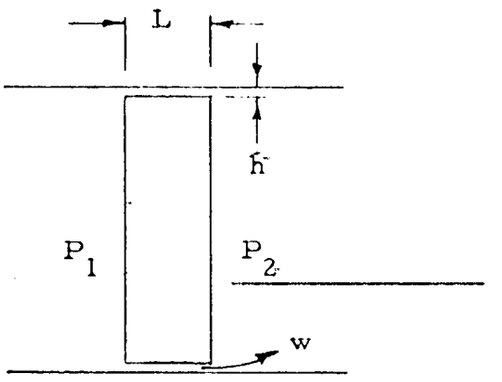


$$w = \frac{g_o \bar{\rho} h^2 A \Delta p}{12 \mu L}$$

where:

| | | |
|---|---|---|
| $g_o$ | = | 100 cm kg/N $s^2$ |
| $\bar{\rho}$ | = | average density in leakage path, $kg/cm^3$ |
| h | = | piston clearance, cm |
| A | = | leakage area, $cm^2$ |
| $\Delta p$ | = | pressure drop along leakage path, $N/cm^2$ |
| $\mu$ | = | viscosity, kg/s cm |
| L | = | length of leakage path, cm |
| w | = | flow rate, kg/s |

FIGURE 52. PISTON LEAKAGE FLOW

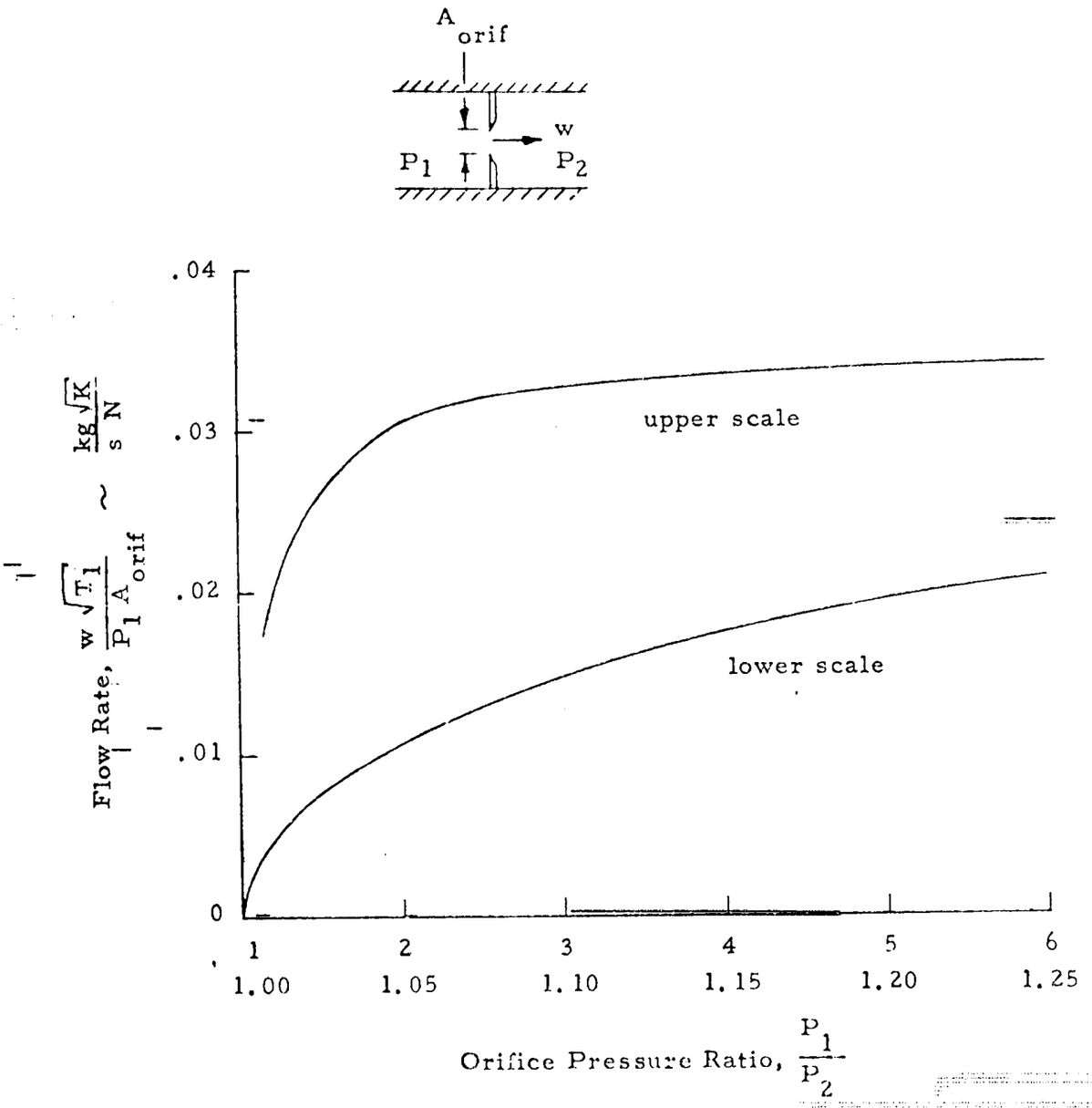


FIGURE 53. ORIFICE FLOW CHARACTERISTICS

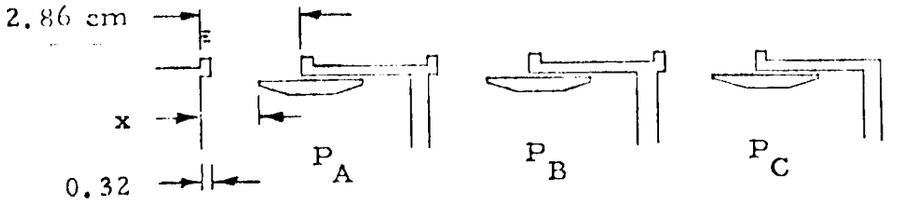


$$F_{aerodynamic} = C_1 (P_A + P_B + P_C)$$

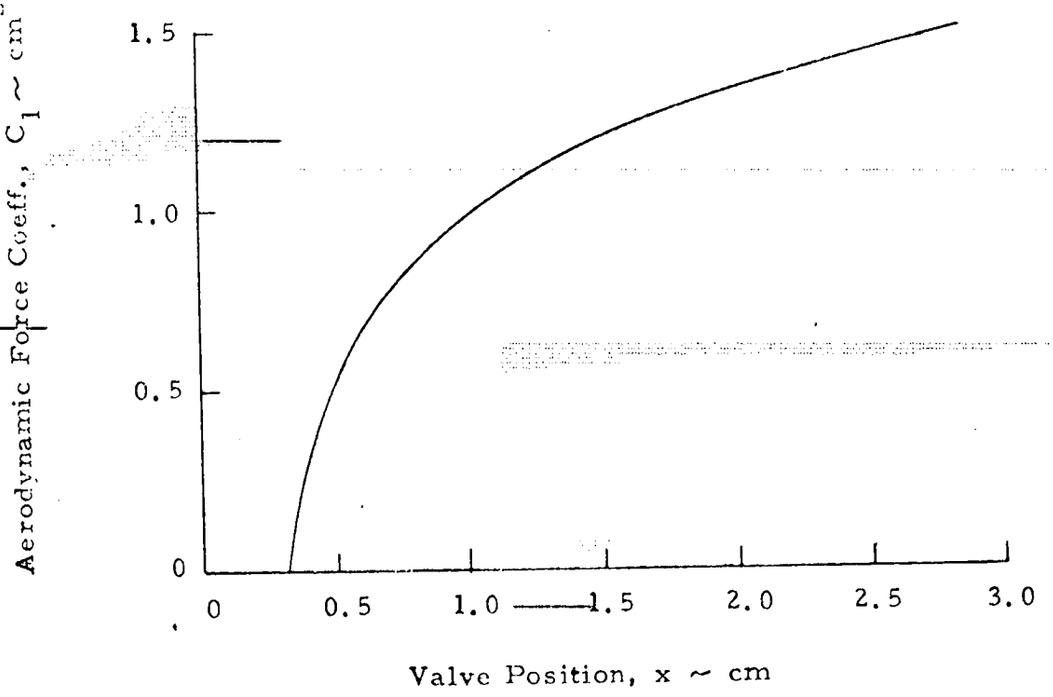


FIGURE 54. AERODYNAMIC FORCE ON SLIDE VALVE

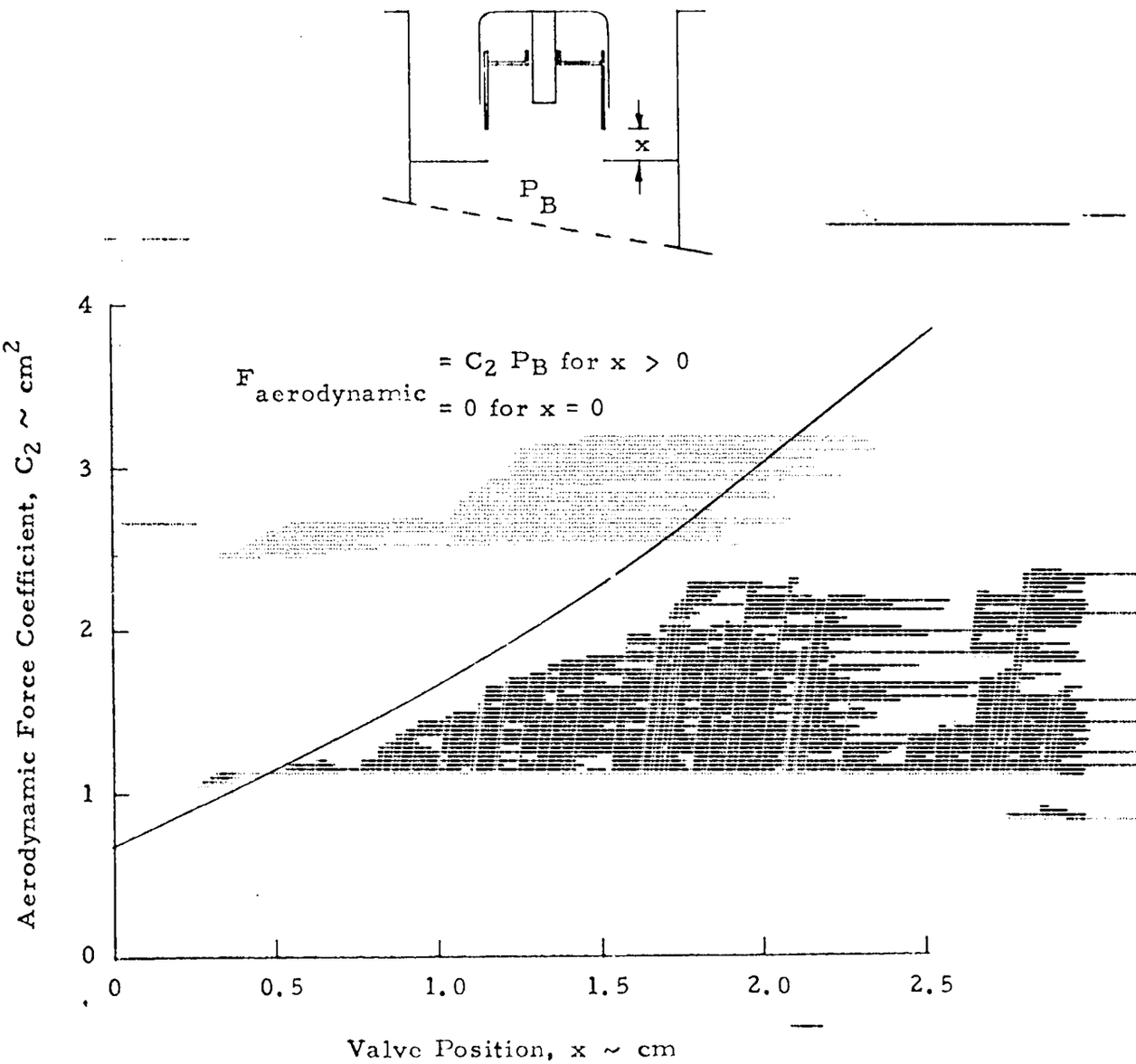


FIGURE 55. AERODYNAMIC FORCE ON UNSHIELDED POPPET VALVE

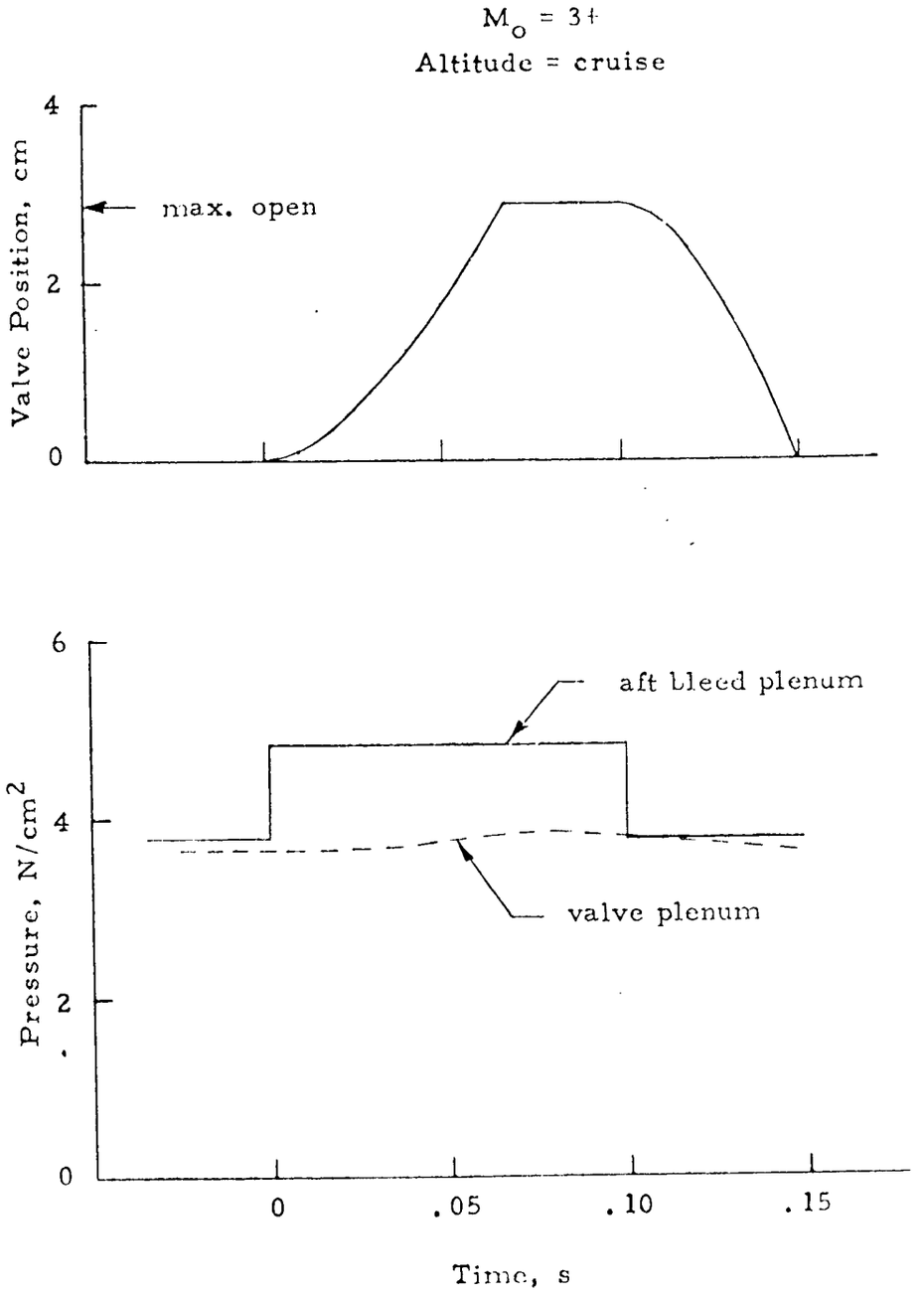


FIGURE 56. RESPONSE OF SLIDE-VALVE TO STEP CHANGE IN BLEED PRESSURE

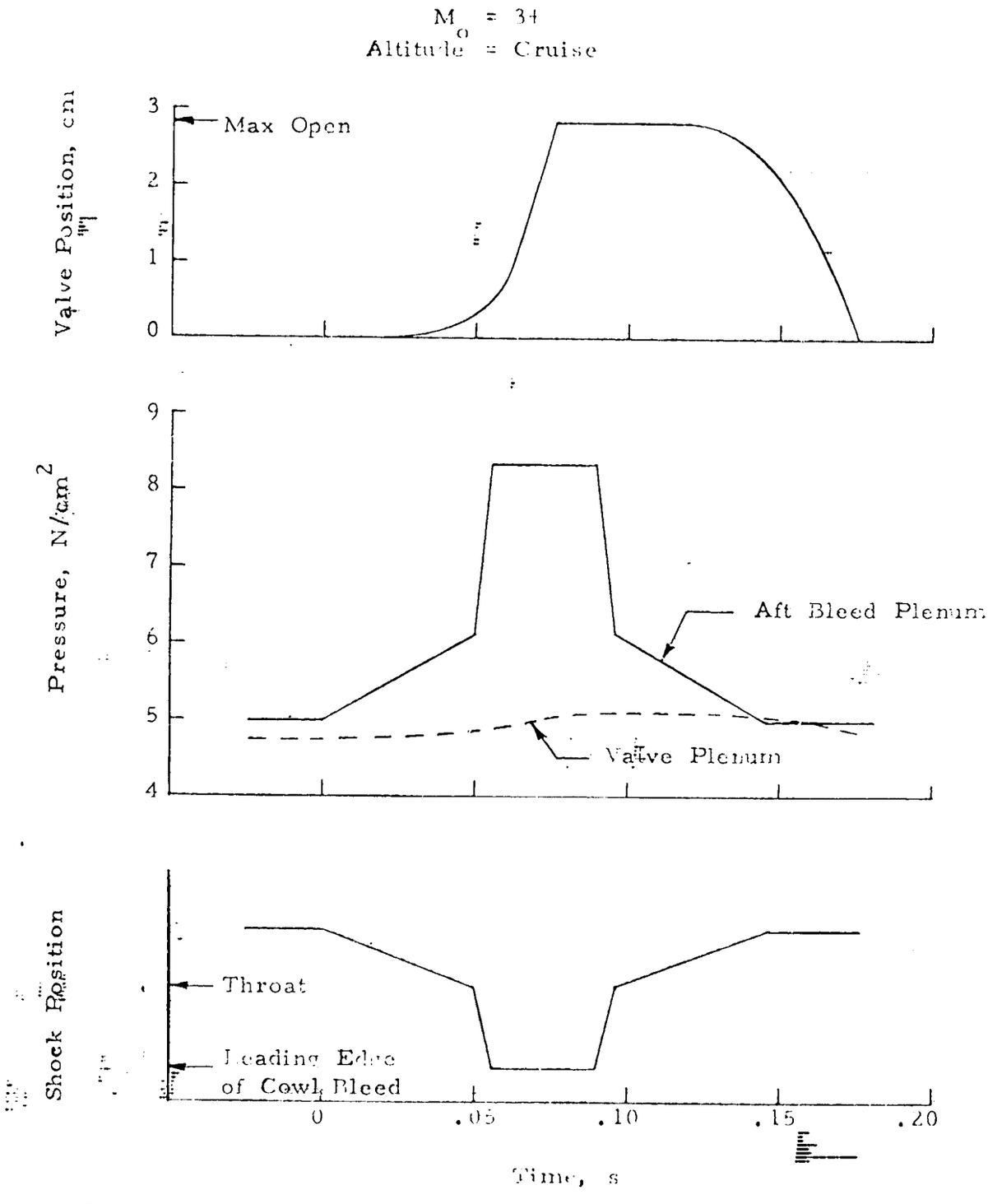


FIGURE 57. RESPONSE OF SLIDE VALVE TO TERMINAL SHOCK MOVEMENT

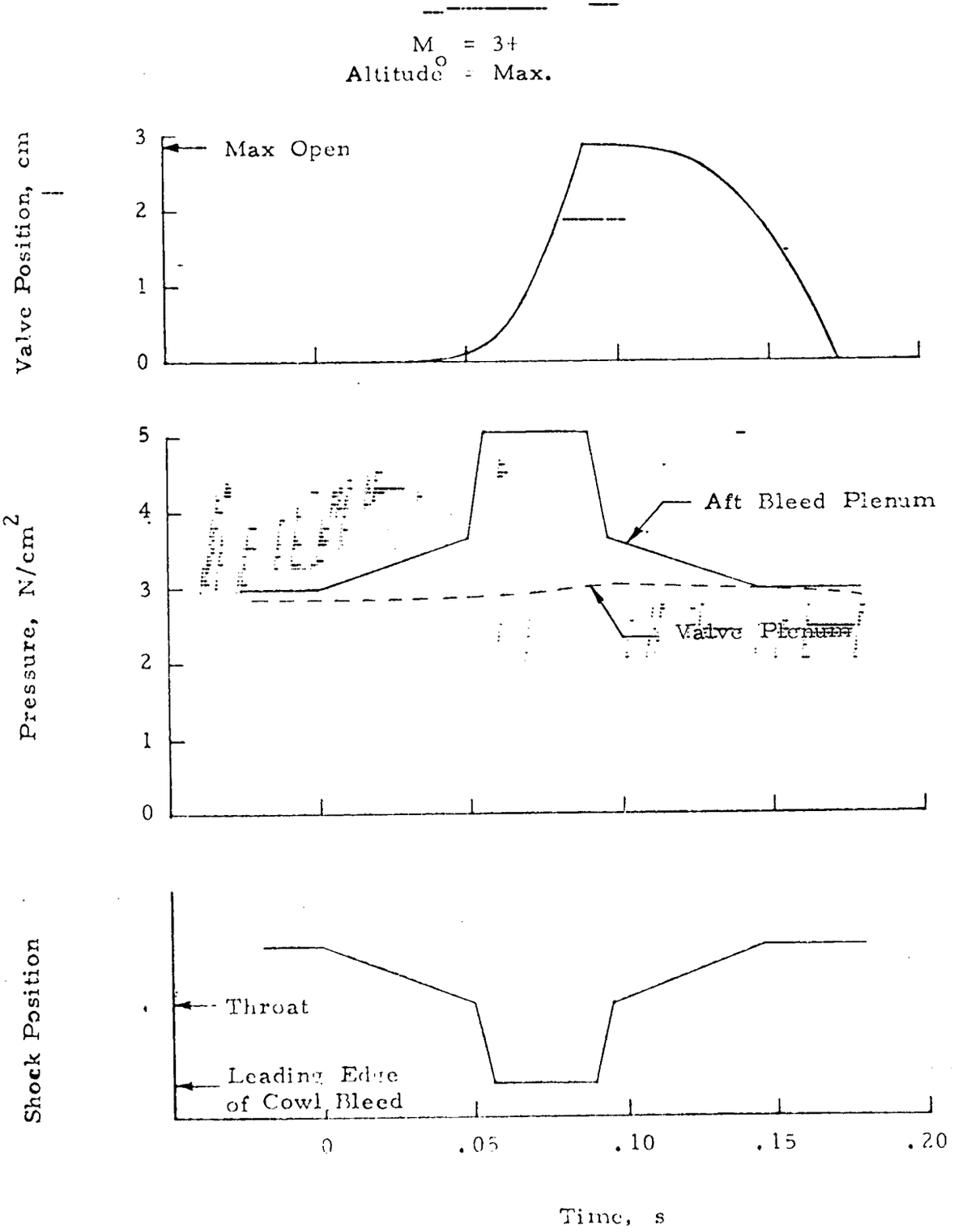


FIGURE 58. RESPONSE OF SLIDE VALVE TO TERMINAL SHOCK MOVEMENT

$M_o$ = 3+
Altitude = Cruise

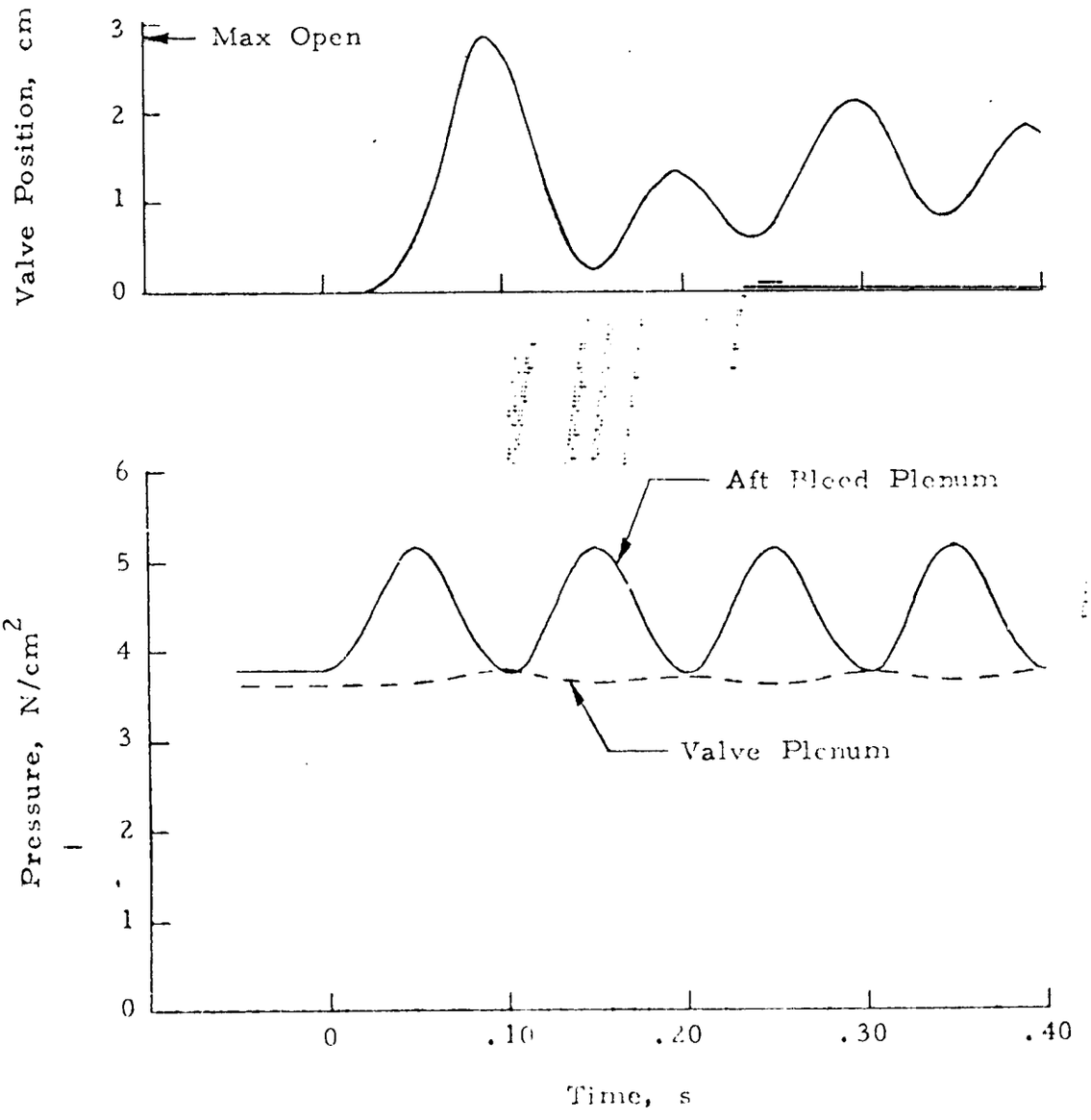


FIGURE 59. RESPONSE OF SLIDE VALVE TO 10 HERTZ BLEED PRESSURE OSCILLATION

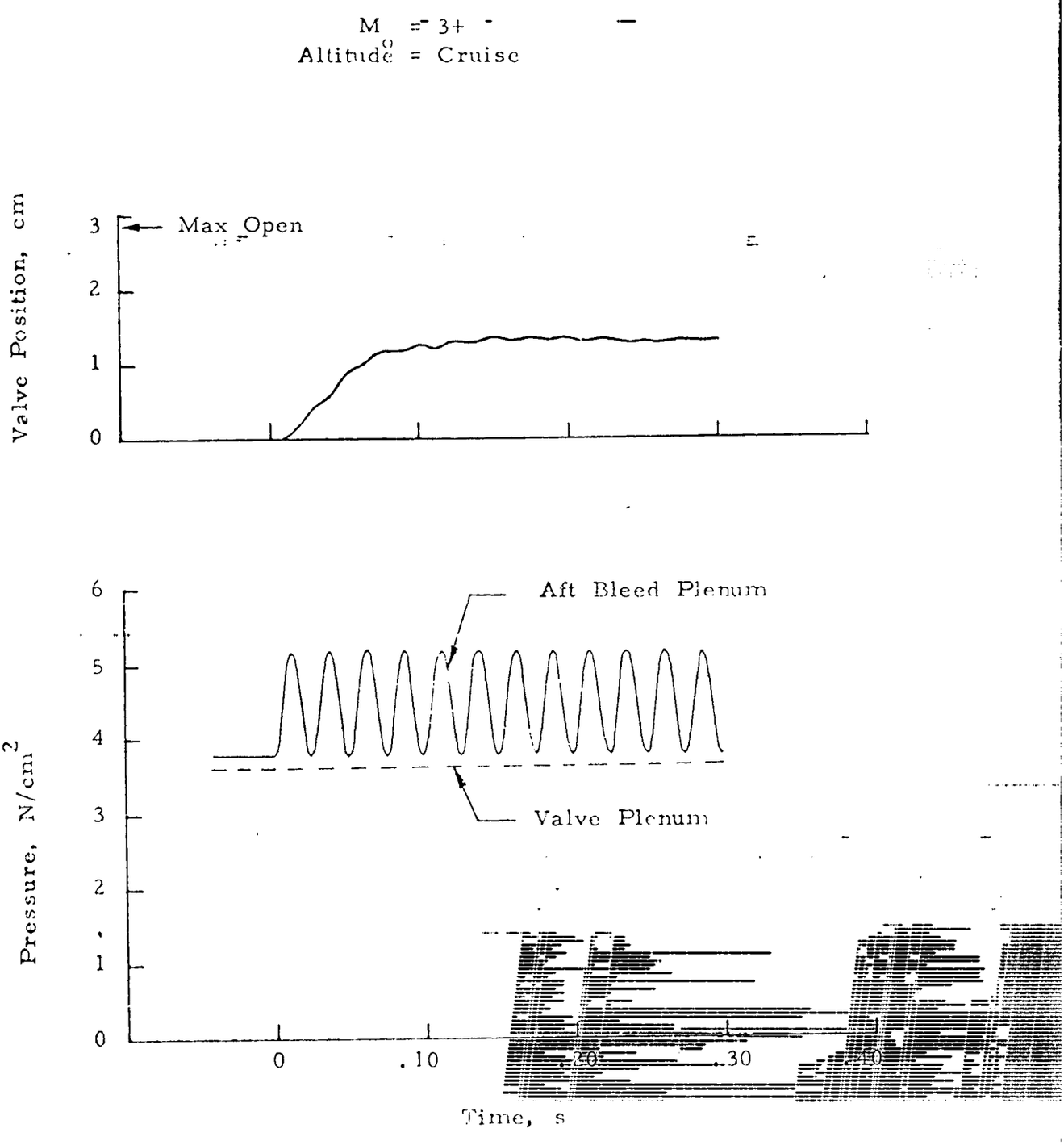


FIGURE 60. RESPONSE OF SLIDE VALVE TO 40 HERTZ BLEED PRESSURE OSCILLATION

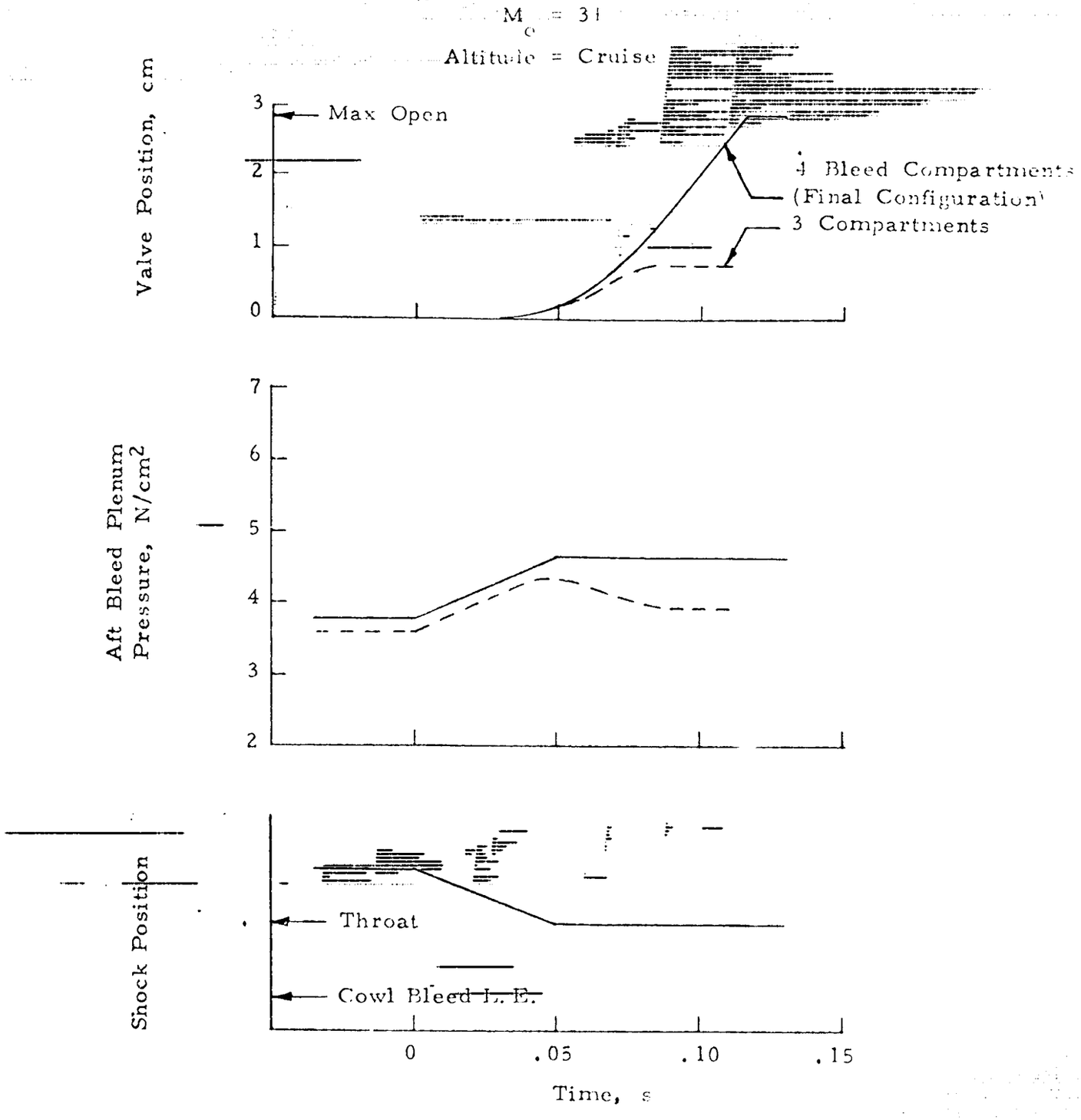


FIGURE 61. EFFECT OF BLEED COMPARTMENTATION ON SLIDE VALVE RESPONSE

$M_o$ = 3+

Altitude = Cruise

Preliminary Configuration
with Orifice Damper Valve

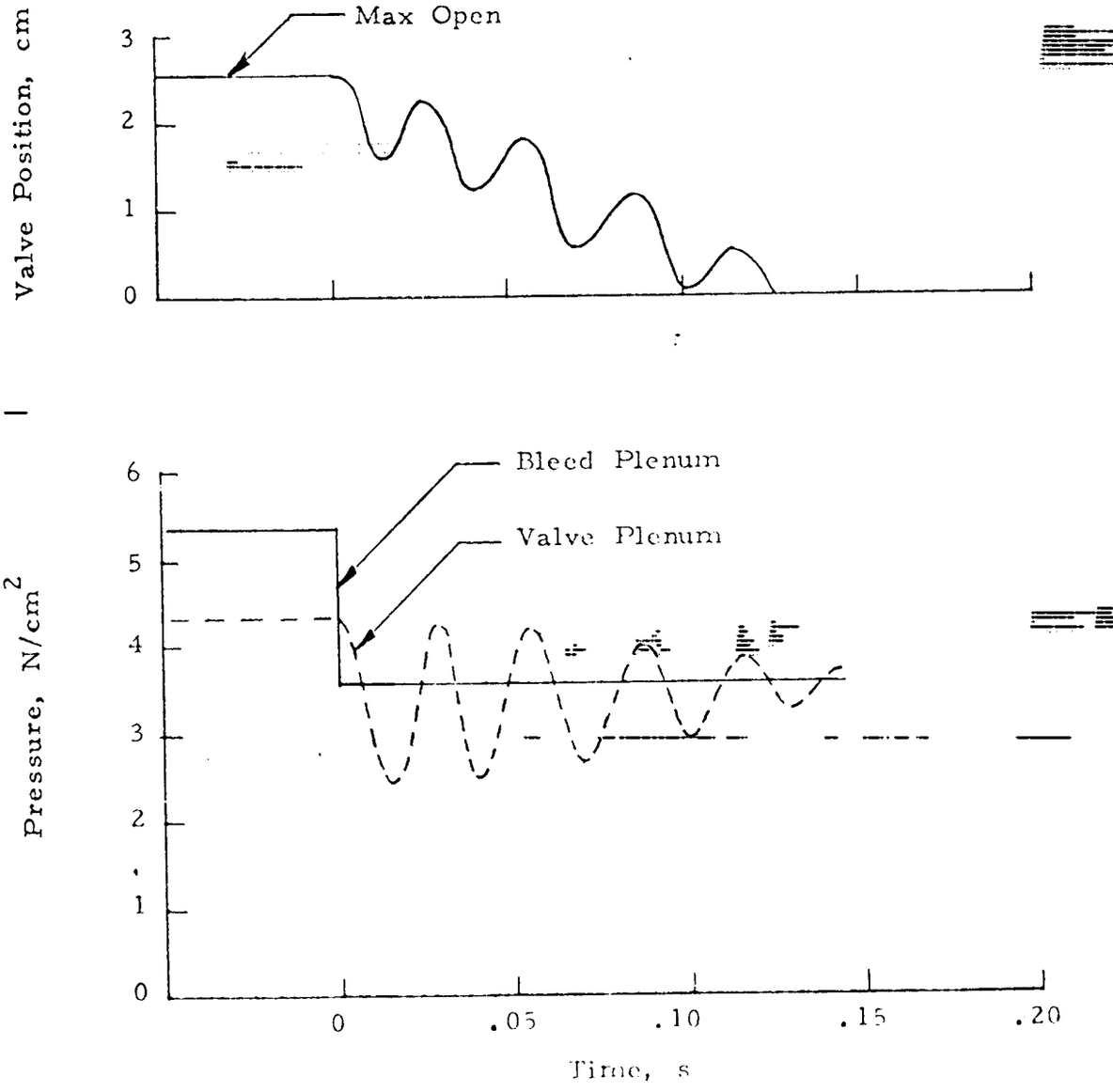


FIGURE 62. AFT POPPET VALVE CLOSING DYNAMICS

$M_o$ = 3+

Altitude = Cruise

Preliminary Configuration
with Orifice Damper Valve

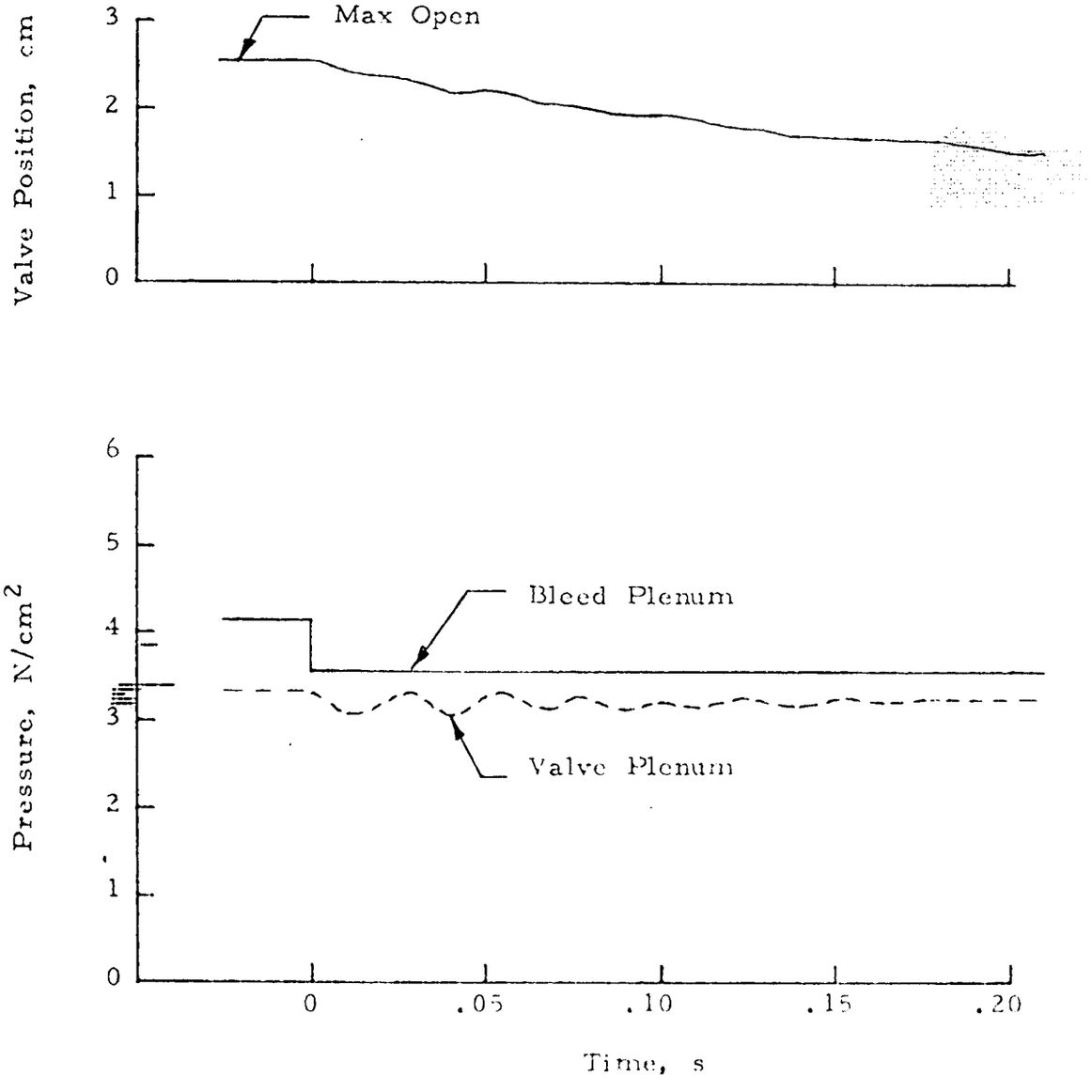


FIGURE 63. AFT POPPET VALVE CLOSING DYNAMICS

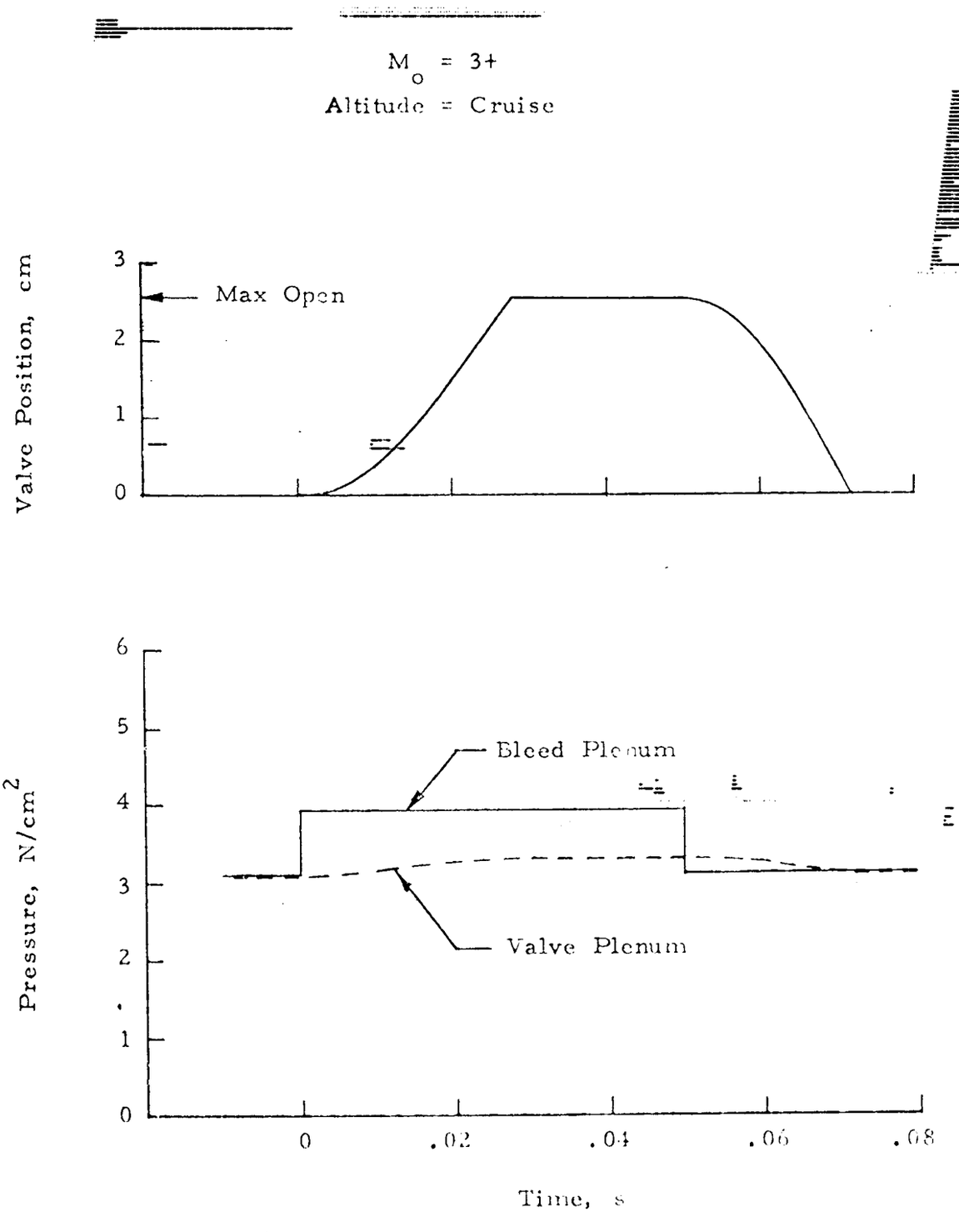


FIGURE 64. RESPONSE OF UNSHIELDED AFT POPPET VALVE TO 27 PERCENT STEP CHANGE IN BLEED PRESSURE

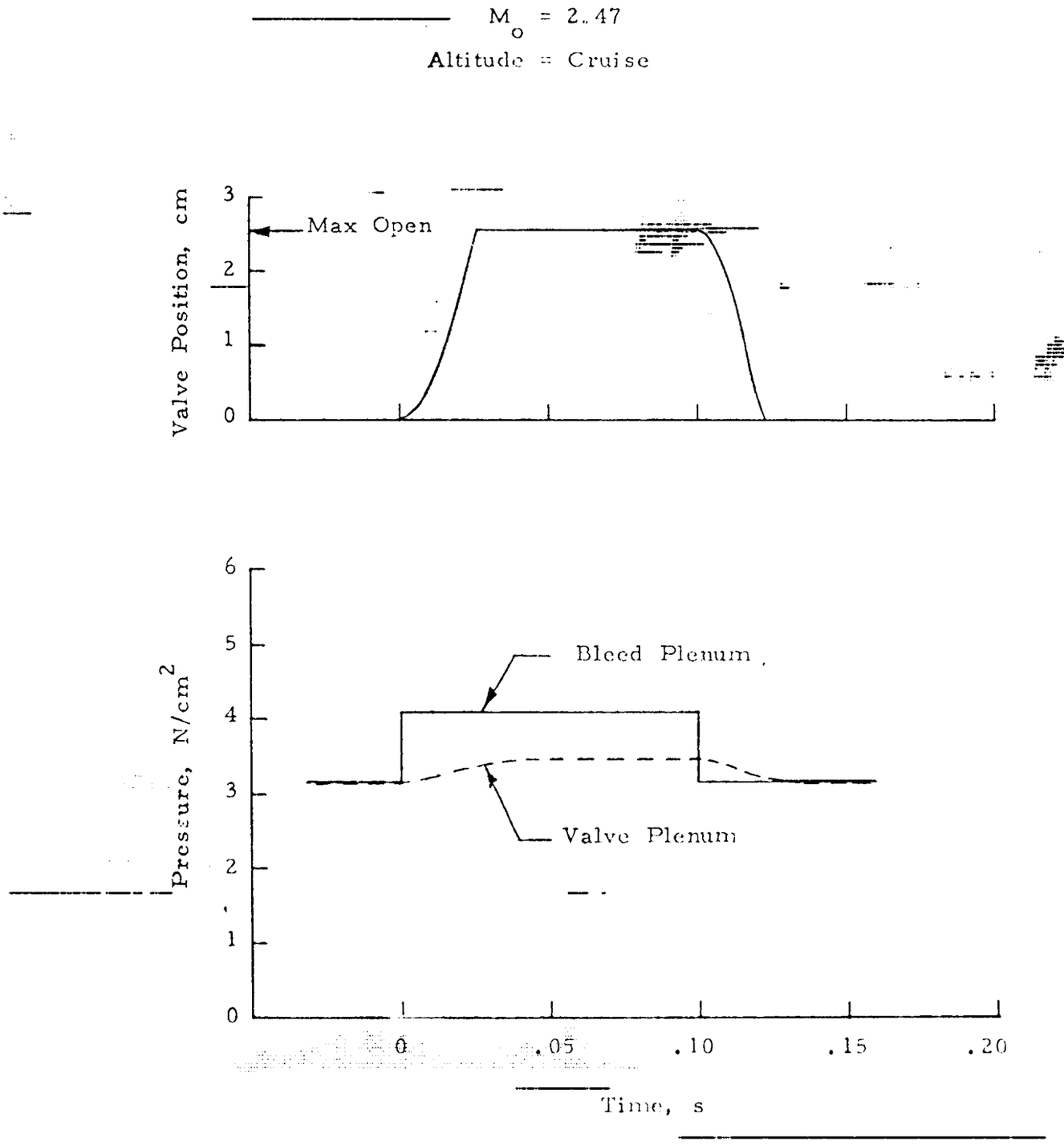


FIGURE 65. RESPONSE OF UNSHIELDED AFT POPPET VALVE TO 27 PERCENT STEP CHANGE IN BLEED PRESSURE

$M_o$ = 3+

Altitude = Cruise

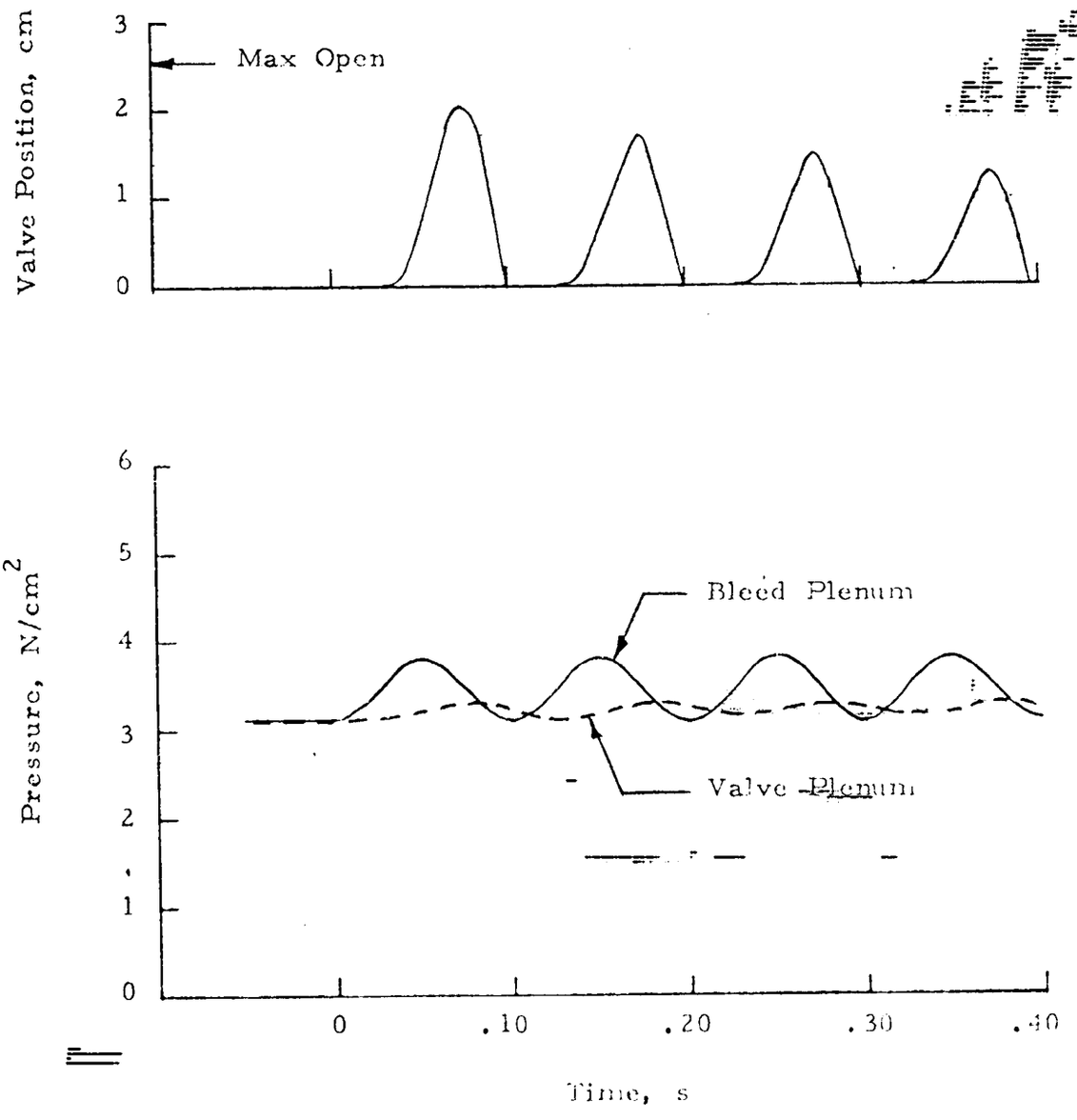


FIGURE 66. RESPONSE OF UNSHIELDED AFT POPPET VALVE TO 10 HERTZ BLEED PRESSURE OSCILLATION

$M_o$ = 3+

Altitude = Cruise

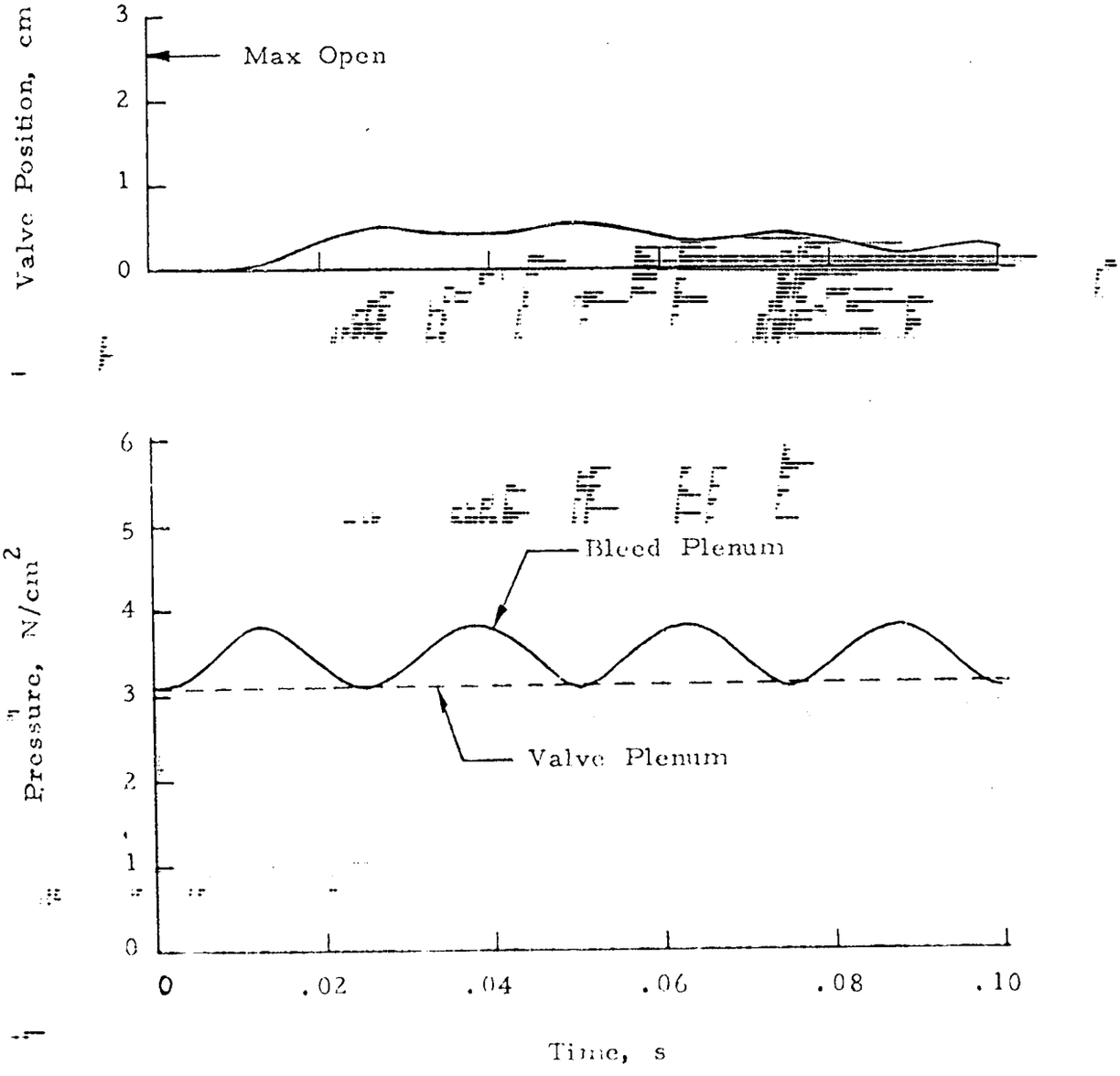


FIGURE 67. RESPONSE OF UNSHIELDED AFT POPPET VALVE TO 40 HERTZ BLEED PRESSURE OSCILLATION

$M_o$ = 3+

Altitude = Min.

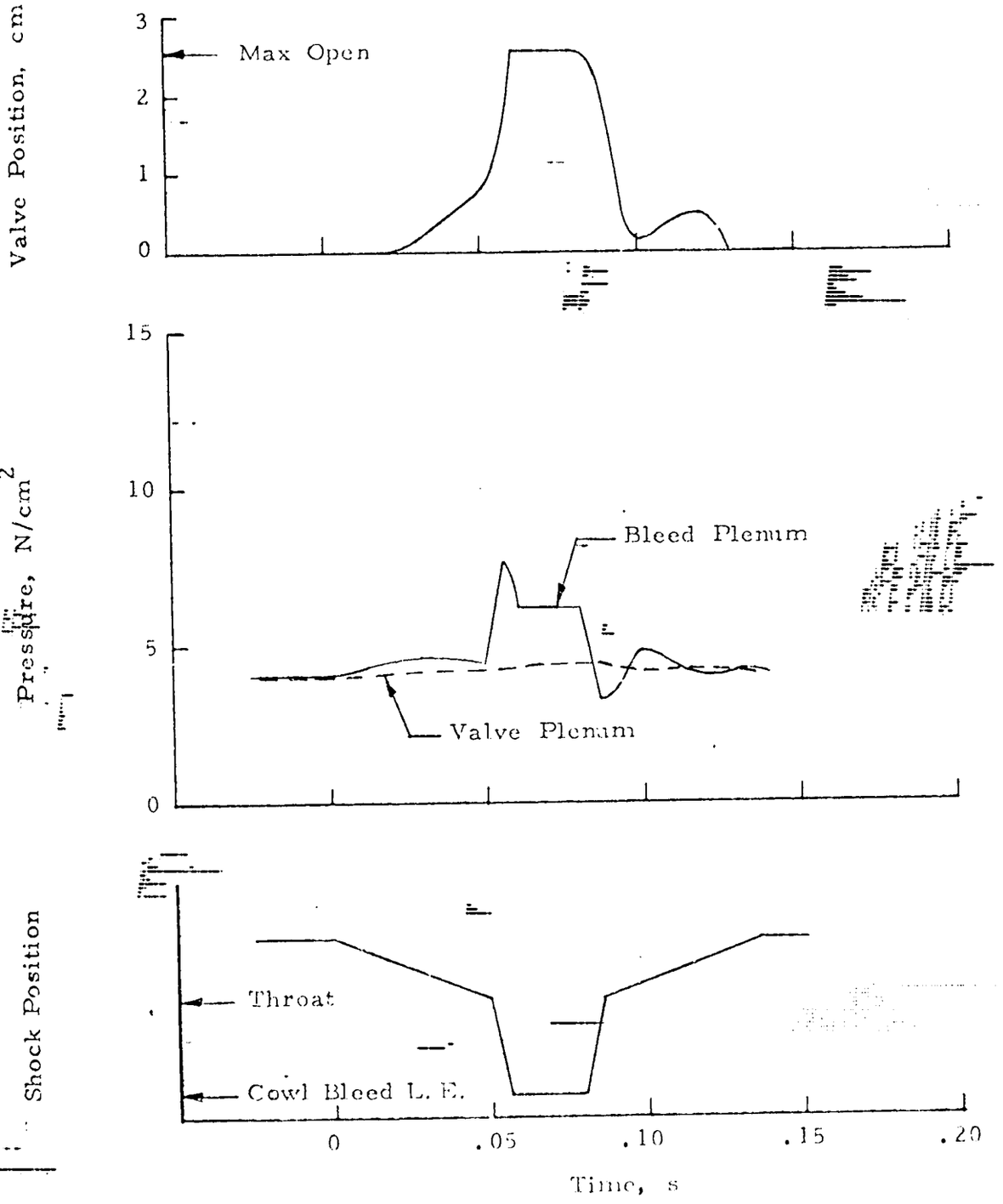


FIGURE 66. RESPONSE OF RESPELLED AFT POPPET VALVE TO TERMINAL SHOCK MOVEMENT

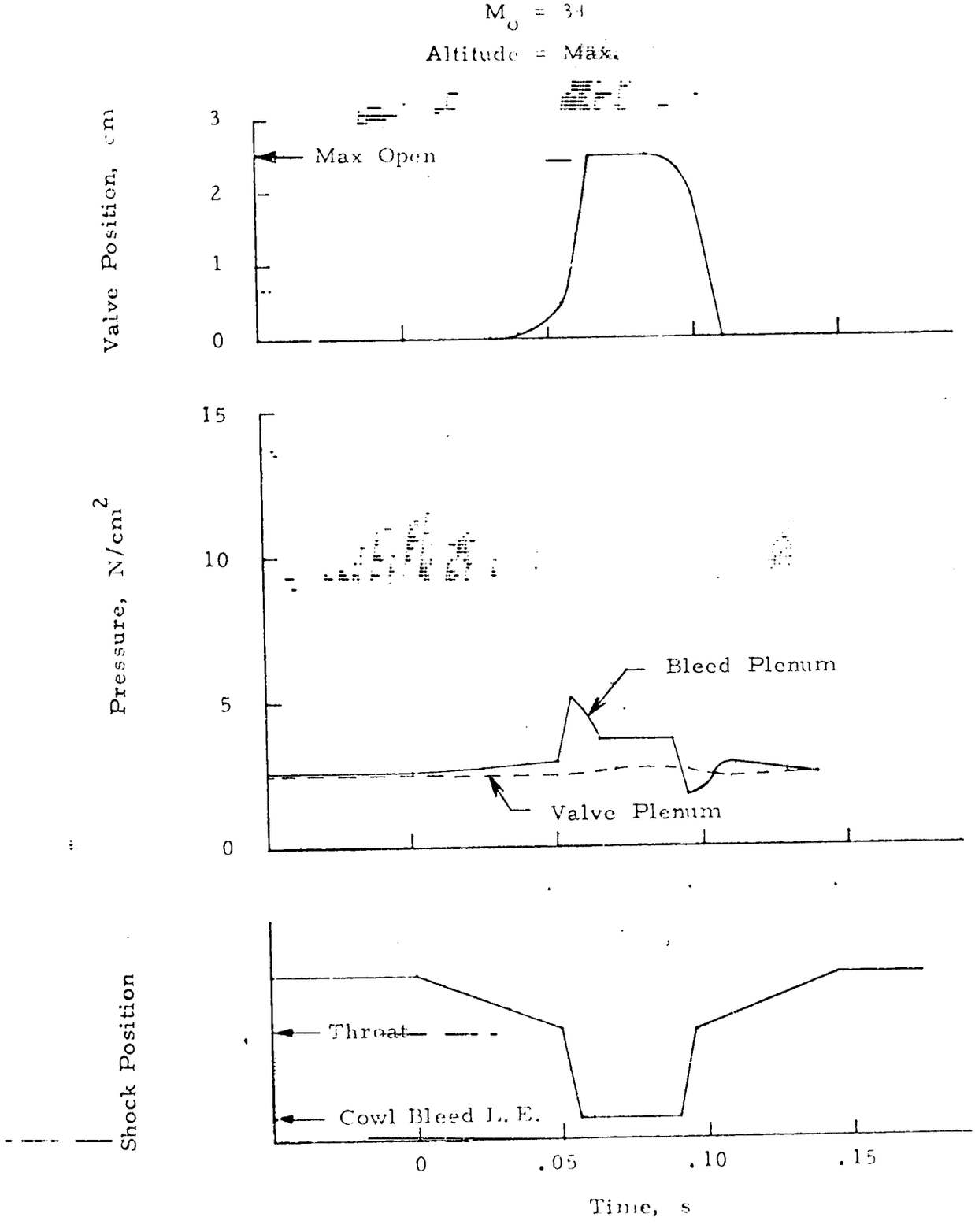


FIGURE 69. RESPONSE OF UNSHIELDED AFT POPPET VALVE TO TERMINAL SHOCK MOVEMENT

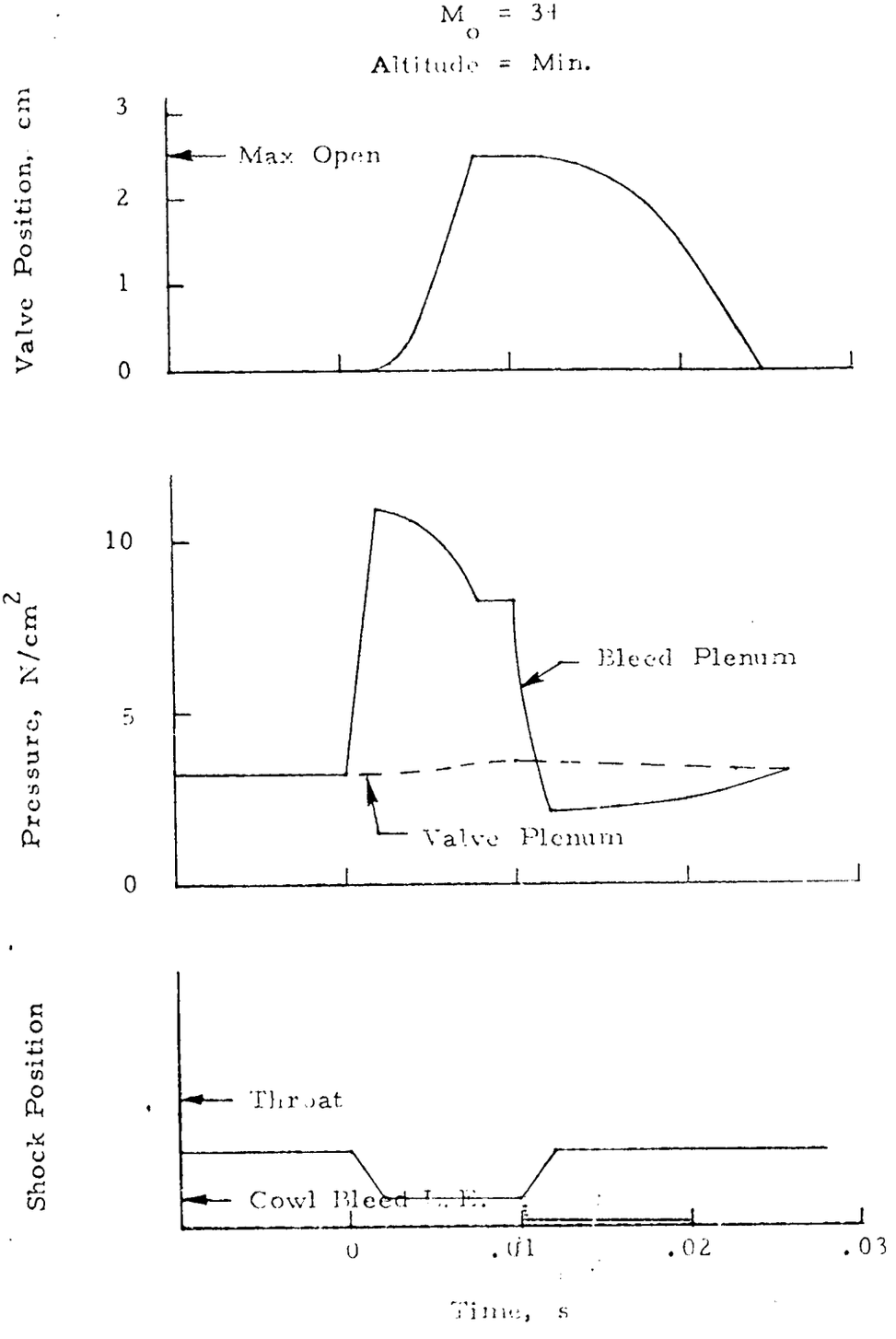


FIGURE 70. RESPONSE OF UNSHIELDED FORWARD POPPET VALVE TO TERMINAL-SHOCK MOVEMENT

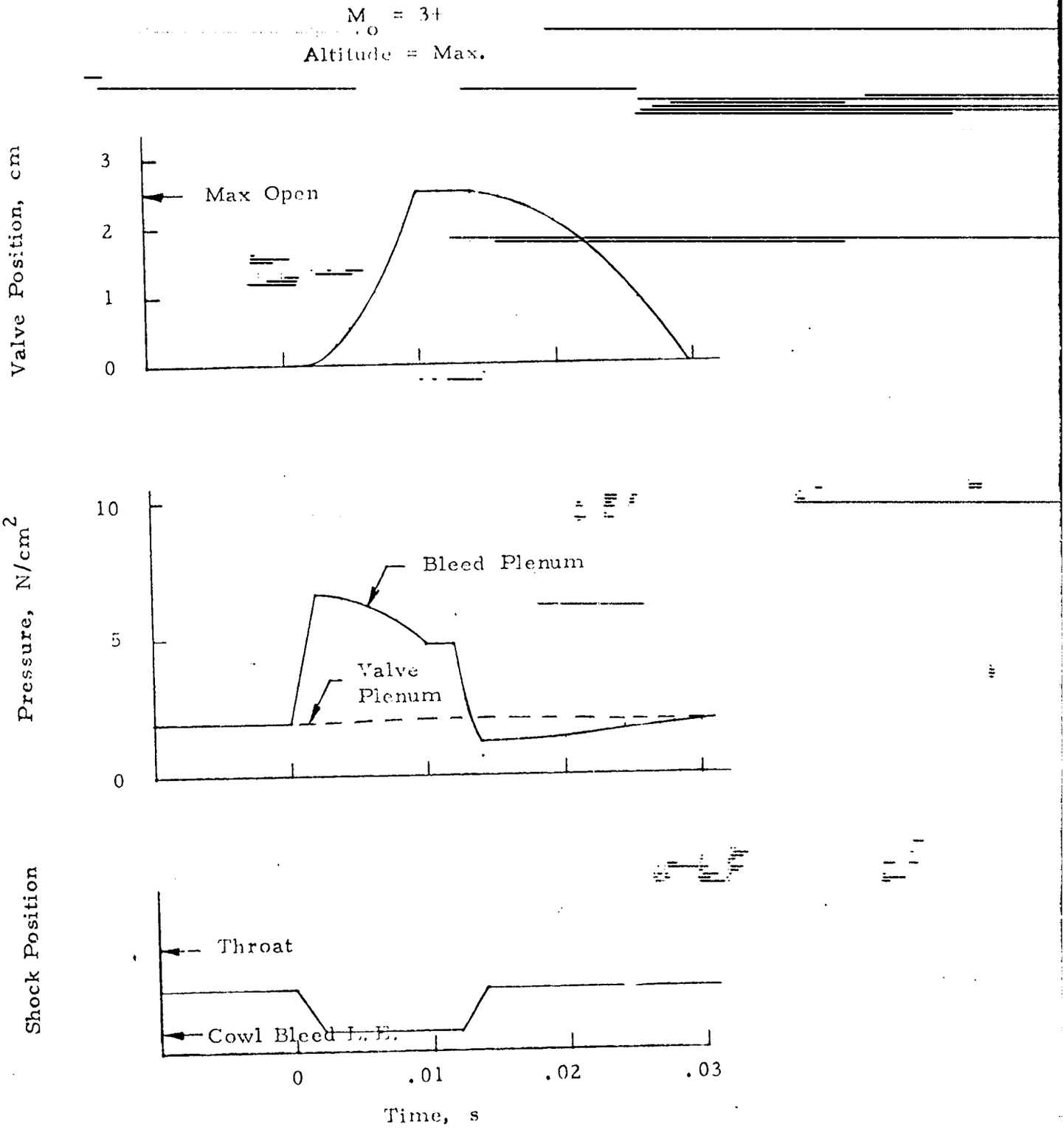


FIGURE 71. RESPONSE OF UNSHIELDED FORWARD POPPET VALVE TO TERMINAL SHOCK MOVEMENT

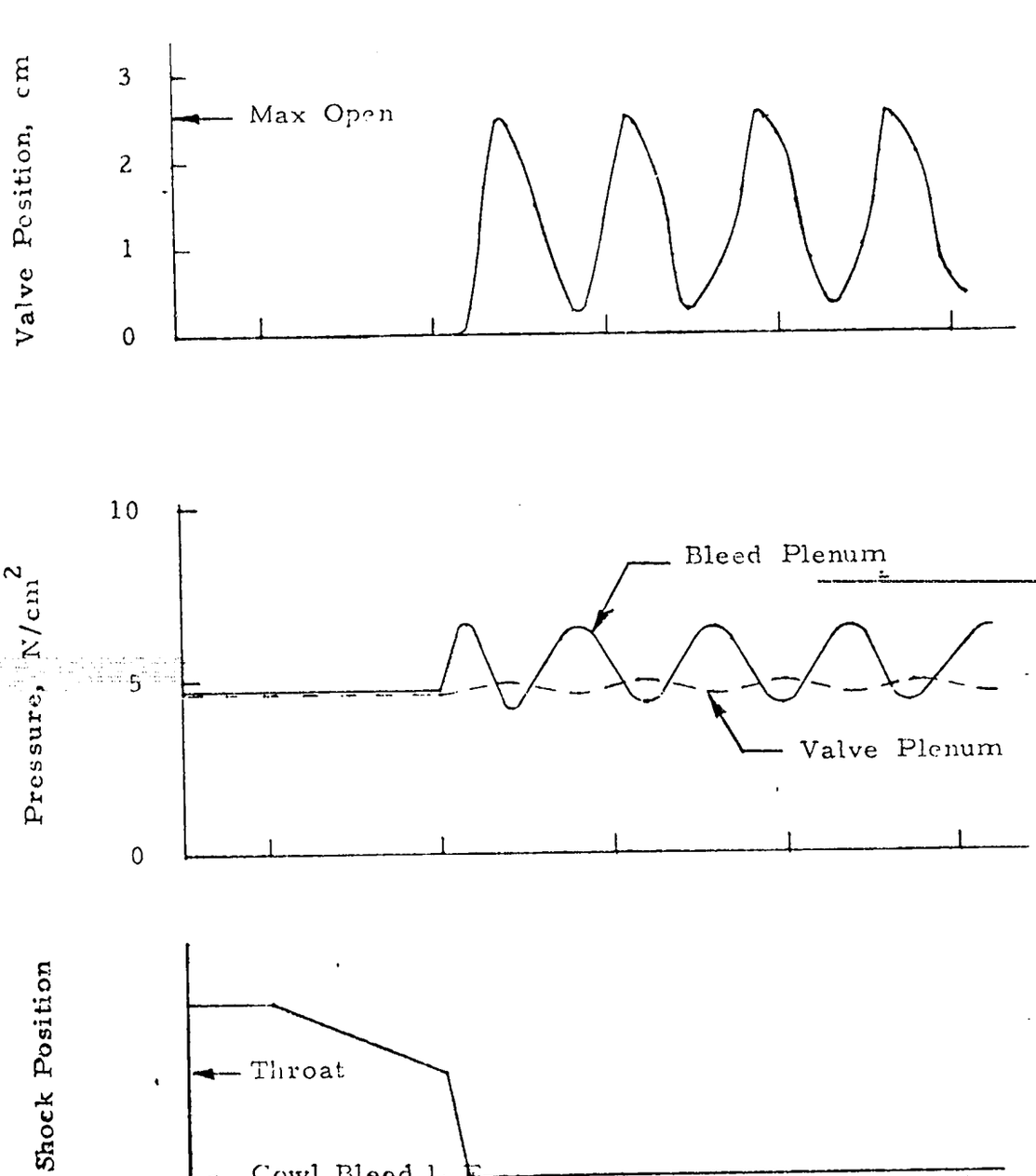


FIGURE 72. RESPONSE OF UNSHIELDED AFT POPPET VALVE TO TERMINAL SHOCK MOVEMENT

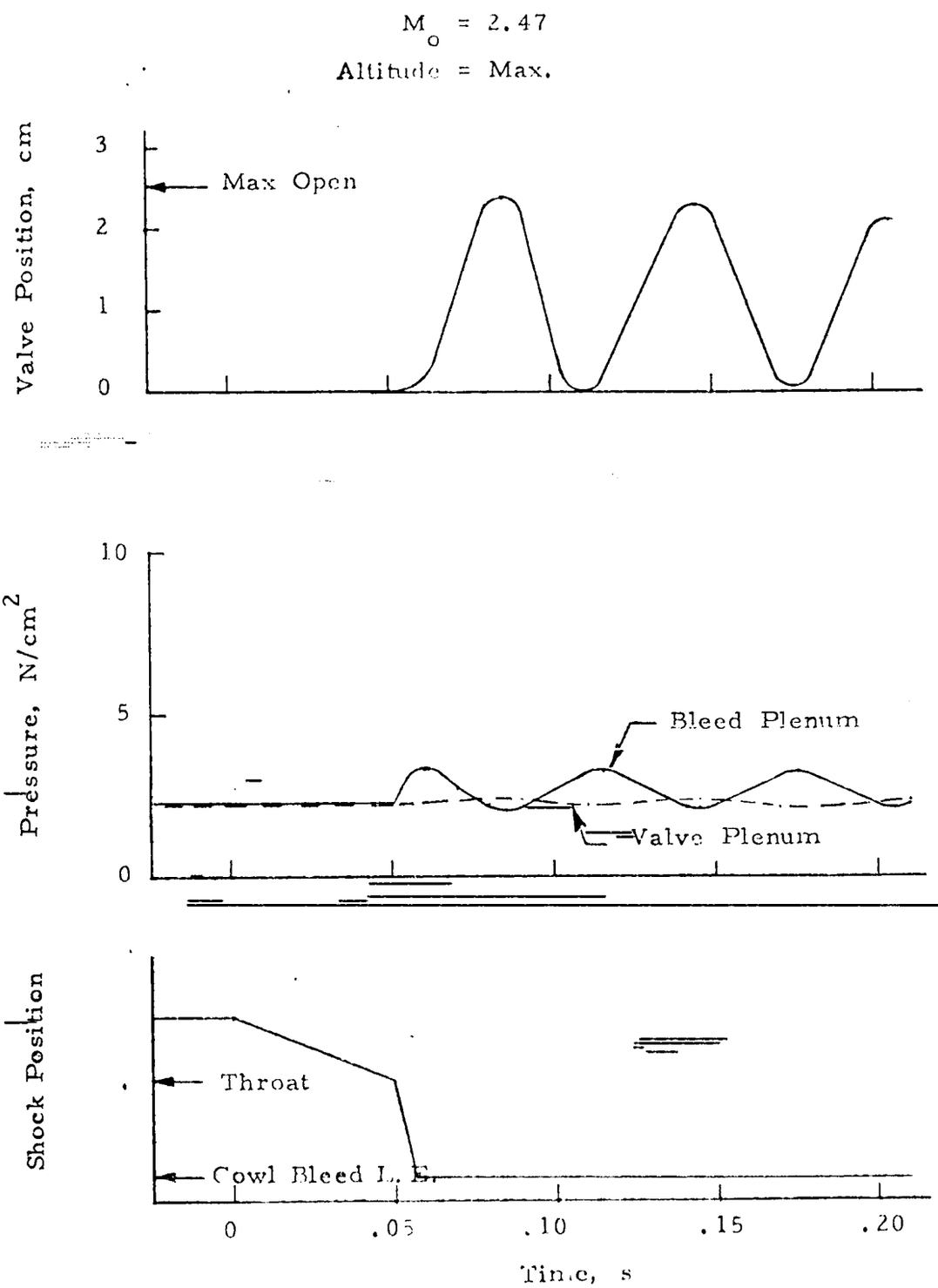


FIGURE 73. RESPONSE OF UNSHIELDED AFT POPPET VALVE TO TERMINAL SHOCK MOVEMENT

$M_o$ = 2.47

Altitude = Min.

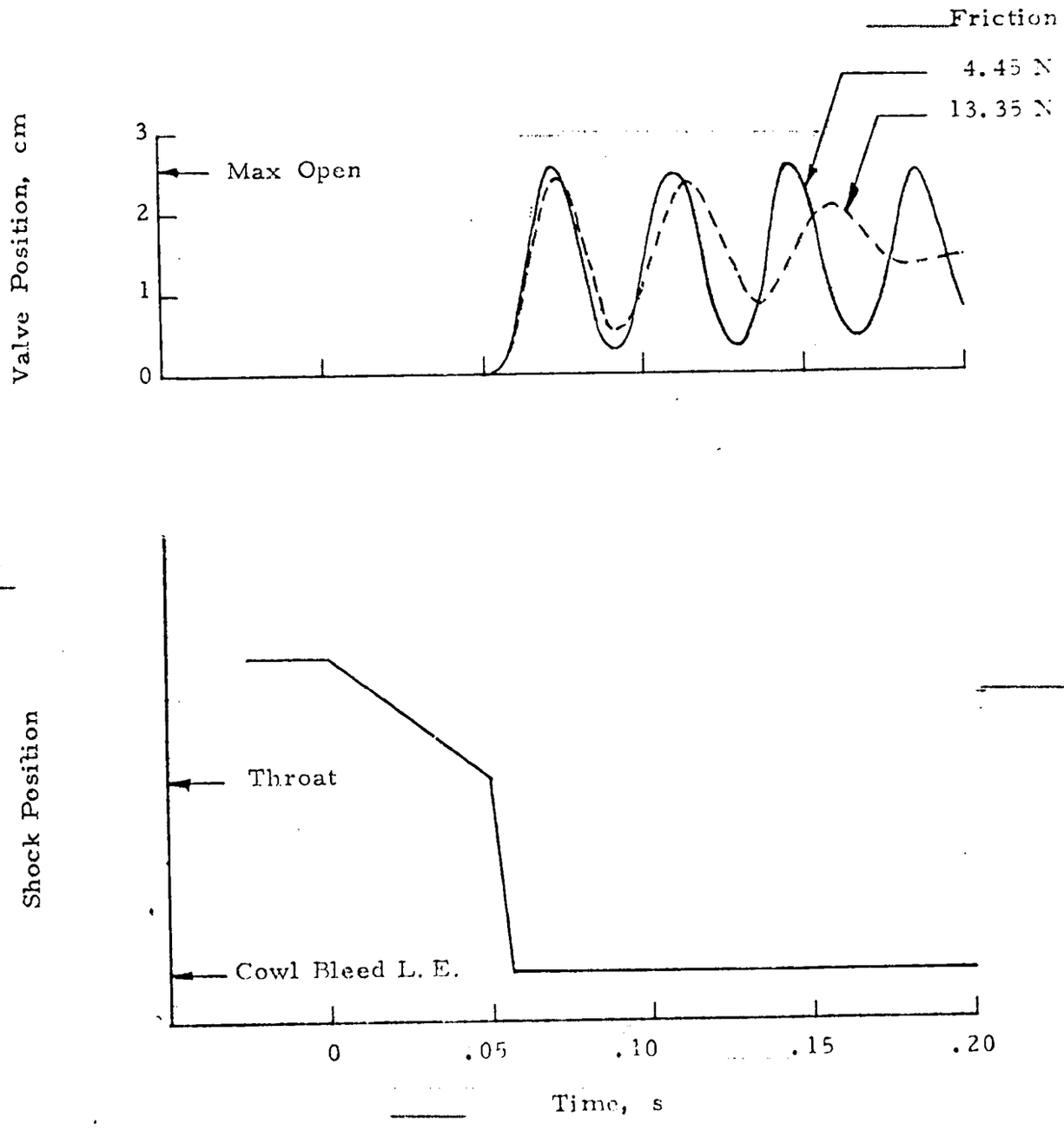


FIGURE 74. EFFECT OF FRICTION ON RESPONSE OF UNSHIELDED AFT POPPET VALVE TO TERMINAL SHOCK MOVEMENT

$M_o = 2.47$

Altitude = Min.

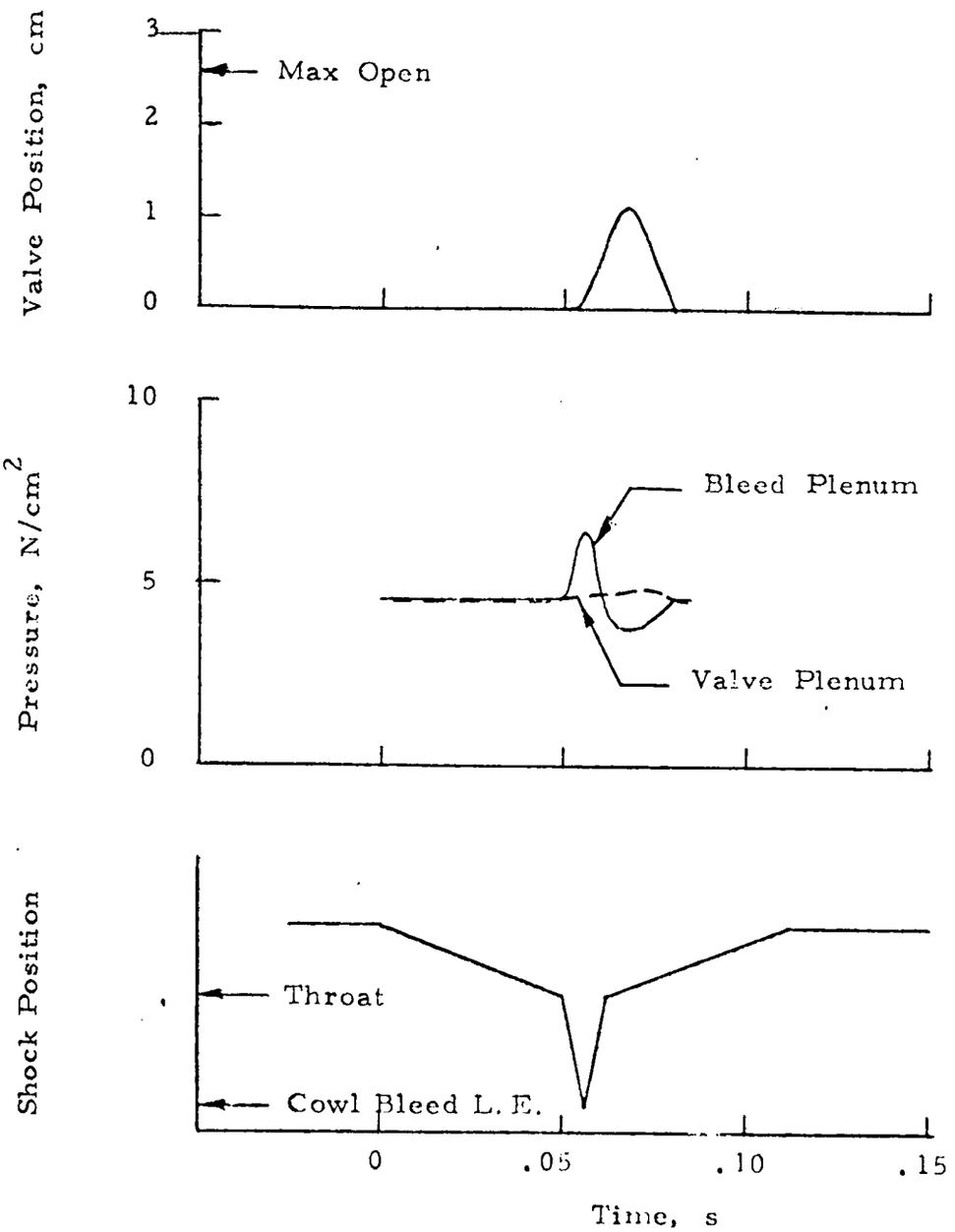


FIGURE 75. RESPONSE OF UNSHIELDED AFT POPPET VALVE TO TERMINAL SHOCK MOVEMENT

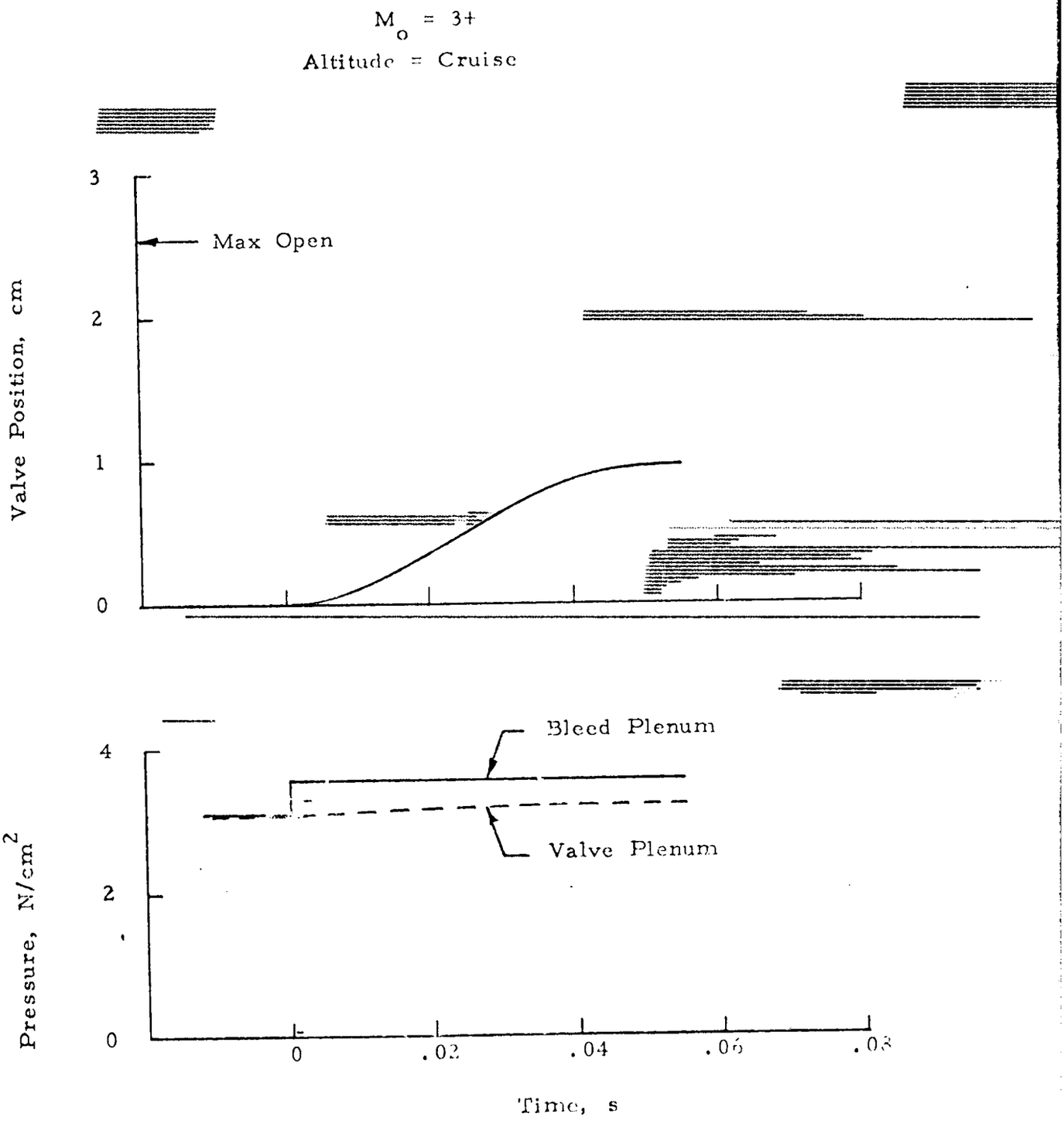


FIGURE 76. RESPONSE OF UNSHIELDED AFT POPPET VALVE TO 15 PERCENT STEP CHANGE IN BLEED PRESSURE

$M_o$ = 3+

Altitude = Cruise

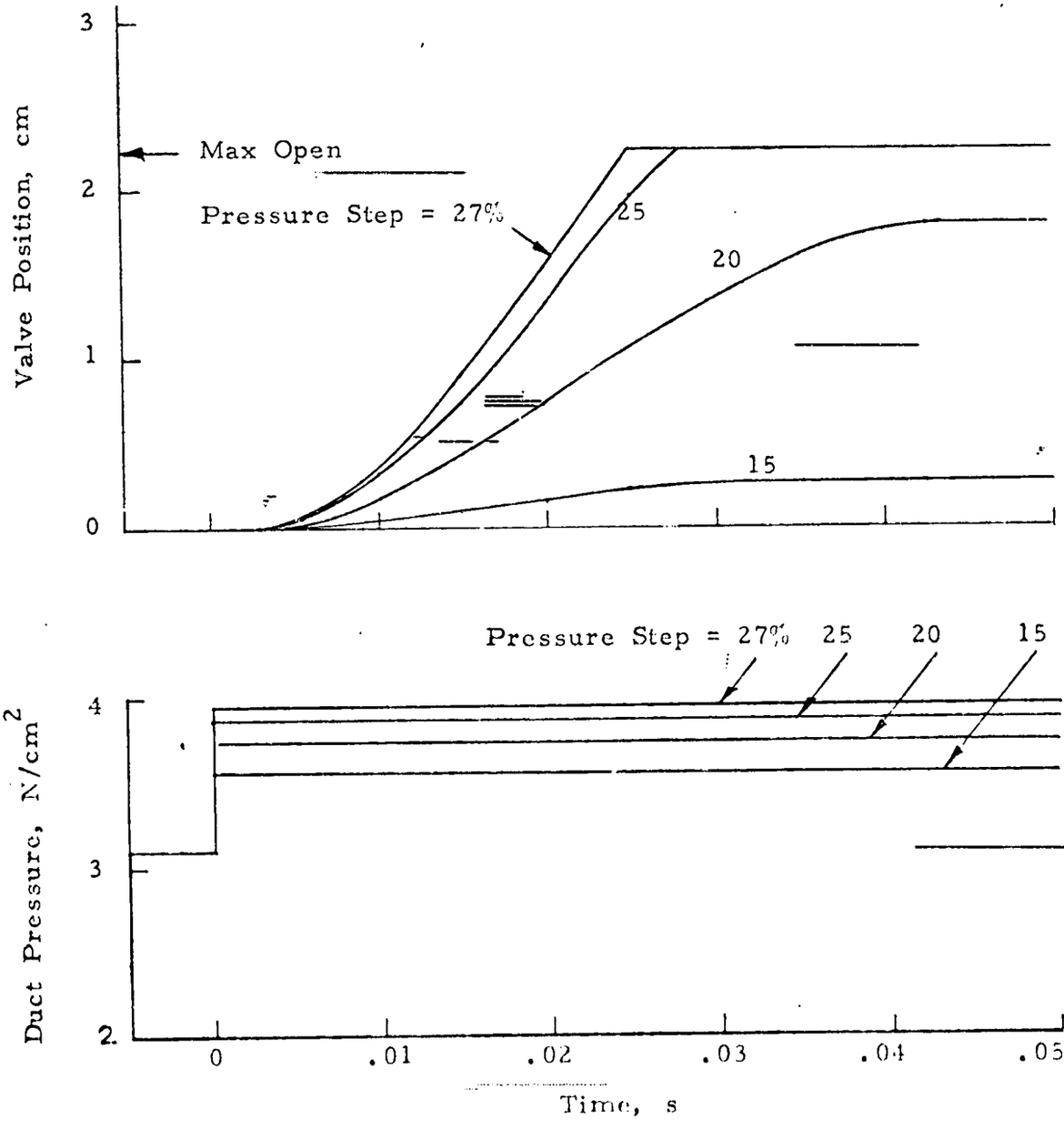


FIGURE 77. RESPONSE OF SHIELDED AFT POPPET VALVE TO STEP CHANGES IN DUCT PRESSURE

$M_o$ = 3+

Altitude = Max

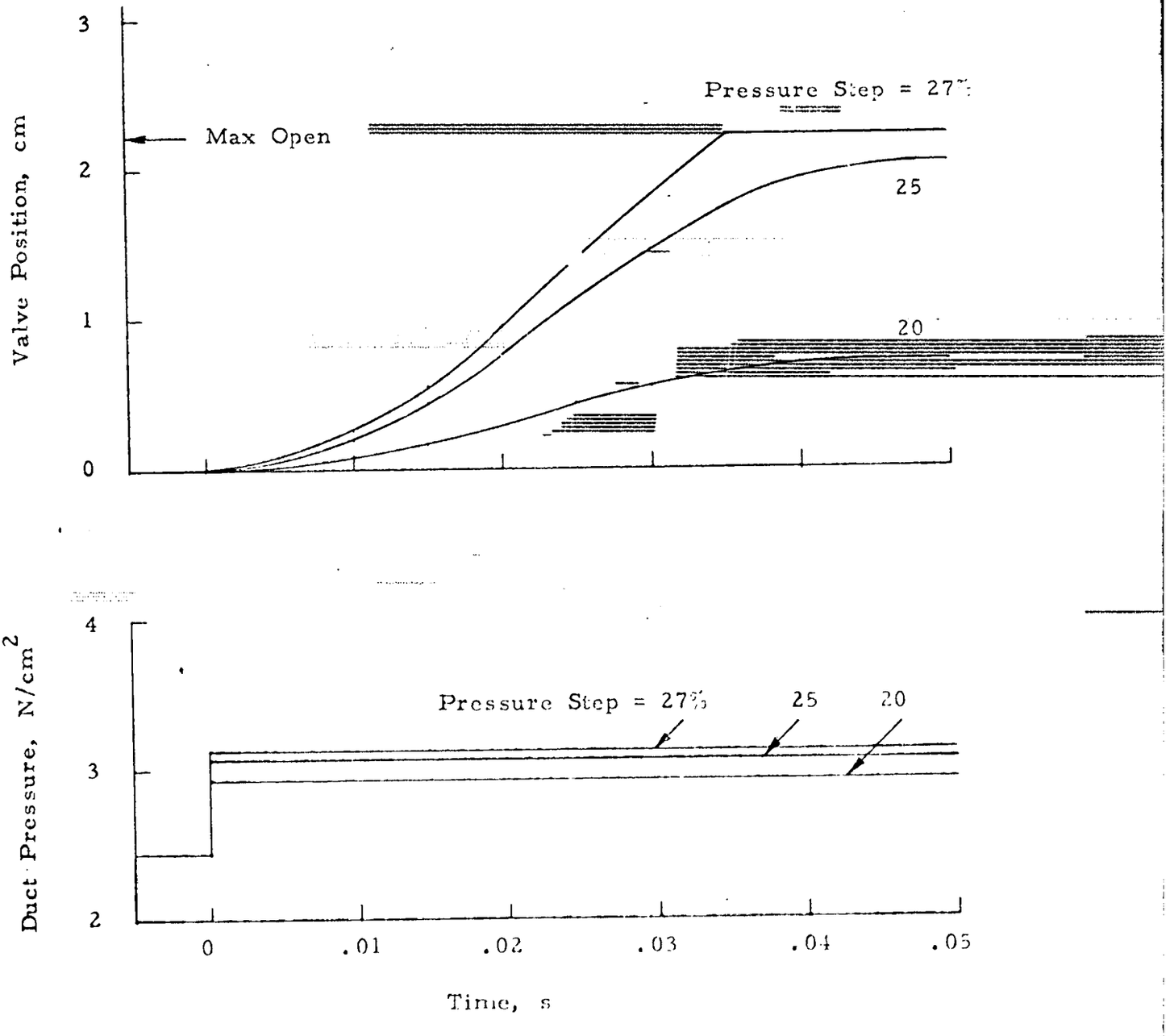


FIGURE 78. RESPONSE OF SHIELDED AFT POPPET VALVE TO STEP CHANGES IN DUCT PRESSURE

$M_o$ = 3+

Altitude = Cruise

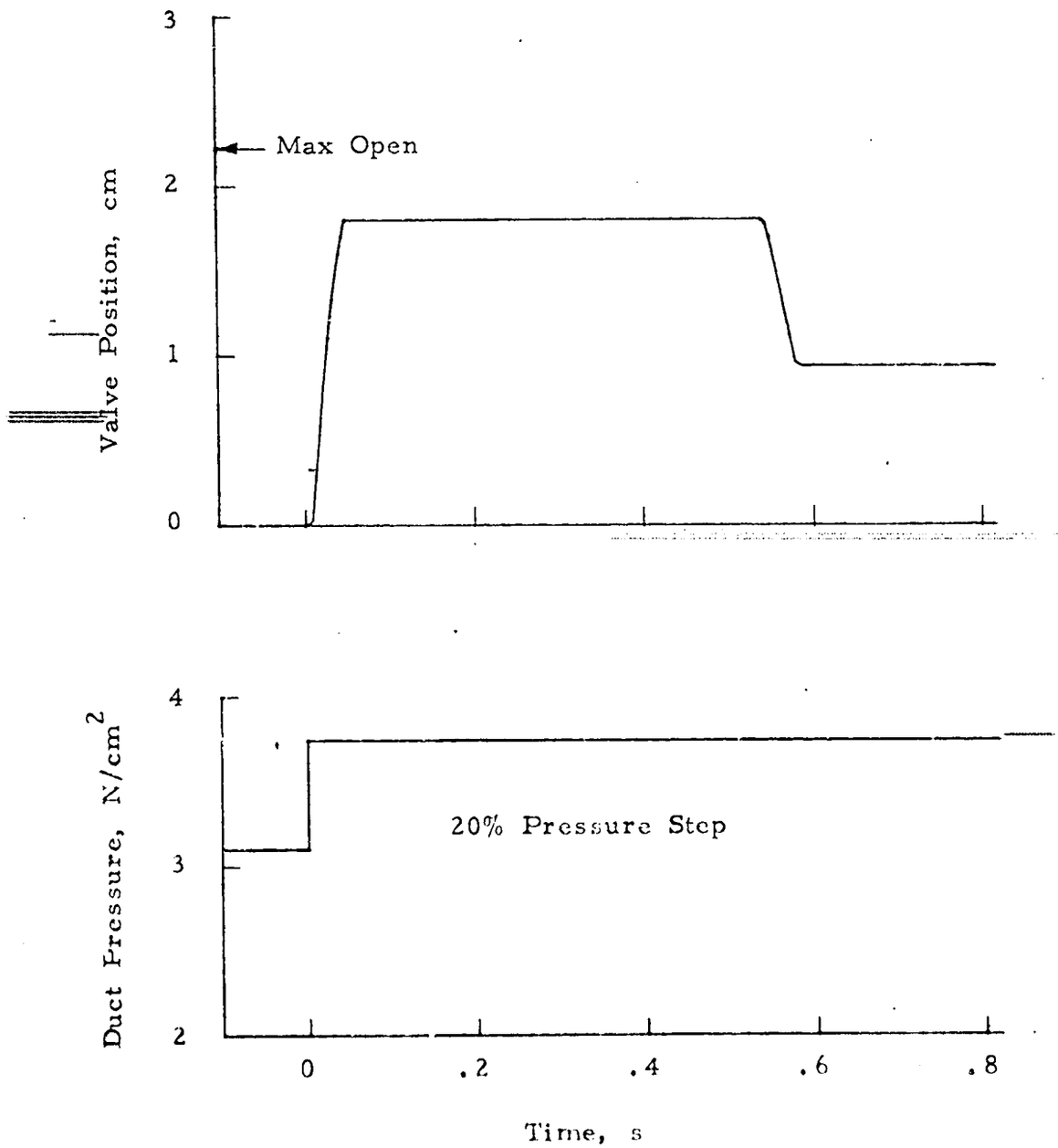


FIGURE 79. RESPONSE OF SHIELDED AFT POPPET VALVE TO 20 PERCENT STEP CHANGE IN DUCT PRESSURE

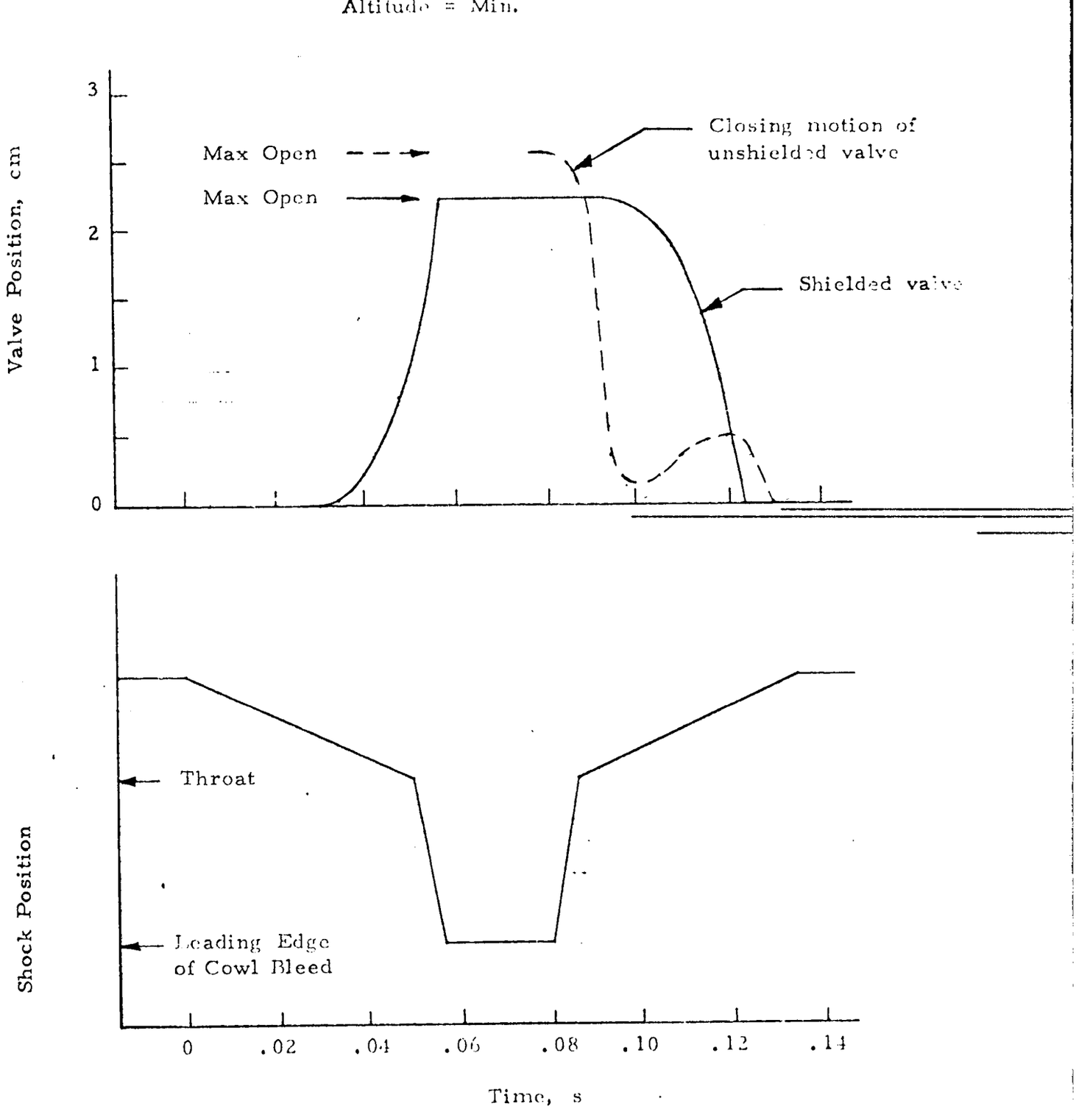


FIGURE 80. EFFECT OF SHIELD ON RESPONSE OF AFT POPPET VALVE TO TERMINAL SHOCK MOVEMENT

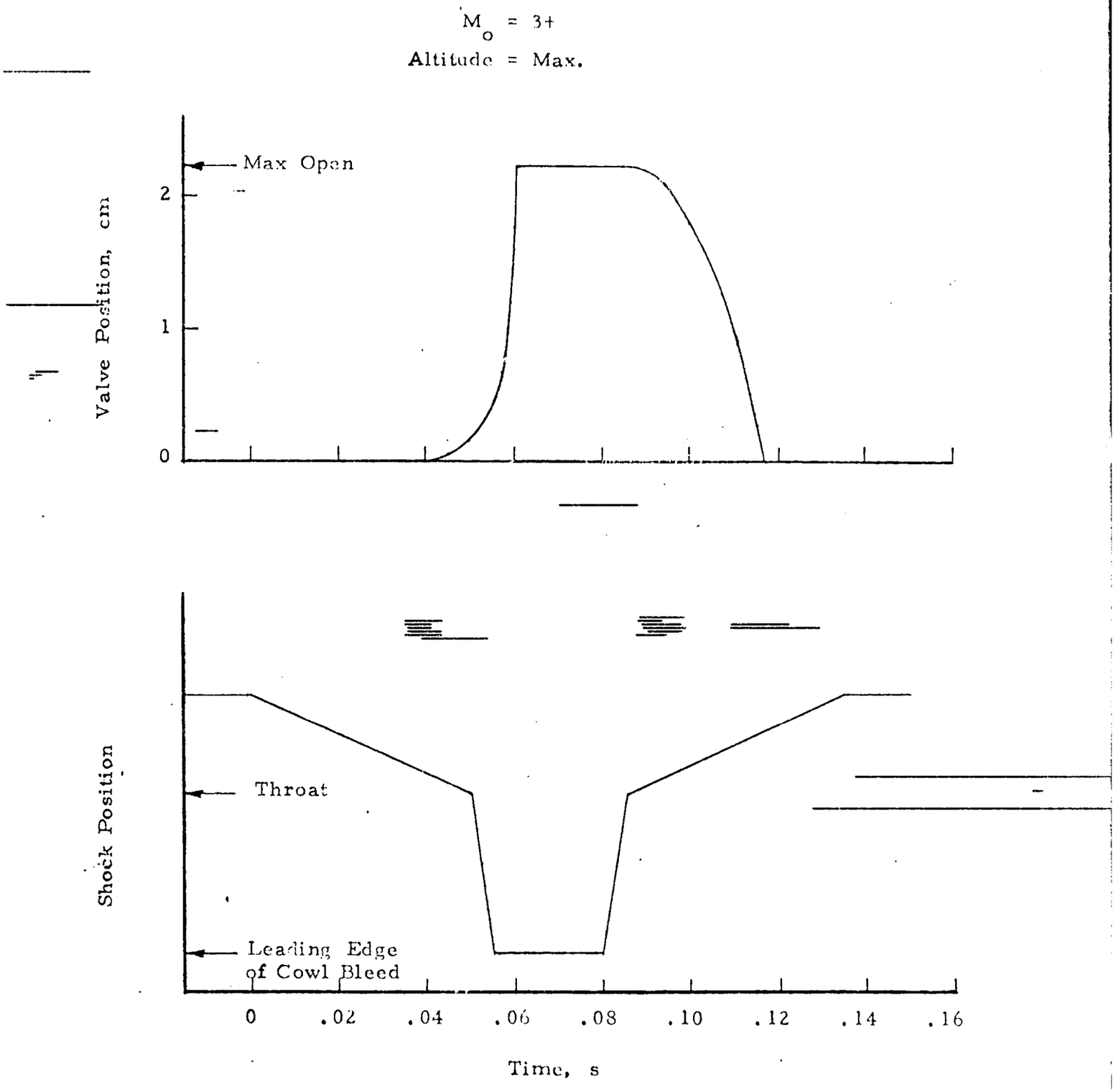


FIGURE 81. RESPONSE OF SHIELDED AFT POPPET VALVE TO TERMINAL SHOCK MOVEMENT

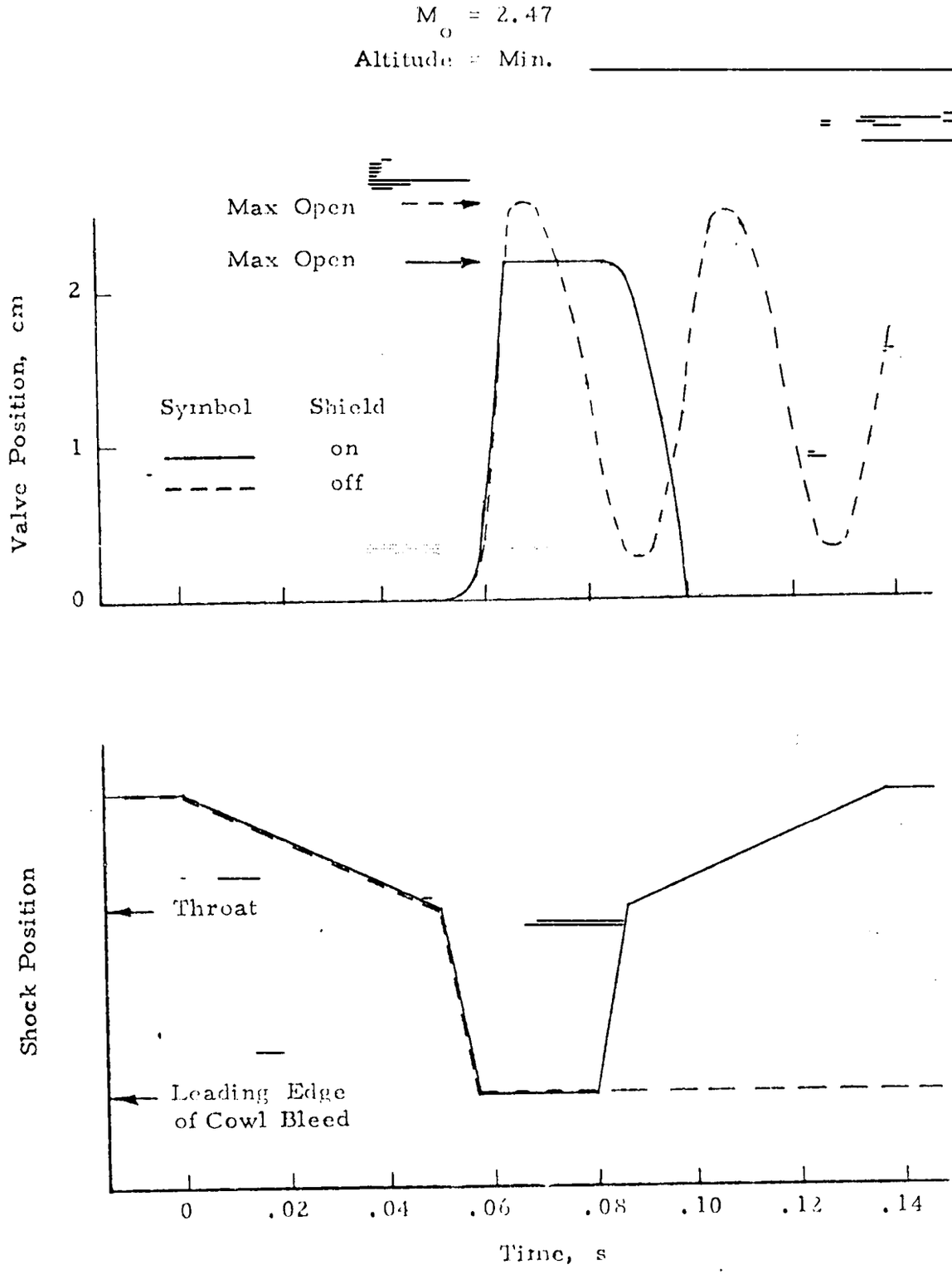


FIGURE 82. EFFECT OF SHIELD ON RESPONSE OF AFT POPPET VALVE TO TERMINAL SHOCK MOVEMENT

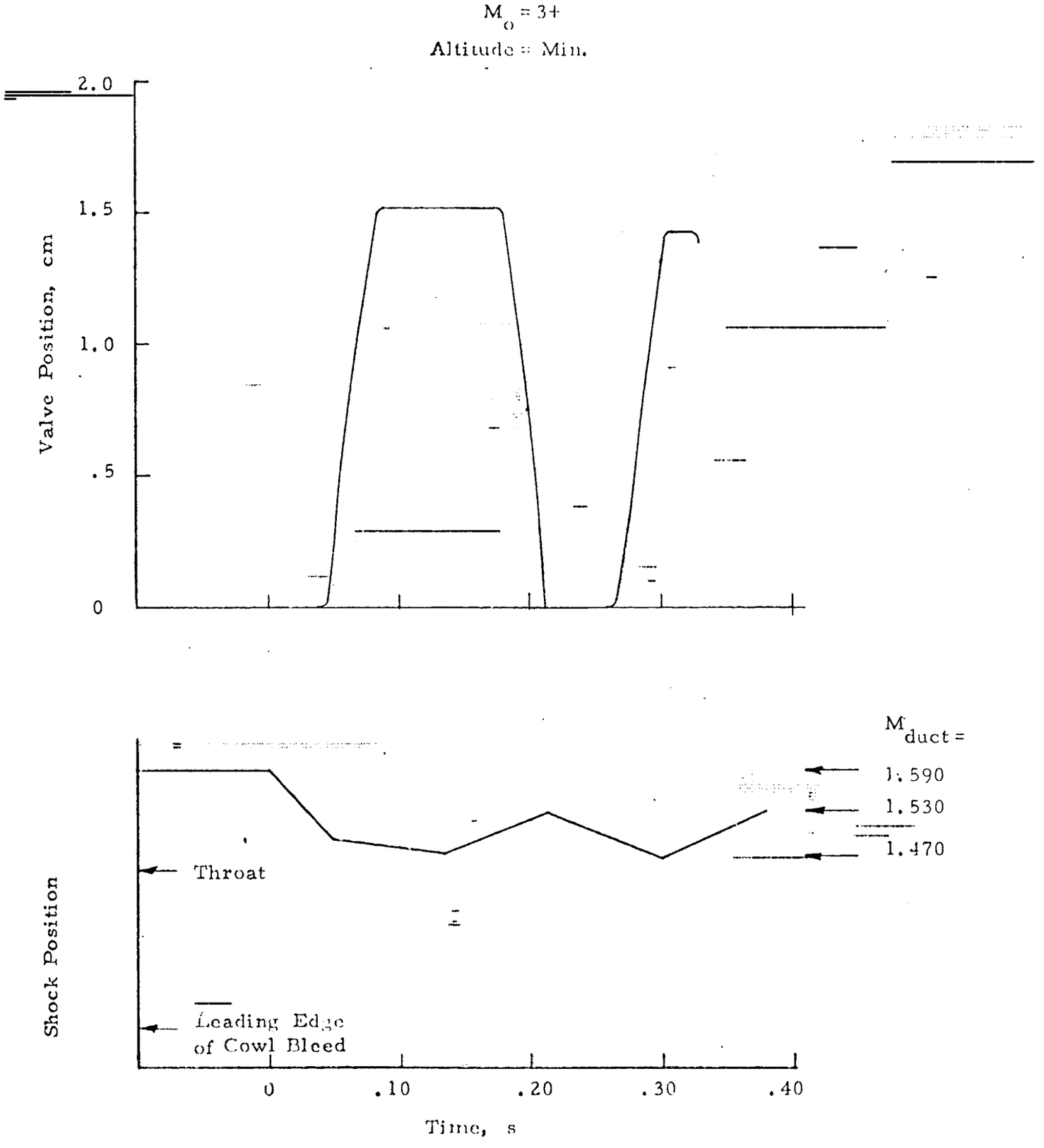


FIGURE 83. RESPONSE OF SHIELDED AFT POPPET VALVE TO 6 HERTZ BLEED PRESSURE OSCILLATION

$M_o$ = 3+

Altitude = Min.

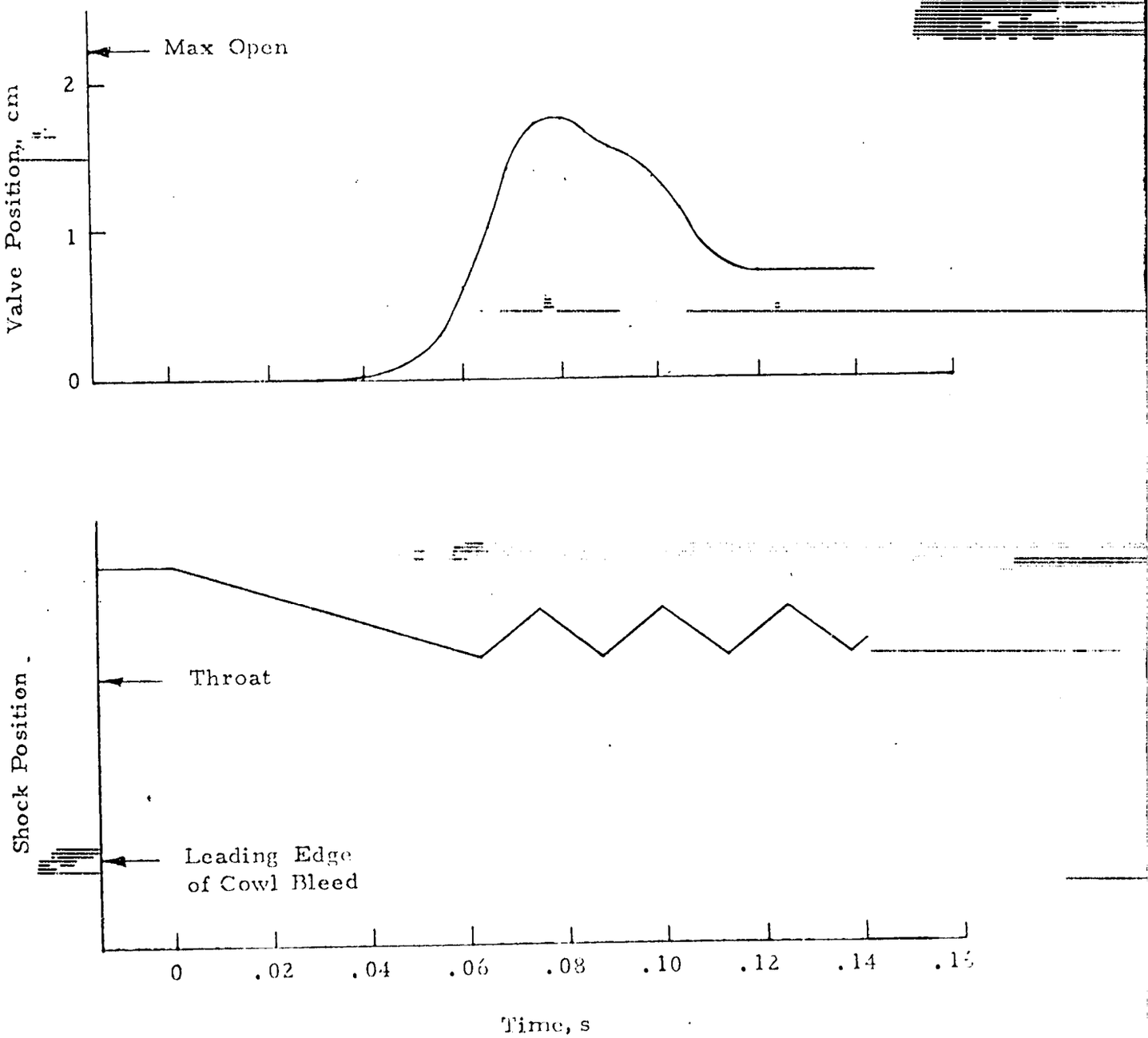


FIGURE 84. RESPONSE OF SHIELDED AFT POPPET VALVE TO 40 HERTZ BLEED PRESSURE OSCILLATION

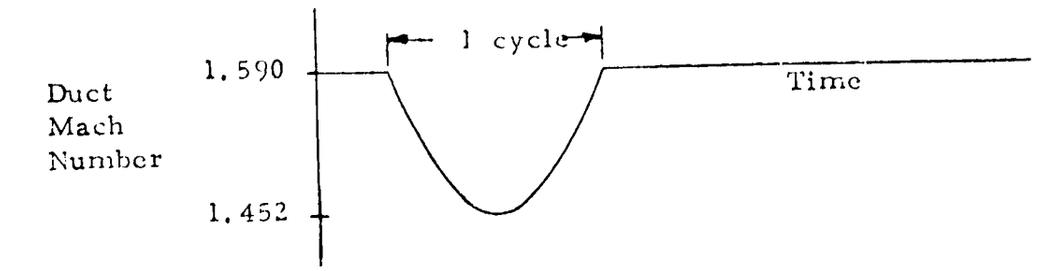


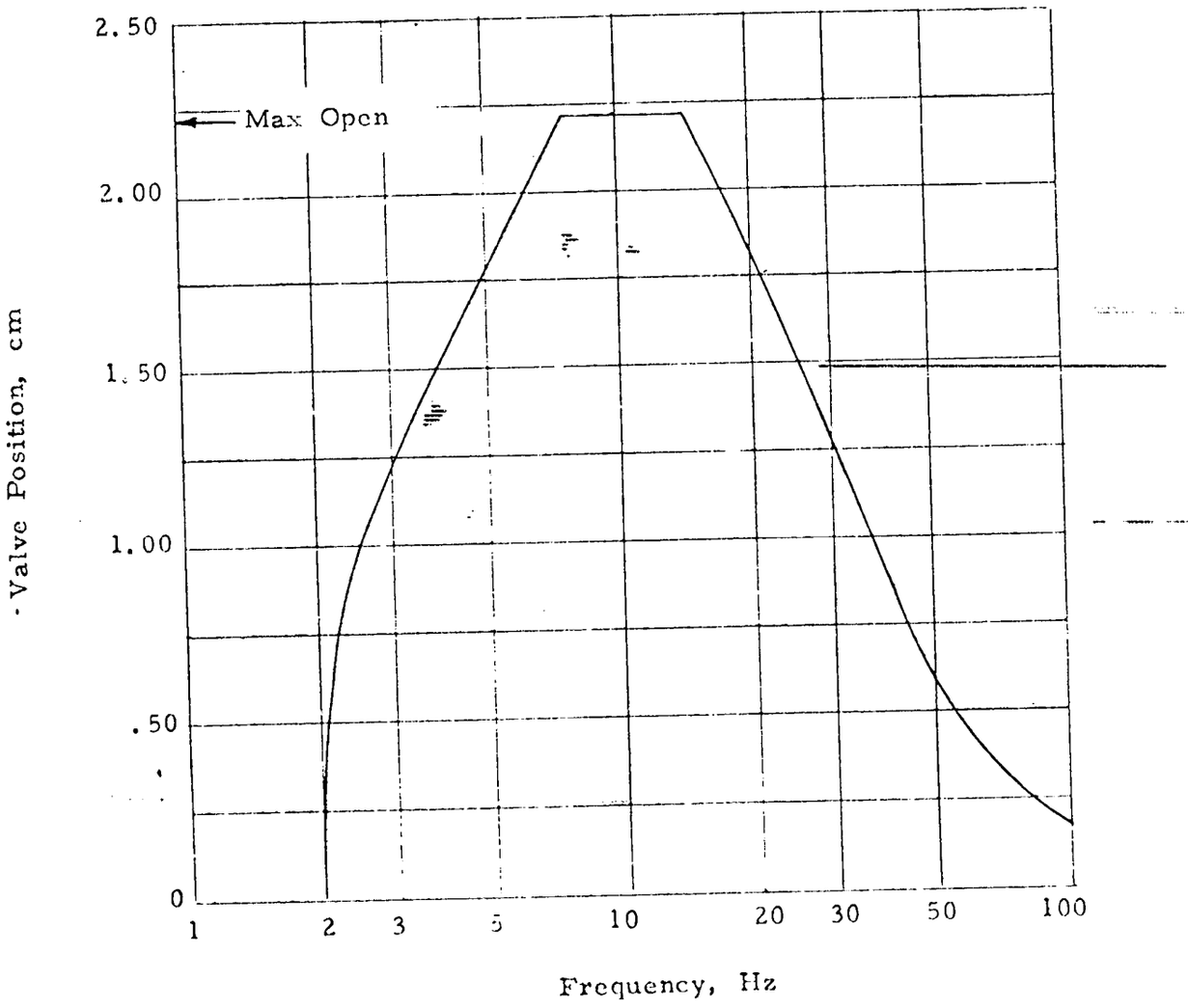


FIGURE 85. RESPONSE OF SHIELDED AFT POPPET VALVE TO A DUCT MACH NUMBER PULSE

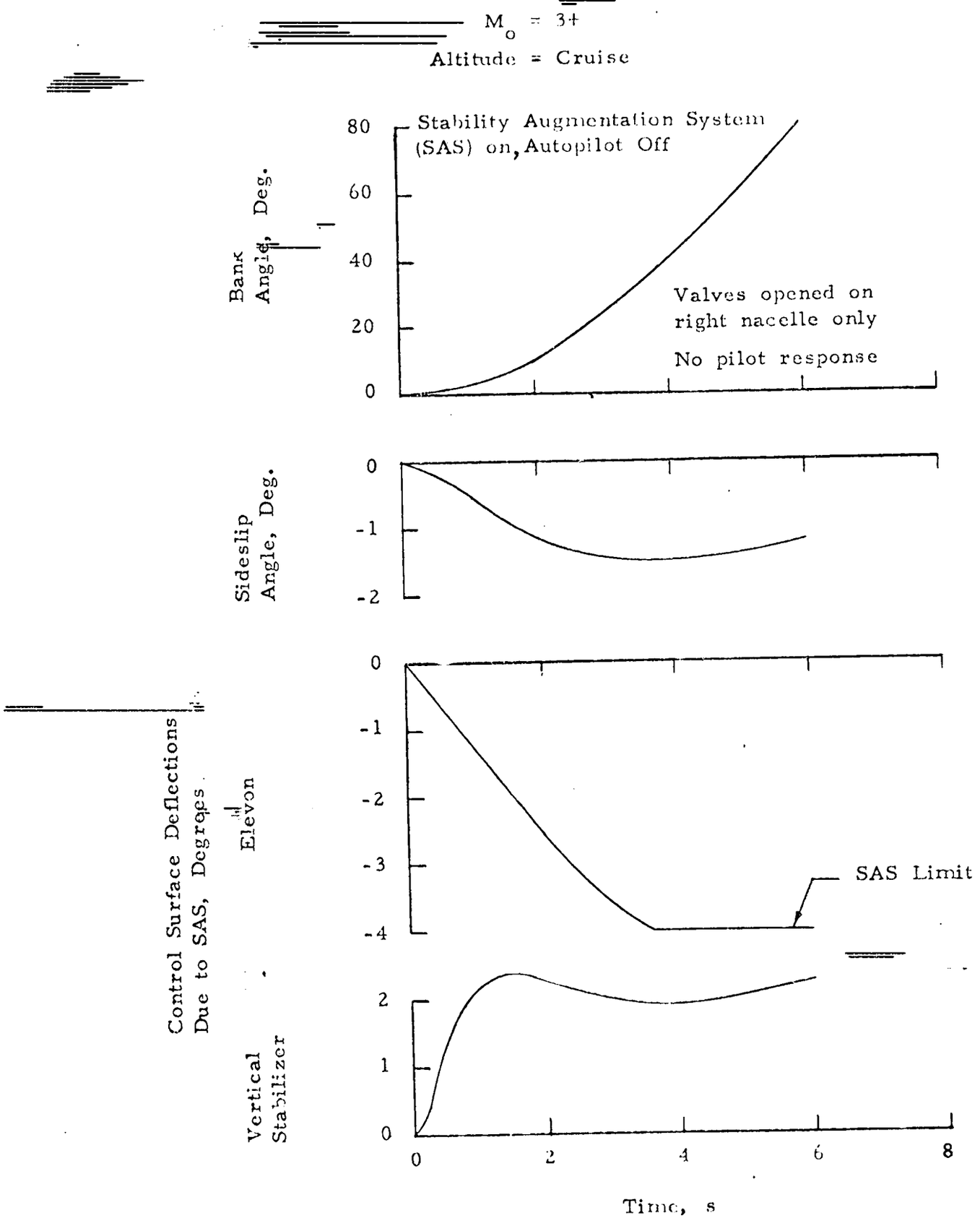


FIGURE 86. AIRCRAFT RESPONSE TO UNSYMMETRICAL OPENING OF SHOCK STABILITY VALVES

FIGURE 87. 'BEARING TEST FACILITY

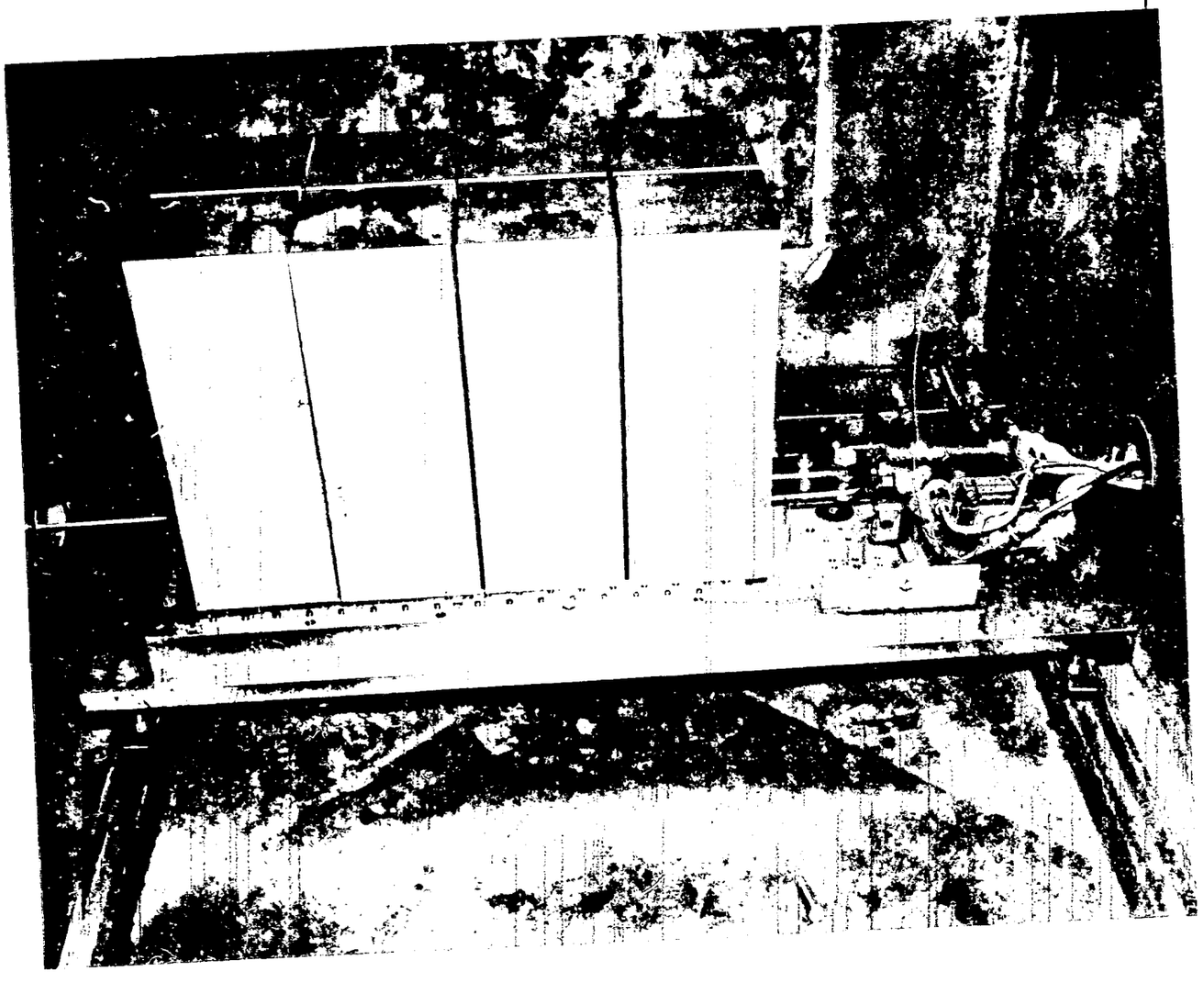

FIGURE 88. LOADING BLOCKS INSTALLED ON BYPASS DOOR ASSEMBLY

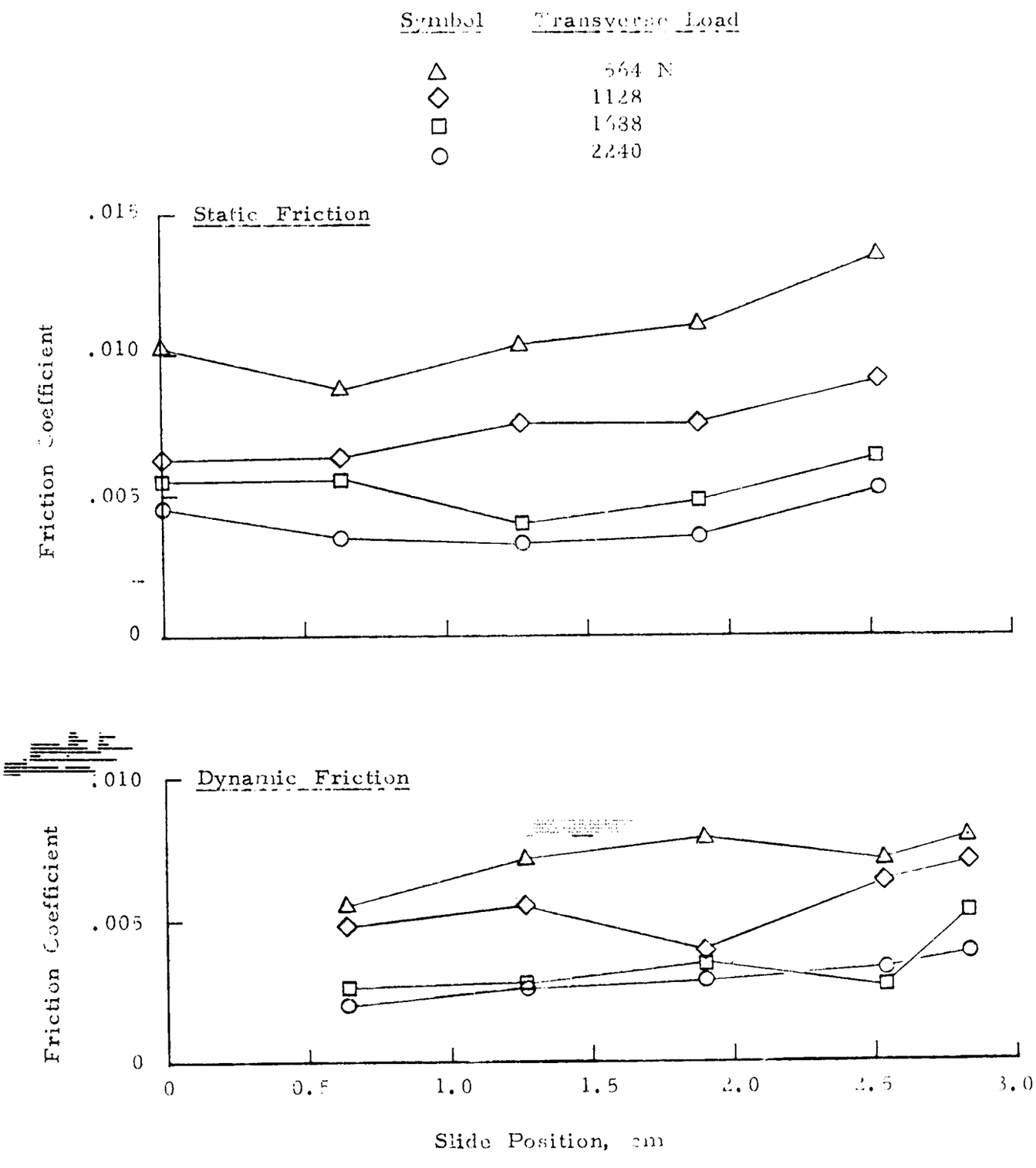


FIGURE 89. BEARING FRICTION AT 294°K BEFORE HEATING

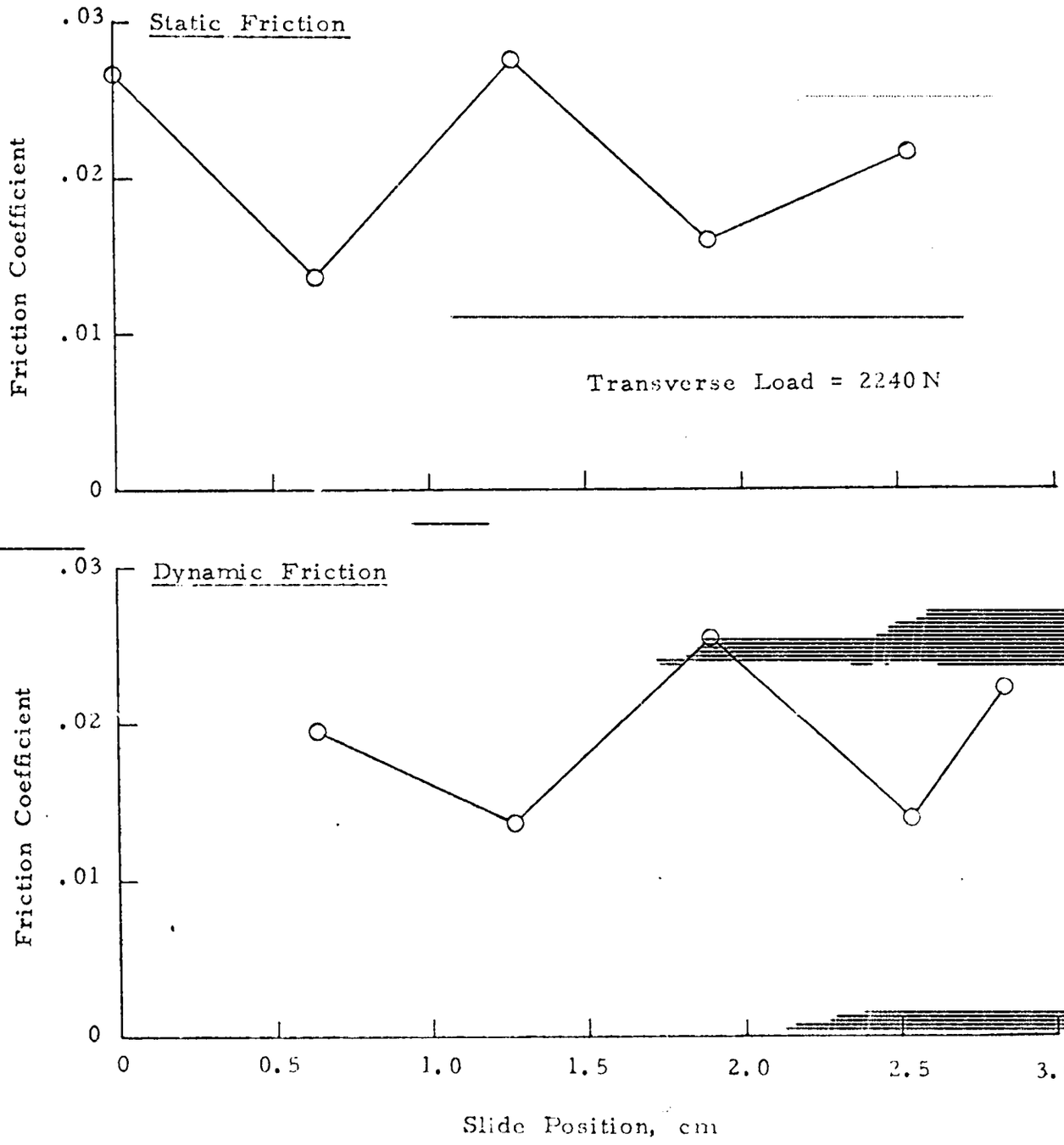


FIGURE 90. BEARING FRICTION AT 664°K

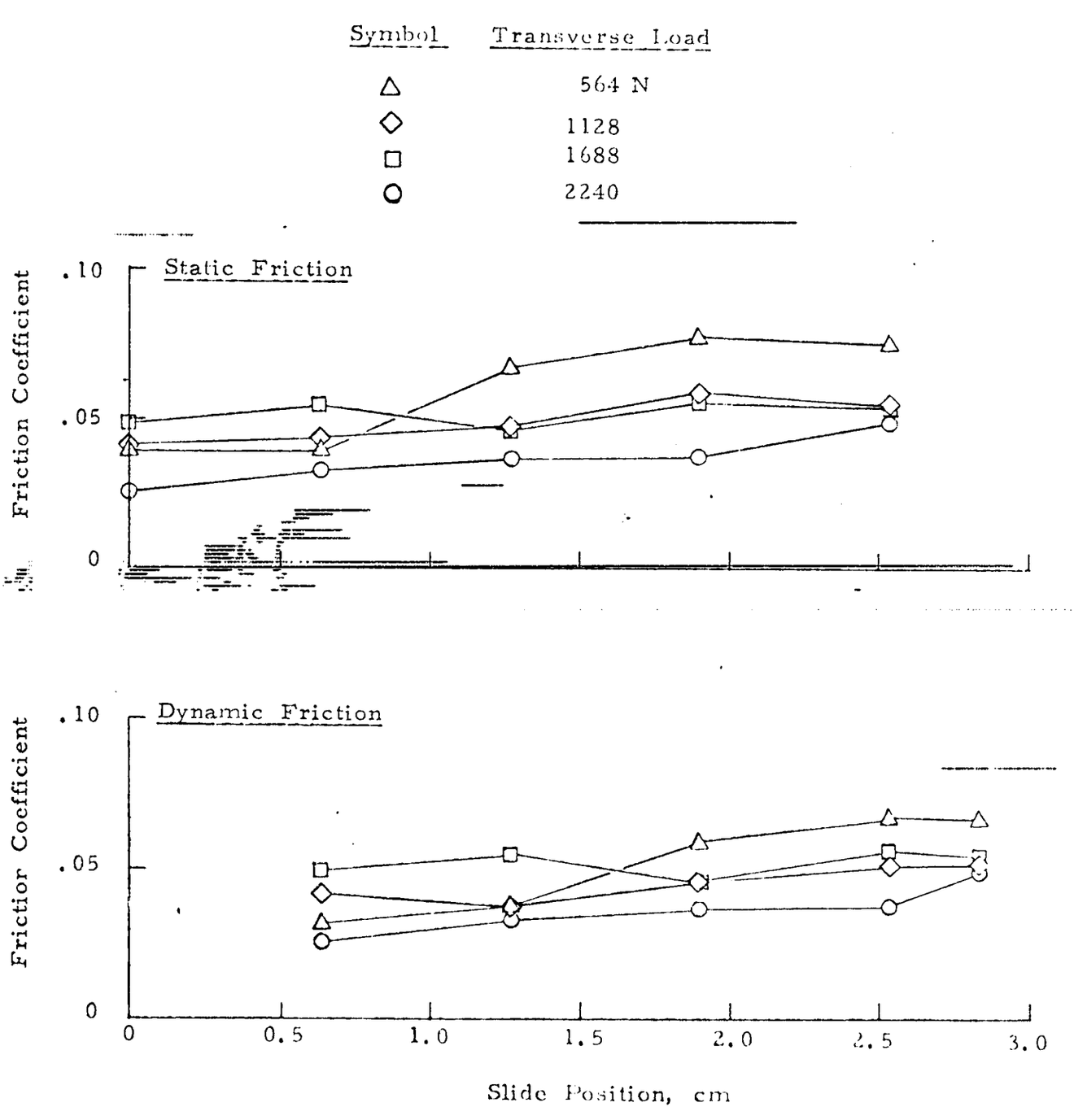


FIGURE 91. BEARING FRICTION AT 294°K AFTER HEATING

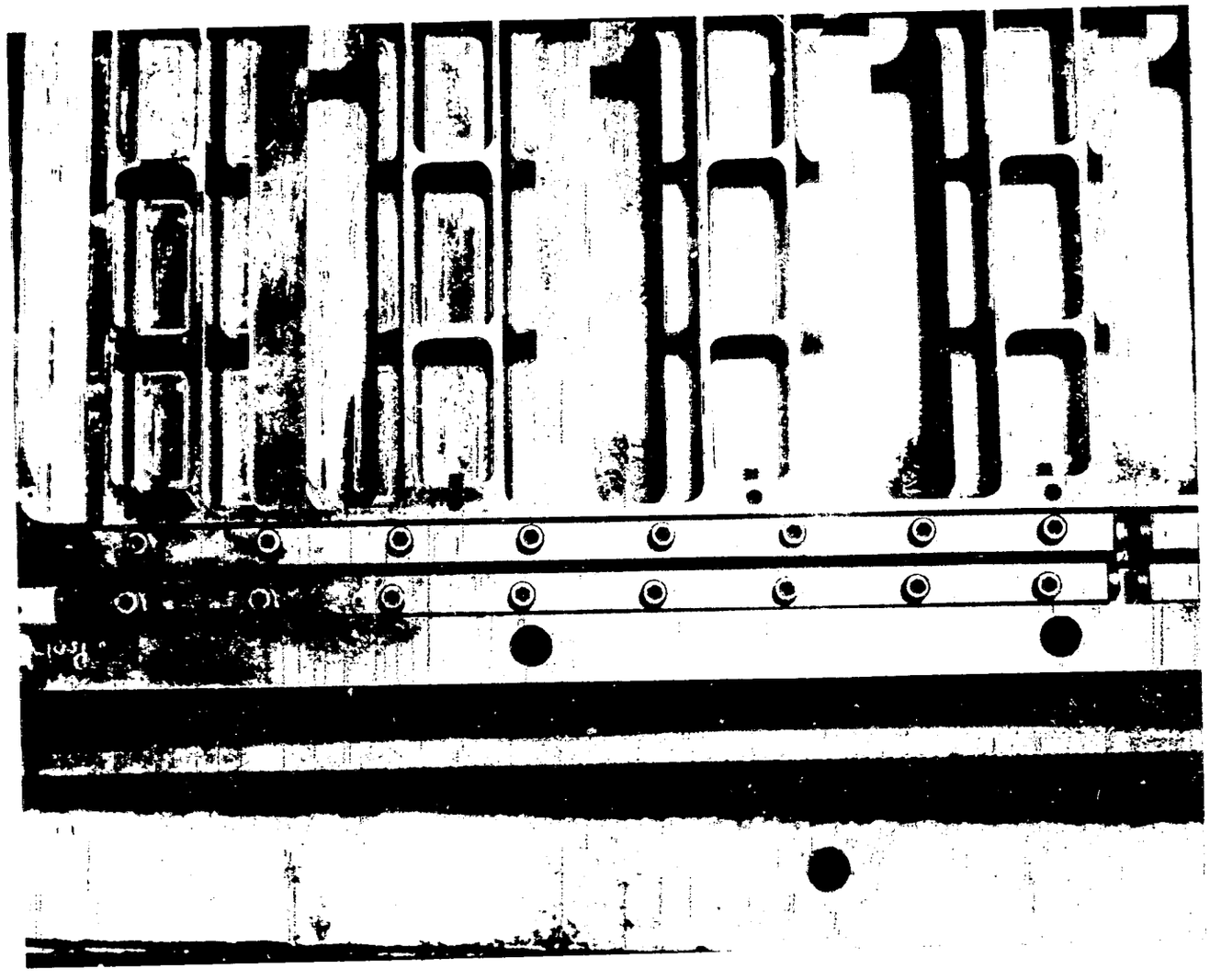

FIGURE 92. BYPASS DOOR ASSEMBLY AFTER HIGH TEMPERATURE FRICTION TEST

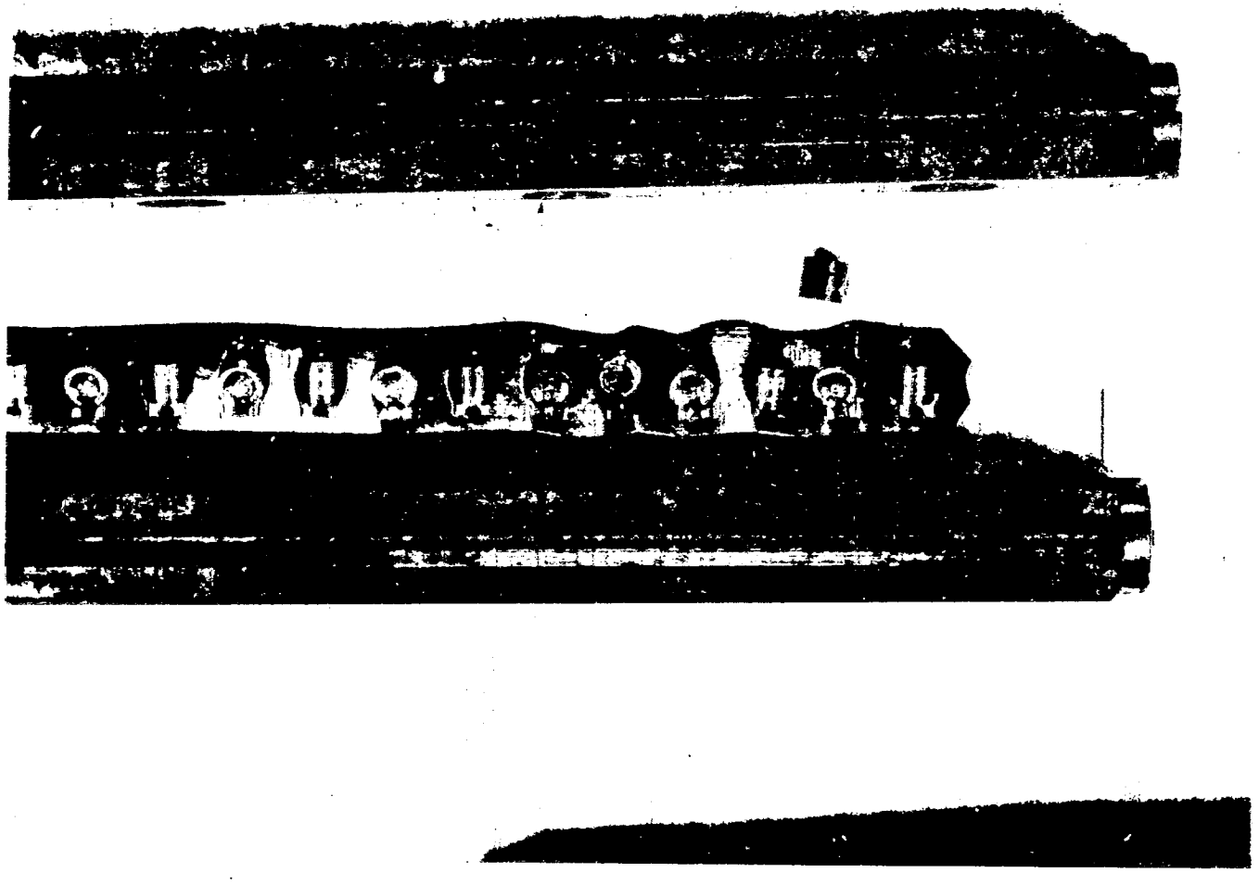

FIGURE 93. DISASSEMBLED BEARINGS AFTER HIGH TEMPERATURE FRICTION TEST

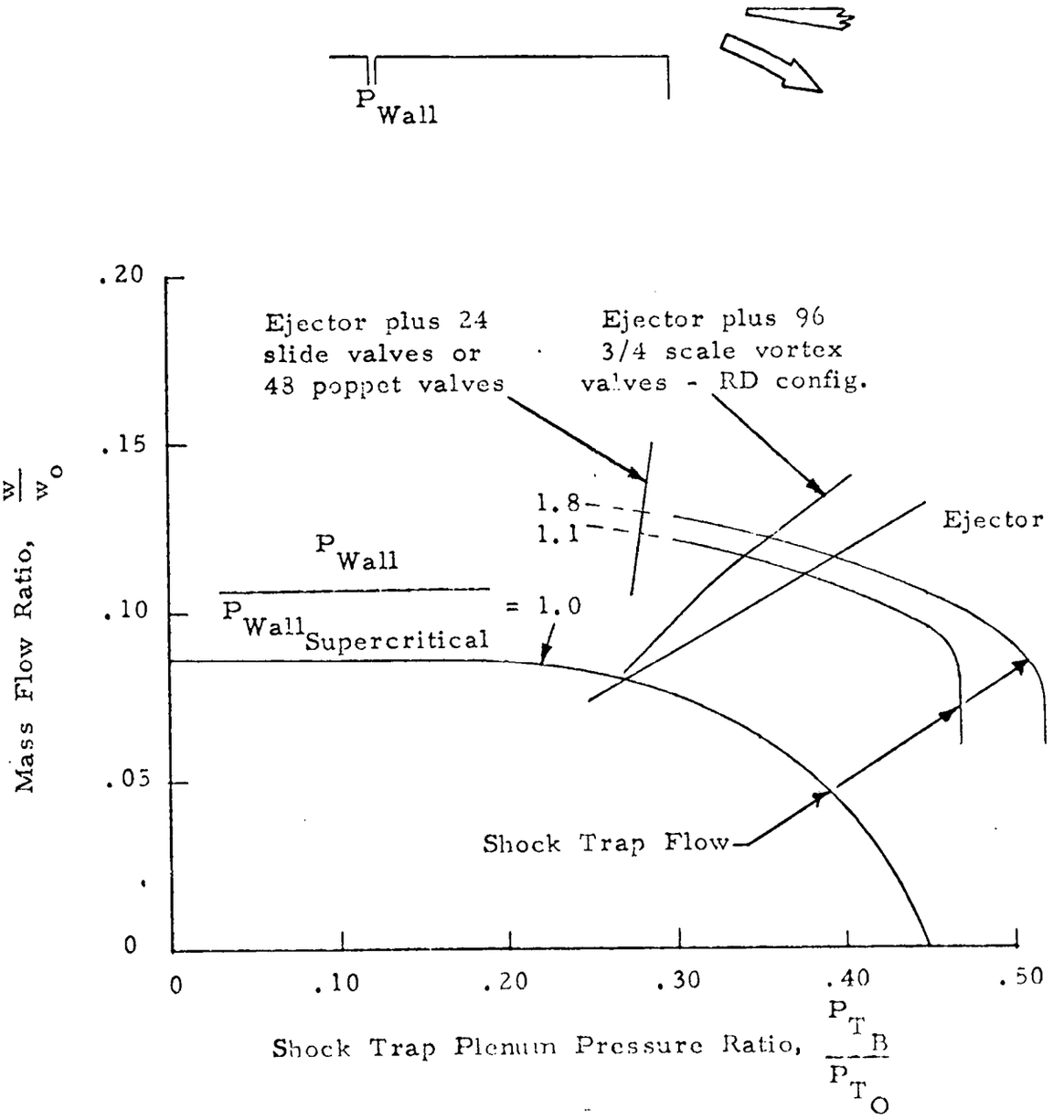


FIGURE 94. EFFECT OF BLEED VALVES ON SHOCK TRAP/EJECTOR MATCHING

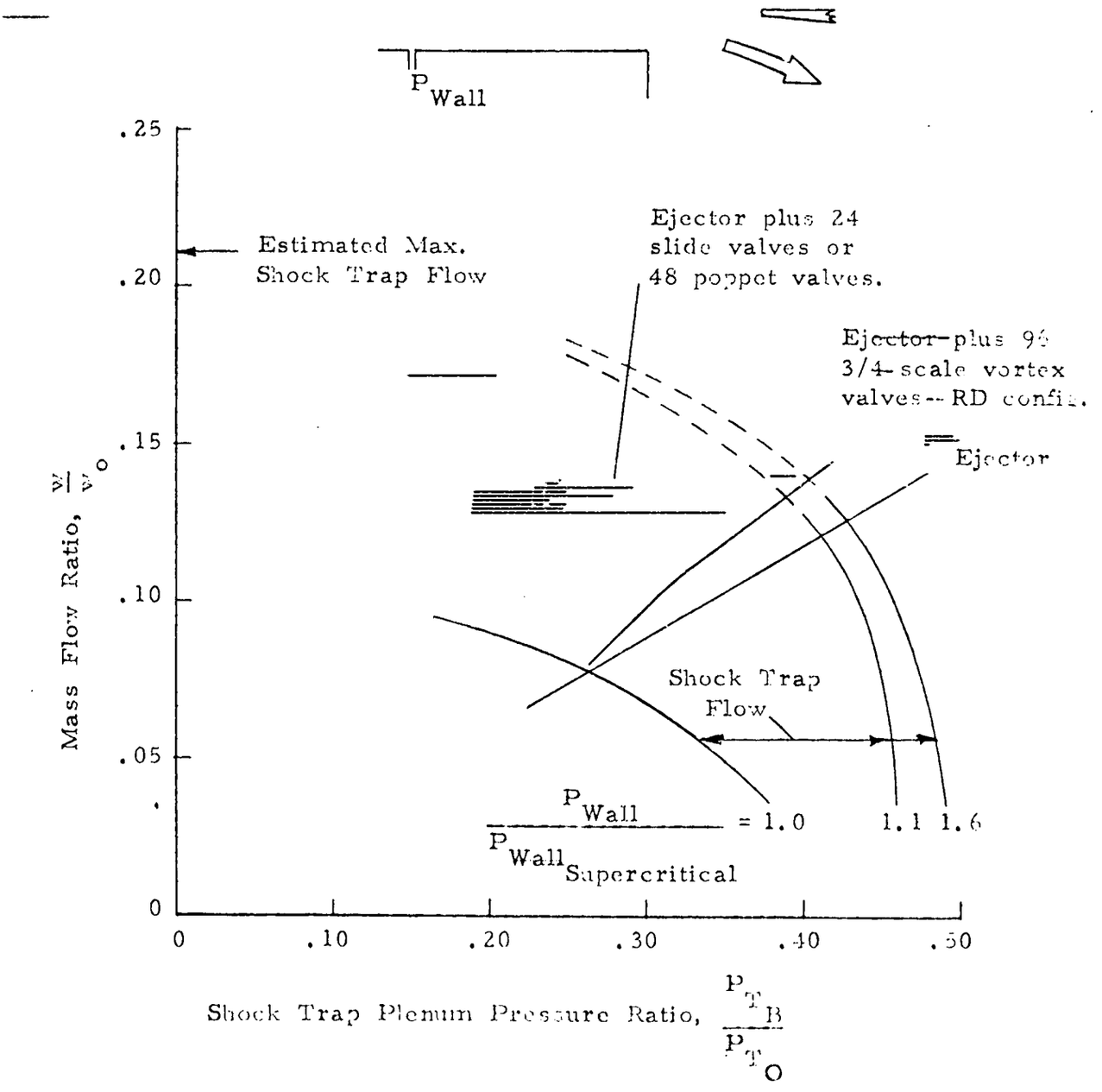


FIGURE 95. EFFECT OF BLEED VALVES ON MATCHING OF ENLARGED SHOCK TRAP WITH EJECTOR

$M_o = 3+$

| Location | Type | No. | Increase in Valve Flow $\Delta m_V/m_o$ | | Increase in Valve Plus Ejector Flow $\frac{\Delta m_V}{m_o} + \frac{\Delta m}{m_o}$ EJ | |
|---|---|---|---|---|---|---|
| | | | 27% Step In Bleed Plenum Pressure | Terminal Shock Standing Ahead of Bleed | 27% Step In Bleed Plenum Pressure | Terminal Shock Standing Ahead of Bleed |
| Cowl | Unshielded Poppet | 50 | .173 | .257 | .205 | .293 |
| | Shielded Poppet | 50 | .135 | .214 | .167 | .250 |
| | Slide | 25 | .156 | .220 | .188 | .256 |
| | Vortex | 96 | .011 | .032 | .043 | .068 |
| Present Shock Trap | Unshielded Poppet | 48 | | | * | .012 |
| | Slide | 24 | | | * | .012 |
| | Vortex | 96 | | | .005 | .005 |
| Enlarged Shock Trap | Unshielded Poppet | 48 | | | * | .048 |
| | Slide | 24 | | | * | .048 |
| | Vortex | 96 | | | .010 | .013 |

*Maximum attainable pressure increase is less than 27%.

FIGURE 96. COMPARISON OF BLEED FLOWS WITH VALVES FULLY OPEN

$M_o = 3+$

Valves Installed in Cowl

| Configuration | Time Req'd For Full Valve Opening After 27% Step in Bleed Plenum Pressure | Increase in Cowl Bleed Mass Flow Ratio (Valves Plus Shock Trap) After .056 Second Shock Movement to Bleed Leading Edge | | Natural Frequency of Installed Valve with Inlet Terminal Shock Position Fixed | |
|---|---|---|---|---|---|
| | Cruise Altitude | Min. Altitude | Max. Altitude | Min. Altitude | Max. Altitude |
| Unshielded Poppet | .028 Sec. | .107 | .080 | 22 Hz | 17 Hz |
| Shielded Poppet | .025 | .242 | .100 | 11 | 10 |
| Slide Valve | .068 | .066 | .036 | 4 | 3 |

FIGURE 97. VALVE DYNAMIC RESPONSE COMPARISON

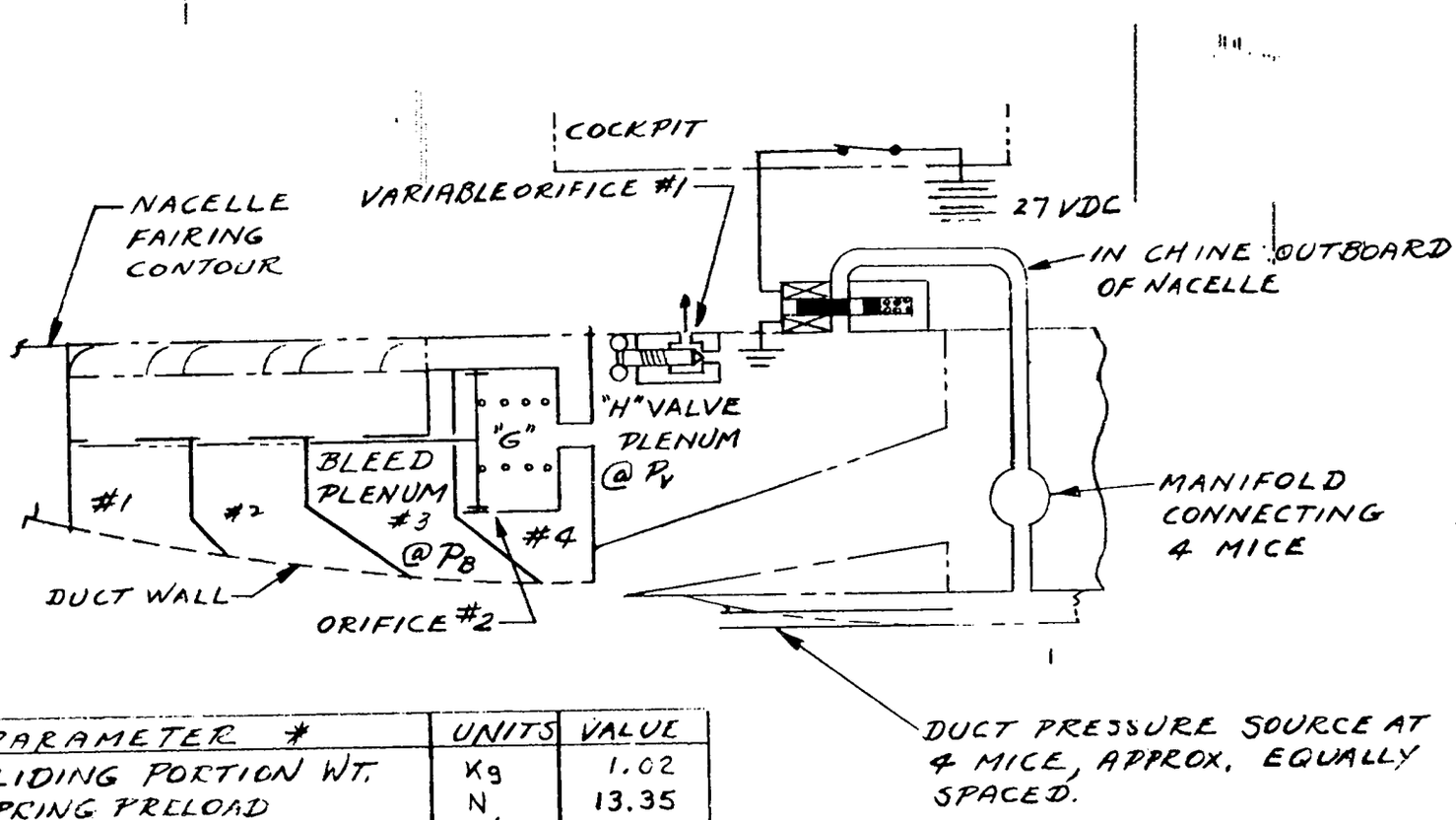


| PARAMETER * | UNITS | VALUE |
|---|---|---|
| SLIDING PORTION WT. | Kg | 1.02 |
| SPRING PRELOAD | N | 13.35 |
| SPRING RATE | N/cm | 1.75 |
| FRICTION COEFF. (MAX.) | — | .025 |
| SLIDE MAX. TRAVEL | cm | 2.86 |
| SLIDE VALVE OVERLAP | cm | .318 |
| ORIFICE #1 AREA (NOM.)** | $cm^2$ | .0045 |
| ORIFICE #2 AREA/VALVE | $cm^2$ | .0116 |
| SLIDE PLANFORM AREA | $cm^2$ | 122.5 |
| PLENUM G VOLUME | CC | 116.0 |
| PLENUM H VOLUME | CC | 2720.0 |

* ALL DATA PER BLEED VALVE.
** ADJUSTABLE ORIFICE

DRAWING 1. SLIDE VALVE INSTALLATION SCHEMATIC

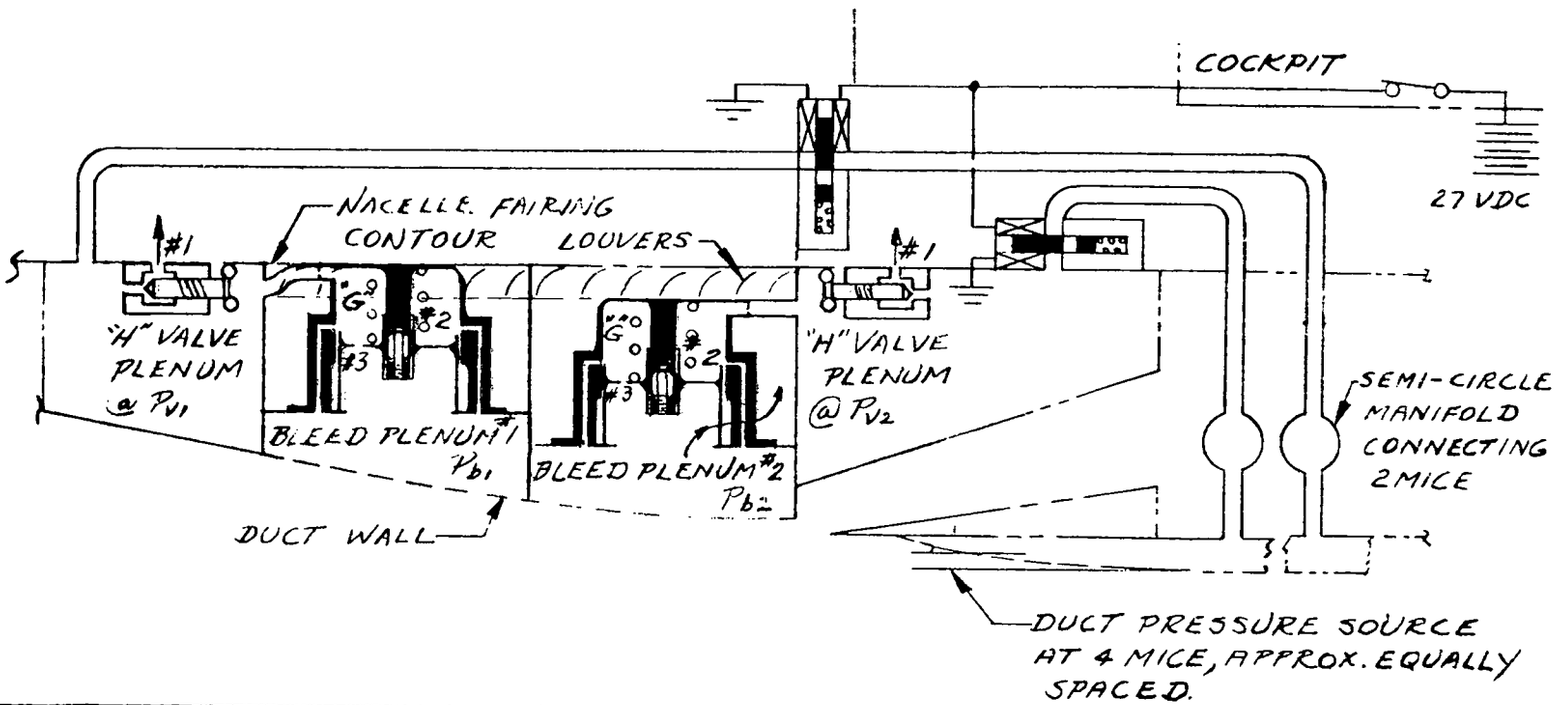


| PARAMETER * | UNITS | FWD VALVE | AFT VALVE |
|---|---|---|---|
| POPPET WT. | Kg | .318 | .318 |
| SPRING PRELOAD (CLOSED) | N | 13.35 | 13.35 |
| SPRING RATE | N/cm | 3.5 | 3.5 |
| MAX. POPPET TRAVEL | cm | 2.54 | 2.54 |
| ORIFICE #1 (NOM.) AREA** | $cm^2$ | .0106 | .0077 |
| ORIFICE #2 AREA | $cm^2$ | .129 | .129 |
| ORIFICE #3 AREA | $cm^2$ | .0129 | .0129 |
| PLENUM G VOL./VALVE | CC | 221.0 | 221.0 |
| PLENUM H VOL./VALVE | CC | 2750.0 | 2700.0 |
| POPPET FRICTION | N | 4.45 | 4.45 |

* ALL DATA PER BLEED VALVE
** ADJUSTABLE (0 TO NOM. AREA + 33%)

DRAWING 2. UNSHIELDED POPPET VALVE INSTALLATION SCHEMATIC

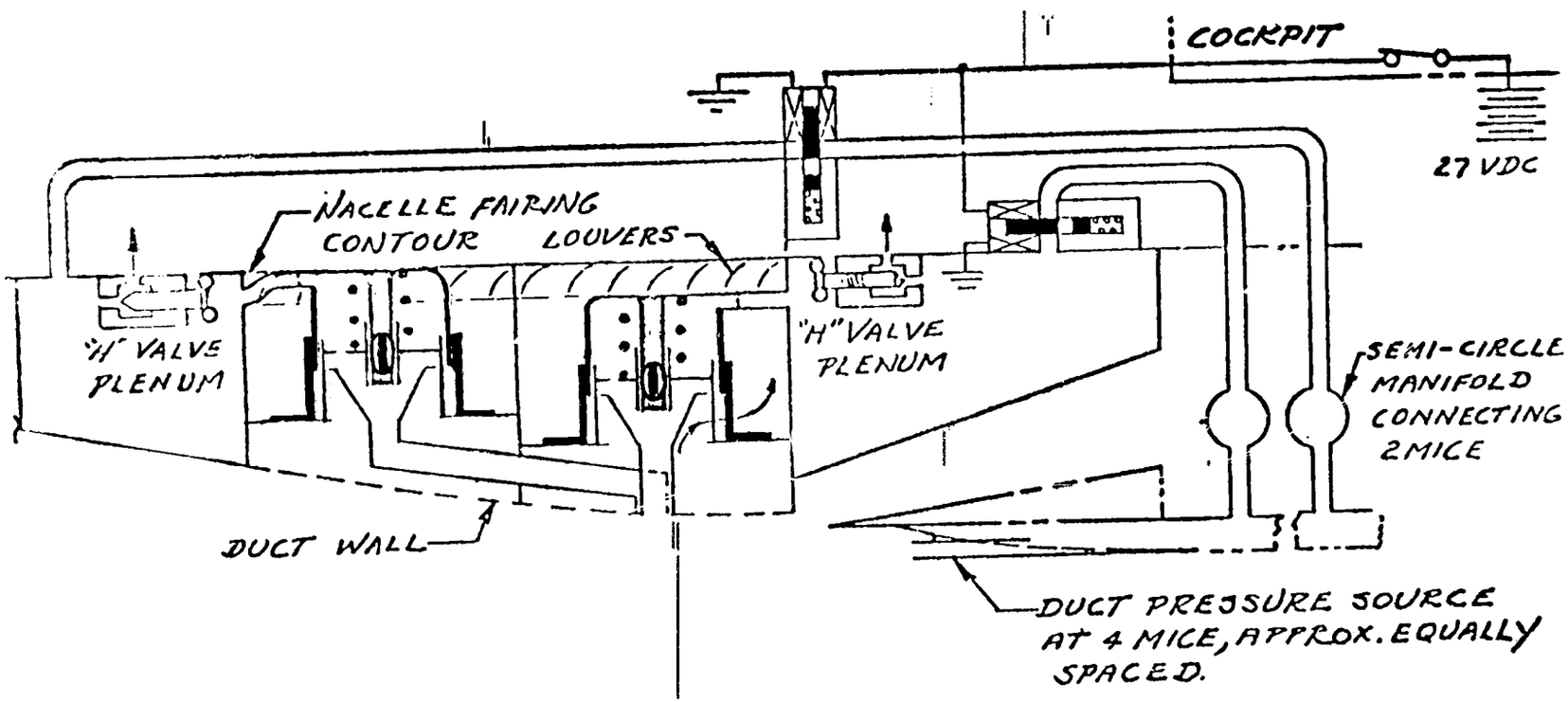


DRAWING 3. SHIELDED POPPET VALVE INSTALLATION SCHEMATIC

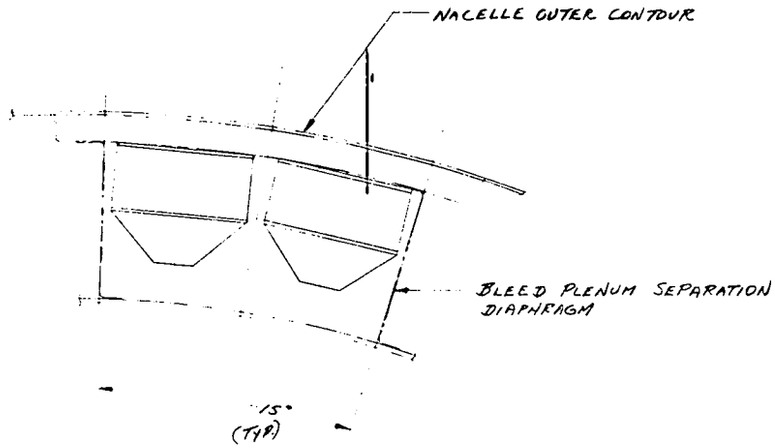


DRAWING 4. FULL SCALE VORTEX VALVE INSTALLATION

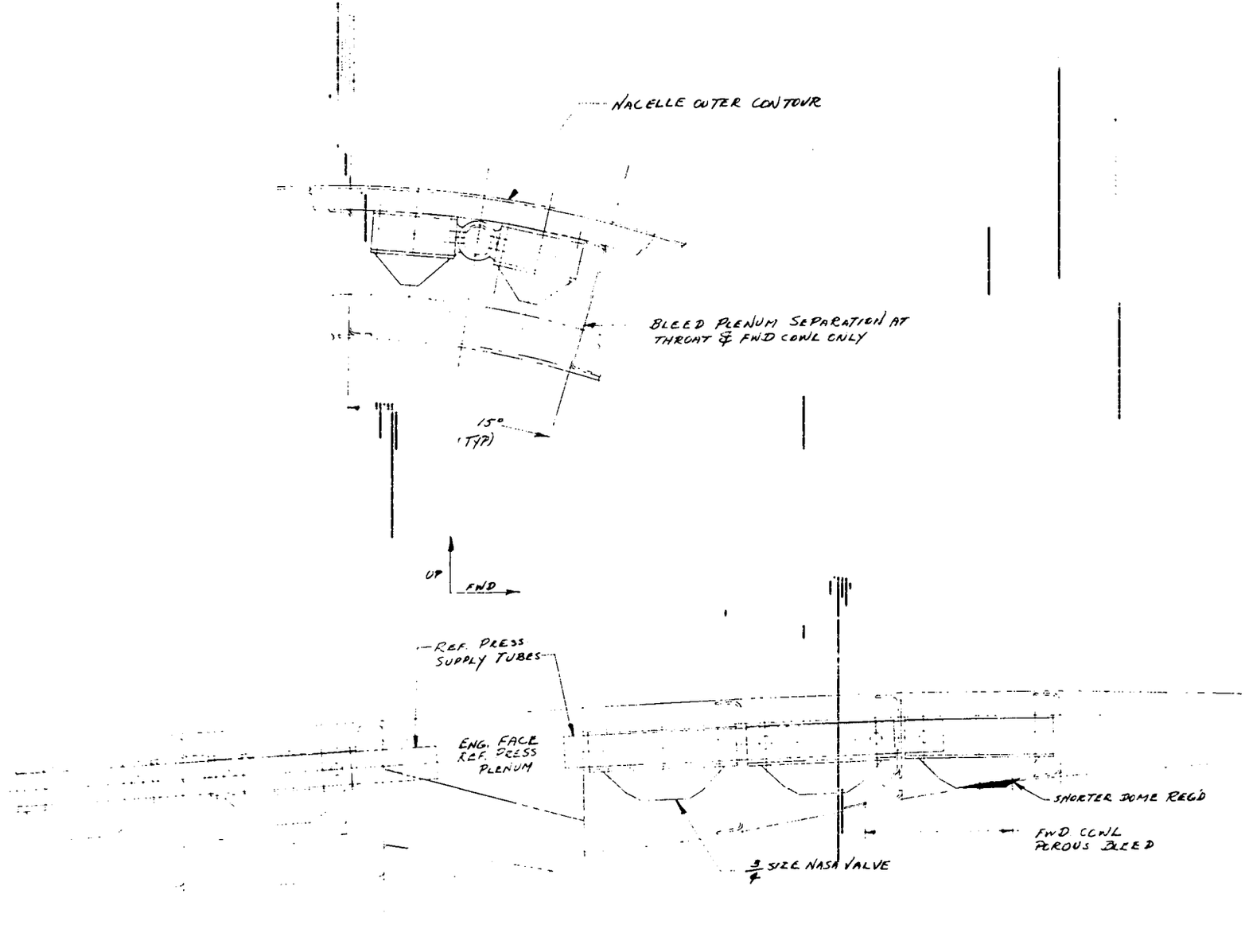


DRAWING 5. THREE-QUARTER SCALE VORTEX VALVE INSTALLATION

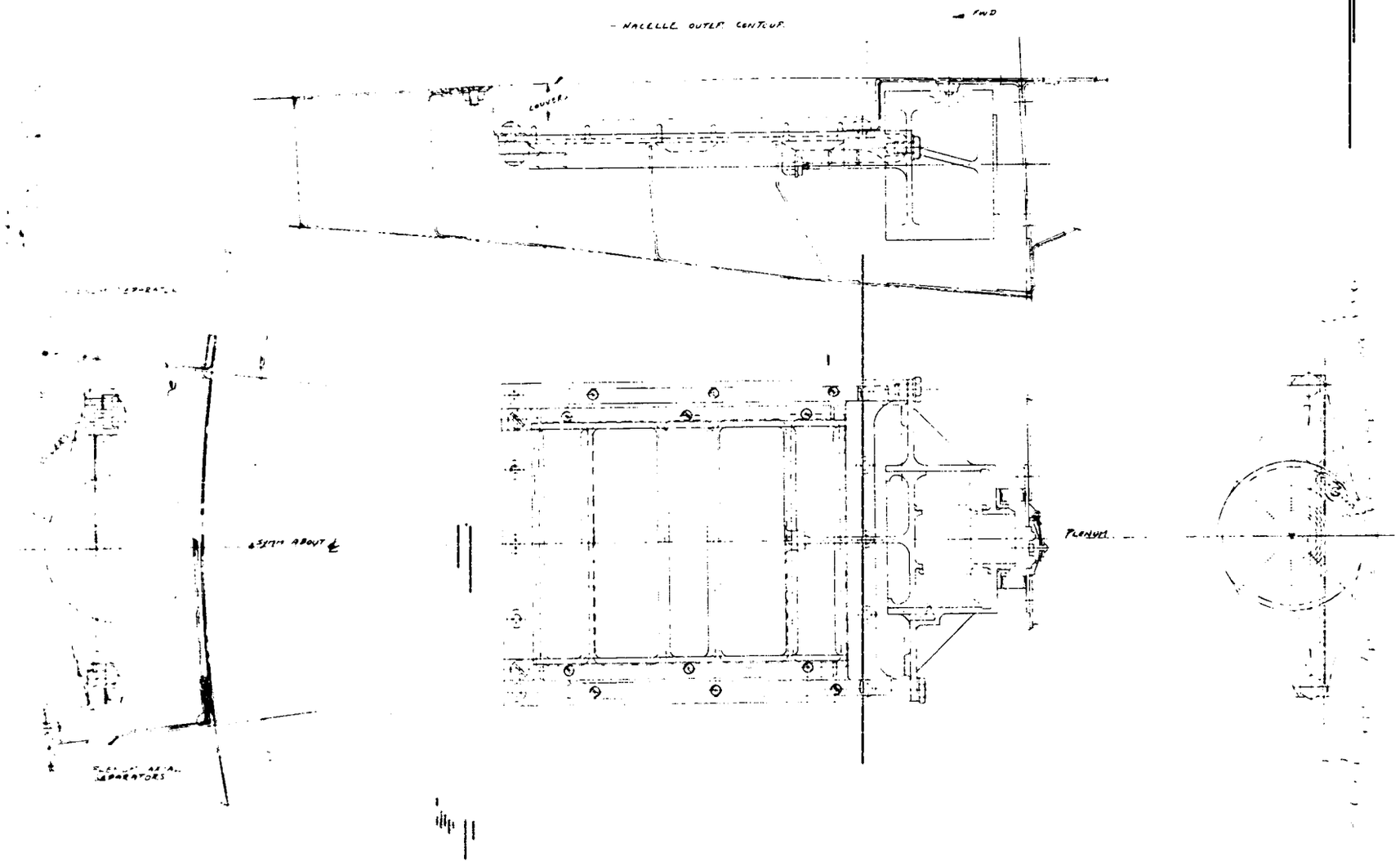


DRAWING 6. PRELIMINARY INSTALLATION OF SLIDE VALVES IN COWL

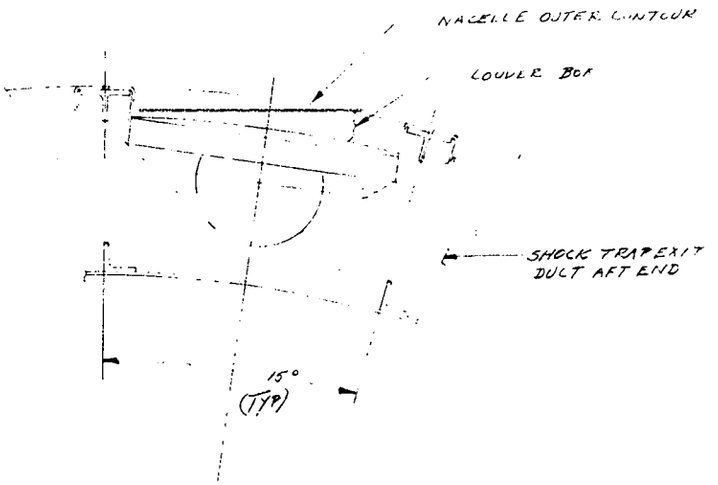


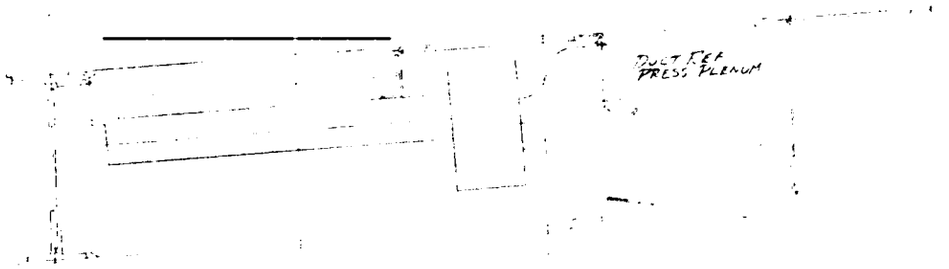


DRAWING 7. SLIDE VALVE INSTALLATION IN SHOCK TRAP PLENUM

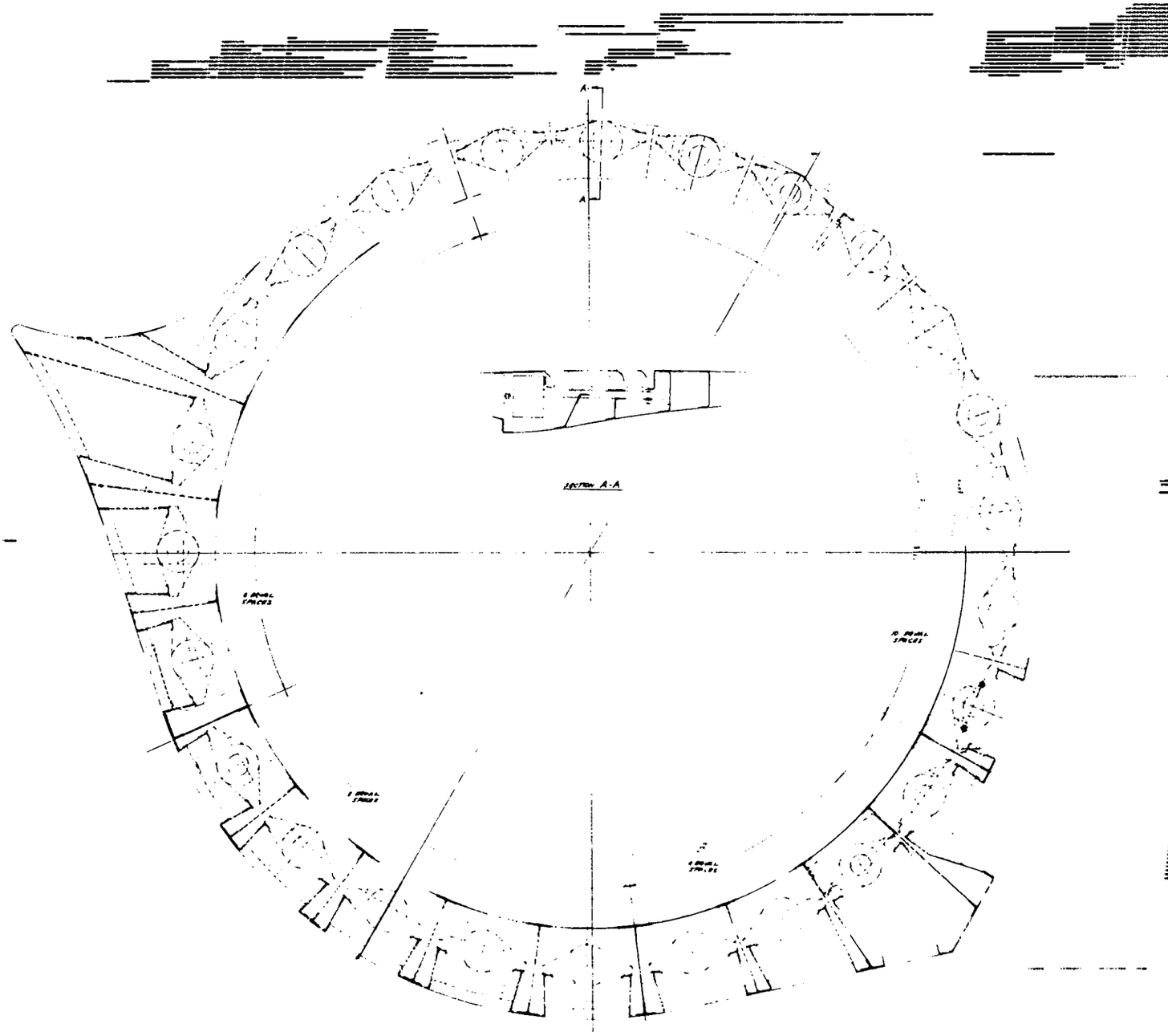


DRAWING 8. CIRCUMFERENTIAL LOCATION OF SLIDE VALVES IN COWL

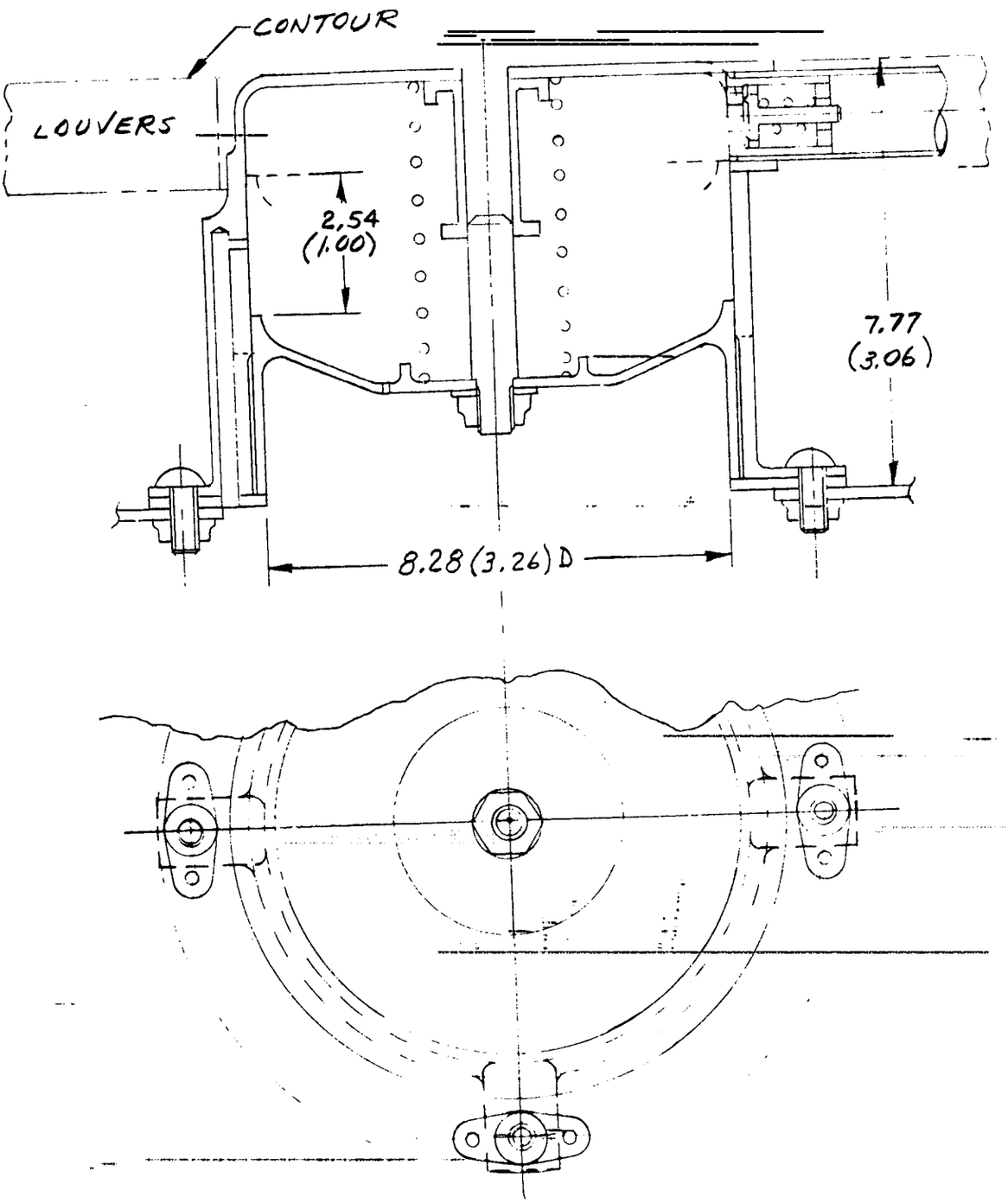


DRAWING ~~9.~~ UNSHIELDED POPPET VALVE ~~PRELIMINARY VERSION~~

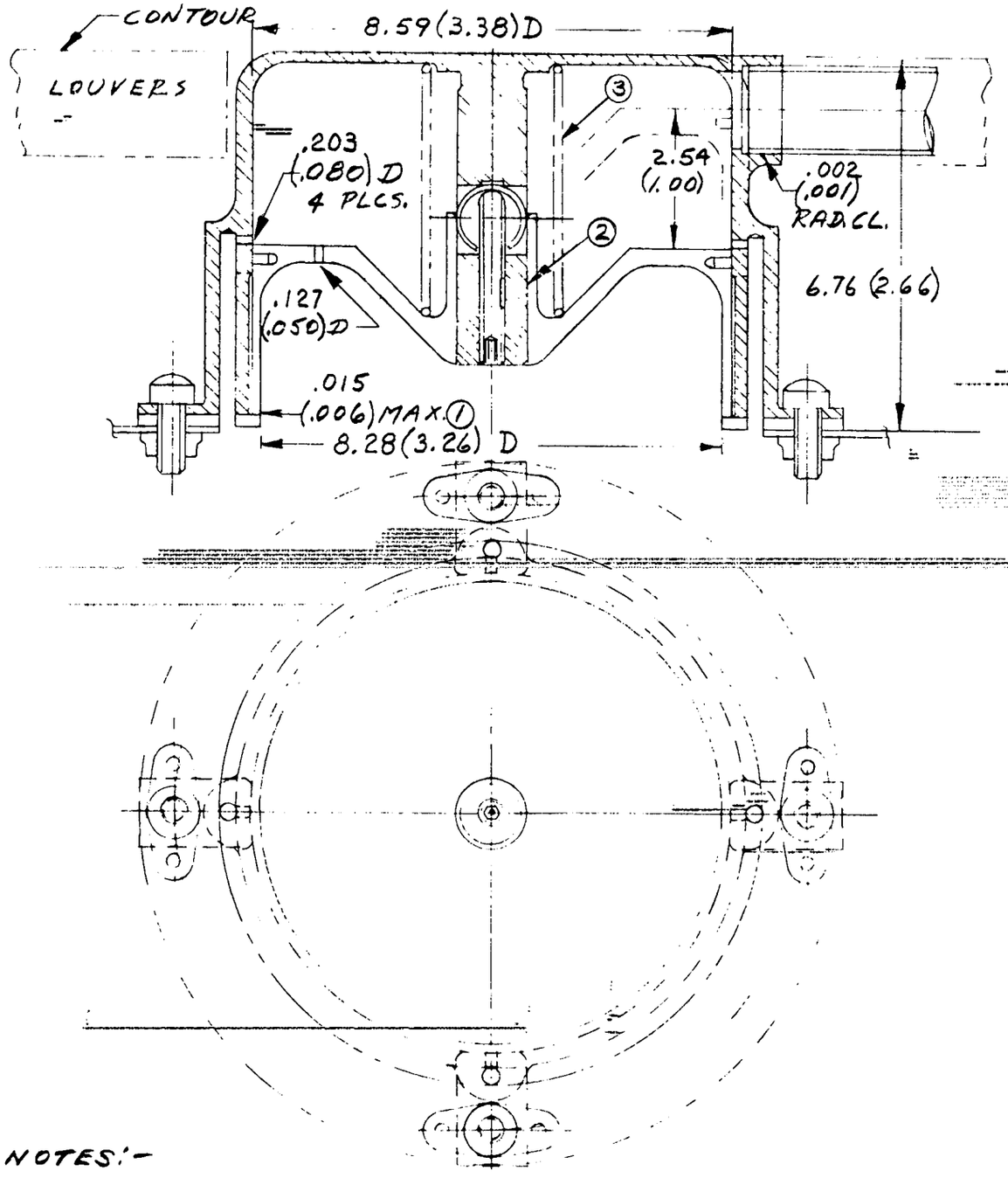


NOTES:-

(1) VALVE CLOSED (2) .0063 (.0025) RAD. CLEARANCE.
(3) 1.33N (3LB.) INSTALLED, RATE .337 N/cm.

DRAWING 10. UNSHIELDED POPPET VALVE, FINAL VERSION

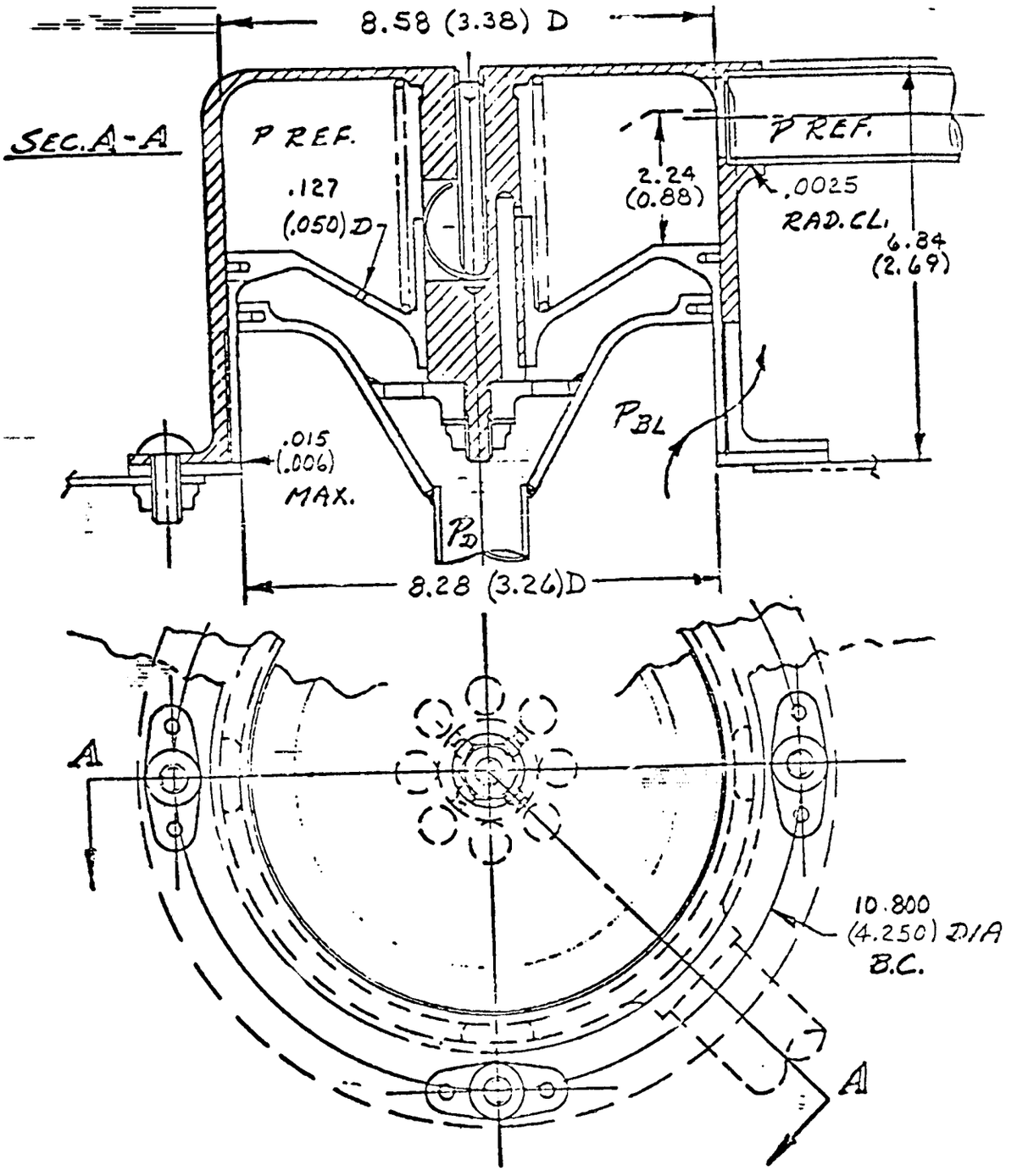


DRAWING 11. SHIELDED POPPET VALVE

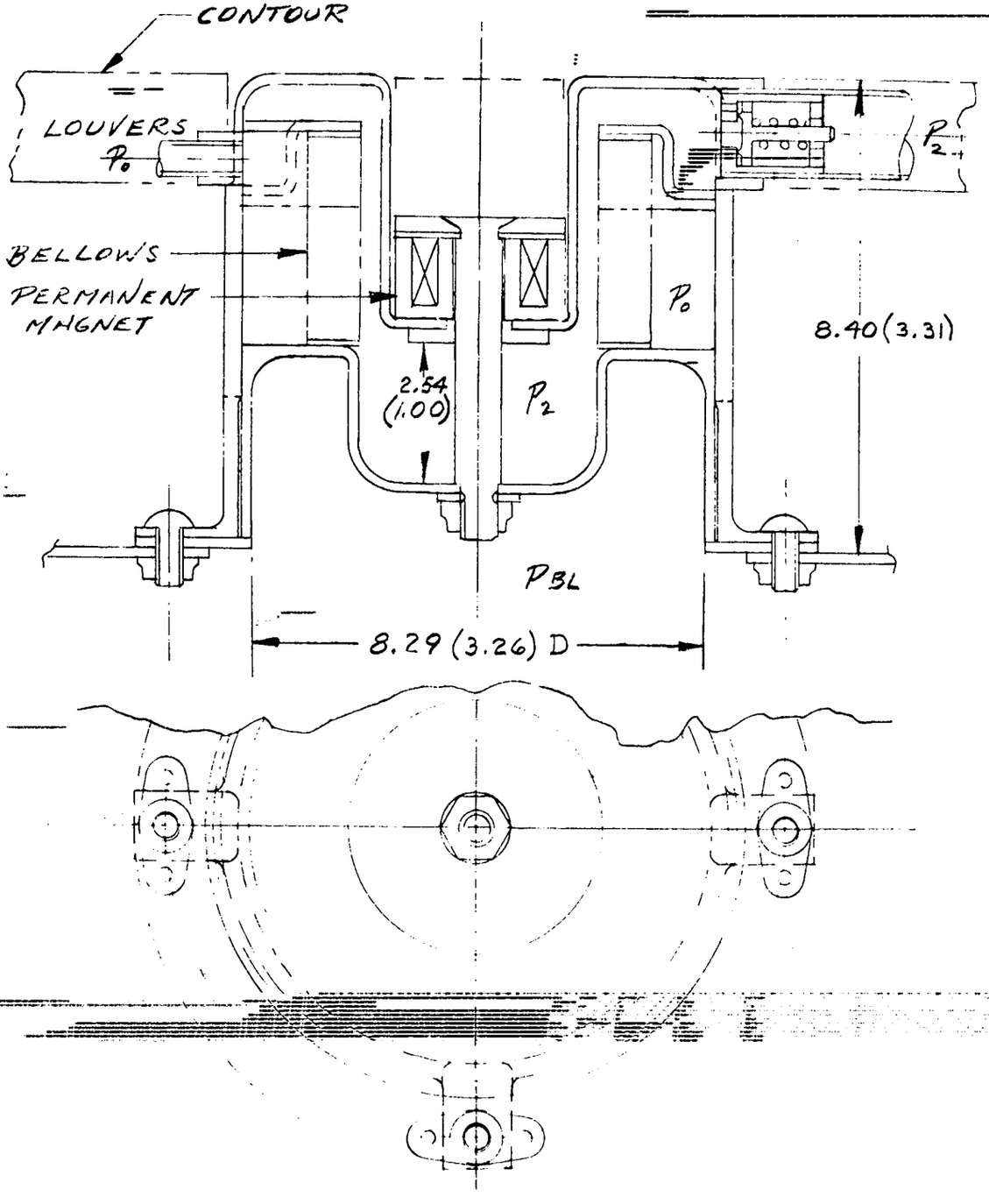


DRAWING 12. BELLOWS-OPERATED POPPET VALVE, PRELIMINARY VERSION

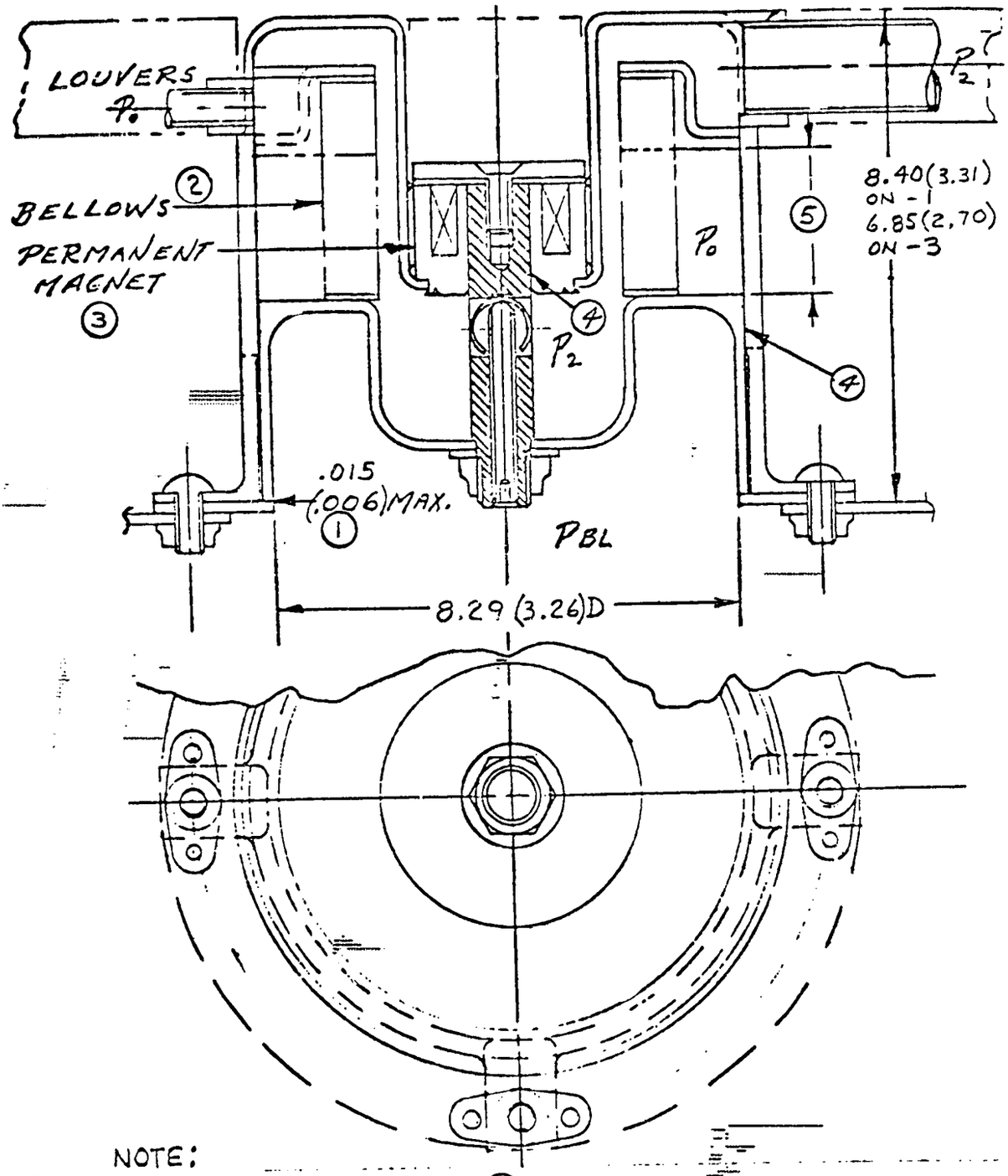


NOTE:

① WITH POPPET TOUCHING SEAT ② METAL BELLOWS CORP.
③ 1.56 N (.35 LB.) WITH .19 (.075) CRES. WASHER ④ .0635 (.0025) RAD. CLEAR.
⑤ 2.54 (1.00) ON -1, 1.75 (.69) ON -3.

DRAWING 13. BELLOWS-OPERATED ~~POPPET~~ VALVE, FINAL VERSION

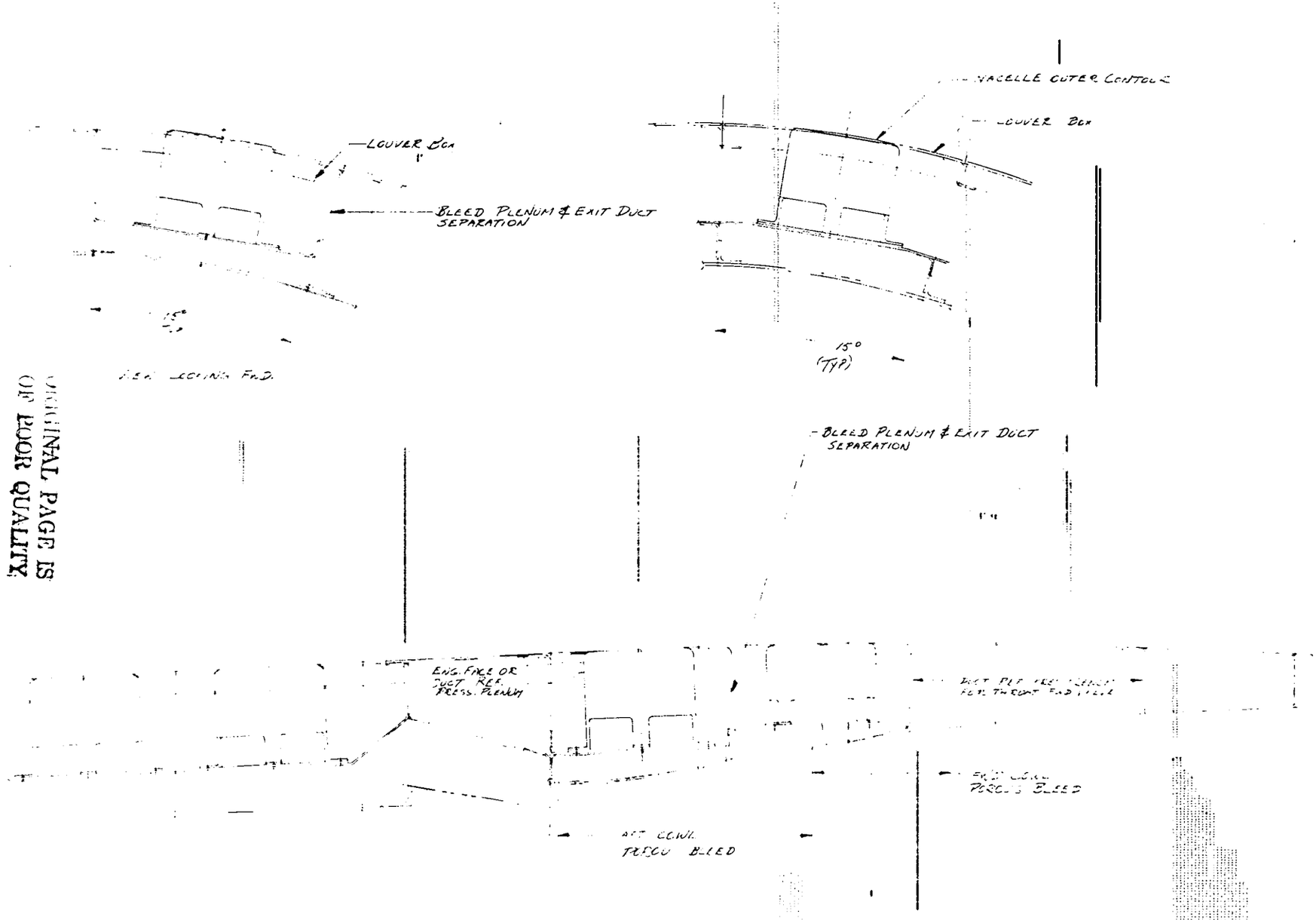


DRAWING 14. PRELIMINARY INSTALLATION OF POPPET VALVES IN COWL AND SHOCK TRAP PLENUM

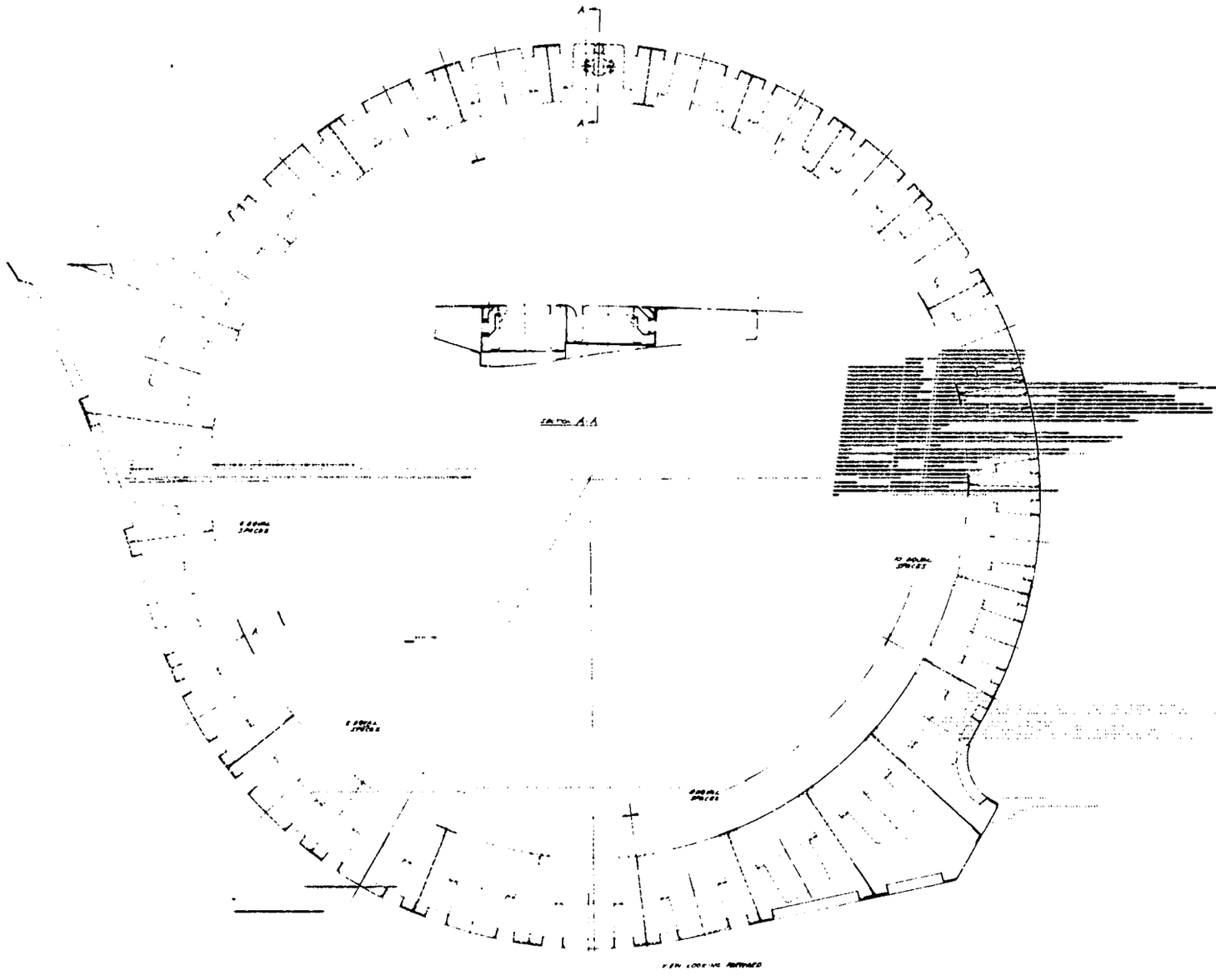

DRAWING 15. CIRCUMFERENTIAL LOCATION OF POPPET VALVES IN COWL

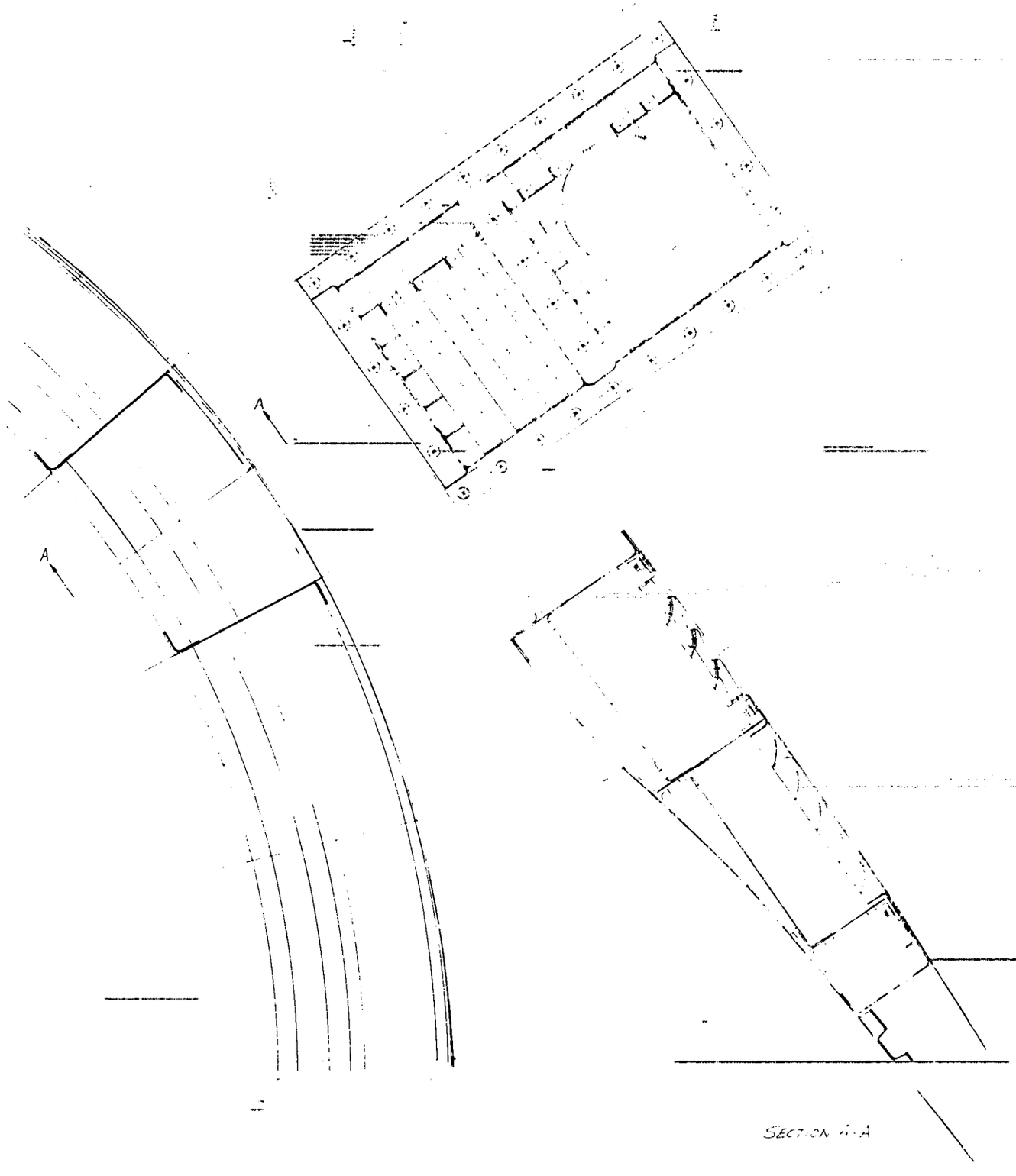


DRAWING 16. POPPET VALVE EXIT LOUVERS

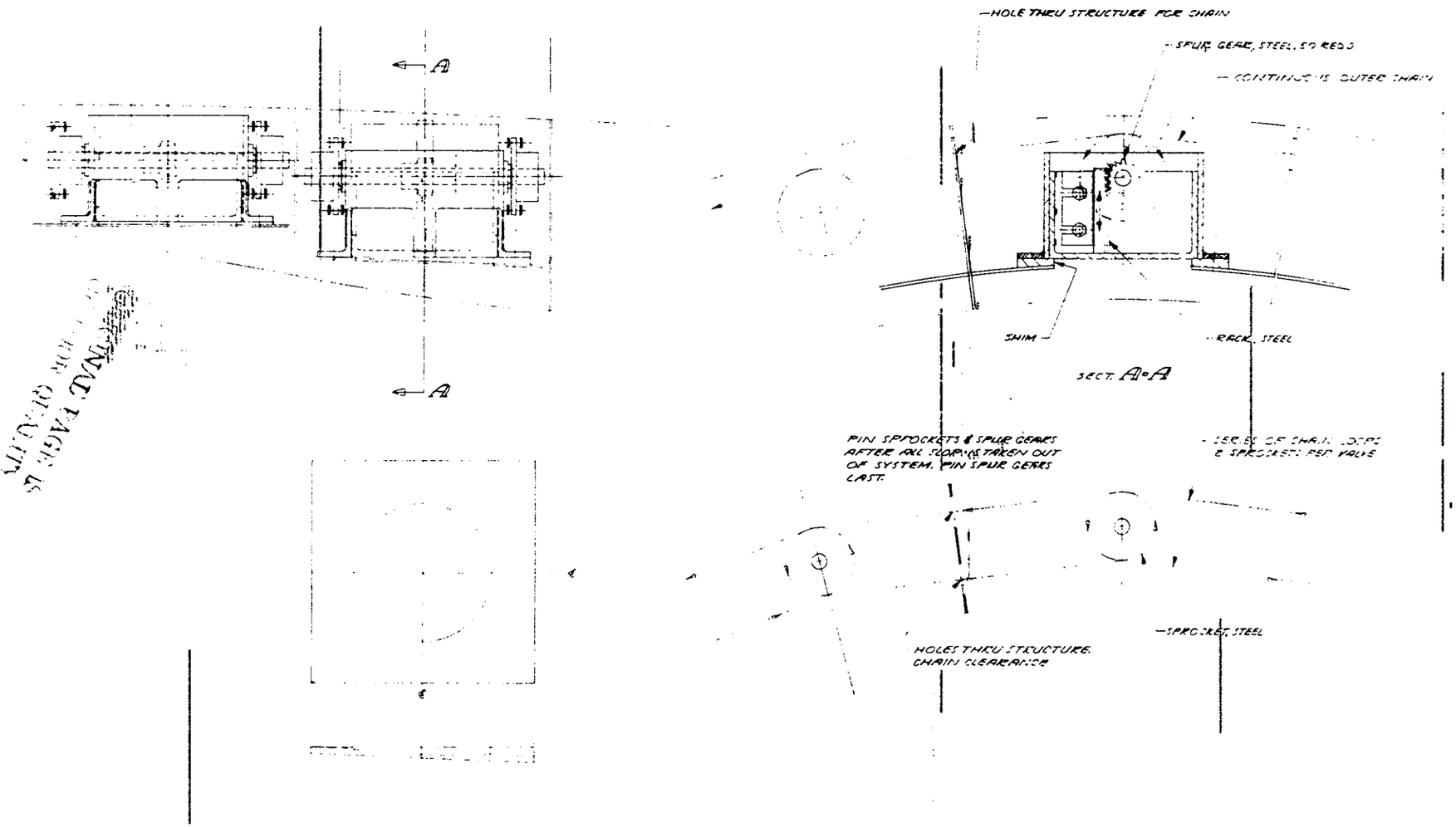


DRAWING 17. BLEED ACTUATOR FOR WIND TUNNEL MODEL

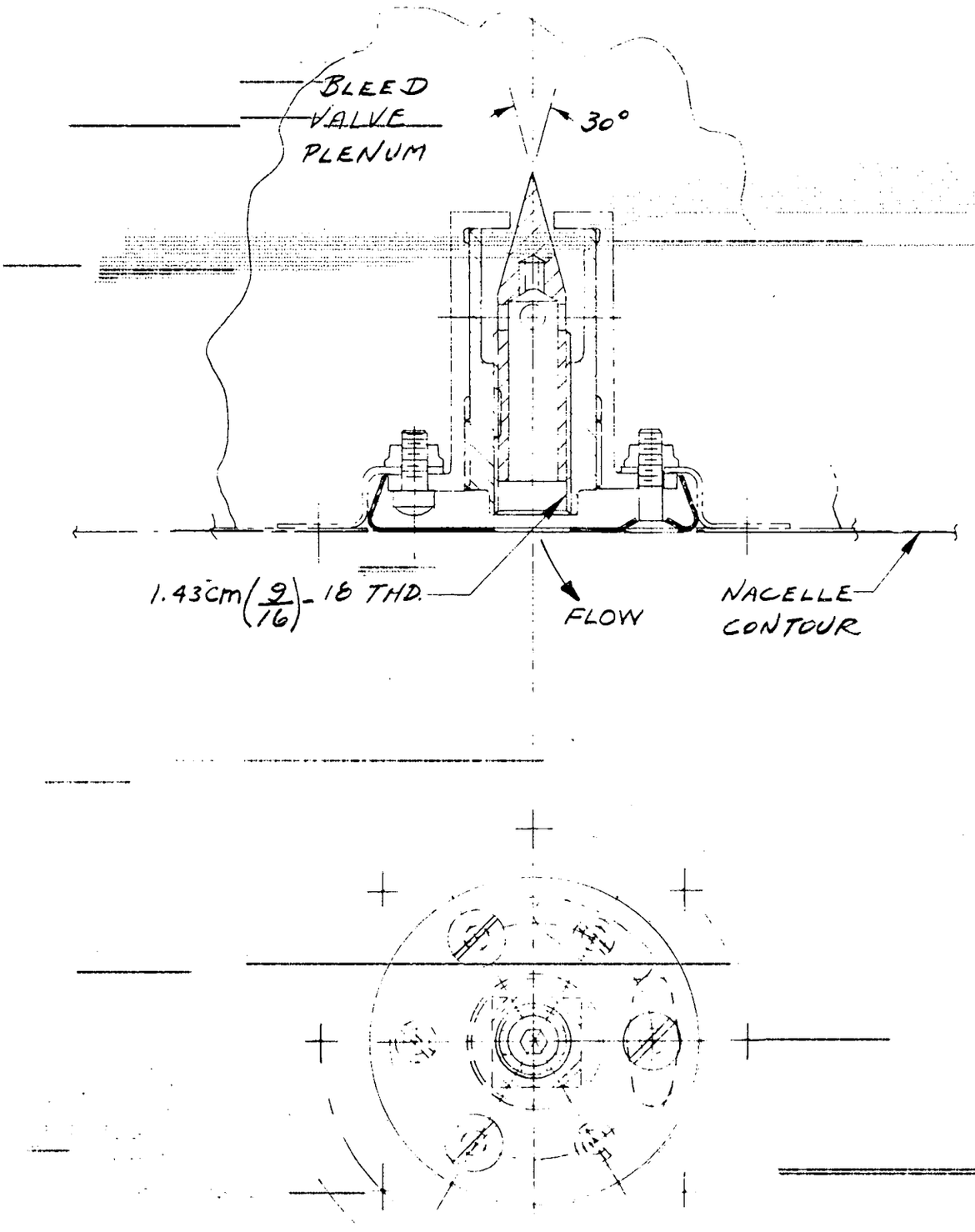


DRAWING 18. VARIABLE-OVERBOARD-ORIFICE

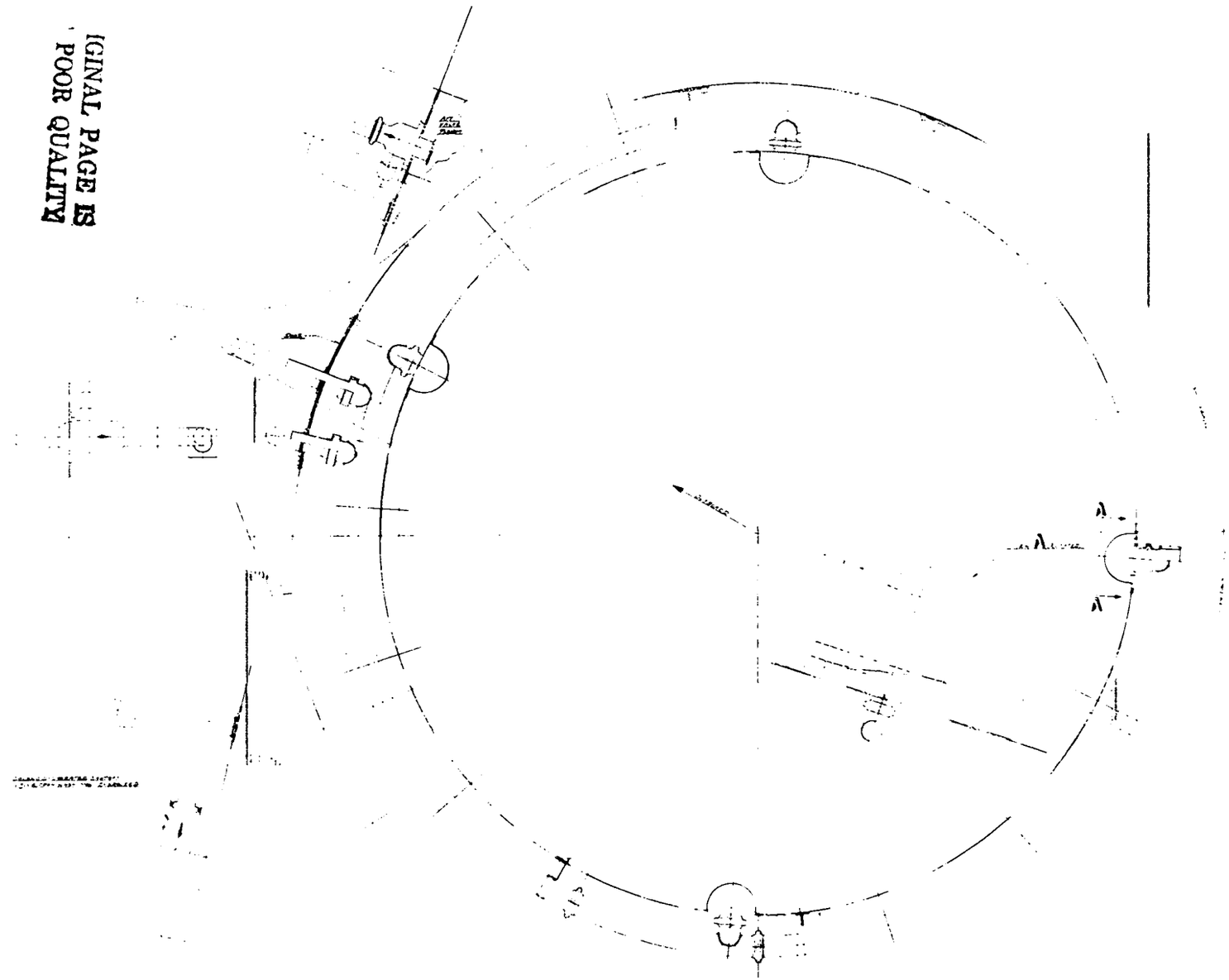

DRAWING 19. BLEED SHUT-OFF SYSTEM

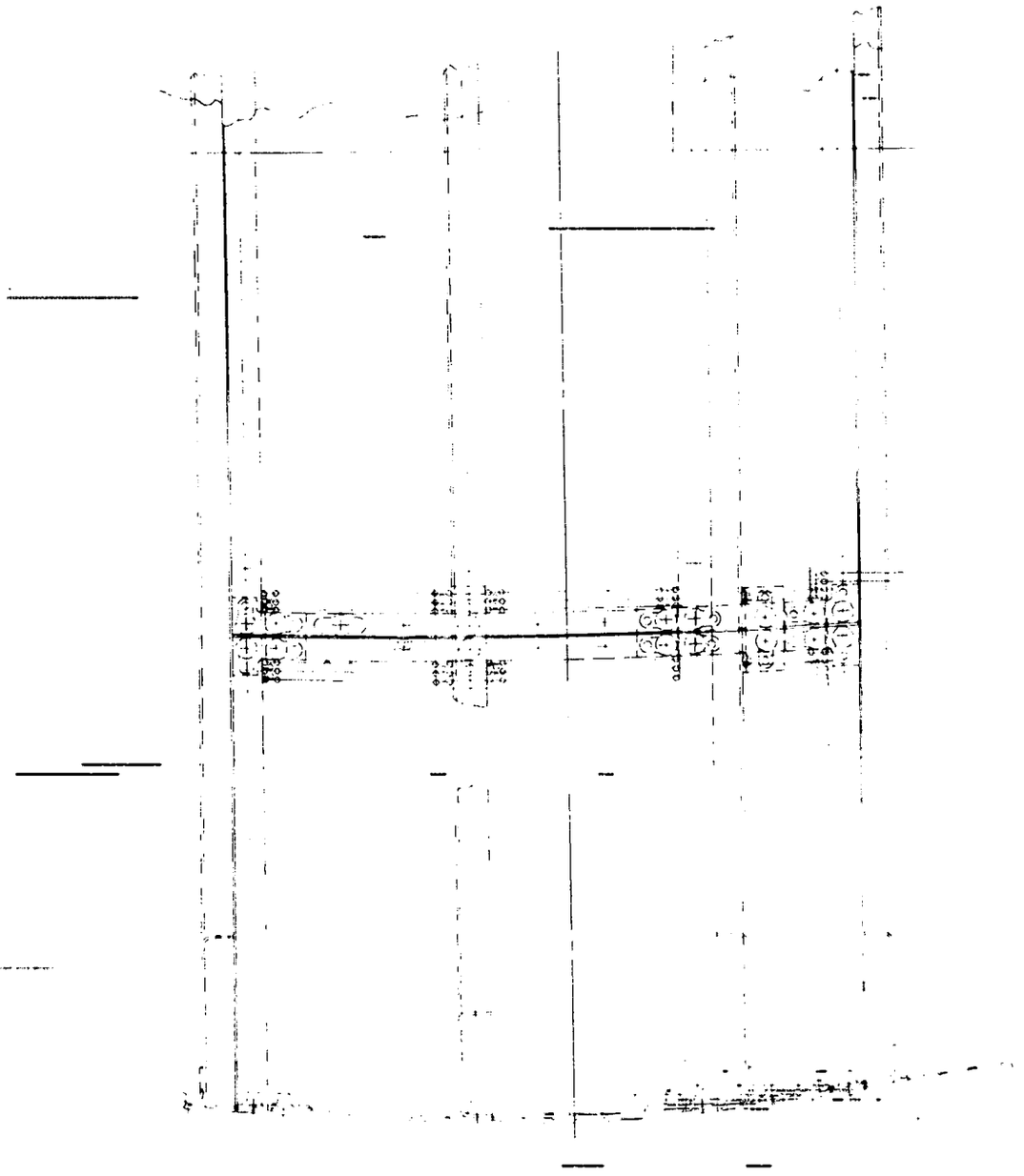

DRAWING 20. INLET CENTERBODY BLEED PERFORATIONS